THIRD HARMONIC MANAGEMENT AND FLEXIBLE CHARGING FOR THE INTEGRATION OF ELECTRIC VEHICLES INTO THE GRID

A Dissertation
Presented to
The Academic Faculty

By

Jorge E. Hernandez C.

In Partial Fulfillment
Of the Requirements for the Degree
Doctor of Philosophy in Electrical & Computer Engineering

Georgia Institute of Technology

May, 2015

THIRD HARMONIC MANAGEMENT AND FLEXIBLE CHARGING FOR THE INTEGRATION OF ELECTRIC VEHICLES INTO THE GRID

Approved by:

Dr. Santiago Grijalva, Advisor
School of Electrical & Computer Engineering
Georgia Institute of Technology

Dr. Ronald G. Harley
School of Electrical & Computer Engineering
Georgia Institute of Technology

Dr. Thomas G. Habetler
School of Electrical & Computer Engineering
Georgia Institute of Technology

Dr. Maryam Saeedifard
School of Electrical & Computer Engineering
Georgia Institute of Technology

Dr. Dario Solis
Office of the President
Texas Tech University

Date Approved: December 17, 2014

To my wife, Marguerite,
parents, Jorge and Edith,
and brother, Jonathan,
with all my love.

ACKNOWLEDGEMENTS

Fulfilling the Ph.D. process at Georgia Tech has been a dream come true. Having had the opportunity to study, work, and learn from some of the brightest minds in the world is an experience that I will always treasure. However, this process has been far from easy and was only accomplished with the support of many to whom I am indebted. First and foremast, I would like to give thanks to my family. My wife, Marguerite, has been an endless source of patience, support, and encouragement, always inspiring in me a positive attitude, particularly during the low points of my graduate studies. I would also like to give a huge thanks to my parents for their teachings throughout my life and installing in me the passion to never stop learning. The support and encouragement of my in-laws has also been instrumental during this process.

I am deeply thankful to my current advisor, Dr. Santiago Grijalva, for his support, encouragement, and advice, both in academic and non-academic matters. His dedication on making a difference in the field is truly inspiring. I would also like to express my gratitude to my previous advisor, Dr. Deepak Divan, for his support and timely suggestions. His view on the importance of asking the right questions and willingness to work on subjects outside of his comfort zone have influenced my professional growth.

I also owe a special thanks to Dr. Thomas Habetler, Dr. Ronald Harley, Dr. Maryam Saeedifard, and Dr. Dario Solis for taking the time to serve as members of my dissertation committee. Their suggestions during the dissertation process have been invaluable.

The financial support from the Government of the Republic of Panama, NEETRAC, and Varentec received during my graduate studies is acknowledged.

I would like to thank Frank Lambert for his support on various projects I have had the opportunity to work on. I am also grateful to James Steinberg for making himself available when his ingenuity was much needed in building different components of the experimental setups. Similar thanks are due to NEETRAC personnel for overseeing the experimental tests and ensuring safety procedures were followed. Deborah King was helpful in providing the logistics for purchasing components. The efforts of Marty Page from Georgia Power to provide the distribution feeder data and coordinate the field measurements made the system impact study of the proposed filter possible.

I would like to express special gratitude to Prasad Kandula for his assistance in building and testing the experimental setups and developing its control software. Without his help the experimental portion of this work would not have been possible. I would also like to thank my fellow graduate students, Frank Kreikebaum, James Thomas, Rohit Moghe, Amrit Iyer, Debrup Das, and Anish Prasai, with whom I had the privilege to work with.

Finally, I would like to thank all my friends back in Panama and here in Atlanta for providing me with the social support and much needed distraction to maintain my sanity during stressful moments of the Ph.D. process.

TABLE OF CONTENTS

LIST OF TABLES

LIST OF FIGURES

ABBREVIATIONS

ASD	Adjustable speed drive
BTB	Back-to-back
CC/CV	Constant current/constant voltage
CFL	Compact fluorescent lighting
DOE	Department of Energy
ED	Economic dispatch
ERCOT	Electric Reliability Council of Texas
EV	Electric vehicle
EWITS	Eastern Wind Integration and Transmission Study
FFT	Fast Fourier Transform
HEV	Hybrid electric vehicle
ICEV	Internal combustion engine vehicle
ISO	Independent system operator
IWC	Infrastructure Working Council
LC	Inductance-capacitance
LDV	Light-duty vehicle
LV	Low voltage
MILP	Mixed integer linear programming
MV	Medium voltage
NEETRAC	National Electric Energy Testing, Research and Applications Center
NEV	Neutral-to-earth voltage
NHTS	National Household Travel Survey

PR	Power router
PSCAD	Power system computer aided design
PST	Phase-shifting transformer
PT	Potential transformer
PWM	Pulse-width modulation
RC	Resistive-capacitive
RPS	Renewable portfolio standard
SOC	State of charge
THD	Total harmonic distortion
UC	Unit commitment
UPFC	Unified power flow controller
V2G	Vehicle-to-grid
VSI	Voltage source inverter
ZEV	Zero emission vehicle

SUMMARY

Electric vehicle (EV) development has gone into an accelerated pace in recent years to address pressing concerns on energy security, the environment, and the sustainability of transportation. The future market success of EVs is still uncertain, but the current shift in the automotive industry is indicating a possible bright future for EVs. Because of its unique load characteristics, an extensive deployment of EVs will not only bring challenges to power systems, but will enable new opportunities as well. The objective of this work is to address the increased third harmonic currents expected with the introduction of EVs and to explore the potential of leveraging flexible EV charging to increase wind power production.

Since EV chargers rely on a nonlinear power conversion process to obtain a controllable DC source from the utility AC supply, it is expected that these devices will aggravate third harmonic current issues. In fact, utility harmonic field data show that, even without EVs, distribution feeders are already experimenting elevated levels of third harmonic currents. To address present and future utility harmonic filtering needs, a practical third harmonic hybrid active filter for medium voltage (MV) applications is proposed. Its design is based on strict utility requirements of cost, reliability, and ease of system implementation. The operation and performance of the proposed filter is verified through simulations and two experimental setups, one tested at 7.2 kV. Furthermore, a system impact study of the proposed filter is performed using actual data for a typical residential/small commercial distribution feeder.

Because vehicles remain stationary most of the time, EVs have the potential of being flexibly charged, providing a spectrum of opportunities for system operators. The recent

increase in wind power penetration in the U.S. is raising concerns on how to accommodate this stochastic renewable energy resource in day-ahead scheduling operations. In this work, a detailed integrated day-ahead scheduling framework is developed to explore the impact of leveraging flexible EV charging to balance out the variability and uncertainty of wind power generation. It is determined that the full benefits of balancing wind power generation with flexible EV charging may not be achieved in congested power systems. A potential solution based on deploying power routers (PRs) to augment the flexibility of the transmission system is proposed. Simulation results are presented for a test system based on the IEEE 39-bus system.

1 INTRODUCTION

This chapter presents the motivation for this research, discusses the scope of work, and provides the outline of this document.

1.1 ELECTRIFICATION OF THE LIGHT-DUTY VEHICLE FLEET

The U.S. Energy Information Administration recently published in [1] figures on the total energy and electric energy consumption of the transportation sector in 2012 that reveal the tremendous opportunity for electrifying portion of the light-duty vehicle (LDV) fleet. LDVs, which consist primarily of automobiles and light trucks, dominate the total energy usage in the transportation sector (57.9%), followed far behind by freight trucks and air transportation. However, considering the level of electric energy consumed by the transportation sector, LDVs only represent just under 2% of this energy, while intercity, transit, and commuter rail collectively account for 98% of electric transportation today. As observed, LDVs represent the largest opportunity for electrification in the transportation sector, since they dominate total energy usage while the penetration of electric LDVs still remains low. The readily available options for electric LDVs are all-electric vehicles, which operate solely on energy stored in an on-board battery, and plug-in hybrid electric vehicles, which are able to operate both on fossil-fuel and energy stored in a battery. These two electric vehicular options are collectively referred to as "electric vehicles" (EVs) in this document.

The vision of having a considerable portion of the LDV fleet being electrified is not new though. Beginning in the early 1830s, numerous small-scaled electric vehicles were built around the world. Those early electric carriages were too rudimentary and

unsuitable for practical implementation [2], but even with their deficiencies their development was markedly ahead of internal combustion engine vehicles (ICEVs), which did not appear until 50 years later [3]. The deficiencies of early EVs were mainly due to the unavailability of practical rechargeable batteries until the mid-19th century. The first practical rechargeable lead-acid battery cell came at the hands of Gaston Plante in 1859, which was later improved by Camille Faure in 1881 into a successful commercial product [2-4], paving the road for the success of the EVs of the following decades. In the late 1800s, France and England were the first countries to support the widespread development of EVs [3]. It was not until 1895 that the U.S. became interested in EVs, after William Morrison introduced his six-passenger wagon in 1891 [4, 5], considered the first successful EV built in U.S. After this many innovations followed, and the U.S. quickly positioned itself as a leader in the production and acceptance of EVs.

The U.S. was prosperous and automobiles, available in electric, steam, and gasoline versions, were very popular by the turn of the last century. At the time, EVs outsold all other types of vehicles and represented 38% of automobiles on U.S. roads [3]. Early EVs suffered from limited range, low speeds, and careful and frequent battery maintenance, but were considered silent, odorless, reliable, and simple to operate compared to its counterparts [4, 5]. Furthermore, EVs did not require wrestling with a gear shifter and were exempt from the dangerous effort of manually crank starting the vehicle, as was the case with early ICEVs [3, 6]. However, the introduction of the mass-produced Ford Model T and the motorized assembly line by Henry Ford in the late 1900s quickly changed the U.S. automotive landscape. By re-branding EVs as luxury town cars, sales peaked in 1912 [3, 5], but at that point only constituted about 1% of the U.S. automotive

market [6]. Sales rapidly declined soon thereafter, and by the 1920s EVs ceased to be a viable commercial product. Other major contributing factors to the demise of early EVs include the slow and uneven spread of electrification during the first two decades of the past century, the invention of the electric self-starter by Charles Kettering in 1912, and the discovery of large crude oil reserves in Texas and the extension of highways in the 1920s [3, 5, 6]. Electric delivery, heavy cargo, and work trucks remained popular for a longer period, but with time also became unable to compete with speedier gasoline and diesel versions and almost all eventually disappeared. After this, electric propulsion was restricted to limited range applications, such as golf carts and airport transporters [5, 6].

Research, development, and commercialization of EVs remained stagnant until interest in them was reawaken again in the 1960s and 1970s. In the mid 1960s, the smog produced by ICEVs became a major concern, prompting the U.S. government in 1966 to introduce the earliest bills that promoted EVs as a means to reduce exhaust emissions [7]. The big U.S. automakers Ford and General Motors both produced EVs in the late 1960s to support this effort [8]. Ultimately, this attempt to promote EVs failed since engine development were able to catch up with emission standards as they got tighter and tighter [9], making ICEVs the lowest cost and highest performance alternative. Also, because most electricity came from high-sulfur coal there were many questions on the effectiveness of EVs in improving air quality. However, the 1973 Oil Embargo and subsequent gas crunch brought renewed hope for the EV. The motives this time around were mainly political, to reduce the dependence on oil from the Arab countries, and economic, to improve the foreign trade position of the U.S [8]. In response to these concerns, the Department of Energy (DOE) created the Electric and Hybrid Vehicle

Program with the purpose of promoting research on EVs and demonstrations to gain public acceptance [8, 10]. Although some EV models enjoyed considerable success during the 1970s, their prosperity was only temporary as consumers were not interested in purchasing the more expensive and less performing EVs after the oil crisis was over.

After a period of slow developments, several U.S. legislative and regulatory actions renewed EV development efforts. Primary among these were the U.S. 1990 Clean Air Act Amendment [11], the U.S. 1992 Energy Policy Act [12], and, particularly, California's landmark Zero Emission Vehicle (ZEV) mandate [13], which required 2% of vehicles to be ZEVs (a category that originally only included EVs) by 1998 and increasing up to 10% ZEVs by 2003. Several other states followed suit issuing ZEV mandates of their own [8]. Prompted by these requirements, major automakers reassumed production and sales of EVs, among the most popular were General Motors's EV1, Ford's Ranger EV, Chevy's S-10 EV, Honda's EV Plus, and Toyota's RAV4 EV [7]. This period also saw the birth in 1997 (Japan) of the first commercially mass-produced hybrid electric vehicle (HEV), the Toyota Prius, a vehicle consisting of an internal combustion engine, a battery, and an electric drive, albeit without the possibility of charging from the grid. By 1998, EVs satisfied the driving requirements of many fleet operators and two-car-owning families, however, they still remained considerably more expensive than ICEVs. As ZEV mandates weakened over the years, the major automakers stopped offering EVs by 2003 [10].

To address pressing concerns on energy security, the environment, and the sustainability of future transportation, EV development has gone into an accelerated pace in recent years. As observed, the idea of electrifying a substantial portion of the LDV

fleet has been resurrected in the past for political, economic, and environmental reasons; however, never before have all simultaneously served to strongly motivate the return of EVs, gaining the support of politicians, automakers, and consumers. In his 2011 State of the Union address, President Obama called for putting one million EVs on the road by 2015, with the goal to position the U.S. as a global leader in the production and deployment of EVs. Regulations, such as the recent increases in the Corporate Average Fuel Economy (CAFE) standards that require manufacturers to increase fuel economy, have already been put into effect to encourage the expanded market entry of EVs [7, 14]. In addition, a number of policies have been introduced to spur domestic manufacturing, deployment, and innovation in EV technologies. Such efforts have included $4.4 billion in loans/grants to EV and battery manufactures, $400 million to support EV demonstrations and installation of EV charging points, and an over 30% increase in support for EV technology research and development [14]. Also, incentives to promote consumer adoption are currently being provided, most notably the federal tax credit of up to $7,500 per EV, depending on its battery capacity [15]. Many states and regions of the U.S. have also adopted measures to promote EV usage, including additional tax credits/rebates, exemptions from fees and inspections, and other non-monetary incentives [16]. Another important initiative that has considerably supported EV deployment is the alternative fuel infrastructure tax credit [17], which has helped increase public EV charging points from 541 in 2010 to 19,410 in 2013 [18].

Based on the success of HEVs and stimulated by the recent increase in the price of gasoline and advances in lithium-ion battery technology, almost all manufacturers are offering an EV option as part of their lineup. In 2013, a total of 16 EV models were

available in the U.S. from 10 different manufacturers [19], with 7 more models expected to be released in 2014 [20]. Among the best selling models are the Nissan Leaf, an all-electric vehicle capable of traveling 84 mi powered from its 24 kWh battery [21], and the Chevrolet Volt, a plug-in hybrid electric vehicle which complements its 38 mi all-electric range from its 16.5 kWh battery with an internal combustion engine electric generator [22]. Nissan, who sold 22,610 of its Leaf in 2013, has lifted production of this vehicle by 50% to 3,000 units a month after recently breaking a monthly record sales of 2,500 units [23]. Likewise, General Motors, who sold 23,094 of its Chevrolet Volt in 2013, has recently announced a $450 million investment to booster its electric car research and production capability, this follows an earlier $121 million investment with the same purpose [24]. Other automakers are also taking steps to increase their EV manufacturing capabilities, signaling a promising future for the EV market.

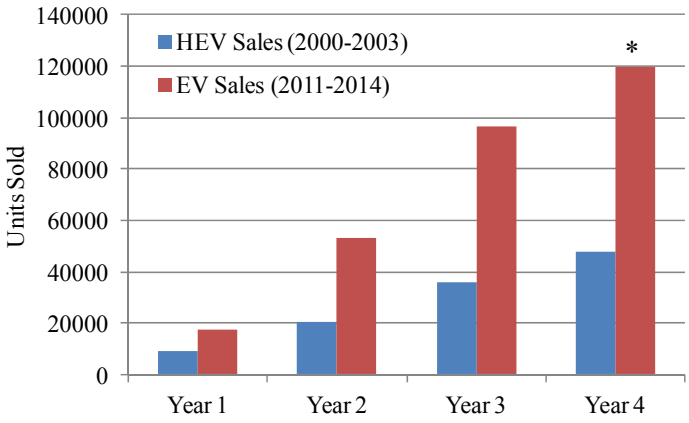

* Projected EV sales from [25]
Actual HEV and EV sales extracted from [26] and [19], respectively

Figure 1. HEV and EV sales in their first four years in the automotive market.

With U.S. EV sales on pace to reach just half of the government's target of one million EVs on the road by 2015, a target considered from the beginning by many

analysts as unachievable, criticism on the market performance of EVs has started to surface. But, the future of the U.S. EV market, currently the largest one in the world [27], is not as gloom as it appears, especially when compared to HEV sales during the same stage of their development, as seen in Figure 1. In the third year after their introductions, EVs outsold HEVs, regarded as a successful vehicle product, by over 168%. In the meantime, as summarized in Figure 2, numerous studies have projected varying levels of market success for EVs, most predicting substantial market growth with time. The reality is, though, that the EV market is still at an early stage and not much historical data exists to accurately predict exact future EV market penetrations. However, based on the current industry shift, it appears evident that the question is no longer if EVs will become a reality, but rather when EVs will transition from clusters of early adopters to national mainstream use. Thus, the moment has come to develop mechanisms so that the electric power industry is prepared to address the challenges and take advantage of the opportunities that EVs will bring with them.

1.2 POWER SYSTEM CHALLENGES AND BENEFITS OF EVS

EVs have already entered the U.S. market, and with the current shift in the automotive industry, it is anticipated that they will play an important role in the future of the LDV transportation sector. EVs are qualitatively different from conventional loads though. First, they are equipped with high-energy-capacity batteries, requiring between 3,000 and 4,500 kWh per year (plug-in hybrid electric vehicles consume about 70-80% of this), slightly more than an average central air-conditioner [28]. Second, although some plug-in hybrid electric vehicle owners will opt to charge using Level I chargers (up to 1.92 kW), the majority of EVs are expected to charge at Level II (up to 19.2 kW), which

represents a greater power consumption than an average household [29]. So, as observed, EVs are a formidable load that can have a significant impact on power systems, especially at the distribution level. However, EVs are more flexible in their operating schedules than traditional loads, in the sense that EV owners may not have a preference about the exact time of charging, as long as the batteries have sufficient energy to complete the next trip [30, 31]. This flexibility can be harnessed by system operators to provide benefits to the power grid. Therefore, all in all, an extensive deployment of EVs will not only bring considerable challenges to power system design and operation, but enable unique opportunities as well. An overview of the main challenges and benefits brought forth by EVs discussed in the literature is given in the following.

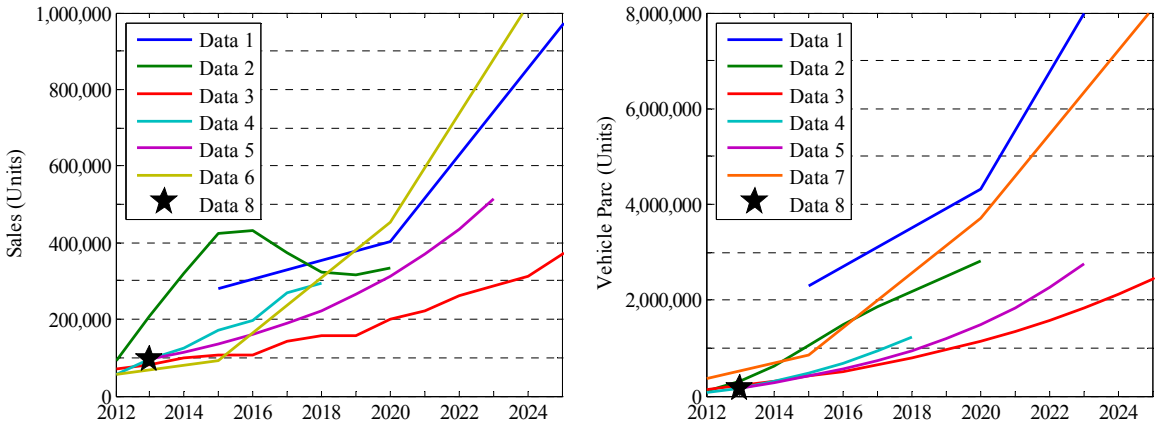

a) b)

Data Sources:
Data 1: Reference [32], gas $4/gal plus subsidy case
Data 2: Reference [33], current policy case
Data 3: Reference [34], reference case
Data 4: Reference [20]
Data 5: Constructed from data given in [27] and [25]
Data 6: Reference [35]
Data 7: Reference [28], medium scenario
Data 8: Actual sales extracted from [19]

Figure 2. EV sales and parc forecasts from various EV market penetration studies.

Because of the comparably high energy and power requirements of EVs, and since they will connect directly to lower network levels, it is widely recognized that EVs will

have the most impact on distribution systems. Also, since EV adoption is not expected to happen uniformly, but rather cluster in particular neighborhoods, the negative consequences on distribution systems are anticipated to be felt even at low national penetration levels [29, 36]. Furthermore, EV charging is expected to coincide with the evening peak of conventional load if allowed to charge freely without any sort of control [29, 37]. This situation would bring voltage stability problems, increase branch congestions, greater losses, and overloading of distribution equipment, which in turn could lead to service outages impacting reliability of supply [37-40]. Of particular concern are the decreases in distribution transformer lifetimes because of temperature-induced insulation aging from capacity overload that will be caused by the additional EV load [36, 41, 42]. In addition, since the loading of distribution feeders is inherently unbalanced in order to serve unequal single- and double-phase loads, EVs will further aggravate the problems arising from this condition [43]. Utilities have also expressed their concerns over the impact harmonics generated by EV battery chargers will have on power quality and their effect on utility and customer equipment [39, 44]. To prepare distribution systems for these challenges, large investments in reinforcement may be required if an uncontrolled EV charging approach is adopted [29, 40].

At the bulk power system level, many studies have shown that, even under uncontrolled EV charging, the U.S. has enough generation and transmission resources to supply energy and power to a substantial portion of its LDV fleet [45, 46], but system operators would need to include this new load in their long-term planning activities [47]. Energy planners, however, have concerns over the increase of electricity production costs with growing EV penetration, which in turn has electric rate impacts on customers.

Depending on the marginal unit that comes online to supply the additional EV load, this increase might be substantial, especially if EVs charge at will and in regions with already high electricity costs [48]. Uncontrolled EV charging might also exacerbate the short-term planning complexity for energy service providers. Not considering EV energy demand appropriately in the day-ahead load schedule will lead to substantial financial penalties [47]. Regulatory issues like development of standards, metering, and billing of EVs need further investigation and are of great interest as well. To address the challenges associated with managing coordinated EV charging, some studies have suggested the emergence of new entities known as EV aggregators. Nonetheless, problems such as how to efficiently integrate these new entities into existing technical and organizational structures of power system operation [47], and the development of an operating framework that determines their purchase of energy and distribution of this energy to EVs [30] still need more attention.

The benefits of EVs are enabled by the possibility of flexibly controlling their charging such that it is advantageous to the power system. At the distribution level, shifting EV charging to periods of low demand allows the grid to operate under less stressed conditions, with improved voltage profiles, lower losses and congestion levels [36, 39, 40]. This helps the system accommodate a larger number of EVs without requiring infrastructure reinforcements, or at least deferring them for a later period [29, 37]. The advantages of employing EVs for load-leveling to increase efficiency and profits was identified by utilities since the early years of the EV [6]. Historically, the fluctuation between generation and transmission resources and customer load has been managed with faster operating, higher-cost cycling power plants. The use of these generation

resources can be reduced if EVs are flexibly charged during off-peak hours, allowing base-load power plants to operate at a uniform power delivery schedule, improving their efficiency and increasing the load factor of the overall system [39, 49]. Another benefit of flexible EV charging is that its characteristics make it suitable for supporting the large-scale integration of variable renewable energy resources, such as wind energy. Many studies have demonstrated the potential of adopting a combined strategy for expanding wind power generation and promoting EVs [31, 40, 50]. The potential impact of flexible EV charging on reducing wind energy prices is twofold: it increases the capacity factor of wind power plants and reduces the requirement for backup capacity and energy storage.

Apart from flexibly charging EVs, many have suggested the possibility of utilizing them as distributed energy storage devices with the capacity of providing power to the grid, a concept referred to as vehicle-to-grid (V2G) [51]. In the literature, V2G is mainly discussed in the context of quick-response, short-duration, high-value electric services, e.g., backup power, frequency regulation, and spinning reserves. However, the degradation of battery life, manufacturer warranty issues, and complexity and cost of added controls and communication with the utility are just but some of the significant barriers for the deployment of this strategy [29, 31]. Beyond the technical challenges, there is also much debate on the economic incentives for V2G operation. Fortunately, even without V2G technology, system operators are still able to use EVs to provide services, such as regulation and spinning reserves, by modulating their unidirectional charging rate [29, 31, 52]. This mode of operation would not be encumbered with the above issues, since it circumvents the warranty issue, has a much more limited impact on battery life, and has simpler charger requirements [29, 31]. In fact, the current SAE

standard J1772 [53], which specifies the electric coupler for EV charging, makes provisions for the communication via the Control Pilot to change the rate at which batteries are charged, making this technology readily applicable. By providing such ancillary services, EVs have the potential of increasing the stability and reliability of the grid, in a cost-effective manner, in addition to also supporting the safe integration of low-cost, variable renewable energy generation.

1.3 SCOPE

The objective of this research is to propose mechanisms to prepare the future electricity grid for the possible large-scale adoption of EVs. As such, this work is not concerned with modeling or predicting the evolution of the EV market penetration, but rather treats the existence of EVs in the power system as an exogenous variable. The focus of this work is on one of the challenges and one of the opportunities that EVs will bring to power system operations of those discussed in the previous section, as illustrated in Figure 3.

The challenge of EVs that will be discussed in this work is the effect that this new load type will have on power system harmonics, specifically on harmonics at the third harmonic frequency. Because of the proliferation of single-phase nonlinear loads on residential/small commercial distribution systems in last few decades, utilities are already concerned about the elevated levels of third harmonic currents flowing in their feeders, especially in the neutral conductor. It is expected that this problem will be exacerbated with the introduction of larger rectifier-end loads, such as EV battery chargers. To address this emerging issue, a practical third harmonic hybrid active filter for medium voltage (MV) utility applications is proposed. The design of the proposed filter has its

foundation on strict utility requirements of low cost, high reliability, and ease of implementation. Simulation studies are performed and experimental setups are designed, built, and tested, to verify the operation and performance of the filter and demonstrate its implementation at utility distribution MV levels. Furthermore, a distribution feeder model is developed for a typical residential/small commercial distribution system from actual utility data and field measurements to make a complete assessment of the benefits of deploying the proposed third harmonic filtering strategy.

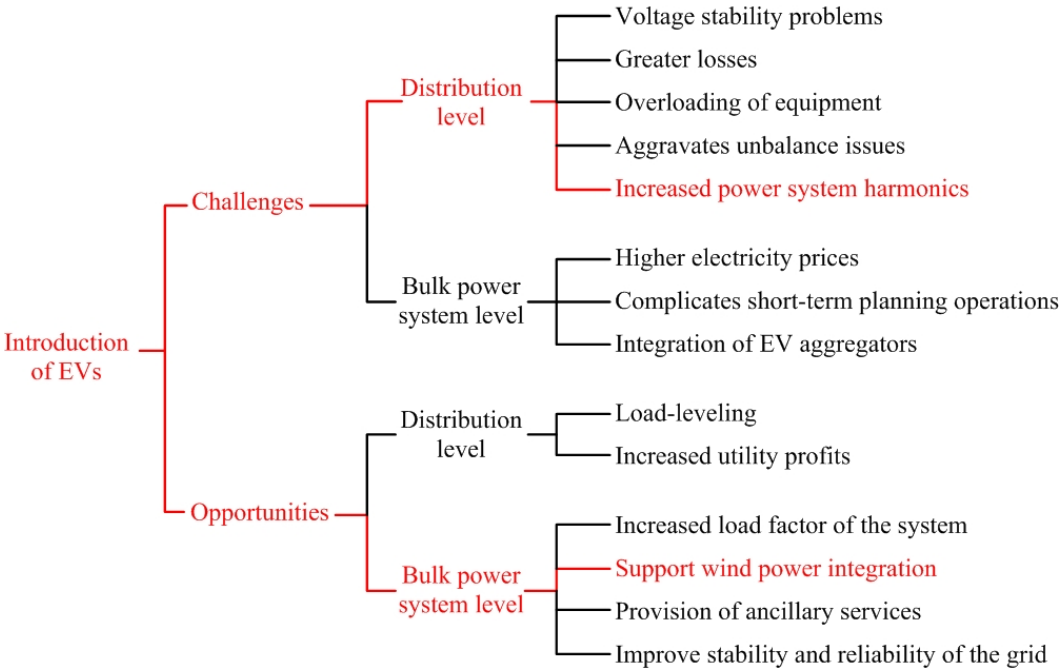

Figure 3. Focus of this work.

The opportunity explored in this research that could be exploited with the wide-spread adoption of EVs is the capacity of this new flexible load in supporting the large-scale integration of highly variable and stochastic renewable energy resources, in particular wind energy. A number of methods have been proposed in the literature and have been implemented by system operators to accommodate a greater amount of wind

energy in current power system operations. Since transportation data reveal that vehicles remain stationary for most of the day, it is believed that EVs could become a resource to balance out the variability and uncertainty of wind power production; especially, if EV charging is flexibly scheduled and EVs are allowed to provide reserve services to compensate for forecast errors. However, the addition of these new highly dynamical components into an already aging grid will most likely aggravate transmission congestion issues. Transmission congestion may limit the benefits achieved by deploying these clean energy technologies and have their adoption occur at a higher societal cost. Recent efforts, though, have led to the development of a new class of power electronics based power routers (PRs) that promise to be considerably more cost-effective than traditional flexible AC transmission systems (FACTS). These PR devices are envisioned to serve as a physical mechanism for alleviating transmission congestion by diverting power flows from congested lines to parallel under-utilized transmission paths. Taking all this into consideration, an integrated day-ahead scheduling/real-time dispatch tool is developed as part of this work, which incorporates wind energy, flexible EV charging, power routers, procurement of reserves, and current practices followed by U.S. independent system operators (ISOs) to accommodate a higher wind capacity in their systems. This tool is applied to a test system based on the IEEE-39 bus system to conceptually demonstrate the benefits of flexible EV charging and allowing EVs to provide system reserves; the potential negative impact of transmission congestion on achieving such benefits; and, the powerful role PRs could assume in scheduling and dispatch power system operations.

1.4 OUTLINE

The rest of this document is organized as follows. Chapter 2 begins by providing a background on the history and origin of power system harmonics, the negative effects of third harmonic currents on distribution systems, and previously proposed approaches for managing elevated third harmonic currents. Work presented in the literature on the harmonic currents generated by EV battery chargers and their potential impact on distribution systems are also reviewed. In this chapter, a practical third harmonic hybrid active filter for MV applications is proposed. The topology, characteristics, and controller design of the proposed filter are described. Simulation results are presented to conceptually demonstrate the operation and benefits of the proposed filter.

Chapter 3 describes two experimental setups that were built and tested to verify the filtering performance of the proposed filter and to demonstrate third harmonic hybrid active filtering at utility distribution MV levels. A detailed description of the design, simulation results, and experimental results for both experimental setups are given. This chapter also includes a system impact study of the proposed filter using actual data for a typical residential/small commercial distribution feeder. Development of a reduced feeder, its validation with field measurements, and simulation results of the impact of deploying the proposed filter are discussed.

Chapter 4 gives an overview of the growth of wind power production in the U.S. in recent years and its projection into the future and discusses the challenges that this renewable energy source is bringing to power system operations. Strategies that have been proposed in the literature to manage high wind power penetration in day-ahead scheduling operations are also briefly discussed. In this chapter, a detailed unit

commitment (UC) problem formulation is developed to explore the benefits of leveraging flexible EV charging to increase wind power production. Simulation results are presented for a modified version of the IEEE-39 bus system, assuming the network has infinite transmission capacity.

Chapter 5 includes modeling of the transmission system in the developed UC framework. The impact of transmission congestion on achieving the full benefits of balancing wind power generation with flexible EV charging is determined for the 39-bus test system. In this chapter, PRs are suggested to improve the utilization of existing transmission assets, and hence to alleviate transmission congestion. Simulation results are provided that show that PRs can facilitate EV-wind balancing in congested power systems.

Chapter 6 presents conclusions, summarizes the contributions of this research, and gives suggestions for future work.

2 MANAGING INCREASED THIRD HARMONICS PRODUCED BY EVS

The introduction of electric vehicles (EVs) into residential/small commercial distribution systems is raising numerous concerns among utilities. A particular concern is the impact of these new load types on power system harmonics. This chapter begins with a background on the history and origin of power system harmonics. The increase of single-phase nonlinear residential loads during the last couple decades has changed the power system harmonic paradigm. Significant harmonic currents are no longer only generated at large industrial and commercial installations, but at numerous smaller residential and commercial establishments as well. The difficulty of enforcing harmonic standards on small customers and the reluctance of manufacturers of applying such standards to individual appliances have made utilities responsible for managing the level of harmonics in their distribution systems. Because of their unique characteristics, currents at the third harmonic frequency are the most cumbersome and represent a formidable challenge for utilities. Their effects on distribution systems are discussed in this chapter.

Work presented in the literature on the harmonic distortion of EV battery chargers and the potential impact of the harmonic currents generated by these devices on distribution systems are also reviewed. Substation harmonic field measurements obtained from utilities are presented to illustrate the level of power system harmonics that typical distribution systems are currently experiencing, even without EVs. In addition, conventional approaches discussed in the literature that utilities can employ to manage third harmonic currents in their distribution systems are reviewed.

To meet near-term utility harmonic filtering needs, a practical third harmonic hybrid active filter is proposed in this chapter. The topology, characteristics, and controller design of the proposed filter are described. Power system computer aided design (PSCAD®) simulations were performed to tune the parameters of the controller and demonstrate the correct and stable operation of the proposed hybrid active filtering system. Comparisons of the proposed filter with conventional pure third harmonic active and passive filters were made in terms of filtering performance, power requirements of their components, and total estimated cost. Cost versus performance curves of the proposed filter for the case in which a capacitor bank is retrofitted for this particular application are also presented.

2.1 BACKGROUND

2.1.1 History and Origin of Power System Harmonics

Power system harmonics are defined as sinusoidal voltage and current components at frequencies that are integer multiples of the fundamental frequency of the system [54]. Harmonic related issues in power systems have been heavily studied, probably more any other power quality problem [55], and is still regarded by some as the most significant one there is [56]. This does not come as a surprise as problems associated with harmonic voltages and currents have tormented power system engineers since the very beginning of the electric power industry. Throughout the history of AC power systems, issues caused by power system harmonics have constantly appeared in the literature, bringing with them new symptoms, new views on allowable limits, and new methods with which they were resolved. The earliest records in the literature of power system harmonic problems include the famous motor heating incident at Hartford, CT in 1893, which was traced

back to transmission line resonance [57]; excessive third harmonic neutral currents in solidly grounded wye-connected generators operating in parallel, caused by the improper selection of the armature winding pitch factor [58]; and, power system interference on telephone communication systems as a result of substation and distribution transformers operated in the saturation region [59].

During the decade of the 1920s, a new product came on the market with tremendous economic implications − the mercury arc rectifier [60]. This was the first inherent nonlinear load to experience widespread use and that suddenly made large industrial customers, and not utilities, the main culprits behind power system harmonic problems. There was much concern over these devices because of their harmonic content [61], but they were more efficient and required less maintenance than motor-generator sets. Through time a number of incidents built up from the operation of these devices at early electrochemical installations. The two most noticeable instances occurred at a copper refinery west of Salt Lake City, UT and at a mine site in eastern Canada, causing massive telephone conversation interruptions [62]. In the decades that followed manufacturers, electric utilities, and telephone companies worked together to study and provide solutions, such as multi-phasing the power converters [62], to mitigate the impact of large electrochemical plants on neighboring communication circuits.

Since the introduction of low-cost high-efficiency semiconductor power converters, in the decade of the 1970s, these devices have been adopted for general use in almost all corners of industry, especially in the form of adjustable speed drives (ASDs) for electrical machinery. The widespread use of power electronic converters in higher rating applications was fueled by the 1973 oil embargo and the consequent increase in energy

costs [63]. As a result of this widespread adoption, in 1980 power system harmonics was recognized as a major technical issue in the U.S. Recognizing the potential problems, the Static Power Converter Committee of the Industry Applications Society initiated work on the first IEEE standard dealing with power system harmonics, giving birth to the IEEE Std 519-1981 [64], with a subsequent revision introduced in 1992 [65].

Large industrial customers are characterized by employing a variety of nonlinear loads, such as medium to large ASDs and arcing devices like arc furnaces, arc welders, and discharge-type lighting with magnetic and/or electronic ballasts. Large commercial facilities are also dominated with ASDs in fans and heat pumps of air conditioning systems and elevator drives. In addition, a recent study indicates that fluorescent lighting was used on 77% of commercial floor spaces [56]. This is substantial considering that lighting typically accounts for 40 to 60% of a commercial building load. It was estimated that more than 70% of the loading of large industrial and commercial facilities would be nonlinear by 2010 [66]. However, still to this point harmonic current generation was limited to a relatively few large customers, greatly simplifying the process of locating and managing power system harmonic sources. Once offending harmonic current producers were identified, harmonic standards were enforced so that proper filtering actions would be taken by the customer to prevent troublesome harmonic currents from flowing back into the distribution system [55].

The use of power electronic devices has become commonplace not only in the industrial and commercial sectors. By 2000, it was estimated that nonlinear electronic loads accounted for around half of the U.S. electrical demand, with much of the growth in the previous decade occurring in the residential sector [67]. It is common nowadays to

observe residential and small commercial installations with uninterruptible power supplies (UPS), personal computers (PC), compact fluorescent lighting (CFL), and electronic entertainment devices. A recent U.S. study revealed that energy consumed by appliances, electronics, and lighting increased from 16.7% in 1978 of the total energy consumption in homes to 24.0% and 34.6% in 1993 and 2009, respectively [68].

Power for modern office and residential electronic devices is sourced from the most common producer of harmonics − single-phase power supplies. There exist two types of single-phase power supplies. Order technologies relied on step down transformers to reduce voltages to the level required for the DC bus. Newer technologies are based on switch-mode power supplies, which eliminates the transformer and the input diode bridge is directly connected to the ac line [56]. Among the key advantages of switch-mode power supplies are a lighter weight, more compact size, efficient operation, and immunity to larger input voltage variations. However, removal of the transformer causes increase harmonic current generation. Switch-mode power supplies are known for drawing currents with total harmonic distortion (THD_i) sometimes in excess of 100% [69] and a very high third harmonic content [55, 56, 70]. Even though the rating of these devices are usually small, with typical medium voltage (MV) feeders serving around 2500 low voltage (LV) customers [67], their cumulative effect can have a significant impact on power system operation.

So as observed, once again the paradigm surrounding power system harmonics has changed. Significant harmonic current distortion is not only being generated "centrally" at large industrial and commercial installations, but also in a "distributed" manner by smaller residential and commercial customers. Unfortunately, limits set forth in standards

such as [65] were never intended to cover small single-phase services like residential and small commercial users. The logistics of verifying harmonic performance of each residence makes applying specific limits for residences almost impossible [71]. This difficulty is resolved in some countries by enforcing harmonic standards, such as [72, 73], to individual appliances rather to the residence itself. In the U.S., such proposals have received opposition from manufacturers because of the low return on the investment to have their products comply with such standards [74]. Thus, for the time being the onus is on utilities to manage power system harmonics to allowable limits.

2.1.2 Effects of Third Harmonic Currents

Although harmonic problems receive a great deal of attention, mainly because of their complexity, they are not very numerous with only a few percent of utility distribution feeders in the US having sufficiently severe harmonic problems to require notice [55, 56]. However, third harmonic currents do demand special consideration because their system response is considerably different than for other harmonics. In the US four-wire, multigrounded neutral distribution systems predominate [75, 76]. Assuming balanced conditions, the fundamental current component in the neutral is zero, but the third harmonic component and its odd multiples (also known as the triplen harmonics) are three times that of the phase current since they naturally coincide in phase and time [55, 56]. For this reason triplen harmonics are also referred to as zero-sequence harmonics. In addition, negligible phase diversity and attenuation caused by large number of distributed single-phase nonlinear loads occurs at the third harmonic compared to other harmonic components [70]. Furthermore, the third harmonic component generated by front-end rectifier loads, such as switched-mode power supplies, may be over 80% of the

fundamental [55, 70]. Under balanced conditions, such levels of third harmonic distortion could theoretically lead to neutral currents as high as 173% of the phase currents due to the additive nature of the third harmonic component [77]. Elevated levels of neutral current as a result of increased third harmonic currents poses serious adverse effects to the distribution system.

Third harmonic currents can have negative impacts on a variety of power system equipment, causing additional losses and overloading. Since third harmonic currents are additive in the neutral circuit of a three-phase four-wire distribution system, there are generally concerns for overloading the neutral conductor, especially in older distribution feeders where an undersized neutral may have been installed. These harmonic currents can appreciably increase cable temperatures [55], sometimes even leading to burned neutral conductors [78]. Harmonic problems typically appear first at capacitor banks though, as either blown fuses or capacitor unit failures [79]. The main reason for this is that capacitor banks form part of resonant loops, where the highest current and/or voltage magnification occurs at the bank location. The effects of third harmonic currents are to cause additional heating and higher dielectric stress on capacitors [79]. There is also concern for transformer overheating in the presence of elevated third harmonic currents, particularly of its neutral connection [56, 67]. In addition, in three-legged core designs third harmonic currents generate zero-sequence fluxes that flow and escape the core, causing additional heating in the tanks, core clamps, etc. [54, 56]

Electromechanical, solid state, and even early microprocessor based ground overcurrent relays are prune to nuisance tripping in the presence of third harmonic currents [67, 80]. These devices are employed to protect circuit equipment against ground

faults by sensing the residual current of the phase conductors. In three-phase four-wire distribution systems, an allowance for unbalance must be provided when adjusting the settings of the relay. Third harmonic currents must also be taken into account, further complicating the processes of fine tuning the settings and affecting the coordination with other protection devices [80]. However, it is important to note that modern digital relays are immune to third harmonic currents by implementing a digital filter that extracts solely the fundamental component, allowing for a more sensitive relay setting [80-82].

Apart from adversely impacting power system equipment, third harmonic currents have also other negative side effects, such as increasing neutral-to-earth voltages (NEV) in distribution systems. In four-wire, multigrounded distribution systems, a portion of the neutral current returns to the source via the neutral conductor; while the remaining neutral current flows back through the earth. The resulting voltage potential between a neutral-to-ground bonding point and remote earth is known as NEV [83, 84]. This voltage potential is one of the components that contribute to stray voltage related electrical shock complaints, which are taken quite seriously by utilities. Consequently, NEV should be kept low − typically less than 4 V rms as recommended in [85]. In certain circumstances, even stricter NEV requirements may be warranted as testing has shown that humans react to voltages as low as 2 or 3 V under wet conditions [86]. In Midwestern states, such as Wisconsin, limits are imposed where stray voltage levels may not exceed 1 V to not affect production of dairy farms [86]. Although in the past elevated NEV problems were mainly caused by unbalance and improper grounding, recent studies are indicating strong correlation between increasing levels of NEV and higher third harmonic distortion [83, 84, 87, 88].

Third harmonic currents can also aggravate power system interference with communication circuits sharing a common path, most noticeably with telephone circuits. Harmonics in the neutral return path have the greatest exposure with communication circuits and hence are much more likely to create interference [55, 56]. The additional neutral current caused by third harmonic current also increases magnetic field levels near the distribution feeder [83]. Harmonic currents are coupled into communication circuits by two main mechanisms, induction or direct conduction. Inductive coupling was a more severe problem in the past when use of open-wire telephone circuits was prevalent. Telephone interference is less common nowadays because more immune circuits with shielded cables or fiber optics are employed. However, inductive coupling can still be a problem if high currents are induced in the shield surrounding the telephone conductors. Shield currents can also be generated by direct conduction, since the shield is in parallel with the power system neutral circuit. Currents flowing in the shield, either by induction or direct conduction, create a potential between the ground references at either side of the telephone circuit that could negatively impact conversations [56, 79].

2.1.3 Impact of EV Battery Chargers on Power System Harmonics

In addition to the proliferation of smaller typical nonlinear residential loads, the introduction of new higher rating nonlinear loads for residential use, such as inverter based appliances and EVs, are also becoming an important power quality concern for electric utilities. In particular, chargers for EV batteries form a significant class of harmonic-producing loads, and, as EVs attain technical and commercial success, these chargers will become widespread in residential distribution systems. EV battery charging systems normally rely on a rectifier followed by a DC/DC converter to obtain the

required DC power from the utility grid [89, 90], as depicted in Figure 4. Both power electronics converters can have different topologies and can be arranged together in different ways, the most common of which are discussed in [91]. Because of the nonlinearity of these devices, this electrical energy conversion process produces harmonic currents that flow back into the distribution system [89, 90, 92, 93]. The battery management system monitors key battery parameters, triggers the protection circuits in case of faults, and controls the charging rate to provide the required constant current/constant voltage (CC/CV) charging profile. Typically, the battery charging process is controlled to provide a constant charge current until the battery voltage nears its gassing limit and battery receptivity drops, then maintaining a constant voltage until the full charge level is reached. The THD_i of EV battery chargers varies throughout this charging process, increasing as the battery state of charge (SOC) increases [94].

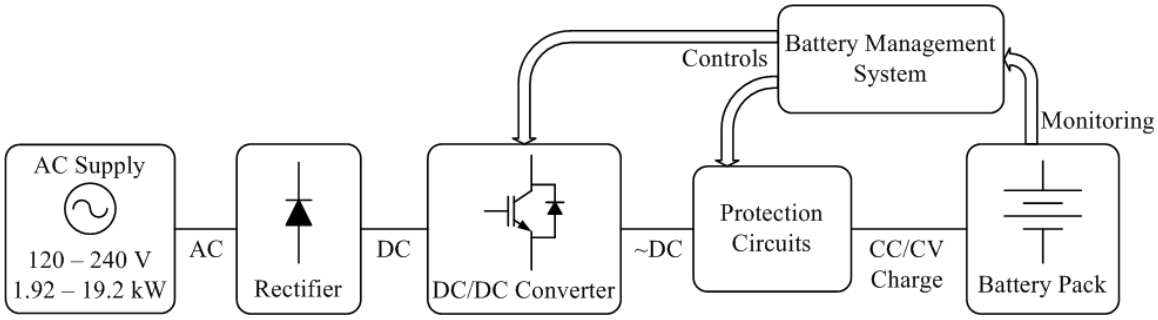

Figure 4. Generic diagram of a Level 1-2 EV battery charging system.

Data on the harmonic performance of commercially available EV chargers directly from manufacturers are difficult to come by. However, there are many reports in the literature indicating varying levels of harmonic distortion of EV chargers. Measurements carried out on commercial chargers have shown THD_i values as high as 60% to 70% [93, 95]. A survey of battery chargers manufactured from 1993 to 1995 presented in [96]

showed that the average total current harmonic distortion decreased from 50.1% to 6.12%. Also important was that third harmonic component values of up to 75% of the fundament component were observed in some EV chargers. In this study, EVs manufactured in 1995, which generated less harmonic currents, implemented more sophisticated chargers. However, no information on the SOC at which measurements were taken was provided. According to [97], THD_i values for actual EV chargers that were analyzed varied from 2.36% and 5.26% at the beginning of charging up to 28% at the end of charging. Similarly, the EV charger analyzed in [98] had a THD_i that varied from 15% to 35% when charging current reduced from 22.5A to 5 A. Coefficients of polynomial functions representing the real and imaginary components of harmonic currents generated by a commercial EV charger versus charging rate, obtained experimentally, are given in [94]. As an example, these polynomial curves were reconstructed in Figure 5a, showing the harmonic characteristics of the charger, which are dominated by the third harmonic component, especially above 35% of the maximum charging rate. Figure 5b displays charging current waveforms for the same charger at different charging rates, demonstrating EV chargers as potential devices for drawing substantially distorted current waveforms from the grid.

Over the years there have been a number of studies that have attempted to predict the impact of harmonic currents produced by EV chargers on the distribution system. One of the first ones was realized in the early 1980s at the same time power system harmonics were recognized as a major technical issue for utilities. This study [99] developed a Monte Carlo simulation procedure to determine the harmonic currents injected into the distribution system by a cluster of EVs, equipped with the "taper current" charger,

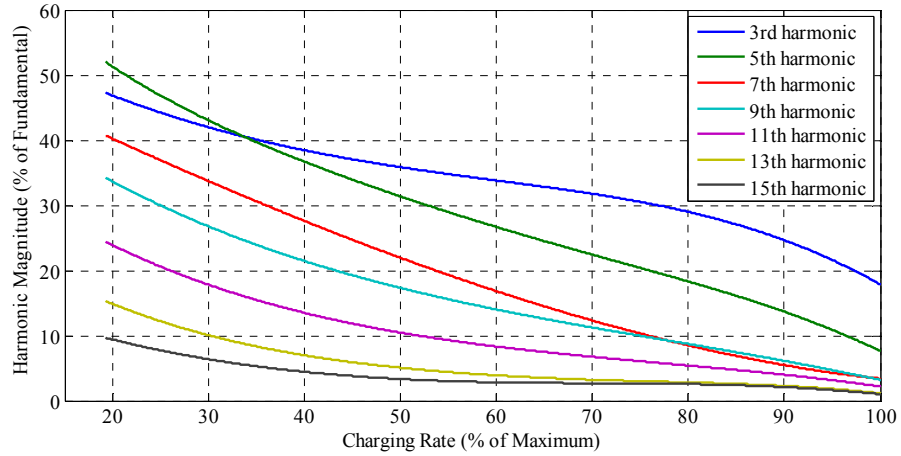

a)

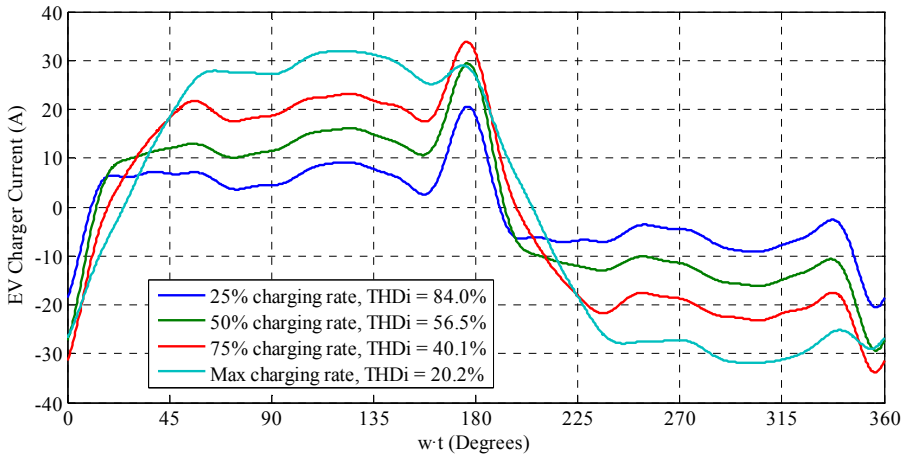

b)

Figure 5. Harmonic characteristics of the commercial EV charger analyzed in [94]: a) Harmonic magnitudes vs. charging rate and b) Charger current waveforms at different charging rates.

charging on a single bus. From the simulation results, it was found that the third harmonic dominated the spectrum, reaching 50% of the fundamental, and third harmonic currents added nearly in phase, indicating negligible phase diversity. The developed framework was extended in [100] to include additional types of EV chargers, randomly distributed on a distribution system, to determine their cumulative effects at the substation level. All of the cases presented produced significant amounts of harmonic current for several hours of the day, with typical third harmonic current values of 20 A

per phase on the MV side generated solely by a 10% penetration of EVs in the distribution system.

A later study [94] presented a statistical method for predicting the net harmonic currents produced by a large number of EVs, utilizing data from a commercially available EV charger. Results from this method indicate that the expected current from a group of these EV chargers would have a THD_i of 49% and be dominated by the third harmonic component with a level of 31.1% of the fundamental. This work was extended in [101] to predict the effect that widespread EV charging will have on distribution system harmonic voltage levels. For the distribution system under analysis, it was determined that during the late evening of a summer day it could accommodate an EV penetration level of 20% before IEEE recommended total voltage harmonic distortion (THD_v) limits were unacceptably exceeded. This penetration level decreased to 15% for spring and fall, largely because there was less linear load to provide harmonic damping. It is important to mention that much of the voltage distortion was due to the third harmonic component and that no other nonlinear load apart from EV chargers were considered in this work.

Other studies have focused on the impact of harmonics generated by EV chargers on the LV secondary distribution system. For example, the effect of EV charger harmonics on distribution transformers was investigated in [93]. In this study it was determined that THD_i of these devices should be limited to 25-30% to have a reasonable transformer life expectancy. However, results presented in [102] showed the possibility of harmonic problems arising only with small transformers and EV chargers engineered to minimum recommendations. For typical test cases, it determined that the introduction of EV

chargers would not result in a significant increase in THD_v in the LV secondary distribution system.

Today every type of EV charger implemented in practice takes a heavily distorted current from the utility grid [93]. However, there is no general agreement among the THD_i values generated by these chargers. Some consider EV chargers as a highly contaminating load, while some manufacturers and researchers claim of having designs with very low THD_i. In the literature, EV charger topologies with THD_i values ranging between 1 and 2%, with a power factor close to unity, can be found [91, 103]. Although achieving such performance metrics is technically possible, there is a tradeoff between harmonic generation and system cost, complexity, and efficiency [96, 100]. Therefore, the implementation of such designs in commercial products is normally not economically justified. To provide some sort of guideline, the National Electric Vehicle Infrastructure Working Council (IWC), based on limits established in [73], have suggested EV chargers be designed to have a minimum power factor of 95% and a maximum THD_i of 20% [97, 102]. Although these IWC guidelines are voluntary, for the most part EV charger vendors have met these requirements [74]. Still, with this THD_i limit, EV chargers are expected to worsen the already growing trend of harmonic distortion in distribution systems, which as discussed in the following section are already experiencing elevated levels of third harmonic currents even without any EV load.

2.1.4 Utility Harmonic Field Data

Experiments were performed to determine the harmonic current signature of various typical single-phase nonlinear loads to study their impact on residential distribution systems [104]. Table 1 and Figure 6 summarize the results of this effort. Table 1 indicates

that in almost all cases the generated harmonics were dominated by the third harmonic component, in some cases exceeding 75% of the fundamental component. Also, as observed in Figure 6, contrary to other harmonics, little phase diversity occurs at the third harmonic frequency, indicating negligible phase cancellation at this frequency component. From these observations, and the zero-sequence characteristics of third harmonic currents, it was concluded that this harmonic component is the most cumbersome one and would represent a formidable task for utilities to manage, as feeders serving an important amount of single-phase nonlinear loads would have significant levels of third harmonic currents in their neutral circuits.

Table 1. Magnitude of Harmonic Currents of Typical Single-phase Nonlinear Loads

Load	THD_i (%)	I_1 (A)	I_3 (%)	I_5 (%)	I_7 (%)	I_9 (%)
CPU (Dell, 1999)	138	0.91	90	75	56	37
CPU (Dell, 2005)	81	1.05	71	34	14	9
CRT Monitor (HP, 1999)	19.7	0.87	176	3.9	4.1	4.96
LCD monitor (Dell, 2005)	147	0.39	89	77	61	46
LCD TV (42", Samsung)	13.5	3.03	7.7	8.5	5.1	3.4
CFL (26 watt, GE)	108	0.23	76	50	34	30
LED (3 watt, ATC)	26	0.2	10	11.6	10	2.2
LED (40 watt, Asian)	4.6	1.97	2.11	< 0.5	< 0.5	< 0.5
Microwave (Emerson)	31	6.84	27	12	5	2.5
Microwave (Sharp)	13.8	13.9	10	7.8	3.5	1.3
Room A/C (Frigidaire)	8.3	8.7	7	2.2	< 0.5	< 0.5
Room A/C (Kenmore)	11.4	6.3	8.7	2.5	1.1	< 0.5
Central A/C (3.5 ton Goodman)	7.5	13.3	7.2	1	< 0.5	< 0.5
Water heater (Airtap)	9.8	5.3	6.1	1.7	< 0.5	< 0.5

To support this conclusion and to align any potential solution with current utility needs, actual harmonic field measurements were obtain directly from utilities. Harmonic measurements taken at the substation of two representative feeders are summarized in Table 2. One serves primarily residential/small commercial customers, while the other serves mainly gas wells with a high number of single-phase adjustable-speed-drive loads.

In both feeders it is observed that the phase current harmonics are dominated by the third harmonic component, more than doubling the fifth component. Third harmonic currents in the range of 11-12% and 20-27% of the fundamental are observed in the feeders serving residential/small commercial loads and gas wells, respectively. In addition, almost all of the third harmonic phase currents flow in the neutral, causing elevated levels of neutral current to circulate in the system with potential adverse effects to the distribution system.

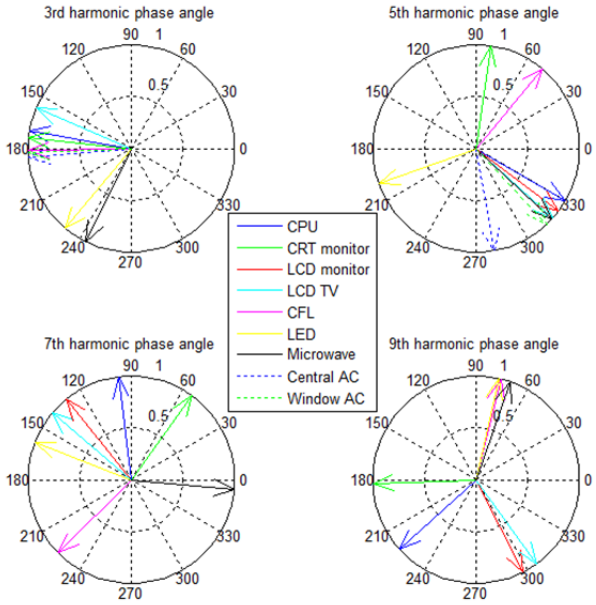

Figure 6. Phase of harmonic currents of typical single-phase nonlinear loads.

2.1.5 Conventional Approaches for Managing Third Harmonic Currents

This work focuses on strategies utilities can adopt to manage third harmonic currents in their residential/small commercial distribution feeders caused by the proliferation of single-phase nonlinear loads and the future penetration of EVs in their systems. Thus, common approaches taken to resolve third harmonic issues at large industrial and

Table 2. Substation Harmonic Field Measurements Provided by Utilities

Feeder serving mainly residential/small commercial loads										
Feeder Voltage	**Conductor**	**Current Harmonic Components (A rms)**								**THD_i (%)**
		h = 1	***h = 3***	***h = 5***	***h = 7***	***h = 9***	***h = 11***	***h = 13***	***h = 15***	
24.9 kV	A	126	15.4	7.7	5.9	1.9	0.4	1	0.9	14.6
	B	132	14.5	6.6	5.3	2.1	0.2	1	0.5	12.9
	C	127	14.9	7.6	5.7	1.3	0.4	1.1	0.8	14.0
	N	2.3	44.5	1.6	1.6	5.3	0.3	0.3	2.1	--
Feeder serving mainly single-phase adjustable-speed-drive loads (gas wells)										
Feeder Voltage	**Conductor**	**Current Harmonic Components (A rms)**								**THD_i (%)**
		h = 1	***h = 3***	***h = 5***	***h = 7***	***h = 9***	***h = 11***	***h = 13***	***h = 15***	
12.47 kV	A	90	18	5	4	0	0	--	--	21.2
	B	100	27	6	5	1	0	--	--	28.1
	C	95	24	5	4	0	0	--	---	26.1
	N	9	68	3	2	1	0	--	--	--

commercial sites are not discussed. Example of such approaches include the use of zig-zag transformers to prevent third harmonic currents from flowing back into the distribution system; series passive and active filtering solutions that would require utilities to open their circuits for installation; and, strategies that would otherwise result prohibitively expensive if realized on a distribution-system scale, such as re-conductoring the neutral or improving the grounding system to reduce NEV. Steps discussed in the literature that utilities can follow to address third harmonic problems in their distribution systems are summarized below.

2.1.5.1 Ground Connection Removal of Grounded Wye-connected Capacitors

The use of power factor correction capacitors to provide voltage regulation could have serious implications on the level of harmonics in a distribution system. Shunt power capacitors, which are generally connected in a grounded-wye configuration, create zero-sequence network loops that could give rise to local or general resonant conditions. Therefore, even though capacitor banks do not generate harmonic currents, they can highly influence the level of harmonic voltages and currents along a distribution feeder.

If third harmonic currents become greater than the allowable limits, one remedy suggested in [105] is to remove the capacitor bank ground connection. This effectively removes the capacitor bank from the zero-sequence network, avoiding possible resonant conditions from occurring at the third harmonic frequency. Recently, a utility implemented such an approach on one of its feeders presenting NEV issues caused by elevated third harmonic currents flowing in the neutral conductor [106]. A reduction in third harmonic neutral current of 40 to 50% was observed. Nonetheless, the neutral current remained at about 55 A, which is still considered to be on the higher side and appeared to be almost entirely dominated by the third harmonic component.

The advantages of this approach is that with minimal system changes considerable third harmonic and NEV reductions can be achieved, provided these issues are caused by resonance. The disadvantages of this approach, though, are that the capacitor switchgear must be upgraded for higher switch recovery voltages and that the capacitor bank must be isolated from ground at full system basic insulation level [105]. But, most importantly, removing the ground connection of grounded wye-connected capacitor banks, instead of providing third harmonic compensation for single-phase nonlinear loads, merely avoids third harmonic current problems from worsening because of resonant conditions. Hence, even when adopting this strategy, with continued increase of these load types on distribution systems, utilities will need to take additional remedial actions to manage third harmonic currents in their systems.

2.1.5.2 Passive Filters

Passive filters, as their name implies, consist of only passive components, typically of an inductance-capacitance (LC) series combination. The values of the inductor and

capacitor are tuned at a particular harmonic frequency to provide a low impedance path for currents at this frequency component [66]. The objective is to shunt a portion of downstream harmonic currents, thereby reducing the amount of harmonic current that flows upstream of the filter. Historically, passive filters have been the solution of choice for diverting harmonic currents generated by large industrial customers because of their low cost and high efficiency. However, passive filters possess serious limitations that make them impractical for MV utility harmonic filtering applications.

First, passive filters are highly susceptible to undesirable resonant conditions and switching transients. Therefore, utmost care must be exercised when implementing these filters to avoid any possible resonant condition [55, 66]. This requires extensive system studies and engineering effort, which may not be justified in MV distribution systems since detailed system models are often not readily available. This could also be extremely difficult to guarantee considering that utilities tend to frequently modify the configuration of their distribution feeders. Even if detailed studies are performed, the expected results of a distributed passive filtering scheme may not be realized [107].

Second, the filtering performance of passive filters is very sensitive to the supply impedance and tuning of its LC components. When connected to a stiff system (i.e., systems with a low supply impedance), it is very challenging for passive filters to divert a significant portion of downstream harmonic currents. Under this conditions it is difficult to design passive filters with sharp tuning and high quality factor (Q) [108]. Tolerance of their LC components and variation of their values with time and temperature may also deteriorate their filtering performance.

Finally, passive filters may become overloaded in the presence of background voltage distortion and/or with the increase of downstream loads, especially when it is finely tuned to a dominant harmonic frequency. To prevent this situation from happening, it is a common practice to mistune the filter, which in turn defeats the purpose of the original filtering action. Because of all these disadvantages of passive filters, there is a worldwide tendency in considering active harmonic filtering solutions for utility distribution systems [109].

2.1.5.3 Active Filters

The active filter is a mature technology, with first conceptual designs introduced back in 1976 [110]. Since then, a number of conventional three-phase four-wire active filter topologies and sophisticated controllers have been proposed that not only provide harmonic compensation, but VAR compensation and phase balancing as well [111]. In theory, virtually any power quality problem utilities face could be solved by employing an active filtering scheme. Among the most popular filter topologies that have been developed over the years for three-phase four-wire systems are the voltage source inverter (VSI) based split capacitor, four-leg, and three H-bridge active filters. A thorough comparison of the advantages and disadvantages of each of these active filter designs is presented in [112].

Active filters outperform passive filters by relying on power-electronics switching techniques to draw currents that cancel out the harmonic distortion in the load current. Another advantage of active filter over passive filters is that they are able to respond to changing load conditions with no serious ill effect to the distribution system [66]. However, despite their technical maturity, commercially available active filters are only

offered for LV customer applications and are prohibitively expensive [66, 67]. The main reason for the latter is that high active power ratings are required to provide useful levels of harmonic compensation. Since cost is one of the major drivers for a technology to be adopted by utilities, active filters are considered unlikely to become a realistic filtering solution for MV utility applications in the foreseeable future.

To overcome the inherent disadvantages of pure passive and active filters, hybrid active filter counterparts have also been proposed throughout the years. A comprehensive review of common hybrid active filter topologies is provided in [113]. Hybrid active filters normally consist of an LC passive filtering component connected in series with an active filtering component. The LC branch is tuned to provide a low-impedance path for the active filter, greatly reducing the rating of its power converter and hence reducing overall cost. There also exists more complex topologies that take advantage of special star/delta or zig-zag transformers to reroute zero-sequence harmonic currents to reduce the rating of their active filtering components [114-116].

As with pure active filters, hybrid active filters are able to adapt to changing load conditions and are not prone to resonance. However, since an LC branch can only be tuned at a single harmonic frequency, hybrid active filters can solely be used to target a single harmonic current component. In addition, the grand majority of hybrid active filters that have been proposed in the literature are mainly targeted for installation at industrial and commercial sites, as opposed to along primary distribution feeders, with hardware implementations limited to conceptual demonstrations at low-voltage levels. Also, much of the research on (hybrid) active filters has been focused almost entirely from an academic standpoint, often neglecting factors important to utilities, such as cost,

reliability, ease of implementation, and system impact. These are some of the reasons that could explain why hybrid active filters have not been extensively deployed in the field.

2.2 PROPOSED THIRD HARMONIC HYBRID ACTIVE FILTER

In this research, an attempt was made to develop a practical solution for near-term utility harmonic filtering needs [117, 118]. To achieve such an objective, work for this project was realized in close interaction with National Electric Energy Testing, Research and Applications Center (NEETRAC) utility and industry members. From early discussions, it was quickly determined that the major drivers for a technology to be adopted in a utility application are cost, reliability, and ease of implementation. Therefore, these factors were heavily weighted in the design of the proposed filter and its controller. This process, together with simulation results, is discussed in the remainder of this chapter.

2.2.1 Topology and Description

A schematic diagram of the proposed third harmonic hybrid active filter is presented in Figure 7. Significant cost reduction is achieved by designing a harmonic filtering solution that provides compensation only for third harmonic currents, which are the harmonic currents utilities are currently having issues with. This considerably reduces the rating of the power converter. Also, the active component of the proposed filter was located in the neutral path, which implies using one single-phase power converter for a three-phase four-wire system as opposed to three single-phase power converters or a three-phase one as for the conventional filters discussed in [112]. So, as observed, this filtering strategy takes advantage of the zero-sequence nature of third harmonic currents and the fact that almost all of it flows in the neutral circuit as indicated by previous work

and field data. Because of this design choice, the application of the proposed filter can readily be extended to any distribution voltage level and to provide compensation at a different zero-sequence harmonic frequency, i.e., triplen harmonic frequency. Additional cost reduction was accomplished by opting for a hybrid filter configuration; where possible, retrofitting existing power factor correction capacitors; and, employing the proposed filter as part of a distributed harmonic filtering solution.

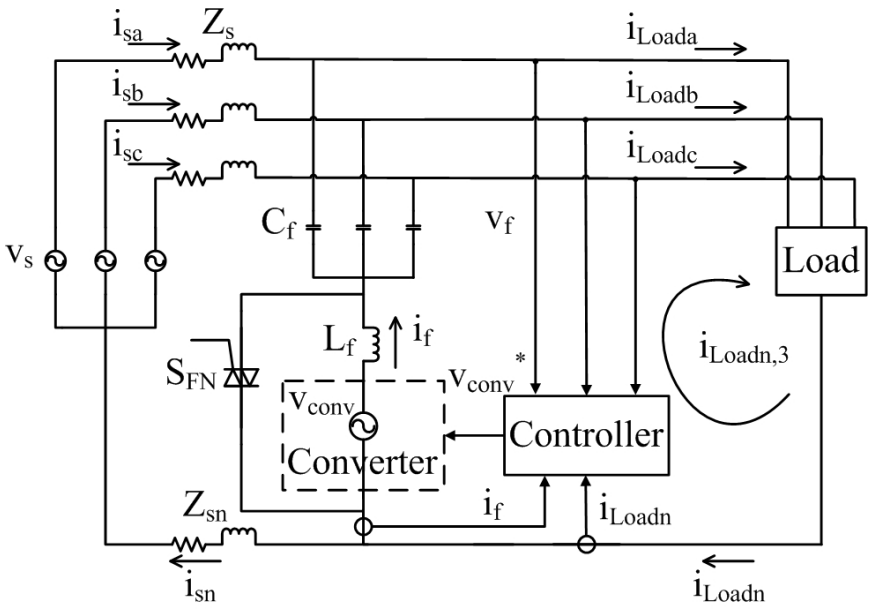

Figure 7. Schematic diagram of the proposed third harmonic hybrid active filter.

The active component of the proposed filter compensates for LC mistuning, yielding ideal notch-filter characteristics at the third harmonic frequency, while providing third harmonic isolation, blocking incoming upstream third harmonic current caused by background voltage distortion. The power converter represents the active component of the proposed filter and is implemented in this work with an H-bridge VSI as discussed in the next chapter. The passive component provides a low-impedance path for the third harmonic current generated by the power converter. This is accomplished by selecting an

inductor value that tunes the LC branch closely to the third harmonic frequency. Note that by placing the inductor in the neutral circuit, instead of in series with each single-phase capacitor unit, the need for three inductors is avoided, plus its value is only one-third of the inductance that would otherwise be required. It also eliminates additional positive sequence voltage stress across the capacitor units and facilitates the design of the filter protection scheme. The inductance value required for the proposed filter can be computed using:

$$L_f = \frac{V_{C_f,3\phi}^2}{27\omega_1 Q_{C_f,3\phi}\left(1-k_{mistune}\right)^2}, \tag{1}$$

where ω_1 is the fundamental angular frequency of the system, $V_{C_f,3\phi}$ and $Q_{C_f,3\phi}$ are respectively the three-phase voltage and power ratings of the capacitor bank, and $k_{mistune}$ is the factor by which the LC branch is intentionally mistuned. To give a sense of the inductance required for the proposed filter, Table 3 presents inductor values for capacitor banks rated at different kVAR and voltage levels typically used in distribution systems, assuming a 5% filter mistune. The power rating of the inductor is dependent on the amount of third harmonic neutral current the filter is designed to compensate, $I_{n,3}$, and can be estimated using the following:

$$Q_{L_f} = 3\omega_1 I_{n,3}^2 L_{f.} \tag{2}$$

Existing power factor correction capacitors on distribution feeders could be retrofitted into the proposed third harmonic hybrid active filter. In [119], IEEE establishes that power capacitor units should be capable of operating continuously without damage provided none of the following limits are exceeded:

- 110% of rated RMS voltage,
- 120% of rated peak voltage, including harmonics, but excluding transients,
- 135% of nominal RMS current, based on rated kVAR and voltage, and
- 135% of rated kVAR.

A capacitor manufacturing company was consulted on the possibility of utilizing this additional margin of power capacitor units to provide third harmonic compensation. It was confirmed that, although these limits are provided for rare emergency situations, the extra margin is available and useable under normal conditions as well, and that normally capacitor banks are oversized in practice. To take advantage of this opportunity, a mechanism was included in the controller of the proposed filter to provide partial third harmonic compensation based on the loading conditions of the capacitor bank, thus augmenting its functionality to the distributions system. This avoids exceeding the maximum operating limits of existing capacitor banks, allowing them to be retrofitted for this particular application to achieve greater cost savings as discussed below.

Table 3. Inductance Required for the Proposed Filter as a Function of Capacitor Bank Ratings

kVAR Rating	**Inductance (mH)**	
	Terminal-to-Terminal Cap Bank Voltage Rating (3ϕ Dist. Syst. Voltage)	
	7.2 kV (12.47 kV)	14.4 kV (24.94 kV)
300	56.43	225.73
600	28.22	112.86
900	18.81	75.24
1200	14.11	56.43
1500	11.29	45.15

Power systems are required to have extremely high levels of reliability. In the US, power system reliability figures in excess of 99% are observed. Meanwhile, commercially available power electronics systems for solving power quality issues have

reliability numbers in the range of 96-97%. To meet utility reliability requirements, a fail-normal switch (S_{FN}) was included in the design of the proposed filter, as observed in Figure 7. In practice, this switch can be implemented with a thyristor pair. These devices have very short operating times and are capable of handling high levels of fault current. The fail-normal switch is activated during faults and filter shutdown, bypassing the inductor and power converter of the filter. This returns the system back to its original state, i.e., a simple capacitor bank, hence maintaining the original level of reliability of the system.

2.2.2 Principle of Operation and Controller Design

The controller of the proposed third harmonic hybrid active filter was designed to minimize the power requirements of the power converter when the filter is controlled to provide partial third harmonic compensation. The condition to achieve this can be explained with the phasor diagram of Figure 8, which shows filter voltage and current variables of the zero-sequence equivalent circuit of the system in Figure 7. In practice, LC passive filter components are slightly mistuned such that the resulting filter impedance is inductive at its dominant harmonic frequency. If the impedance were capacitive, it would have the potential of series resonance with the supply inductance in the presence of background voltage distortion [120]. Therefore, in the diagram of Figure 8, it is assumed that the LC filter is slightly inductive, i.e., slightly mistuned under the third harmonic frequency.

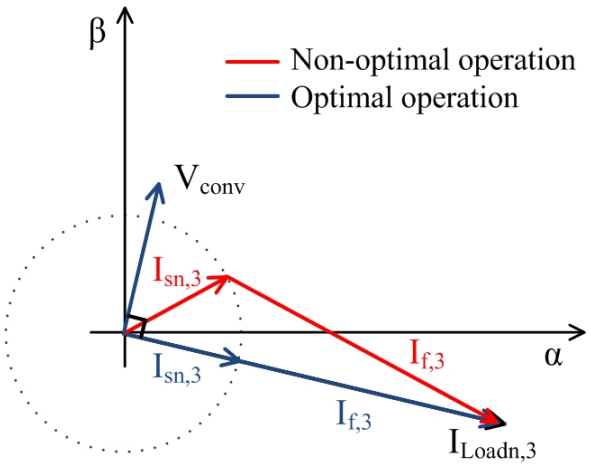

Figure 8. Phasor diagram of filter voltages and currents of Figure 7.

As observed, when the hybrid active filter provides full third harmonic compensation only one possibility exists, the filter current must equal the third harmonic neutral load current. On the other hand, when it provides partial harmonic compensation, the filter current can assume different values to achieve the same level of source-side third harmonic neutral current. However, as shown in Figure 8, minimum control effort, i.e., minimum filter current, is only guaranteed when the filter current is in phase with the third harmonic neutral load current. Furthermore, this figure also shows that the converter voltage, V_{conv}, must lead the third harmonic component of the filter current, $I_{f,3}$, by 90º. This can be derived by noticing that V_{conv} must counteract the voltage drop across the LC branch impedance, Z_f, to provide a zero-impedance path for the third harmonic neutral load current. That is,

$$V_{conv} = Z_f \cdot I_{f,3} = jX_f \cdot I_{f,3}, \tag{3}$$

where again the filter reactance, X_f, is assumed to be inductive.

The structure of the controller is defined by the operating principles described above. Figure 9 shows a block diagram of the controller of the proposed third harmonic hybrid

active filter. It is based on synchronous reference frame theory and direct generation of power converter reference voltage. The direct generation of power converter reference voltage allows the use of voltage based pulse-width modulation (PWM) schemes, which can be implemented by simple and constant switching frequency sine-triangle or space vector PWM schemes. Hysteresis based current regulators have several undesirable characteristics, such as low-frequency current errors, limit cycles in current, and variable switching frequency. In general, voltage based PWM schemes have lower bandwidth requirements than conventional current regulated PWM schemes and hence are preferred in high power applications [120]. This is an important distinction between the filter proposed in this work and shunt third harmonic hybrid active filters presented in the literature that follow conventional controller designs that generate current references for the power converter, such as the one proposed in [121].

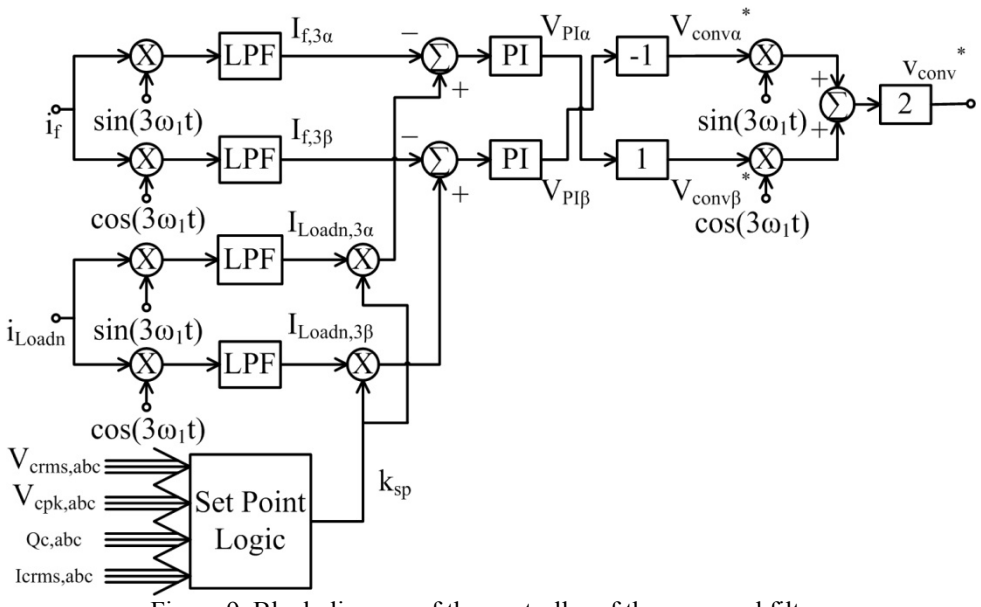

Figure 9. Block diagram of the controller of the proposed filter.

The controller senses the filter current, i_f, and the load neutral current, i_{Loadn}. Their respective DC components on an orthogonal reference frame rotating at the third harmonic frequency, with axes labeled here as α and β, are extracted so that PI controllers could be employed. This is done for the filter current through the following computation:

$$\begin{aligned} i_f \cdot \sin(3\omega_1 t) &= \left[I_{f,1} \sin(\omega_1 t - \phi_1) + I_{f,3} \sin(3\omega_1 t - \phi_3) + I_{f,5} \sin(5\omega_1 t - \phi_5) + \ldots \right] \sin(3\omega_1 t) \\ &= 1/2\, I_{f,3} \cos\phi_3 + \sum_n 1/2 \Big[-\text{sign}(n-3)\, I_{f,|n-3|} \cos\left(n\omega_1 t - \text{sign}(n-3)\, \phi_{|n-3|} \right) \\ &\qquad + I_{f,(n+3)} \cos\left(n\omega_1 t - \phi_{(n+3)} \right) \Big] \quad \text{for } n = 2,4,6,8,\ldots \\ &= I_{f,3\alpha} + \tilde{i}_{f,3\alpha} \end{aligned} \tag{4}$$

$$\begin{aligned} i_f \cdot \cos(3\omega_1 t) &= \left[I_{f,1} \sin(\omega_1 t - \phi_1) + I_{f,3} \sin(3\omega_1 t - \phi_3) + I_{f,5} \sin(5\omega_1 t - \phi_5) + \ldots \right] \cos(3\omega_1 t) \\ &= -1/2\, I_{f,3} \sin\phi_3 + \sum_n 1/2 \Big[\text{sign}(n-3)\, I_{f,|n-3|} \sin\left(n\omega_1 t - \text{sign}(n-3)\, \phi_{|n-3|} \right) \\ &\qquad + I_{f,(n+3)} \sin\left(n\omega_1 t - \phi_{(n+3)} \right) \Big] \quad \text{for } n = 2,4,6,8,\ldots \\ &= I_{f,3\beta} + \tilde{i}_{f,3\beta}, \end{aligned} \tag{5}$$

where $\omega_1 t$ is the electrical angle of the phase A filter voltage, v_{fa}, obtained using either a single-phase or three-phase phase-locked loop (PLL); $I_{f,3\alpha}$ and $I_{f,3\beta}$ are the DC α and β third harmonic components of the filter current, respectively; and, $\tilde{i}_{f,3\alpha}$ and $\tilde{i}_{f,3\beta}$ are the AC components of the filter current on the α-β orthogonal third harmonic rotating reference frame. Similar expressions can be formulated for the load neutral current. From (4) and (5) it is observed that only the third harmonic components of the filter and load neutral currents contribute to their respective DC third harmonic orthogonal components. Current components at all other frequencies are mapped into AC components in the third harmonic rotating reference frame. The DC third harmonic orthogonal components of the filter and load neutral currents can therefore be extracted by means of low-pass filtering.

In this work, fourth-order low-pass filters with a cutoff frequency of 5 Hz were employed.

The DC third harmonic orthogonal components of the filter current are then compared to the corresponding components of the load neutral current. Such an approach allows for the introduction of a compensation set point signal to scale the components of the load neutral current, thus controlling the amount of third harmonic compensation provided by the proposed filter. The results of these comparisons are fed to PI controllers to reduce any steady-state error, yielding the following:

$$V_{PI\alpha} = k_{P\alpha}\left(k_{sp}\cdot I_{Loadn,3\alpha} - I_{f,3\alpha}\right) + k_{I\alpha}\int\left(k_{sp}\cdot I_{Loadn,3\alpha} - I_{f,3\alpha}\right)\cdot dt \tag{6}$$

$$V_{PI\beta} = k_{P\beta}\left(k_{sp}\cdot I_{Loadn,3\beta} - I_{f,3\beta}\right) + k_{I\beta}\int\left(k_{sp}\cdot I_{Loadn,3\beta} - I_{f,3\beta}\right)\cdot dt, \tag{7}$$

where $V_{PI\alpha}$ and $V_{PI\beta}$ are the output voltages of the α- and β-component PI controllers, respectively; $k_{P\alpha}$ and $k_{I\alpha}$ are the proportional and integral gains of the α-component PI controller, respectively; $k_{P\beta}$ and $k_{I\beta}$ are the proportional and integral gains of the β-component PI controller, respectively; and, k_{sp} is the third harmonic compensation set point scaling value determined by the compensation set point logic block. Notice that (6) and (7) ensure that the filter current remains in phase with the third harmonic neutral load current.

As explained previously, the converter voltage must lead the filter current by 90º to adequately provide harmonic compensation. Therefore, the α and β components of the converter reference voltage, $V^{*}_{conv\alpha}$ and $V^{*}_{conv\beta}$, can be determined from the output variables of the PI controller by using the 90º rotation matrix as shown in the following:

$$\begin{bmatrix} V^*_{conv\alpha} \\ V^*_{conv\beta} \end{bmatrix} = \begin{bmatrix} \cos\theta & -\sin\theta \\ \sin\theta & \cos\theta \end{bmatrix}\Bigg|_{\theta=90^\circ} \begin{bmatrix} V_{PI\alpha} \\ V_{PI\beta} \end{bmatrix} = \begin{bmatrix} 0 & -1 \\ 1 & 0 \end{bmatrix} \begin{bmatrix} V_{PI\alpha} \\ V_{PI\beta} \end{bmatrix} = \begin{bmatrix} -V_{PI\beta} \\ V_{PI\alpha} \end{bmatrix}. \tag{8}$$

Finally, the converter reference voltage, v^*_{conv}, is obtained by transformation back to the stationary reference frame with the following computation:

$$v^*_{conv} = 2\left[V^*_{conv\alpha} \sin\left(3\omega_1 t\right) + V^*_{conv\beta} \cos\left(3\omega_1 t\right) \right], \tag{9}$$

where the factor 2 was included to compensate for the factor 1/2 that appeared in (4) and (5). In this work, the gate signals for the power switching devices of the proposed filter are generated from the converter reference voltage using a conventional sine-triangle PWM scheme.

It is important to notice that since the power converter reference voltage is constructed independent of the LC components and system impedances, it eliminates the possibility of producing resonance. Another important observation is that the source-side third harmonic neutral current is defined by the vector difference of the third harmonic neutral load current and the filter current. In the situation where the proposed hybrid active filter is controlled to provide full third harmonic compensation, the source-side third harmonic neutral current is forced to zero. Therefore, the proposed filter not only acts as a sink for downstream third harmonic neutral currents, but also blocks any upstream third harmonic neutral current from flowing because of supply background voltage distortion. This property defines the directionality feature of the proposed filter.

When part of a distributed third harmonic filtering solution, multiple of the proposed filters are installed on a single distribution feeder. During transient conditions, interactions could take place among different filter controllers located on the same feeder. However, since speed is not a major requirement in harmonic filtering applications, lower

gains in the control loop could be selected to mitigate negative interactions among filter controllers during transients. Selecting sufficiently low gains was a condition determined in [122] to avoid hunting and instability problems when multiple power converters are installed on a single system. Under steady-state conditions, since the proposed filter is connected in shunt, each filter operates to suppress upstream third harmonic neutral current by circulating downstream third harmonic neutral current, as depicted in Figure 10. This allows the filtering burden among different filters to be shared naturally, based on their respective positions in the network and the amount of downstream single-phase nonlinear loads. However, this is only guaranteed in radial distribution systems. Fortunately, the overwhelming majority of distribution feeders have a radial configuration [75]. The implementation of the proposed filtering strategy on meshed distribution networks might require the development of a coordinated control strategy to obtain the required level of harmonic compensation, while appropriately sharing the burden among different filters. This is a subject of future research, outside of the scope of this work.

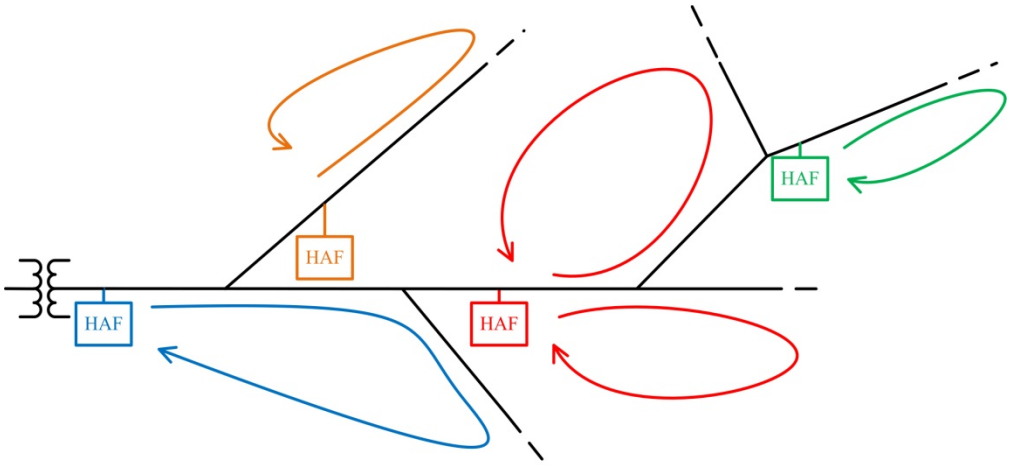

Figure 10. Harmonic compensation burden sharing among multiple shunt filters installed on a single feeder.

As discussed earlier, provisions were made in the controller to dynamically adjust the level of third harmonic compensation provided by the proposed filter based on the loading conditions of its passive components. As already observed, in [119] IEEE establishes operating limits for the capacitor RMS voltage, peak voltage, RMS current, and reactive power under which it can operate continuously without being damaged. These critical capacitor variables need to be monitored by the compensation set point logic block. If necessary, inductor variables can also be monitored to prevent any passive component overload caused by the increase in downstream loads. In summary, the set point logic must increase the compensation set point if all the monitored variables are under their maximum operating limits; decrease it if at least one of the variables is over its maximum operating limit; and, maintain it at a constant level if at least one of the variables has reached its maximum operating limit. The output of the set point logic must also be limited between 0 and 1. A simple approach for accomplishing all this is through the decision and logic circuitry depicted in Figure 11. As with the main control loop, this set point logic block can easily be implemented in a digital controller.

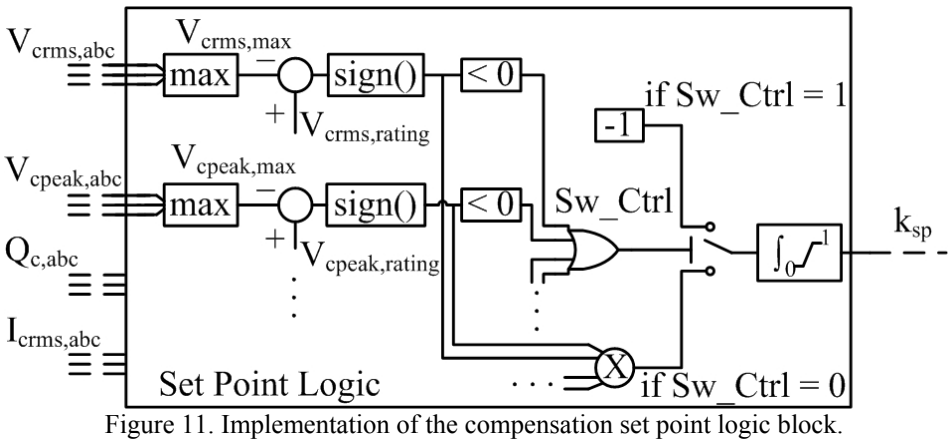

Figure 11. Implementation of the compensation set point logic block.

With the inclusion of the set point logic block, when one of the monitored capacitor variables reaches its maximum operating limit, the controller of the proposed filter becomes a control system with a varying reference. The PI controller was conceived mainly as a system regulator with fixed reference signals. If the reference changes slowly, i.e., is within the bandwidth of the system, the PI controller can follow it if properly tuned. Otherwise, a more complex controller specifically designed for tracking should be employed. In practice, PI controllers are the preferred alternative in a wide variety of power system applications, especially at the device level when speed of response is not an issue, as for the particular application discussed in this work. Because of the popularity and simplicity of PI controllers, more complex controllers were not considered here. The approach that was followed to avoid undesired interactions between the set point logic block and the main control loop was to first determine the process dominant time constant of the proposed filter when controlled to provide full harmonic compensation. The gain of the integrator in Figure 11 could then be selected such that its integral time constant is greater than the computed time constant of the response of the system. Adequate tuning of the parameters of the controller, and correct and stable operation of the proposed third harmonic hybrid active filter is verified in this work through simulation studies.

2.3 SIMULATION RESULTS

Simulations in PSCAD® were performed using the lumped system of Figure 7 to test the dynamic response of the controller and the compensation set point logic of the proposed third harmonic hybrid active filter. The harmonic data of the 24.9 kV residential/small commercial feeder in Table 2 were used to construct the system load.

The three phase system load was modeled with three Norton equivalent circuits consisting of a resistive-inductive branch connected in parallel with harmonic current sources, as depicted in Figure 12 for phase A. System impedances were selected based on information provided by utilities. A positive sequence impedance of 0.328 + j8.063% and a zero sequence impedance of 0.332 + j8.163%, both at a base of 12 MVA, were used. The phase shift between the voltage and current fundamental components was established based on substation power flow measurements. The capacitor bank was chosen to improve the resulting power factor to be in the range of 0.97-0.98 lagging. Three 14.4 kV, 300 kVAR single-phase capacitor units were selected for this purpose. An inductance value of 75.24 mH was chosen to tune the filter 5% under the third harmonic frequency. Situations with both no background voltage distortion and 3% third harmonic background voltage distortion were considered.

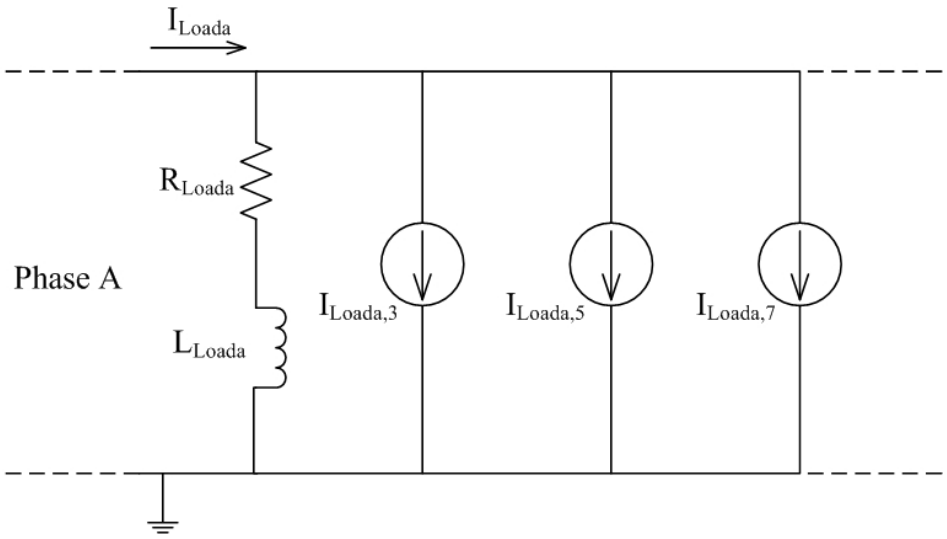

Figure 12. Norton equivalent circuit of nonlinear loads for harmonic system studies.

2.3.1 Dynamic Response

The dynamic response of the proposed third harmonic hybrid active filter was tested assuming a third harmonic background voltage distortion of 3%. Also, the filter was controlled to provide full compensation for the third harmonic neutral load current. Figure 13a shows how the error between the α and β components of the third harmonic neutral load current and the filter current vary throughout the simulation. Compensation was initiated at 8 s, and a few seconds after the filter was activated both error components were driven to zero. Figure 13b displays the source-side third harmonic neutral current reduction of 59.1 A after full compensation was provided. This result proves the directionality feature of the proposed filter in blocking upstream third harmonic current caused by background voltage distortion. The source-side current waveforms of phase A before and after third harmonic compensation was provided are presented in Figure 14. The harmonic spectra of these current waveforms are compared in Figure 15. Note that since most of the third harmonic current in the phase conductors flow in the neutral, the proposed filter does a good job of reducing the source-side third harmonic phase currents to negligible levels. These results demonstrate excellent filtering and dynamic performance of the proposed filter and its controller.

2.3.2 Passive Component Overload Prevention Feature

The compensation set point logic was tested assuming no background voltage distortion. The chosen values for the proportional and integral gains of the PI controllers of the main harmonic compensation control loop were 0.2 V/A and 12 V/A·s, respectively. With these gains, it was determined that the resulting time constant of the proposed hybrid active filter system was 0.816 s when providing full harmonic

compensation. To avoid undesired interactions with the main control loop, a gain of 1 1/s was selected for the integrator of the compensation set point logic block.

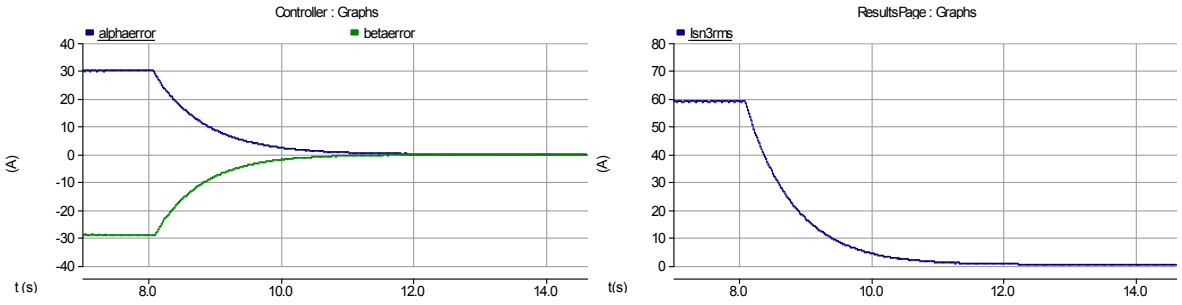

a) b)

Figure 13. Results from the dynamic response simulation: a) α and β error components and b) The source-side RMS third harmonic neutral current.

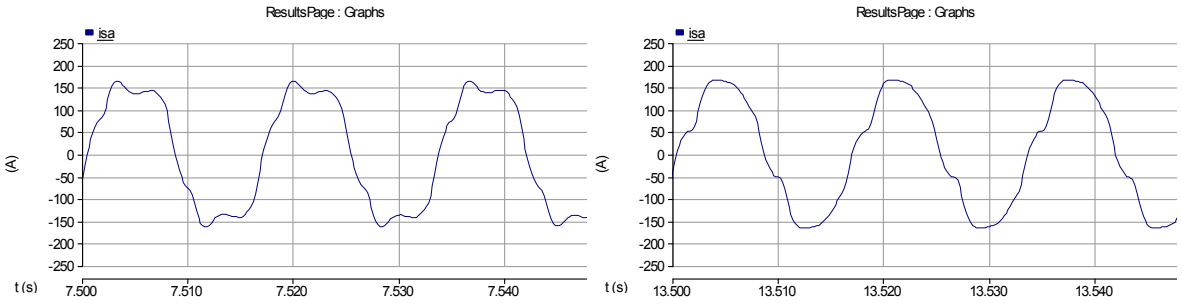

a) b)

Figure 14. Source-side phase A current waveform: a) Before and b) After third harmonic compensation.

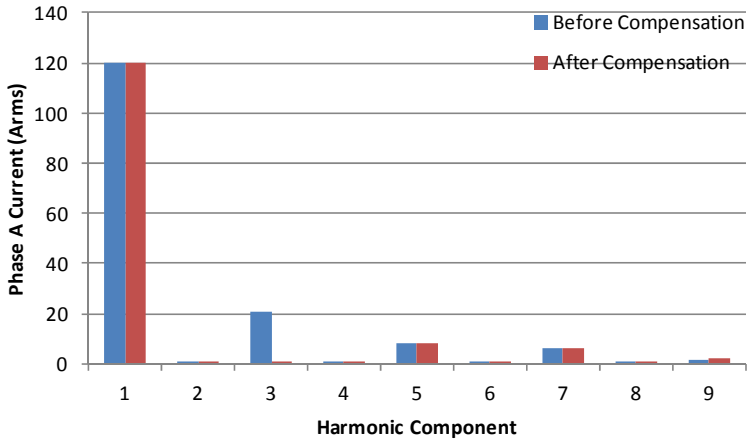

Figure 15. Spectrum of the source-side phase A current before and after third harmonic compensation.

The critical capacitor values for which continuous maximum operating limits were given in [119] were monitored by the compensation set point logic block, and the third harmonic compensation set point was adjusted to not exceed their maximum limits. The simulation results are shown in Figure 16. By examining Figure 16a and Figure 16b, it is clear that no negative interaction occurs between the set point logic block and the main harmonic compensation control loop. Harmonic compensation was initiated at 5 s, while the load was increased to 140% and then decreased to 80% of its original value at 11 and 17 s, respectively. Figure 16a and Figure 16b show that with the original load the compensation set point settled at 0.91 (i.e., the filter was controlled to compensate for only 91% of the third harmonic neutral current), and the source-side third harmonic neutral current was reduced from 38.9 A to 4.2 A. When the load increased to 140%, the set point was adjusted to 0.67 to avoid overloading the capacitors. In this case the source-side third harmonic neutral current could only be reduced to 21.2 A. With only 80% of the load connected, the capacitor bank had enough margin to allow for full third harmonic compensation. Therefore, the set point increases to 1.0 and the source-side third harmonic neutral current is reduced to a negligible level.

The capacitor bank peak voltage and RMS current remained well below their maximum operating limits throughout the simulation. In this case the limiting factors were the RMS voltage and the reactive power, which came close to exceeding their respective operating limits. As observed in Figure 16c and Figure 16d, the compensation set point logic block operated properly to prevent this from happening. For the results presented in this section, the maximum operating limits the capacitor could reach, before the compensation set point logic adjusted the level of harmonic compensation, were those

given in [119]. In practice, an additional safety band could be left to provide an additional level of security to prevent the capacitor units from overloading.

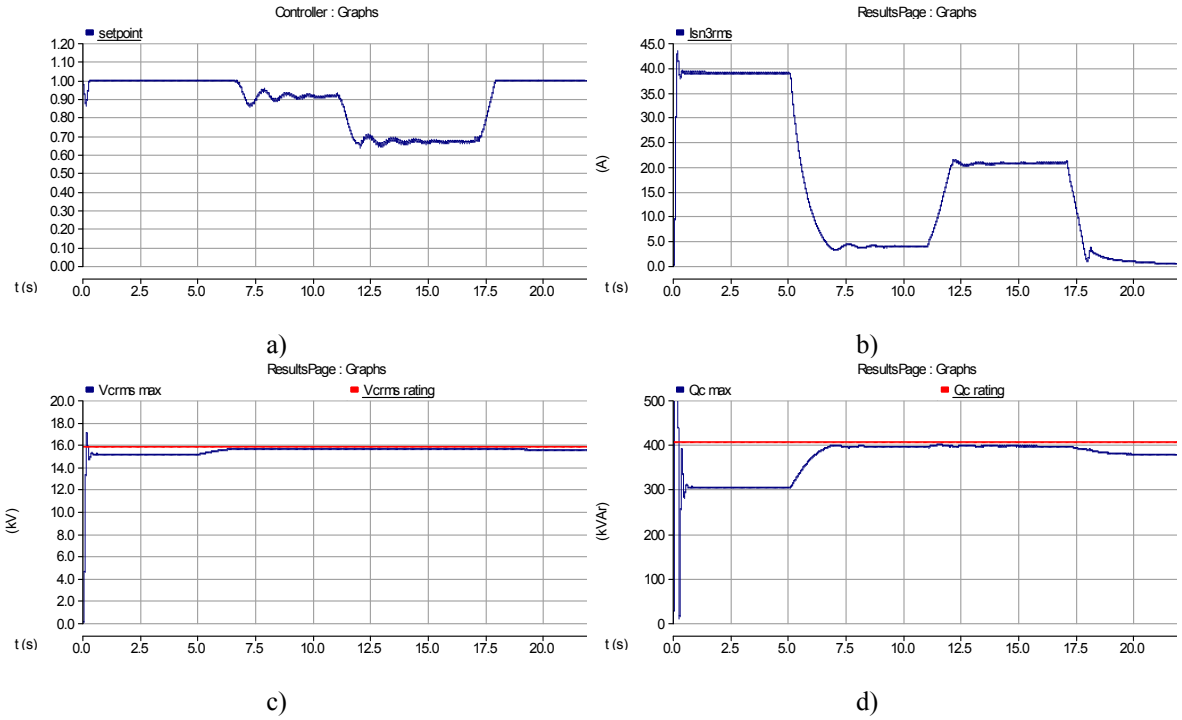

Figure 16. Results from the overload prevention feature simulation: a) The compensation set point, b) The source-side RMS third harmonic neutral current, and the capacitor bank maximum c) RMS voltage and d) Reactive power.

2.4 COMPARISON WITH CONVENTIONAL FILTERING APPROACHES

The results of simulating the proposed third harmonic hybrid active filter in the lumped system of Figure 7 were compared to that of conventional harmonic filtering approaches, mainly pure third harmonic active and passive filters. The same harmonic data for the residential/small commercial feeder of Table 2 and system parameters assumed in the previous section were used again for this analysis. The comparison was made in terms of filtering performance, power requirements of filter components, and

estimated cost of each filtering strategy, assuming both no background voltage distortion and 3% third harmonic background voltage distortion.

Table 4 summarizes the filtering performance of the different filters when applied to the system of Figure 7. Results show that the active filter offers the best performance, achieving the greatest reduction in phase THD_i, regardless of the presence or not of background voltage distortion. The reason for this is because the active filter does not only compensate for zero-sequence third harmonic current, but for third harmonic currents in the positive and negative sequences as well. The table also highlights two of the greatest disadvantages of passive filers: the sensitivity of their filtering performance to filter tuning and their vulnerability to resonance. The harmonic reduction of the passive filter is effectively the same as the proposed hybrid active filter if it is perfectly tuned and there is no background voltage distortion. However, considerable reduction in filtering performance is observed at only 5% filter mistune, compensating for merely 12.6% of the third harmonic neutral current. At the same time, even in the presence of a small amount of background voltage distortion, perfectly tuned filters can introduce serious resonance conditions, as shown in Table 4 for a 1% mistuned passive filter. Resonance effects can even be noticed in the 5% mistuned passive filter. The resonant issues surrounding passive filters are of great concern to utilities and are the main reason that renders them impractical for utility applications. On the other hand, the proposed hybrid active filter fully compensates for the third harmonic neutral load current whether background voltage distortion is present or not.

Table 4. Filtering Performance of Different Third Harmonic Filtering Approaches

Filtering Approach	Phase THD_i (%)			$I_{sn,3}$ (A RMS)
	A	*B*	*C*	
Assuming no background voltage distortion				
No Filter	14.6	12.9	14.0	44.5
Active Filter	7.9	6.7	7.6	0.0
Passive filter (h = 2.85)	14.3	12.5	13.8	38.9
Passive filter (h = 3.00)	8.9	7.6	8.8	0.5
Hybrid filter (h = 2.85)	8.9	7.6	8.8	0.0
Hybrid filter (h = 2.97)	8.9	7.6	8.8	0.0
Assuming 3% third harmonic background voltage distortion				
No Filter	15.4	13.6	15.0	48.4
Active Filter	7.9	6.7	7.6	0.0
Passive filter (h = 2.85)	18.5	16.2	19.9	59.1
Passive filter (h =2.97)	43.4	40.2	45.6	154.4
Hybrid filter (h = 2.85)	8.9	7.6	8.8	0.0
Hybrid filter (h = 2.97)	8.9	7.6	8.8	0.0

The power requirements and estimated cost of the filters applied to the system of Figure 7 are presented in Table 5. The cost estimate was made based on the power requirements of each filter component and assuming a cost of $10/kVAR for the capacitor bank, $20/kVAR at a 60 Hz equivalent cost for inductors [123-125], and $80/kVA for the power converter. Although active filters provide the best filtering performance, Table 5 indicates that this technology is prohibitively expensive compared to its counterparts. This is the major drawback of active filters and the reason they are considered impractical for utility filtering applications. With no background voltage distortion, the most inexpensive solution are passive filters, however recall the poor filtering performance of the 5% mistuned passive filter. At the same time, Table 5 also shows that in the presence of background voltage distortion, finely tuned passive filters experience extremely high power requirements because of resonance, making their application unrealistic. Results show that the active rating of the proposed hybrid active filter is only a small fraction of the capacitor rating, 0.3-2.3%, depending on the tuning of the LC branch and on the presence of background voltage distortion. This small active

rating compared to the rating of its passive elements permits the proposed filter to have a cost not that much greater than passive filters, while making it the only reasonable third harmonic filtering solution in the presence of background voltage distortion. This makes a strong business case for the proposed third harmonic hybrid active filter.

Table 5. Power Requirements and Estimated Cost of Different Third Harmonic Filtering Approaches

Filtering Approach	Cap. kVAR	Ind. kVAR	Active kVA	Estimated Cost (k$)
Assuming no background voltage distortion				
Active Filter	0.0	0.0	645.4	51.63
Passive filter (h = 2.85)	894.0	2.73	0.0	8.96
Passive filter (h =3.00)	1124.9	154.9	0.0	12.28
Hybrid filter (h = 2.85)	1127.9	173.9	17.0	13.80
Hybrid filter (h = 2.97)	1128.5	160.5	3.2	12.61
Assuming 3% third harmonic background voltage distortion				
Active Filter	0.0	0.0	707.3	56.58
Passive filter (h = 2.85)	1141.3	181.9	0.0	12.63
Passive filter (h =2.97)	3202.5	1983.4	0.0	-
Hybrid filter (h = 2.85)	1172.0	206.7	27.4	15.29
Hybrid filter (h = 2.97)	1172.1	190.3	21.1	14.68

2.5 COST VERSUS PERFORMANCE CURVES OF THE PROPOSED FILTER IN RETROFIT APPLICATIONS

For this analysis the inductor was chosen to tune the proposed third harmonic hybrid active filter to four different values below the third harmonic frequency to capture the sensitivity of the filter cost to the tuning of its LC components. The cost estimate of the proposed filter was made based on the power requirements of each of its components and the same cost assumptions of the previous section. Since the objective of this section is to give a sense of the cost savings of the proposed filter in retrofit applications, the capacitor bank cost was included in the total cost only when any capacitor unit within the bank exceeded its continuous operating limits as defined in [119].

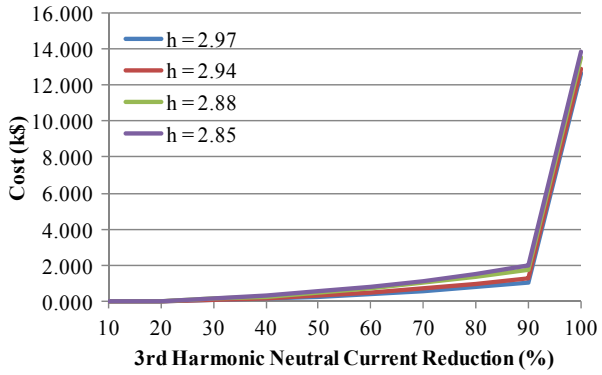

a)

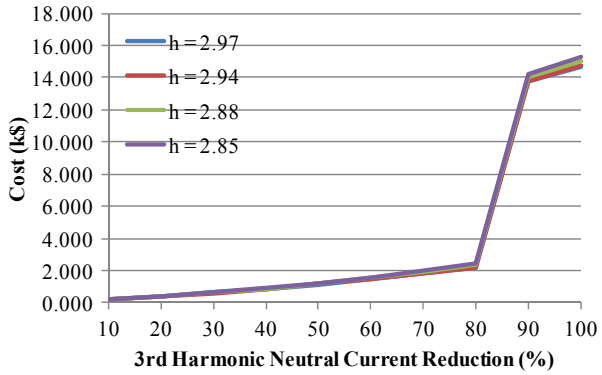

b)

Figure 17. Cost vs. performance curves of the proposed filter assuming: a) No background voltage distortion and b) 3% third harmonic background voltage distortion.

The harmonic data for the residential/small commercial feeder of Table 2 was used again for this analysis. Using these data, cost versus performance curves of the proposed filter were constructed, assuming no supply voltage distortion and 3% third harmonic background voltage distortion. The results are displayed in Figure 17. Notice that even in the worst case, it is observed that if the third harmonic compensation of the proposed filter is limited to 80%, savings in excess of 80% are achieved by retrofitting the existing capacitor bank for this particular application. If background voltage distortion were negligible, the harmonic compensation set point of the filter could be further increased to 90%, while obtaining the same savings. Bear in mind that if a retrofit application is pursued, the compensation set point logic function of the controller can automatically

adjust the level of harmonic compensation provided by the proposed filter to protect the capacitor units from overloading.

It is important to mention that despite the lump harmonic filtering solution assumed in this section, the proposed filter is intended to be part of a low-cost distributed solution, as discussed in the system impact study presented in the next chapter. In such a case, the limits given in [119] would most likely be sufficient to provide full third harmonic compensation at each filter location; although this determination will vary on a case-by-case basis. An additional observation is that, as observed in Figure 17, the filter cost does not appear to be too sensitive to the tuning of its LC components. Also important is that the capacitor cost represents the greatest share of the total filter cost. The power converter and inductor resulted in only a fraction of the cost of the capacitor bank. For this test case, these components represented only 11.7-22.3% of the capacitor cost, depending on the tuning of the filter and on the presence of background voltage distortion. This makes the proposed third harmonic hybrid active filter an attractive potential MV harmonic filtering solution for utility applications.

2.6 SUMMARY

The advent of EVs is raising concerns among utilities over the impact of this new load type on power system harmonics. EV chargers rely on power electronic systems to obtain a controllable DC source from the utility supply to charge the battery of the vehicle. Because of the nonlinearity of this electrical energy conversion process, these devices are generally regarded as a high-harmonic contaminating load. This chapter gives a historical perspective on power system harmonics, detailing the shift in recent years of utility concerns from large industrial and commercial customers to their residential/small

commercial distribution feeders. In these systems, third harmonic currents are of special interest because of their zero-sequence nature and negligible phase diversity. These currents add in the neutral creating problems such as overheating of power system equipment, nuisance tripping of protection relays, elevated NEVs, and interference with communication circuits. Utility harmonic field data indicate that even without EVs, distribution feeders are already experimenting elevated levels of third harmonic currents, especially in the neutral conductor. Conventional approaches utilities can employ to manage third harmonic currents in their systems were reviewed, and the reasons why they are not extensively implemented in practice are explained.

In this chapter, a practical third harmonic hybrid active filter is proposed to meet current utility harmonic filtering needs. To accomplish this goal, strict utility requirements of cost, reliability, and ease of system implementation were heavily taken into consideration. The lowest possible cost was achieved by targeting only third harmonic currents with a single active component located in the neutral circuit; opting for a hybrid filter configuration; and, where possible, employing existing power factor correction capacitors. A fail-normal switch was included in the design to maintain the original level of reliability of the system. The controller of the proposed filter is based on synchronous reference frame theory and direct generation of power converter reference voltage. It was structured to allow the inclusion of a set point logic block that adjusts the level of harmonic compensation provided by the filter based on the loading conditions of its passive elements. This enables existing capacitor banks to be retrofitted for this particular application. Simulation results demonstrate good filtering and dynamic performance of the proposed filtering system, including its controller and set point logic

block. Comparisons with conventional pure third harmonic active and passive filtering approaches indicate that the proposed hybrid active filtering solution is a better alternative to meet the combined requirements of low cost and level of performance demanded by utilities. Finally, cost versus performance curves were developed to give a sense of the cost savings of retrofitting existing capacitor banks into the proposed filter.

In discussions with utilities, it was determined that demonstrating the operation of a proposed technology experimentally, especially at the target voltage level, is an important requirement for it to be considered for practical implementation. The outcomes of appropriate system impact studies to determine the effects of deploying such technologies in their systems are equally important. The latter task is often overlooked in device-level research. These two efforts are discussed in the following chapter.

3 EXPERIMENTAL IMPLEMENTATION AND SYSTEM IMPACT STUDY OF THE PROPOSED FILTER

In the previous chapter, a third harmonic hybrid active filter was proposed to manage elevated third harmonic currents caused by the proliferation of single-phase nonlinear loads and to prepare the grid for the introduction of higher rating nonlinear loads into residential distribution systems, such as electric vehicles (EVs). Simulation studies were used to conceptually demonstrate the operation and benefits of the proposed hybrid active filter solution.

Continuing with this work, the first two portions of this chapter discuss a couple of experimental implementations that were developed as part of this project. The first experimental setup is used to experimentally demonstrate the directionality feature of the proposed filter and its filtering performance when compensating for an actual rectifier front-end load. The second experimental setup is employed to demonstrate the operation of a third harmonic hybrid active filter at utility distribution medium voltage (MV) levels. Power system computer aided design (PSCAD®) simulations were performed during the design of these experimental implementations and to test their correct and safe operation before conducting the experimental process. A detailed description of the design, simulation results, and experimental results for both experimental setups are presented.

The last portion of this chapter is dedicated to a system impact study of the proposed filter. For this study, actual data for a typical residential/small commercial distribution feeder was provided by a National Electric Energy Testing, Research and Applications Center (NEETRAC) utility member. This information was utilized to develop a reduced feeder model so that electromagnetic transient simulations could be performed with the

proposed filter. The developed reduced feeder model was validated with field measurements taken on the actual distribution feeder and then was used to evaluate the impact of the proposed filter on third harmonic neutral current and neutral-to-earth voltage (NEV) reduction.

3.1 350 V Experimental Implementation

The operation and performance of the proposed third harmonic hybrid active filtering approach is first verified at 350 V. As explained later, generating harmonic currents at MV levels utilizing actual loads becomes a prohibitively expensive task. Therefore, working at lower voltage levels allows to demonstrate the performance of the proposed filter when compensating for loads that have the same front-end configuration of typical single-phase nonlinear residential loads. It also enables the demonstration of the directionality feature of the proposed filter.

A schematic circuit of the 350 V experimental setup of the proposed filter is displayed in Figure 18. Because of the unavailability of a three-phase adjustable voltage supply, a single-phase implementation of the proposed filter was pursued. This approach actually results in a disadvantage compared to a three-phase implementation, since in such a configuration the fundamental current flowing through the filter capacitor also flows through the power converter and inductor. Bear in mind that the rationale for placing these components in the neutral circuit was to reduce their power requirements and hence their cost.

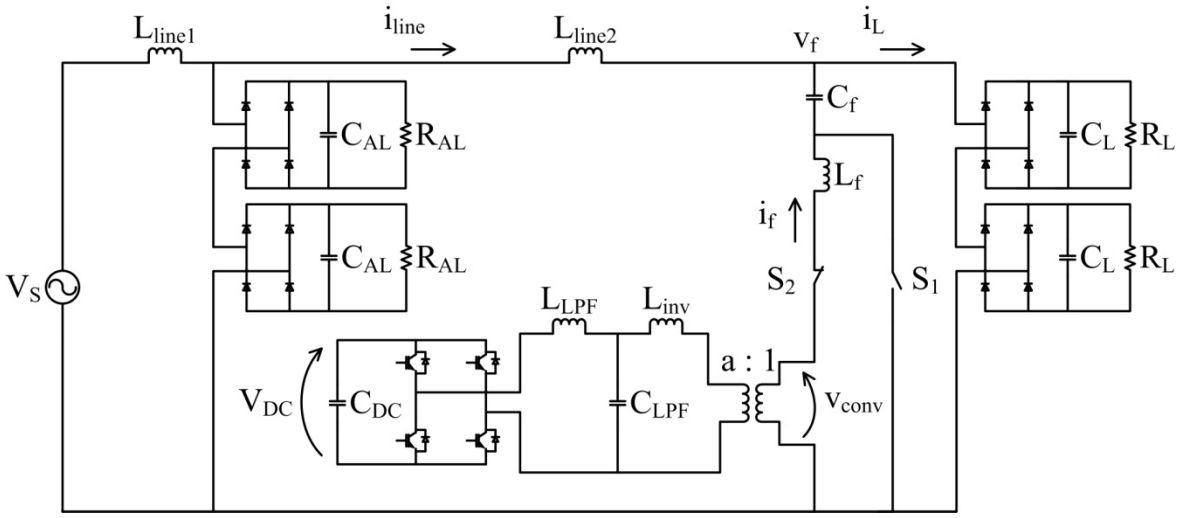

Figure 18. Schematic of the 350 V experimental implementation of the proposed filter.

The experimental setup consists of four resistive-capacitive (RC) rectifier loads. Two were connected in series to form the ambient load to generate third harmonic background voltage distortion. This allows testing of the directionality feature of the proposed filter. The other two, also connected in series, form the load for which harmonic compensation will be provided. The filter capacitor, C_f, and filter inductor, L_f, were tuned at the third harmonic frequency to provide a low impedance path for currents at this harmonic frequency. Low pass filtering elements C_{LPF}, L_{LPF}, and L_{inv} were used to filter unwanted high frequency components generated by the power converter. An isolation transformer was also included in the design for safety and to step down the power converter voltage so that an adequate DC link voltage could be employed.

The power converter was implemented with a single-phase H-bridge inverter. The mechanical design of the power converter was carried out in Solidworks®. Figure 19 displays three-dimensional CAD drawings that were developed in the design stage of the power converter. Notice that bus planes were employed to connect the switching

elements and DC link capacitors. This was done to minimize parasitics and be conservative because of the operating levels the power converter could be exposed to during experimentation. Photographs of the actual power converter before and after assembling the bus planes are shown in Figure 20. Nomex® paper was used to insulate the positive and negative bus planes.

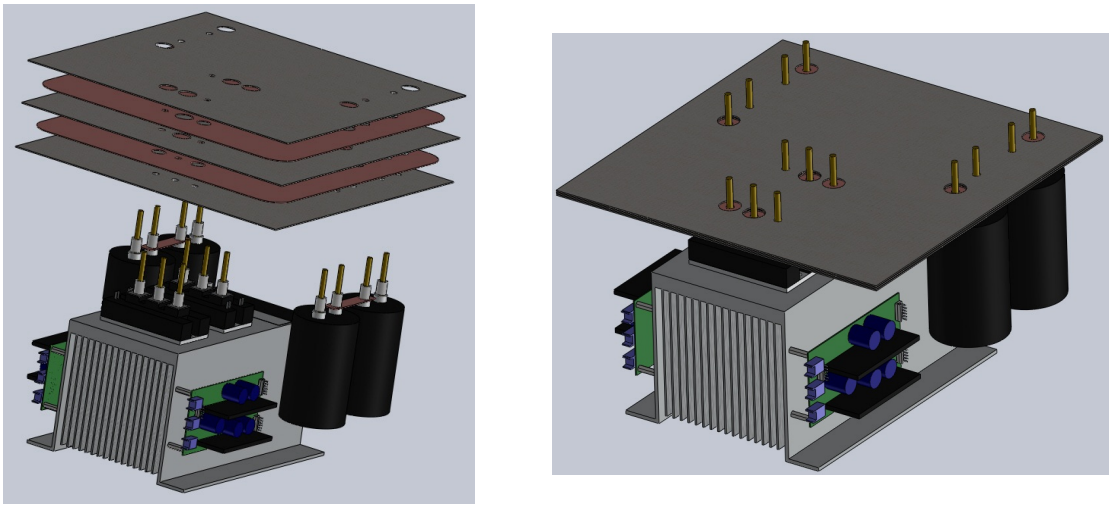

Figure 19. Three-dimensional CAD drawings of the H-bridge inverter.

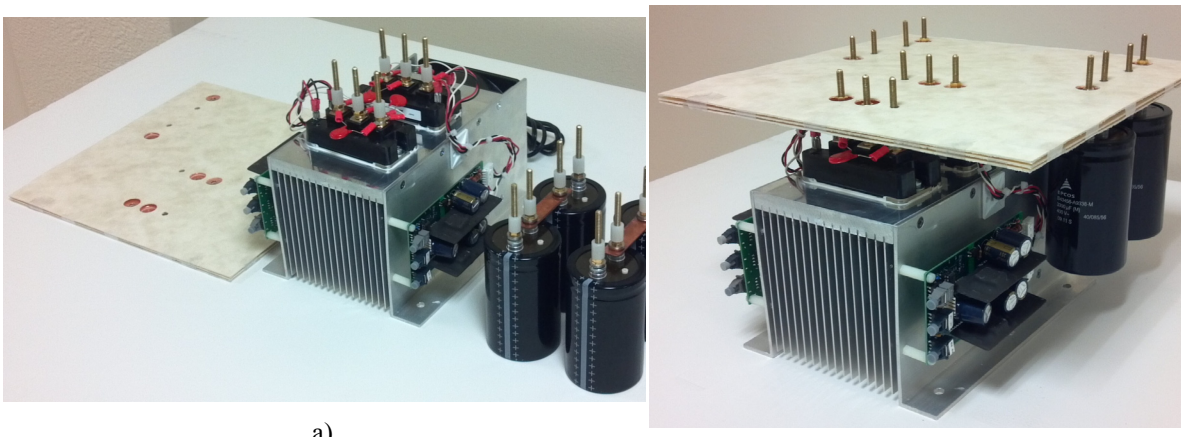

a) b)

Figure 20. Photographs of the H-bridge inverter: a) Before and b) After assembling the bus planes.

The DC link voltage of the power converter must be properly regulated to ensure suitable operation of the proposed filter. If sufficient fundamental current flows through

the power converter, the need for an external energy supply to maintain this voltage can be avoided. This, however, requires the addition of a DC link voltage control loop to the third harmonic compensation control loop introduced in the previous chapter. Since fundamental current flows through the power converter in a single-phase implementation of the proposed filter, this approach was chosen for the experimental setup.

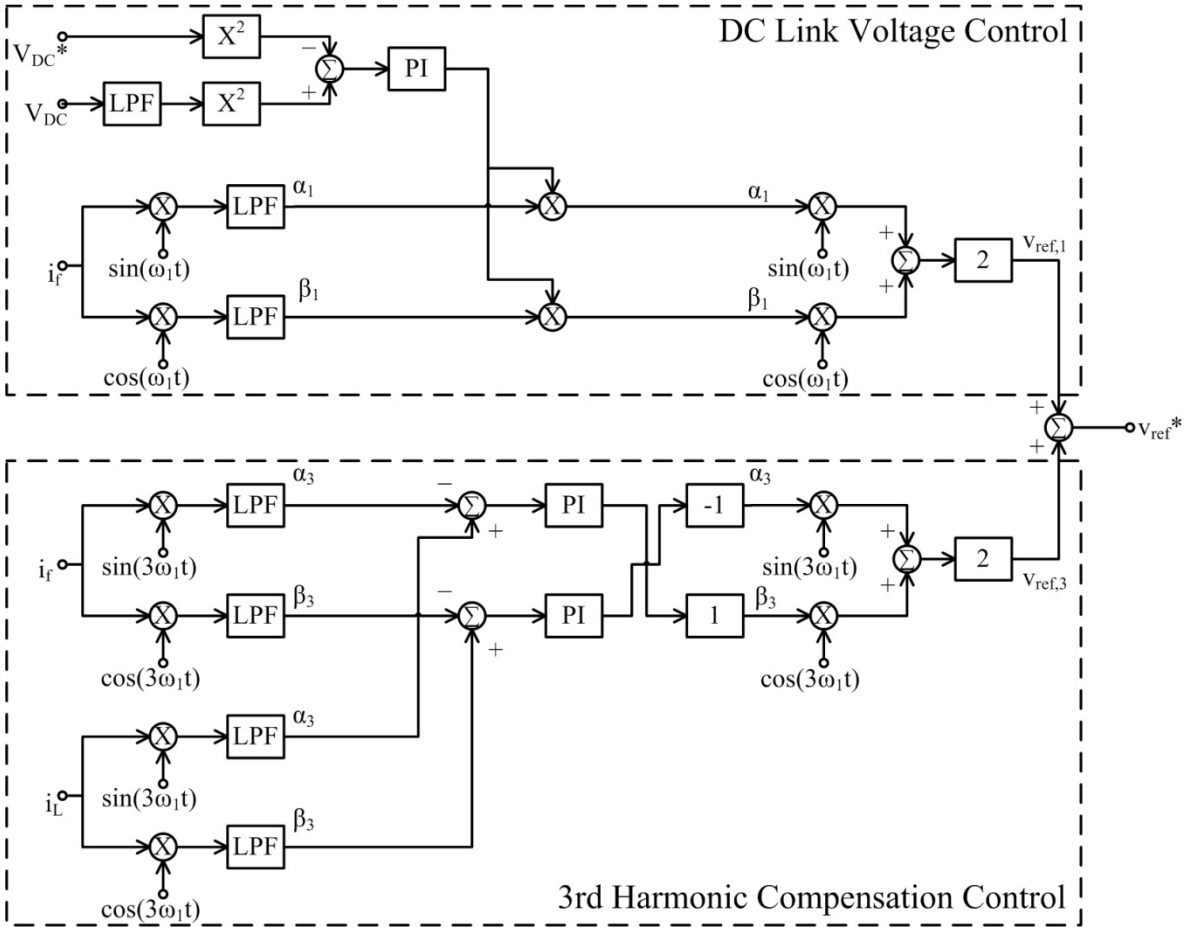

Figure 21. Block diagram of the controller employed in the experimental implementation of the proposed filter.

A block diagram of the controller used for the experimental implementation of the proposed filter is shown in Figure 21. As the third harmonic compensation control loop, the DC link voltage control loop is based on synchronous reference frame theory and

direct generation of power converter reference voltage. The DC link voltage is monitored, low pass filtered, squared, and compared to the square of its reference value. The advantages of working with the squares of the DC link voltage and its reference in terms of stability are detailed in [126]. The steady-state error in DC link voltage is driven to zero by a PI controller. The output command signals of the PI controller are multiplied with the DC components of the filter current on a reference frame rotating at the fundamental frequency, ensuring that the resulting power converter fundamental reference voltage is in phase with this current. Notice that this makes the power converter consume energy.

Recall that the third harmonic voltage generated by the power converter is in quadrature with the third harmonic component of the filter current; hence, it does not consume active power when the proposed filter provides the third harmonic filtering action. Therefore, the energy consumed by the power converter is mainly used to balance out system losses so that the DC link voltage is maintained at its reference value. Because of this, the power converter fundamental reference voltage should be much smaller than the third harmonic reference voltage. These two reference voltage components are summed to obtain the actual reference voltage for the power converter. This reference voltage was synthesized in the experimental setup using a conventional sine-triangle PWM scheme. Following the general design guidelines given in [127], the power converter was selected to operate at a switching frequency of 5 kHz.

This method for providing DC link voltage regulation depends on the amount of fundamental current flowing through the power converter. In [126], the DC link voltage was properly regulated to its reference value with neutral currents as low as 3.2 A by

employing such an approach. However, in a three-phase implementation of the proposed filter in practice, enough fundamental current may not flow through the power converter to provide this functionality. In such a case, an external energy supply to maintain the DC link capacitor at a constant voltage level will most likely be required. This can easily be accomplished by supplying the DC link capacitor with a phase-to-phase voltage through a step down transformer and rectifier, as depicted in Figure 22. The turns ratio of this transformer is selected to obtain the required DC link voltage level. Again, since the power converter does not consume active power when providing the third harmonic filtering action, energy from the supply is only drawn to compensate for system losses. Therefore, the current drawn by the power converter is much smaller than the line currents and hence will have a negligible impact on the filtering performance of the proposed filter. Results from simulations on various systems comparing the two DC link voltage regulation approaches were basically indistinguishable from each other.

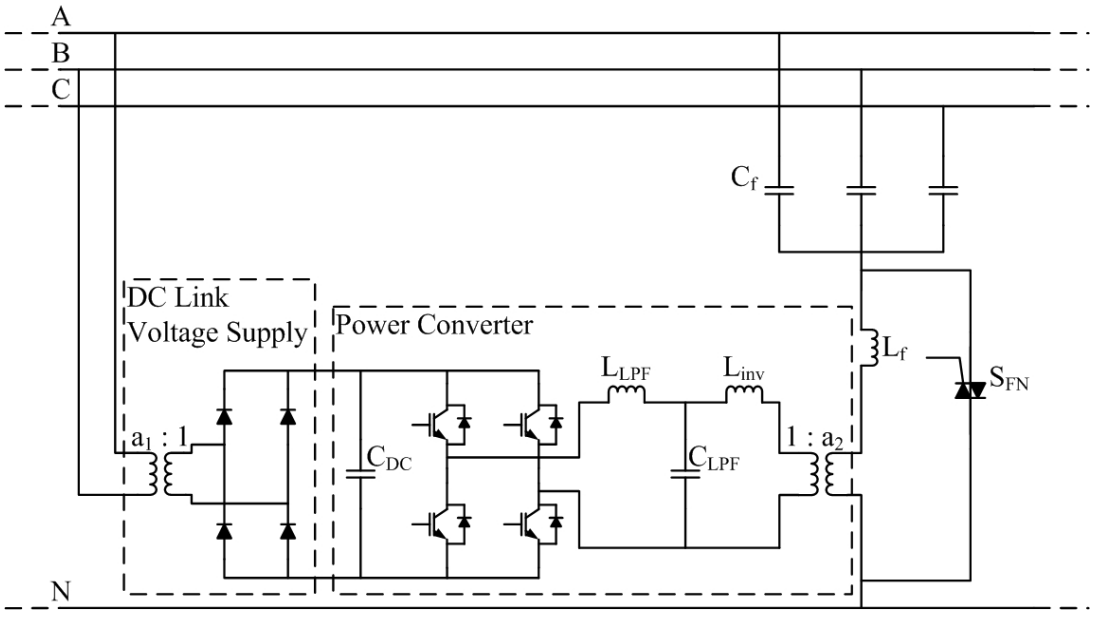

Figure 22. External supply to regulate the DC link voltage of the proposed filter.

A controller board containing input/output ports, signal conditioning, and signal processing circuitry was designed and built for the experimental setup. Design of this controller board was done using EAGLE®. Schematic diagrams and printed circuit board layout are included for reference in Appendix A. LEM® LA 100-P current transducers and LEM® LV 100-750 voltage transducers were used as sensors to provide input signals to the controller board. The controller shown in the block diagram of Figure 21 was digitally implemented in a Texas Instruments® TMS320F2812 DSP.

Two mechanical switches, S_1 and S_2, were included in the design of the 350 V experimental setup. S_1 was employed as the fail-normal switch, bypassing the inductor and power converter when faults were detected or when the proposed filter was turned off. S_2 was included to isolate the power converter from the experimental setup when it was not in operation. The fault/shutdown sequence routine was also programmed into the digital controller. When the controller board detected a fault or a shutdown signal, it would immediately, through analog circuitry, send a signal for S_1 to close. Then the digital controller would send signals for the IGBTs to turn off and for S_2 to open. During the experimentation process, the fault/shutdown sequence and fail-normal operation of the filter satisfactorily isolated the power converter from the rest of the experimental setup when faults were detected and during filter shutdown.

Correct sizing of the components of the experimental setup of Figure 18 was realized through simulation studies in PSCAD®. Table 6 summarizes the values and ratings of the actual components that were used in the experimental setup. Photographs of the setup after assembly are shown in Figure 23.

Table 6. Components Used in the 350 V Experimental Setup of Figure 18

Component	Value, Ratings
V_S	0-560 V, 60 Hz, 100 kVA
L_{line1}	692 µH
L_{line2}	113 µH
C_{AL}, C_L	1.2 mF, 400 V
R_{AL}	44 Ω, 5 kW
R_L	20 Ω, 4 kW
C_f	40 µF, 740 Vrms
L_f	22.26 mH
C_{DC}	3.3 mF, 400 V, 62 Apk (ripple)
IGBTs	600 V, 150 A, Si devices
C_{LPF}	50 µF, 370 Vrms
L_{LPF}	519 µH
L_{inv}	36.5 µH
Isolation Transformer a:1	2 : 1 (240/120 V), 3 kVA
S_1, S_2	Relay, 600 VAC, 30 A, 12VDC coil

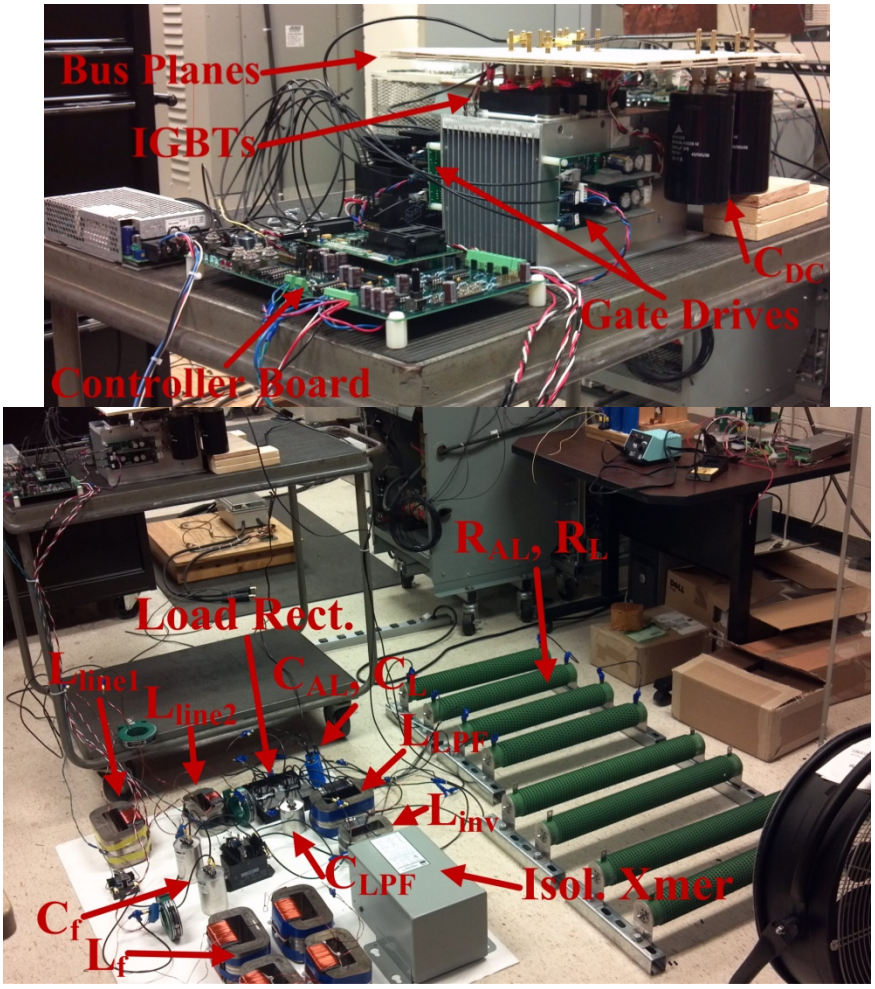

Figure 23. Photographs of the 350 V experimental setup of the proposed filter.

3.1.1 Simulation Results

The 350 V experimental setup of Figure 18 was first simulated with the component values of Table 6 to verify its operation before conducting the experiments. As observed from this table, the LC branch was mistuned by 6.3% (i.e., at h = 2.81) to take into consideration possible combined device tolerances that could be encountered in practice. For the results presented in this section, S_1 was kept open throughout the simulations. Simulation results for the fault/shutdown sequence were only included in this document for the 7.2 kV experimental setup discussed below. S_2 was originally open at the start of the simulation and was closed at 3 s. At the same time, IGBTs started switching and charging of the DC link capacitor was initiated. After the DC link capacitor is charged to its reference voltage, the power converter only generates a small fundamental voltage to balance out component losses. Therefore, under this operating condition, the filter branch effectively becomes a passive filter. Finally, the power converter starts providing third harmonic compensation at 7 s.

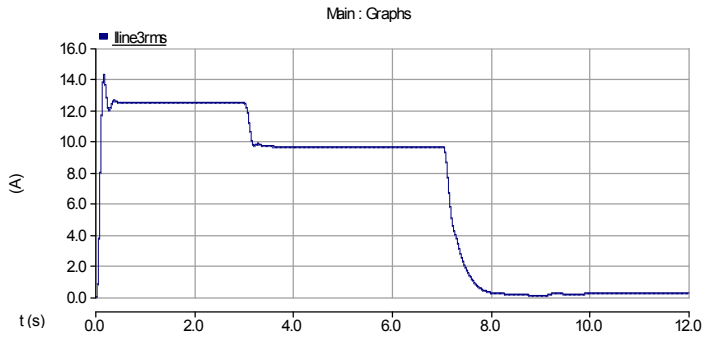

Figure 24. RMS third harmonic line current in the simulation of the 350 V experimental setup.

Figure 24 shows the third harmonic line current throughout the simulation. With no filtering action, the third harmonic line current was 12.5 A. When the filter branch was

connected, the passive LC filter reduced this current to only 9.7 A. As observed by this result, the filtering performance of the passive filter is greatly affected by the mistuning of its LC components. On the other hand, tuning the LC components closer to the third harmonic frequency could have excited a resonant condition in the experimental setup because of the background voltage distortion introduced by the ambient load. For safety, the possibility of this situation occurring was intentionally avoided. After the power converter starts operating, the third harmonic line current is reduced to zero. The third harmonic background voltage distortion introduced by the ambient load was about 1.62% of the fundamental voltage component. Thus, this result demonstrates the directionality feature of the proposed filter.

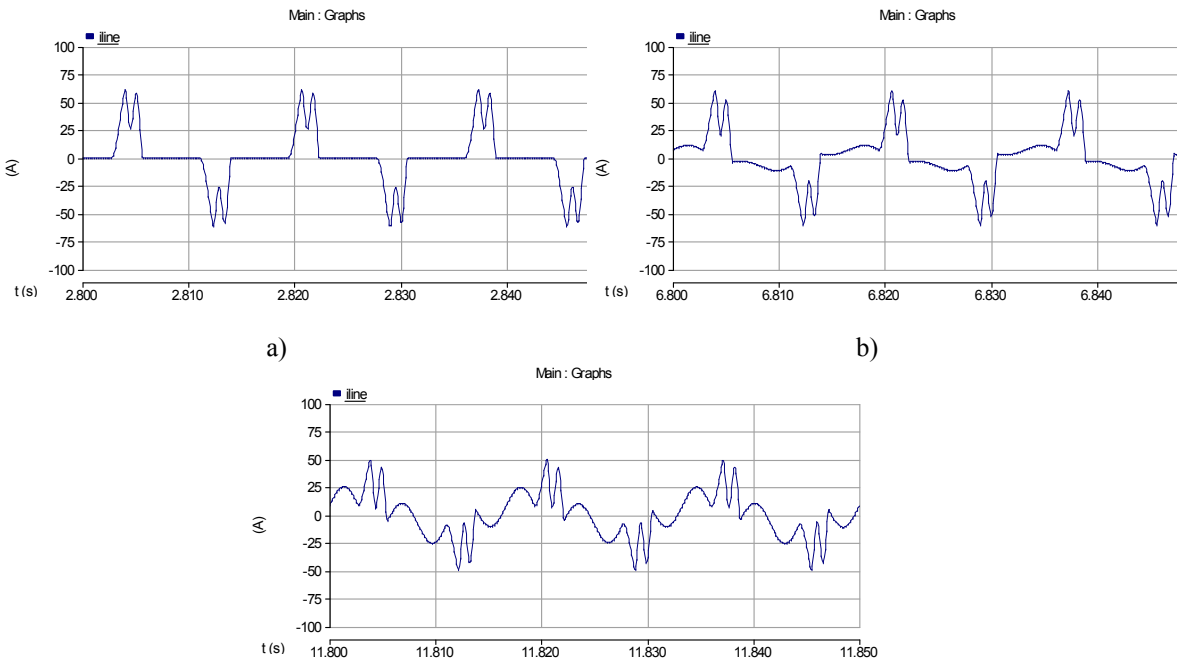

Figure 25. Waveform of the line current: a) With no filter, b) The passive filter, and c) The proposed hybrid active filter.

Time-domain waveforms of the line current of the experimental setup with no filter, the passive filter, and the proposed hybrid active filter are presented in Figure 25. The spectra of these current waveforms are displayed in Figure 26. Notice that the current drawn by the RC rectifier load is rich in third harmonic current, making it adequate for testing the filtering performance of the proposed filter.

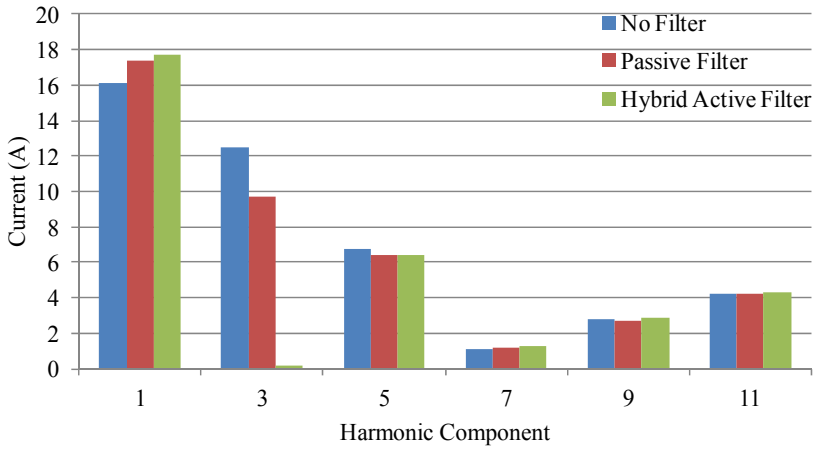

Figure 26. Spectra of the line current waveforms with no filter, the passive filter, and the proposed hybrid active filter.

The spectrum of the voltage injected by the power converter into the filter branch is shown in Figure 27. From this figure it is seen that a third harmonic voltage of only 33.64 V was required to provide full third harmonic compensation for the load. This voltage compensates for both mistuning of the LC components and the third harmonic background voltage distortion. Notice also that only 6.75 V of fundamental voltage was needed to balance out system losses and maintain the DC link voltage at its reference value. Tight DC link voltage control was demonstrated throughout the simulation, as shown in Figure 28. Charging of the DC link capacitor started at 3 s from an initial

voltage of 150 V. A DC link voltage reference of 180 V was selected for this experimental setup.

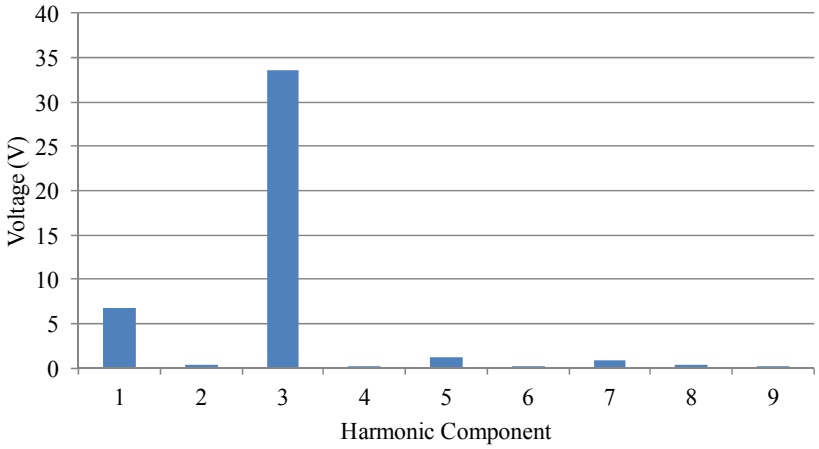

Figure 27. Spectrum of the power converter voltage.

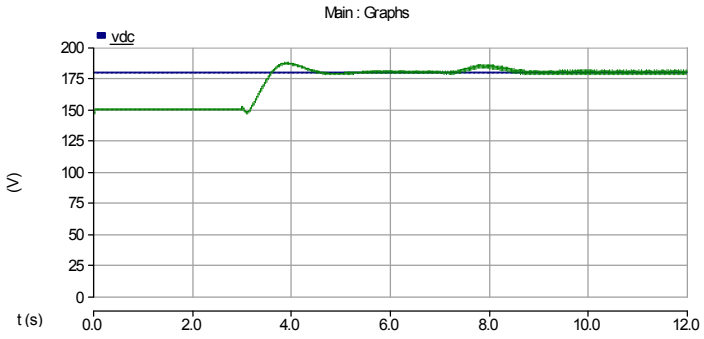

Figure 28. DC link voltage in the simulation of the 350 V experimental setup.

3.1.2 Experimental Results

The experimental setup of Figure 18 was successfully tested at 350 V. Experiments were performed for three different cases: the experimental setup with no filter, with the LC passive filter, and with the proposed third harmonic hybrid active filter. In general, the experimental results that were obtained are in good agreement with simulations. Voltage measurements were taken using Tektronix® P5200 high voltage differential

probes, while current measurements were taking with Pearson® 110 A current sensors. Figure 29, Figure 30, and Figure 31 present oscilloscope screen captures of the relevant waveforms of each case.

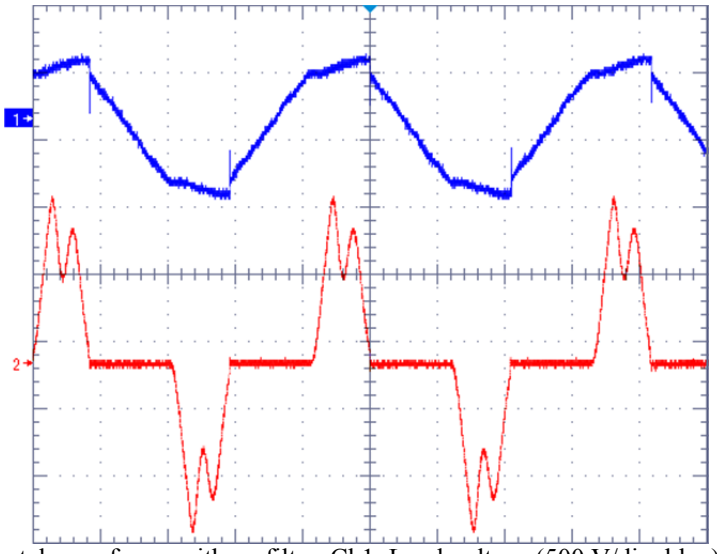

Figure 29. Experimental waveforms with no filter. Ch1: Load voltage (500 V/div, blue); Ch2: Line current (20 A/div, red); time scale 4 ms/div.

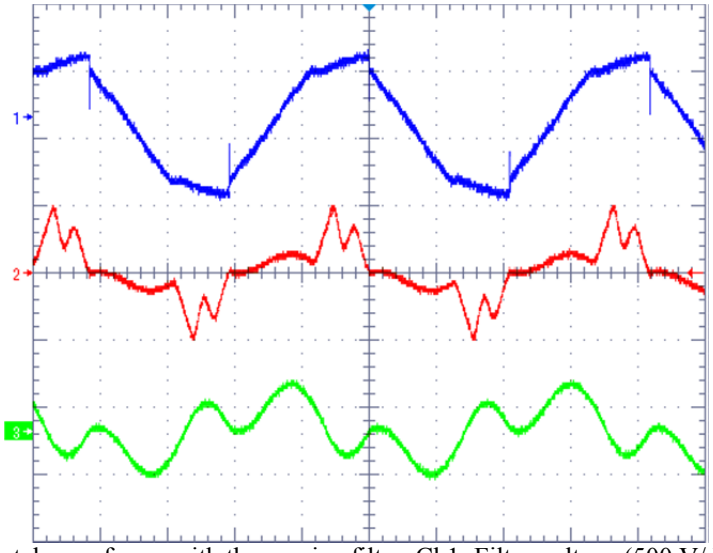

Figure 30. Experimental waveforms with the passive filter. Ch1: Filter voltage (500 V/div, blue); Ch2: Line current (50 A/div, red); Ch3: Filter current (20 A/div, green); time scale 4 ms/div.

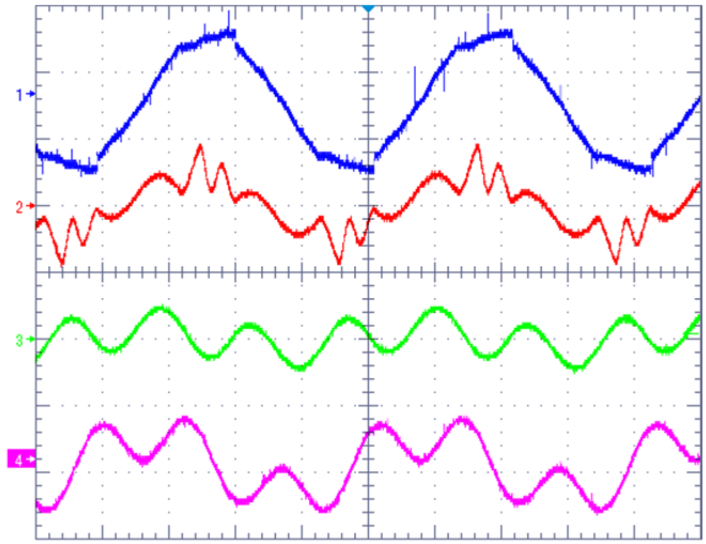

Figure 31. Experimental waveforms with the proposed filter. Ch1: Filter voltage (500 V/div, blue); Ch2: Line current (50 A/div, red); Ch3: Filter current (50 A/div, green); Ch4: Converter voltage (100 V/div, magenta); time scale 4 ms/div.

From these figures it is observed that the filter voltage exhibits a "flat top" in all cases, indicating the presence of non-negligible levels of third harmonic voltage in its waveform. It is also seen that the line current increasingly departs from its traditional RC rectifier profile when the LC passive filter and the hybrid active filter are incorporated into the experimental setup, becoming more "smoother". Bear in mind that the line current remains heavily distorted because the LC components of the passive and the proposed filters are designed to only provide compensation for the third harmonic ėȣ □ꟻ綷 而愀 腑The screen captures for these cases show that the current flowing filter branch is mainly composed of fundamental and third harmonic currents, with increased third harmonic current in the case of the hybrid active filter. In addition, from Figure 31 it is clear that the converter voltage is dominated by the third harmonic component followed by the fundamental component, as it is expected.

To study their harmonic composition, fast Fourier transforms (FFTs) were performed on the line currents for each of the cases. The results of this process are presented in

Figure 32. As noted, the LC filter managed to reduce the third harmonic line current from about 10 A to roughly 6 A, representing a third harmonic current reduction from 70% to 40% of the fundamental component. On the other hand, Figure 32c demonstrates the capability of the proposed filter in reducing third harmonic currents to negligible values.

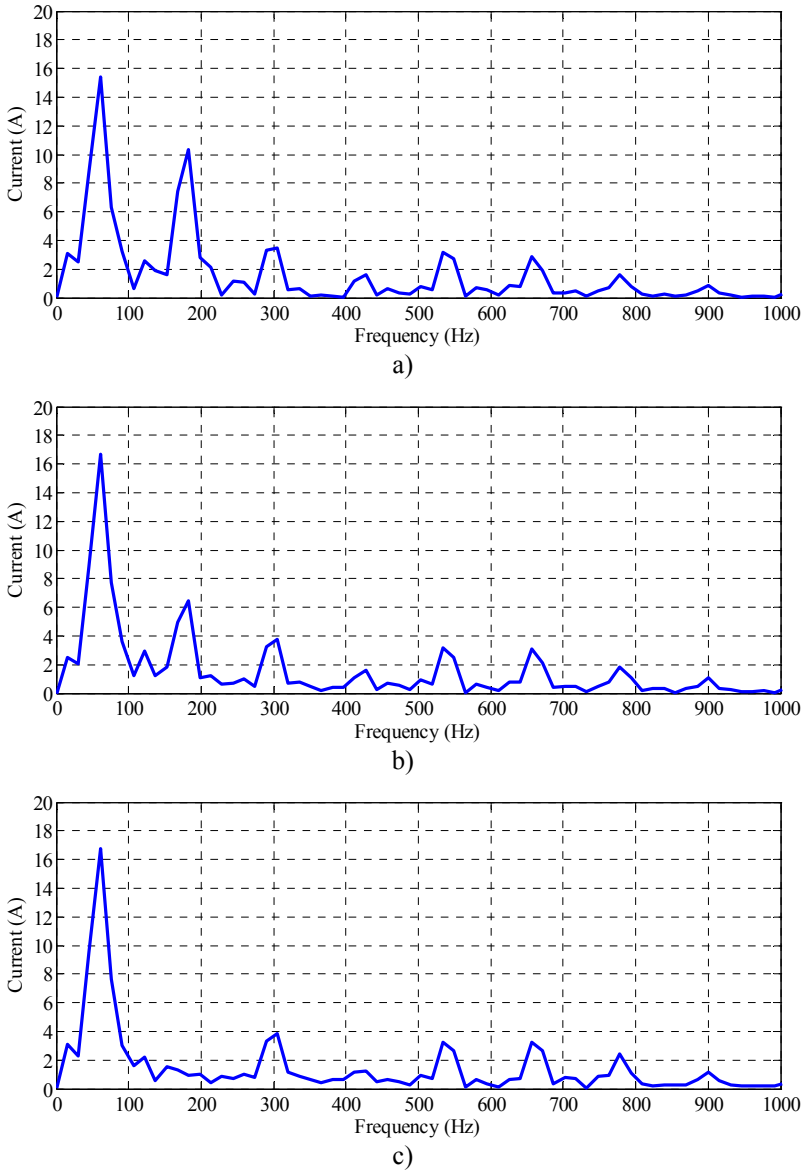

Figure 32. FFTs of the line current with a) No filter, b) The passive filter, and c) The proposed filter.

This result is also confirmed in Figure 33, which shows that the α and β components of the error between the third harmonic load current and the third harmonic component of the filter current computed by the DSP reach a steady-state value close to zero. This experimentally proves the directionality feature of the proposed filter. Throughout the experiments, good DC link voltage control was also observed, as shown in Figure 33. The DC link voltage was controlled to roughly 170 V.

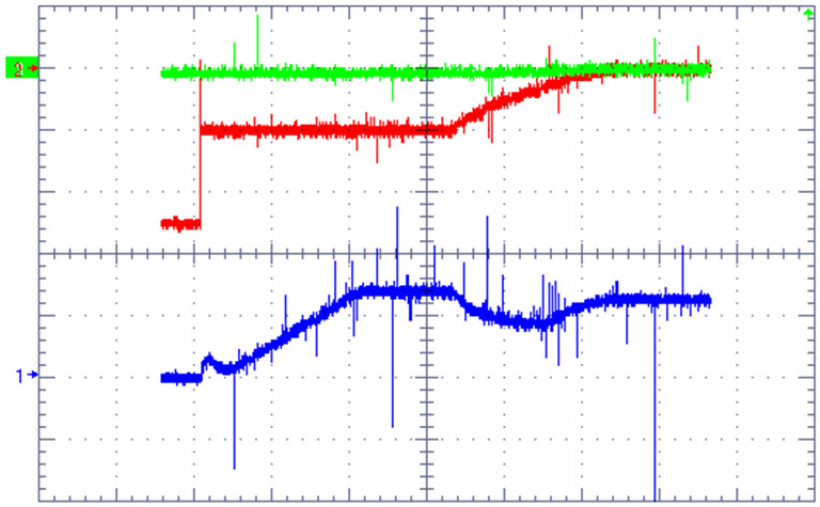

Figure 33. Experimental waveforms of V_{DC} (Ch1: 120 V/div, blue), and α (Ch2: 10 A/div, red) and β (Ch3: 10 A/div, green) error components; time scale 40 s/div.

Note that although the LC components were mistuned by over 6%, an ambient load was used to generate background voltage distortion, the third harmonic component of the load current was 70% of the fundamental, and full fundamental filter current flowed through the power converter, its power requirement was limited to 510 VA. This value represents only 6.26% of the load rating and 4.41% of the power requirements of the LC components. This result stresses again the fact that the proposed filter, by adding a small fractionally rated power converter and inductor to the neutral circuit of capacitor banks, presents a cost-effective potential solution for filtering third harmonic currents.

3.2 7.2 kV Experimental Implementation

A MV experimental setup was built and tested in the Medium Voltage Laboratory at the NEETRAC Campus to demonstrate operation of the proposed filter at utility distribution voltage levels. Figure 34 shows a schematic of the MV experimental setup, while Table 7 summarizes relevant circuit parameters that were employed. Notice that, because of equipment limitations, a single-phase implementation was chosen over a three-phase one. From a third harmonic standpoint both configurations are equivalent, with the only difference that in the single-phase case not only third harmonic current, but also fundamental current flows through the inductor and power converter, requiring components with higher ratings. Photographs of the actual experimental setup after assembly are presented in Figure 35.

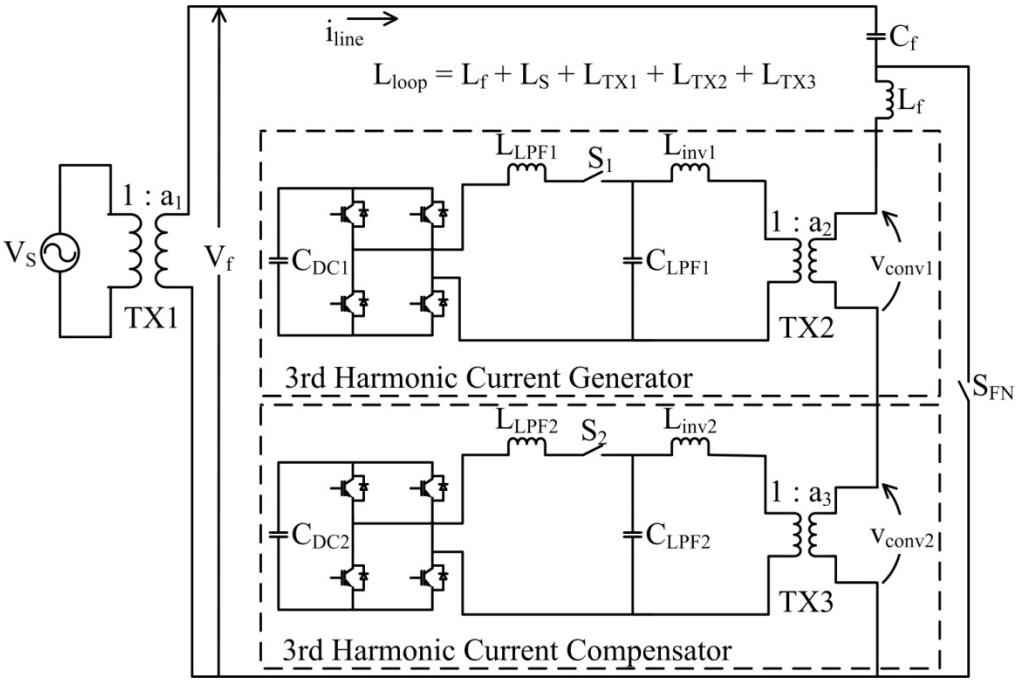

Figure 34. Schematic of the MV experimental setup of the proposed filter.

Table 7. Components Used in the MV Experimental Setup of Figure 34

Parameter	Value	Parameter	Value
V_s	0 - 240 V, 50 kVA	C_{DC1}, C_{DC2}	3.3 mF, 400V
$1 : a_1$	1 : 30 (240 V : 7.2 kV), 100 kVA	IGBTs	600 V, 150 A
C_f	2.56 µF (2 x 100 kVAR, 7.2 kV)	L_{LPF1}, L_{LPF2}	507 µH
L_{Loop}	347 mH (L_f = 35.9 mH)	C_{LPF1}, C_{LPF2}	50 µF
S_{FN}	8 kV, 25 A	L_{inv1}, L_{inv2}	35 µH
S_1, S_2	600 V, 30 A	$1 : a_2$, $1 : a_3$	1 : 2 (240 : 480 V), 3 kVA

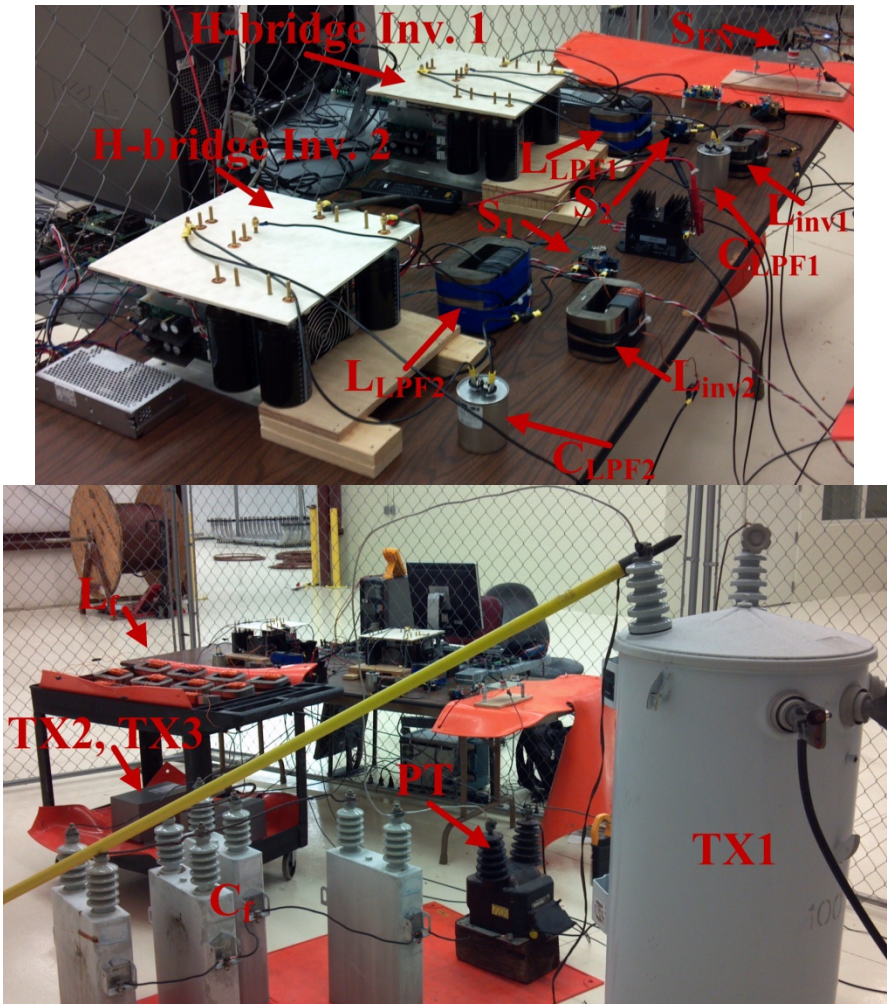

Figure 35. Photographs of the MV experimental setup of the proposed filter.

The power source used for the experimental setup was rated at 50 kVA. It consisted of a combination of a 0 – 480 V PowerStat® variable transformer and a 480/240 V step down transformer. The voltage was stepped up by a single-phase 100 kVA 240 V/7.2 kV pole-mounted distribution transformer. Power factor correction capacitors with a voltage

rating of 7.2 kV were used as the filter capacitor of the proposed hybrid active filter. A 7.2 kV/120 V potential transformer (PT) was employed to sense the high-side voltage of the distribution transformer. All these utility distribution equipment were provided by NEETRAC.

Generating third harmonic current at 7.2 kV becomes a prohibitively expensive task when using actual loads. First, these loads would require extremely high ratings to create significant third harmonic current at this voltage level. Second, it would also require the source to have a high rating as well. As observed later, the source operates slightly above its kVA rating with only the filter branch connected to the distribution transformer. To overcome this hurdle, a second power converter was added into the filter branch to generate the required third harmonic current. The controller of both power converters included a DC link voltage control loop, as explained in Section 3.1, to keep their DC link voltages at their reference values. However, the power converter that generates third harmonic current used an open-loop controller to accomplish this function, while the power converter that provides harmonic compensation used a closed-loop controller to drive the third harmonic line current to zero. Again, both converters utilized sine-triangle PWM to synthesize their reference waveforms and were operated at 5 kHz, based on the general design guidelines given in [127]. Low pass filtering elements at the output of the converters filter out unwanted high frequency components from their output voltages. Isolation transformers were also included for safety and so that adequate DC link voltages could be used. In addition, the capacitance value of the DC link capacitors was selected to limit the second harmonic ripple in the DC link voltage to less than 3%.

The values of the filter capacitor and filter inductor were selected to create a low impedance path at the third harmonic frequency, while limiting the fundamental current to less than 10 A to avoid excessive overload of the source. To meet this goal, two 100 kVAR, 7.2 kV power factor correction capacitors were connected in series to obtain an equivalent capacitance rated at 50 kVAR. The filter inductor was selected to tune the circuit loop to the third harmonic frequency. In this process, it was important to consider all of the inductance in the loop, i.e., the leakage inductance of the power source, the step up transformer, and isolation transformers. From the simulation and experimental results, the loop inductance of the experimental setup (including L_f) was estimated to be about 347 mH. With this loop inductance, the filter branch was mistuned 6.2% under the third harmonic frequency.

It is important to mention that even though the upstream inductance was taken into consideration when selecting the value of the filter inductor in this experimental implementation, this will not be the case in an implementation of the proposed filter in the field. Recall that the proposed filter is designed to provide third harmonic compensation by shunting a portion of the downstream third harmonic neutral current through the filter branch and hence only requires the LC components to be tuned at the third harmonic frequency. Furthermore, since the filter is not vulnerable to resonance, there is no need to take into account the source impedance when designing the filter for a particular situation.

A set of switches was incorporated in the experimental setup for protection. A high voltage Kilovac® relay, S_{FN}, was connected across the power converters and the filter inductor to bypass them during downtime and faults. In addition, two low-voltage

mechanical relays, S_1 and S_2, were included to isolate the power converters from the rest of the experimental setup when not in operation. The placement of S_1 and S_2 in Figure 34 was strategically chosen to prevent voltage spikes caused by accidental tripping of current flow. Before activating the power converters, S_{FN} remains closed. At startup, signals are sent to open S_{FN}, close S_1 and S_2, and start switching the IGBTs to initiate charging of the DC link capacitors. When a fault is detected or the power converters are turned off, S_{FN} receives a signal, through circuitry directly on the controller board, to close. Then, the digital controller sends signals to turn off the IGBTs and open S_1 and S_2 to isolate the power converters from the rest of the circuit.

3.2.1 Simulation Results

The MV experimental setup of Figure 34 was first simulated to verify that it operated correctly before performing the experiments. The component values of Table 7 were used in this process. In the simulation, both power converters were activated at 1 s and started charging their respective DC link capacitors. At 4 s, the first power converter started generating third harmonic current, while the second power converter began compensating for this current at 7 s.

Figure 36 displays the third harmonic line current all through the simulation, indicating correct operation and good dynamic performance of the proposed filter. Notice that even though transient operation of the proposed filter is presented throughout this document, utilities are not particularly concerned with its transient response, but are rather interested in the level of harmonic compensation that is provided after it has reached steady-state operation. Line current waveforms before and after third harmonic compensation was provided are presented in Figure 37. The spectra of these current

waveforms are compared in Figure 38. It is observed that the proposed filter effectively suppresses the 1.6 A of third harmonic current (about 20% of the fundamental current component) present in the line. In both cases, all other frequency components, excluding the fundamental, were negligible.

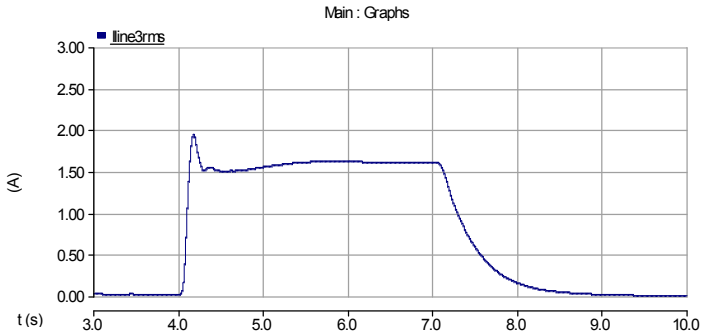

Figure 36. RMS third harmonic line current in the simulation of the MV experimental setup.

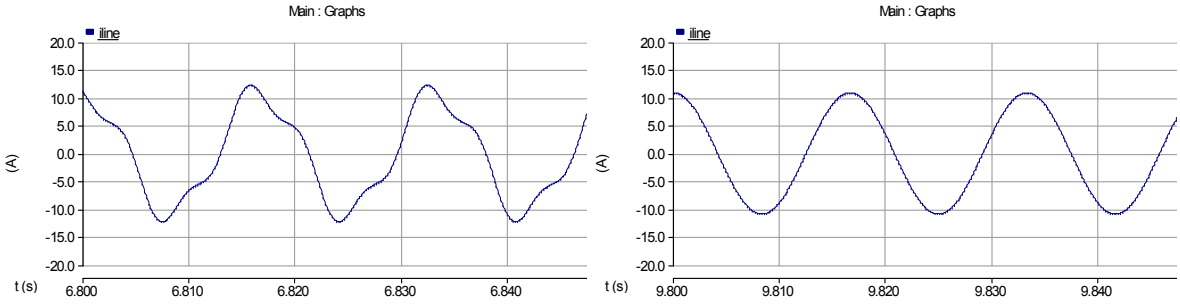

a) b)

Figure 37.Waveform of the line current a) Before and b) After third harmonic compensation.

Good control of the DC link voltage of the power converters was also observed throughout the simulation, as observed in Figure 39. Both converters started charging their respective DC link capacitors at 1 s from an initial voltage of 150 V. A reference voltage of 180 V was selected for the two power converters.

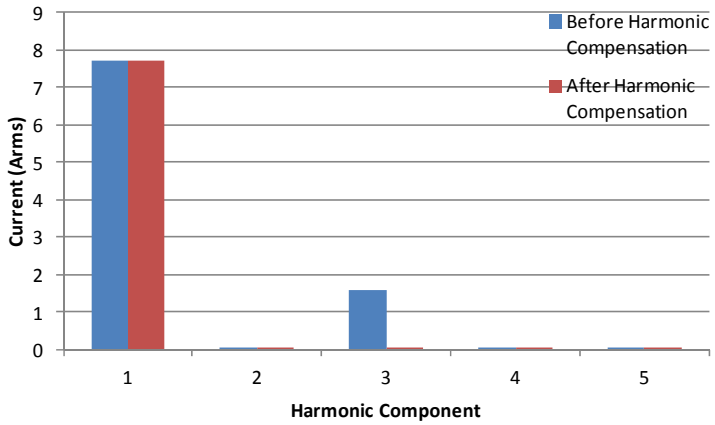

Figure 38. Spectra of the line current waveforms before and after third harmonic compensation.

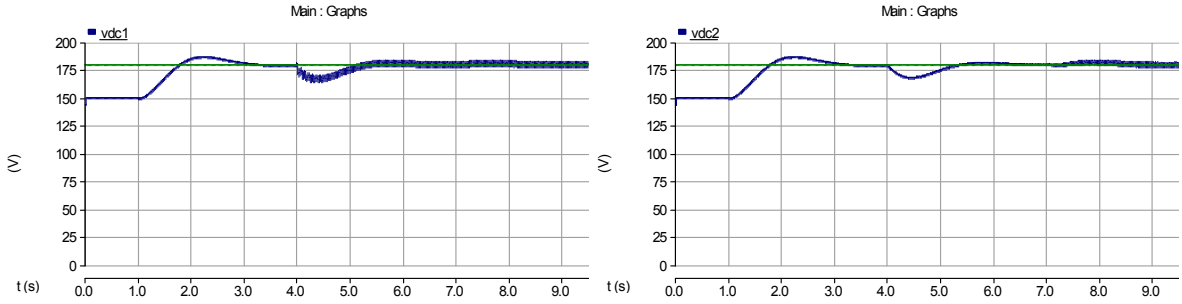

a) b)

Figure 39. DC link voltage of a) The power converter generating third harmonic current and b) The power converter providing harmonic compensation in the simulation of the MV experimental setup.

The MV experimental setup was also simulated to ensure safe operation when the power converters are turned off. To obtain conservative results, delays of the switching elements were modeled for the worst case scenario. When a turn off signal or fault is detected, the controller sends signals to close the fail-normal switch and turn off the IGBTs. With all IGBTs turned off, it is undesirable for the fail-normal switch to remain open as this would cause the DC link capacitor to charge up through the anti-parallel diodes of the IGBTs. In practice, the fail-normal switch should be implemented with a fast device, such as a thyristor pair, capable of handling high fault currents and with

operating times in the range of 100μs. Also, a mechanical switch should be included in parallel with the thyristor pair for extended periods of filter downtime.

In general, IGBTs are faster devices than thyristors. However, whereas the fail-normal switch receives its signal through circuitry on the controller board, IGBTs receive their signals from the digital controller, which has an inherently greater time delay. To be conservative, even though it is expected that the fail-normal switch will receive its signal before the IGBTs, this time difference was neglected, and hence it was assumed that they received their respective signals at the same time. In addition, the turn-off time of the IGBTs was neglected as well. Furthermore, a worst case scenario in which the fail-normal switch closes 400 μs after the IGBTs turn off was assumed.

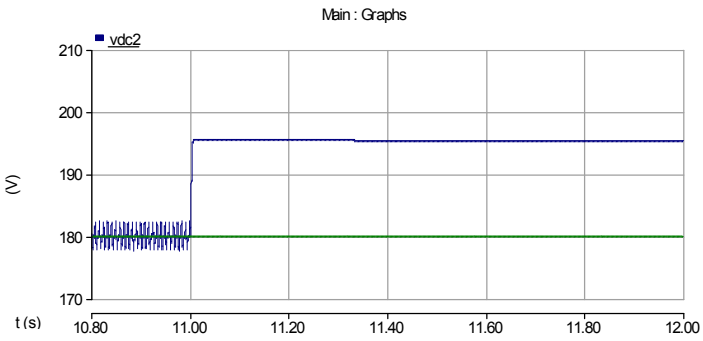

Figure 40. DC link voltage of the power converter providing harmonic compensation during filter turn off.

For the results presented here, the IGBTs were turned off at 11 s. Figure 40 shows that, even under the above conservative assumptions, the DC link voltage build up is minimal. This will always be the case provided the fail-normal switch is implemented with a fast device. Figure 41 displays how the inductor current, after an initial sudden drop, slowly decays to zero and how the current of the filter branch transitions safely to the fail-normal switch.

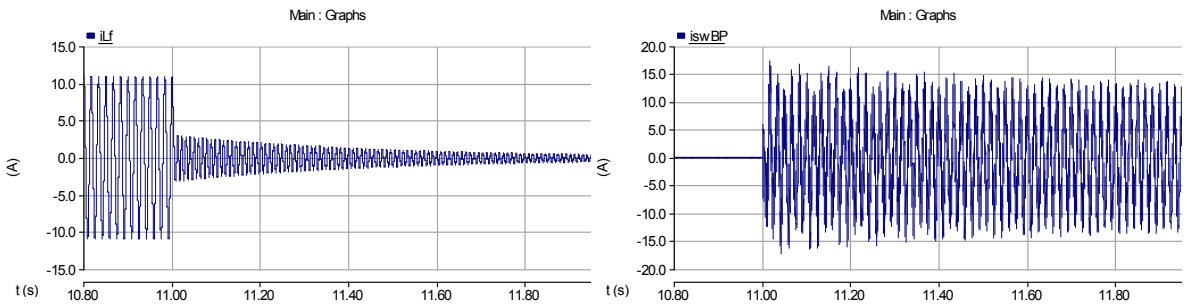

a) b)

Figure 41. Current flowing through a) The filter inductor and b) the fail-normal switch during filter turn off.

Apart from the fail-normal switch and IGBTs, the controller also sends signals to open the switches in the power converter circuits to isolate them from the filter branch. There is no need for these switches to operate as fast as the fail-normal switch, and, in practice, they can be implemented with a much slower technology, possibly with mechanical switches. Here, they were assumed to operate 50 ms after the IGBTs were turned off. When these switches opened, no unwanted voltage spikes across them were observed, as indicated in Figure 42, or elsewhere in the circuit.

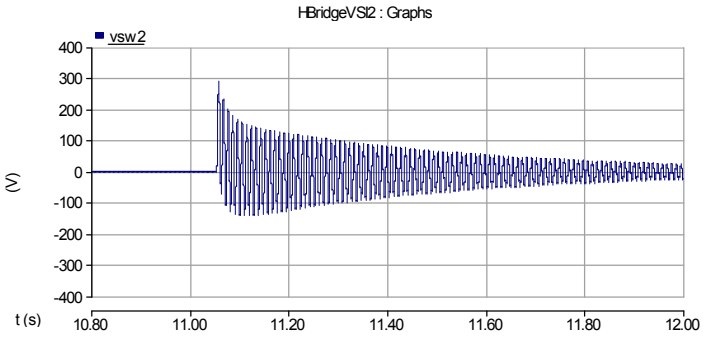

Figure 42. Voltage across S_2 during filter turn off.

These simulation results demonstrate that placement of the switches in the circuit of the MV experimental setup and the design of the shutdown sequence are suitable for

providing adequate protection to the filter components during turn off. This has also been confirmed through the experimental process.

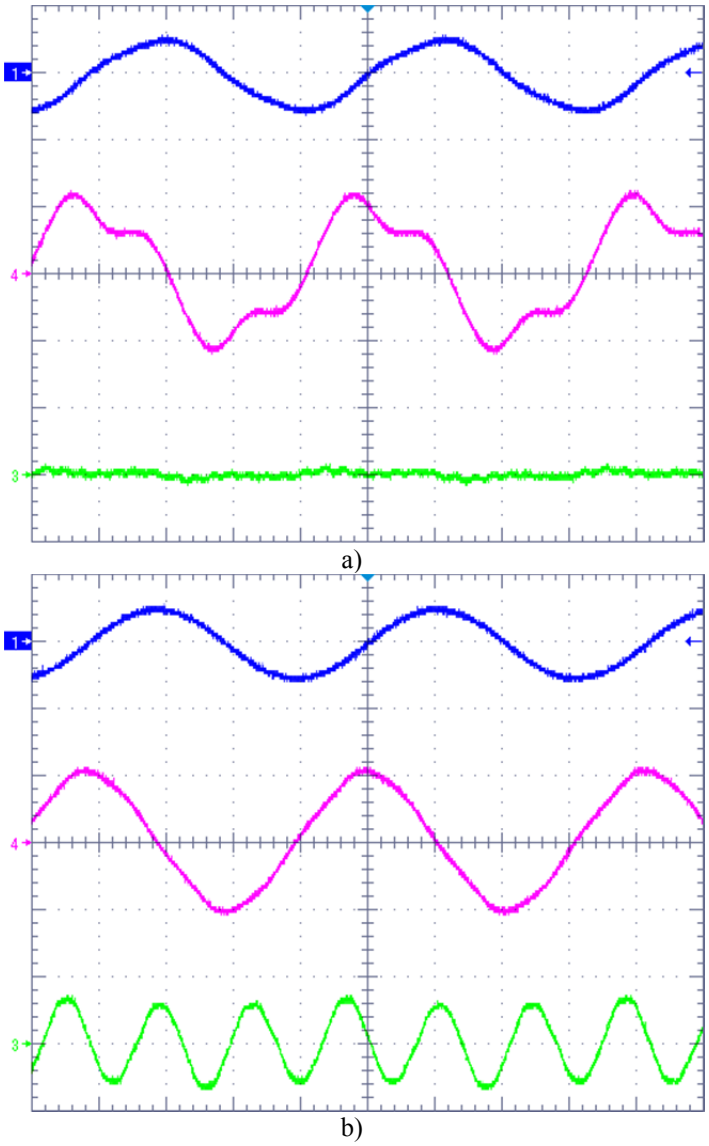

Figure 43. Experimental waveforms of the MV setup a) Before and b) After third harmonic compensation. Ch1: Filter voltage (20 kV/div, blue); Ch3: Output voltage of converter providing compensation (200 V/div, green); Ch4: Line current (10 A/div, magenta); time scale 4 ms/div.

3.2.2 Experimental Results

The MV experimental setup of the proposed third harmonic hybrid active filter was successfully tested at the target voltage of 7.2 kV. Figure 43 exhibits experimental waveforms of the filter voltage, line current, and voltage injected by the power converter providing third harmonic compensation, before and after harmonic compensation was provided. Notice that before compensation the line current was heavily distorted, with some distortion even observed in the filter voltage waveform. However, by generating the appropriate third harmonic voltage, the proposed filter is able to demonstrate good compensation characteristics.

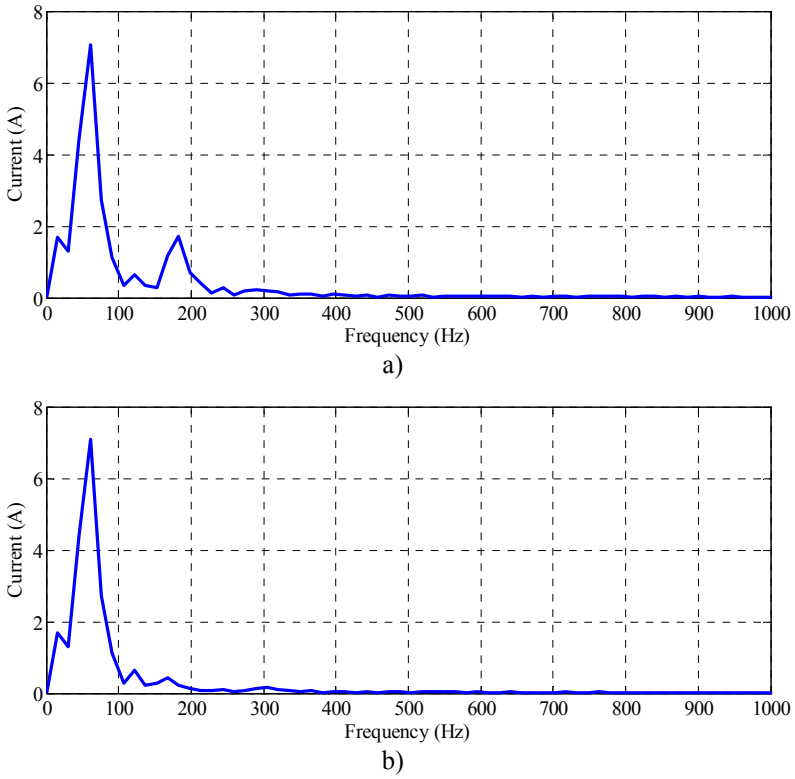

Figure 44. FFTs of the line current a) Before and b) After third harmonic compensation.

The FFTs were computed for the line current waveforms before and after harmonic compensation was provided. The results are compared in Figure 44. Good filtering performance is demonstrated by the proposed filter by reducing the third harmonic line current from 1.7 A (24.3% of the fundamental component) to negligible levels. To accomplish this, the proposed filter only generated about 98 V in the 7.2 kV experimental setup and only required 760 VA, i.e., 1.52% of the 50 kVAR rating of the capacitor bank.

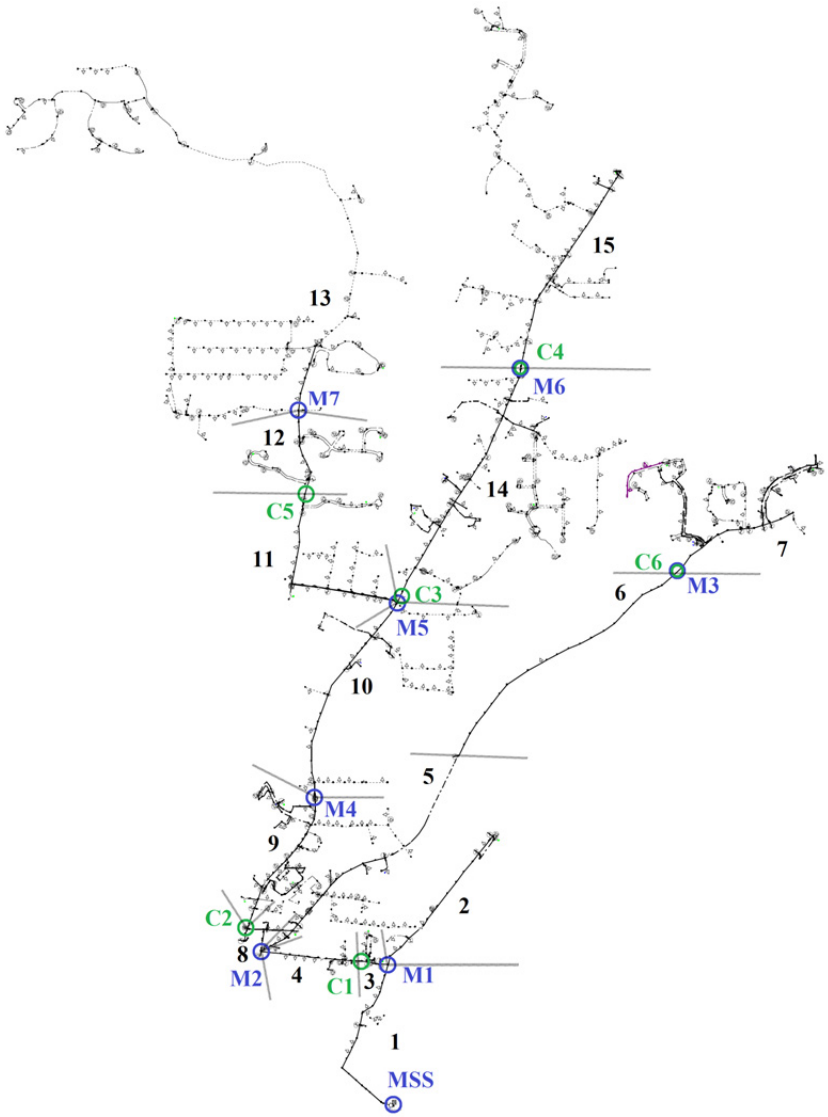

Figure 45. Test case distribution feeder, showing partition, capacitor, and measurement locations.

3.3 System Impact Study on a Typical Residential/Small Commercial Distribution Feeder

A comprehensive system impact study was required to make an adequate assessment of the proposed third harmonic hybrid active filter as a practical filtering solution for MV utility applications. A major requirement to perform such an analysis was to use actual distribution feeder data. To meet this requirement, a NEETRAC utility member provided a detailed model of the actual distribution system shown in Figure 45 to use as a test case for this system impact study. This 12.47 kV system was selected by the utility as a representative distribution feeder serving mainly residential and small commercial customers. The model that was provided consisted of detailed information on the close to 8 mi of three-phase four-wire primary distribution system and includes over 475 loads with an overall maximum designed consumption of 24.1 MVA.

Modeling third harmonic neutral current issues requires the most detailed circuit models for distribution system analysis, except for, perhaps, lightning surge protection analysis. Working with accurate models provides utilities with credible and objective information to quantify third harmonic neutral current related concerns and determine options that will effectively cope with each concern. However, the number and extreme variability of the parameters involved, as well as the need to confirm the model with field measurements, makes developing accurate models an exceptionally challenging process [88]. Because of constantly changing conditions, it results difficult to obtain acceptable accuracies without limiting the flexibility of the model in terms of the number of nodes on the primary distribution feeder [128]. Therefore, a reduced model of the distribution feeder of Figure 45 was developed to achieve a reasonable level of accuracy. The

developed reduced feeder model was validated with phase current and NEV measurements taken along the actual feeder. Finally, this model was used to evaluate the impact of the proposed filter on third harmonic neutral current and NEV reduction. These efforts are discussed in the sections that follow.

3.3.1 Distribution Feeder Modeling

The model of the distribution feeder of Figure 45 was provided as a CYMDIST® self contained study file. There is no single suitable software for modeling every third harmonic neutral current situation. However, since detailed modeling of the proposed filter and its controller are required in the time domain, an electromagnetic transient simulation program was chosen to perform this system impact simulation study. The use of such a software also allows to fully capture the effect of harmonic currents on the system. Unfortunately, CYMDIST® does not provide the capability of performing such simulations or, even more importantly, the modeling of power electronic systems. On the other hand, PSCAD®, the software used for the simulations of the proposed filter presented in Chapter 2, is an electromagnetic transient simulation software and was selected to conduct the system impact study as well. PSCAD® is one of the electromagnetic transient programs recommended in [128] as a suitable modeling software for NEV phenomena.

The CYMDIST® model that was provided for the test case feeder was thus required to be reconstructed in PSCAD®. Since electromagnetic transient simulations are computationally intensive, reasonable assumptions were made to appropriately reduce the feeder model and yield manageable solution times. To accomplish this, all single- and two-phase laterals were aggregated into single point loads. Moreover, the three-phase

circuit of the distribution feeder was partitioned into 15 equivalent line segments, as indicated in Figure 45. These partitions were made according to capacitor placement and locations were measurements were taken along the feeder.

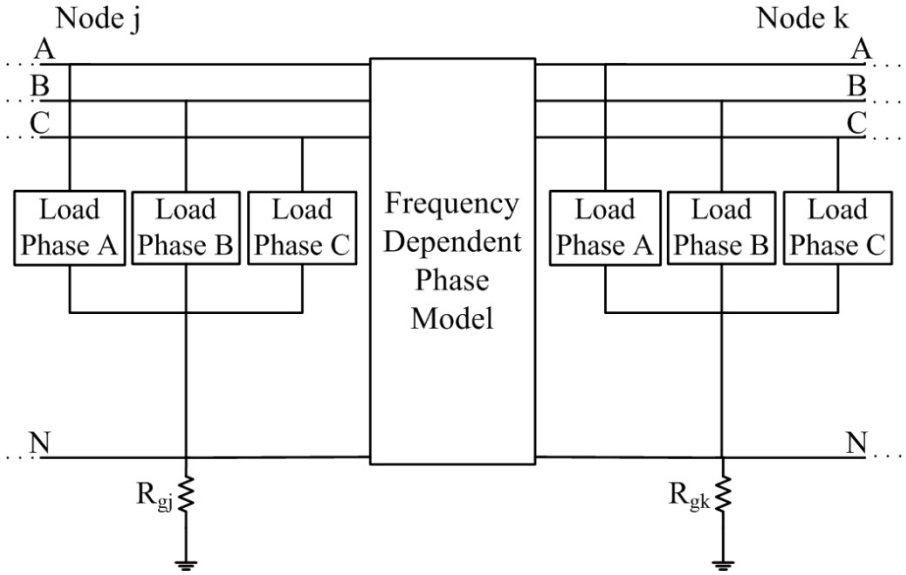

Figure 46. Model used to represent each equivalent line segment of the reduced feeder model.

A schematic of the model that was used to represent each equivalent line segment is presented in Figure 46. Nonlinear loads are generally regarded as harmonic current injection sources into the distribution network. To represent these elements in the reduced feeder model, all loads belonging to a given segment were first aggregated and then divided into two loads placed on either side of the line. Loads of adjacent line segments were summed and modeled using single-phase representations consisting of an RL branch in parallel with harmonic current sources, as was shown in Chapter 2 in Figure 12. This Norton equivalent circuit modeling approach for nonlinear loads is considered suitable and accurate for harmonic system studies [56]. The RL impedance introduces the damping caused by system linear loads [101]. The load model is connected in a

grounded-wye configuration to permit third harmonic currents to flow in the neutral circuit. Since, in general, the grounding resistances are much greater than the neutral conductor impedances, the equivalent grounding resistance of a line segment was assumed to be the parallel combination of all grounding resistances within that particular line segment. All grounding resistances and load parameters of the reduced feeder model were adjusted based on field NEV and phase current measurements.

The overhead distribution lines were modeled using a built-in PSCAD® distributed RLC traveling wave model, known as the Frequency Dependant Phase Model. The Frequency Dependent Phase Model is considered one of the most numerically accurate and robust line models currently available [129]. This model incorporates the frequency dependence of all line parameters and is defined by the configuration of the distribution line itself, including the conductor properties, ground impedance data, and the geometric position of all conductors. Relying on such a model allows to accurately capture the effect of harmonics, unbalanced loads, untransposed lines, and the earth return in the developed reduced feeder model. For the interested reader, the theoretical background of the Frequency Dependent Phase Model is presented in [130], and its actual implementation in the solution engine of PSCAD® is outlined in [131]. In developing the reduced feeder model, a ground resistivity of 100 Ω·m and a relative ground permeability of 1 was assumed. Other major parameters used to construct the model of Figure 46 for each equivalent line segment can be found in Appendix B.

The reduced feeder model that was developed was validated with field measurements taken along the actual feeder. The measurements needed to verify a distribution system model varies with the type of study. In this work, NEV at various pole-down grounds and

phase current measurements taken at the same points were employed. Locations on the feeder where measurements were collected are indicated in Figure 45. NEV readings were made by burying a 4 ft grounding rod as far as feasible into the ground and connecting it to a Fluke® 41B Power Harmonics Analyzer through a 35 ft cable running perpendicular to the distribution feeder. Harmonic current measurements were taken with a SensorLink® Litewire hooked up through a fiber optic link to a Fluke® 43B Power Quality Analyzer. Photographs during moments in which measurements were being taken are presented in Figure 47.

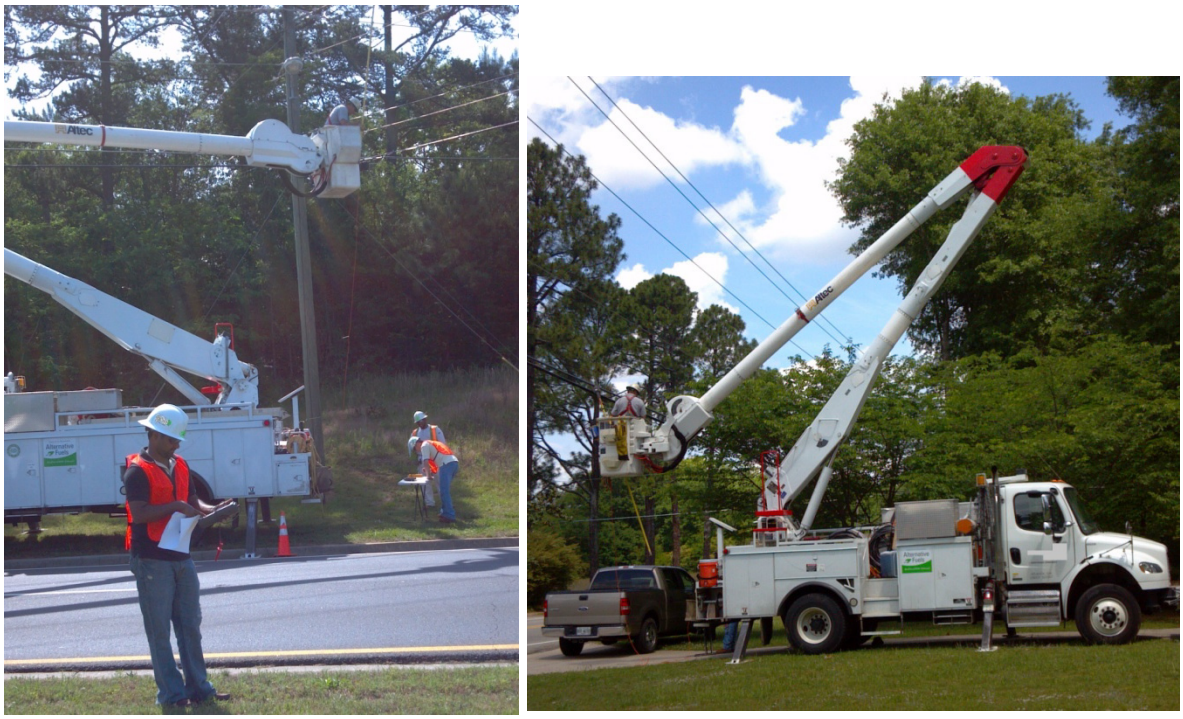

Figure 47. Moments when field measurements were being taken on the test case distribution feeder.

The test case distribution system has six power factor correction capacitors along its primary feeder branches. Locations of these capacitor banks in the actual feeder are indicated in Figure 45. All of them have a 600 kVAR rating, except for C4 which is rated

at 1200 kVAR. It was important to record the connection status of the capacitor banks when the field measurements were being collected to correctly adjust the load parameters of the reduced feeder model. When measurements were being taken, capacitor banks C4, C5, and C6 were connected. Capacitor bank C3 came on line shortly after all measurements were completed. C1 and C2 are manual capacitor banks and were intentionally disconnected before the measurement period.

The filed measurements were taken starting at the substation, during the late morning hours, then at locations increasingly away just as the daily load profile started picking up. This led to situations where some downstream current measurements resulted greater than other measurements taken at upstream locations. So as recommended in [128], the loading data of the substation transformer was recorded for the entire measurement period, as depicted in Figure 48, such that differences in circuit loading could be compensated for in the reduced feeder model. This effect was taken into consideration when validating the model by normalizing the current measurements based on the time they were taken and on the kVA measurements of the substation transformer.

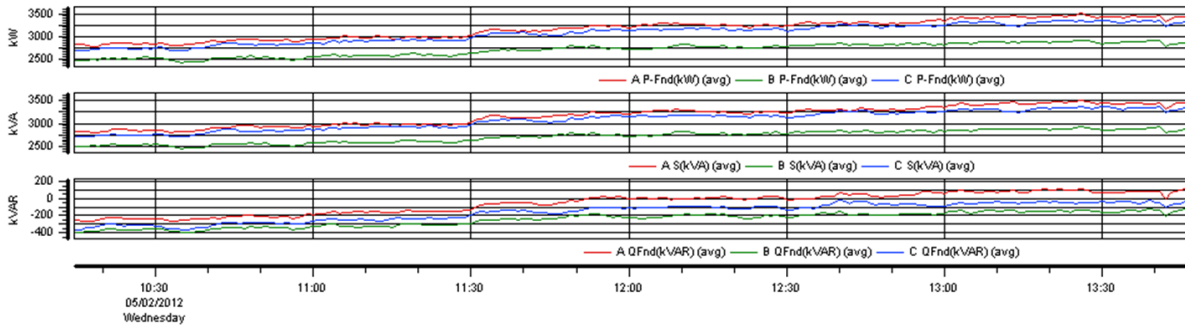

Figure 48. Substation transformer loading data during the field measurement period.

As mentioned previously, the grounding resistances of the reduced feeder model were adjusted to get values close to the NEV field measurements. Likewise, the load factor and load type distribution of individual load models were adjusted so that the fundamental and third harmonic components of the phase currents of the reduced feeder model were comparable to the normalized current measurements. Although neutral current measurements were also taken, these were not employed in this study. The residual current took multiple return paths, including the shield of cable and phone wires, as these are bounded to the neutral conductor at multiple locations. Influence from neighboring circuits was also observed, making these measurements misleading. This gave an indication that fully modeling the neutral return path of a distribution system is a very difficult, if not impossible, task. Therefore, by verifying the reduced feeder model with only phase current measurements, it is implicitly assumed that the residual current only has two return paths, i.e., the neutral conductor and earth, and further neglects the effects of neighboring circuits.

The NEV field measurements are compared to corresponding values obtained from simulation of the reduced feeder model in Table 8. Similarly, in Table 9 the normalized fundamental and third harmonic current field measurements are compared with simulation results. An accuracy within 20% of the base case is regarded as acceptable and accuracies within 10% are considered very good for distribution system models [128]. By limiting the flexibility of the test case distribution feeder to 15 equivalent line segments, an average NEV deviation of 6.90% was achieved in the reduced feeder model with respect to field measurements. In terms of the phase current values, good agreement is observed between the reduced feeder model and the field measurements; except for the

third harmonic components at locations M2 Northeast and M3. A resonant condition created by capacitor bank C6 made the model validation process extremely difficult. In spite of this, good agreement was achieved elsewhere in the circuit. The following section shows results for the main feeder branch, i.e., line segments 1-3-4-8-9-10-14-15. In this branch, average deviations in the fundamental and third harmonic phase currents of 3.93% and 14.10% were obtained, respectively. As observed, the reduced feeder model is in reasonable agreement with field measurements to be employed in the system impact study of the proposed filter.

Table 8. Measured and Simulated NEV Along the Test Case Distribution Feeder

Location	**NEV (V)**		**Location**	**NEV (V)**	
	Meas.	***Sim.***		***Meas.***	***Sim.***
MSS	3.1	3.4	M4	1.2	1.3
M1	1.0	1.2	M5	2.6	2.5
M2	0.9	0.9	M6	1.9	1.9
M3	2.0	2.1	M7	1.2	1.3

3.3.2 System Impact Study Results

Simulation results of the third harmonic neutral current along the main feeder branch are presented in Figure 49. Notice that it increases as it approaches the substation, evidencing its additive nature. The spectrum of the NEV at the substation is exhibited in Figure 50. It is important to note that even though considerable load unbalance is observed in the system, the third harmonic component is almost double of the fundamental. The elevated third harmonic current observed in the neutral conductor poses potential threats to the system, especially as single-phase nonlinear loads in this distribution system continue to increase.

Table 9. Measured (Normalized) and Simulated Fundamental and Third Harmonic Phase Currents Along the Test Case Distribution Feeder

Location	Direction	Phase	Fundamental (A)		3rd Harmonic (A)	
			Meas.	*Sim.*	*Meas.*	*Sim.*
MSS	--	A	364.0	350.1	33.0	30.5
		B	329.0	322.8	31.0	34.4
		C	374.0	373.9	28.6	31.4
M1	North	A	10.5	9.8	0.6	0.6
		B	4.8	4.7	0.2	0.3
		C	5.1	4.9	0.3	0.4
	West	A	347.6	334.5	29.5	28.4
		B	316.9	310.3	28.2	32.8
		C	359.8	359.2	25.7	29.1
M2	Northeast	A	62.7	59.4	2.7	10.3
		B	43.8	44.0	2.1	12.8
		C	57.6	57.9	1.9	10.5
	North	A	268.0	259.9	23.7	20.9
		B	267.1	262.7	22.7	21.2
		C	292.1	292.4	21.0	21.9
M3	--	A	60.9	57.6	0.5	10.3
		B	37.2	37.6	0.8	13.3
		C	32.1	32.2	0.1	12.4
M4	--	A	209.4	202.8	21.2	20.5
		B	219.2	214.0	21.7	21.6
		C	248.8	247.0	20.0	18.9
M5	West	A	113.2	111.6	8.6	8.7
		B	102.2	105.9	8.9	10.2
		C	163.5	164.7	8.0	8.8
	North	A	80.3	71.6	8.8	13.1
		B	84.0	71.3	9.8	14.4
		C	73.0	62.5	8.8	13.2
M6	--	A	43.2	43.9	7.1	7.7
		B	43.2	41.9	7.8	7.8
		C	44.0	45.3	6.6	7.0
M7	--	A	17.1	17.4	0.4	2.5
		B	19.4	20.1	1.0	3.0
		C	30.6	28.9	0.2	4.2

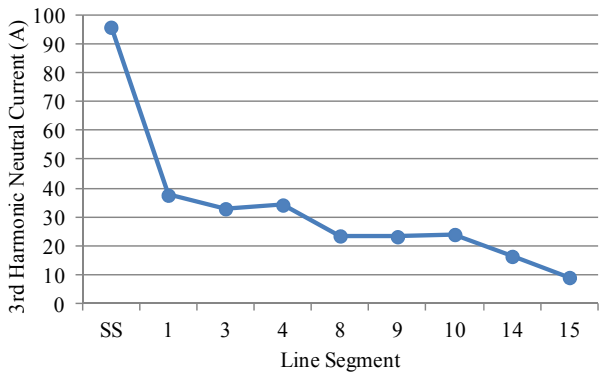

Figure 49. Third harmonic neutral current along the main branch of the reduced feeder model.

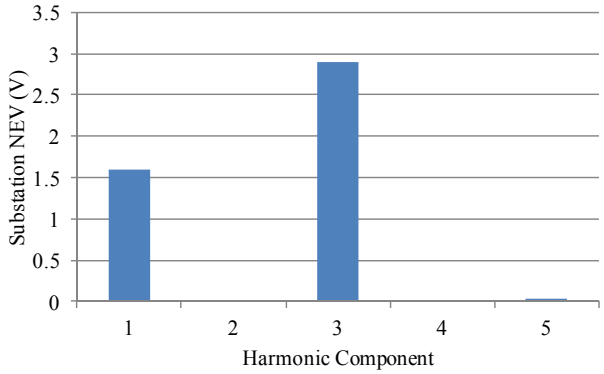

Figure 50. Spectrum of the NEV at the substation of the reduced feeder model.

The capacitor banks on the test case feeder are either fixed or single-step switched banks and thus in theory can be retrofitted into the proposed third harmonic hybrid active filter. Notice that if this is done for a single-step switched capacitor bank, when it is disconnected from the feeder the filter will not provide third harmonic compensation. However, these capacitors are typically connected during periods of increasing load to help regulate the voltage of the feeder. Since third harmonic currents generally increase with the amount of nonlinear load connected to the system, the capacitor would switch onto the system precisely at moments when higher third harmonic compensation is required. Therefore, retrofitting single-step switched capacitor banks into the proposed filter is not discouraged.

Two different scenarios were considered when studying the impact of the proposed filter on the reduced feeder model. For both scenarios the third harmonic neutral current along line segments 1-3-4-8-9-10-14-15 are shown. The fundamental and third harmonic components of the NEV at the substation are also presented. In the first scenario, only the capacitors that were originally connected to the feeder when the field measurements were taken, i.e., capacitors C4, C5, and C6, were assumed to be connected to the feeder. This

case was compared to the situation in which these capacitors were retrofitted into the proposed filter. The results are summarized in Figure 51. Figure 51a shows considerable third harmonic neutral current reduction, especially at the substation where it was reduced from 95.7 A to 53.7 A. The NEV at the substation decreased from 3.4 to 2.3 V. As observed in Figure 51b, all of the NEV reduction at the substation occurs because of the reduction of its third harmonic component.

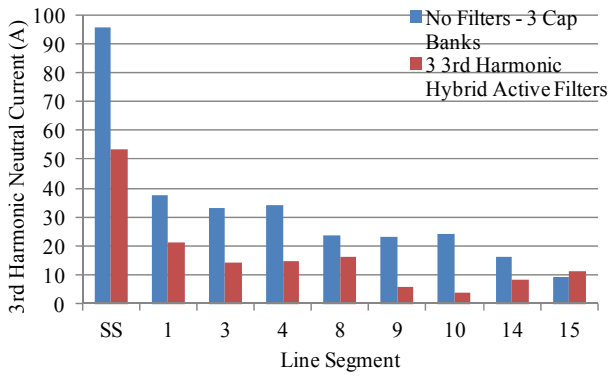

a)

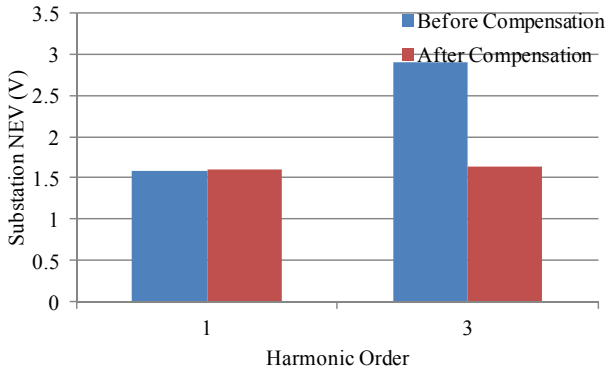

b)

Figure 51. Results for the first filtering scenario: a) Third harmonic neutral current along the main feeder branch and b) Fundamental and third harmonic components of the NEV at the substation.

In the second scenario, it was assumed that all capacitors were connected to the feeder. All other system parameters remained unchanged from the previous scenario. Again, this case was compared to the situation in which all the capacitors were converted

into the proposed filter. Figure 52 summarizes the results. As observed in Figure 52a, the additional filters contribute to a greater reduction of third harmonic neutral current. In this case, this current at the substation decreases from 80.6 to 26.2 A. The NEV at the substation reduces from 3.0 to 1.98 V. Again, this reduction occurs solely because of the reduction of its third harmonic component, as shown in Figure 52b.

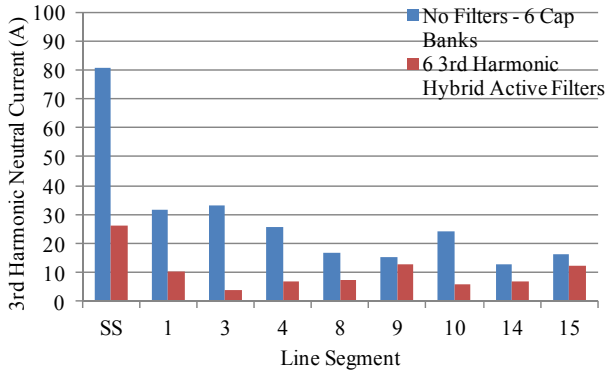

a)

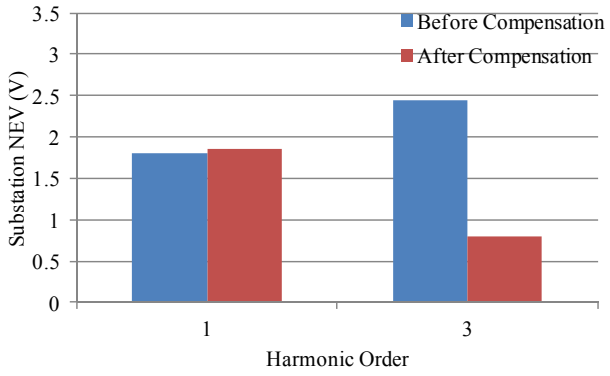

b)

Figure 52. Results for the second filtering scenario: a) Third harmonic neutral current along the main feeder branch and b) Fundamental and third harmonic components of the NEV at the substation.

These preliminary results demonstrate the potential of the proposed third harmonic hybrid active filter in suppressing third harmonic neutral current and reducing NEV in primary distribution systems. The greatest impact of the proposed filter was observed at the substation. This occurs because the proposed filter is designed to mitigate the additive

property of third harmonic currents. Therefore, it is logical to expect that the impact of deploying the proposed filter will become more noticeable as one approaches the substation. At a first glance, it seems that having a greater number of filters on the feeder results beneficial. However, the cost-benefit of adding an additional filter and its system impact are site-specific and must be carefully analyzed.

3.4 SUMMARY

Two experimental implementations were constructed to demonstrate the filtering performance of the proposed filter. Since both implementations were based on a single-phase design, a DC link voltage control loop was included in the controller to take advantage of the fundamental current flowing through the power converter to regulate the voltage across the DC link capacitor. In practice, in a three-phase implementation enough fundamental current may not flow through the power converter, and an external supply may be required. A simple approach of accomplishing this was also discussed in this chapter. The 350 V experimental implementation demonstrated good filtering performance and the directionality feature of the proposed filter. To achieve this result, the power converter only required a fraction of the rating of the load and the LC components. The MV experimental setup was successfully tested at the target voltage of 7.2 kV. A second power converter was included in the filter branch to generate third harmonic current at this voltage level. The power converter providing compensation was able to reduce the generated third harmonic current to negligible levels, while only requiring a fraction of the filter capacitor rating.

Detailed data of an actual residential/small commercial distribution feeder was provided by a NEETRAC utility member to perform a system impact study of the

proposed filter. A reduced feeder model was developed for this test case distribution feeder and validated with field measurements, achieving reasonable accuracy. Results of the system impact study demonstrate that considerable third harmonic neutral current and NEV can be attained in primary distribution systems by deploying the proposed filter. The preliminary results of this chapter thus show the potential of the proposed filter as an effective tool for addressing the anticipated increase of third harmonic currents with the introduction of EVs into residential/small commercial distribution networks.

As discussed in Chapter 1, EVs will not only introduce challenges into power system operations, but will bring a variety of opportunities with them as well. One such opportunity is the flexibility that EV charging could provide to the bulk power system to accommodate greater amounts of highly unpredictable and intermittent renewable energy resources. The following chapter discusses this opportunity in the context of increasing wind power production in day-ahead scheduling operations.

4 MANAGING FLEXIBLE EV CHARGING TO INCREASE WIND PENETRATION

The recent increase of wind power penetration in the U.S., driven by sustainability and environmental efforts, is raising the concern of system operators on how to efficiently and reliably incorporate this stochastic renewable generation resource into power system operations, especially in the day-ahead scheduling process. In this research, the impact of leveraging flexible electric vehicle (EV) charging to balance out the variability and uncertainty of wind power generation is explored.

This chapter begins by presenting the growth of wind power generation in the U.S. over the last decade and its projection into the future, identifying the drivers fueling this growth, and discussing the challenges that this renewable energy source will bring to power system operations. The focus of this work is specifically on the day-ahead scheduling process, also referred to as the short-term planning process. Strategies that have been proposed in the literature to manage high wind power penetration in this power system procedure are also briefly discussed.

The optimal generation schedule to serve a given load demand profile while satisfying system operational constraints is determined through the solution of a unit commitment (UC) problem. A UC problem was developed as part of this research to study the impact of flexible EV charging in systems with high wind penetration. The modeling of flexible EV charging and wind power production in the developed UC framework is discussed in detail. Provisions are made not only to allow for EV load to be flexibly scheduled but for EVs to provide system reserves services if enabled to do so. Also, strategies currently being implemented by U.S. independent system operators

(ISOs) to manage wind power production in their systems, such as employing conservative wind power forecasts and procuring system reserves based on historical wind power forecast errors, are integrated with the developed UC framework.

The developed UC problem formulation is implemented in a MATLAB®/CPLEX® simulation platform. Simulation results are presented for a modified version of the IEEE 39-bus system for varying wind power and EV penetration levels. In this chapter, the cases in which EVs are not and are enabled to participate in the procurement of system reserves are considered. In both cases, the network is assumed to have an infinite transmission capacity.

4.1 BACKGROUND

4.1.1 Increasing Wind Power Penetration

Growing environmental concerns are generating significant public interest in clean energy and have led to the adoption of policies around the world to increase the use of renewable energy. In the U.S., 522.5 TWh of electricity was generated from renewable sources in 2013, 32.1% of which came from wind. When conventional hydroelectric units are excluded, wind represents 66.2% of renewable energy generation [132]. The growth of wind energy generation in the U.S. since 2000 and its projection till 2040 is shown in Figure 53 [1, 133]. Electricity generation from wind has increased from 5.6 TWh at the turn of the century to 160.6 TWh in 2013 and is projected to continue increasing in the next couple of decades. This growth has mainly been fueled by the adoption of renewable portfolio standards (RPS), which requires load serving entities to supply a specified minimum amount of load with electricity from eligible renewable energy sources. As of March 2013, RPS requirements have been established in 29 states, the District of

Columbia, and the U.S. territories [134]. Other initiatives, such as federal and state tax incentives and state renewable energy funds have also contributed to this growth [135]. It is expected that wind will be the most significant component of new renewable generation capacity to be installed in the coming years.

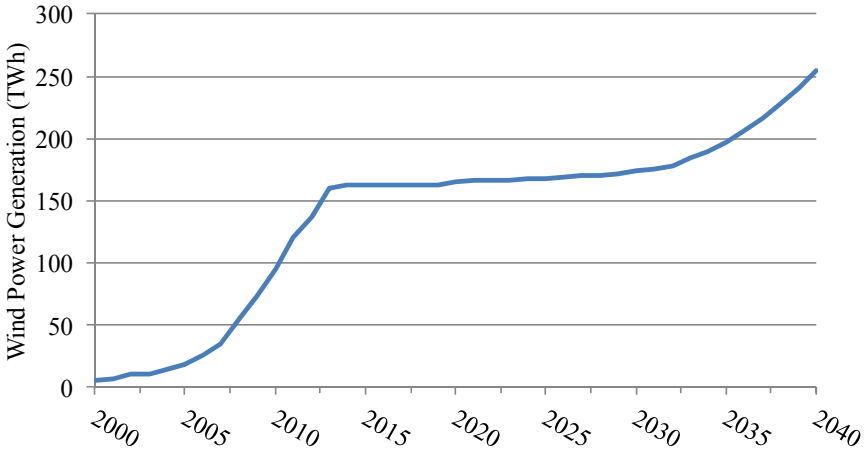

Figure 53. Historical and projected wind power generation in the U.S.

There are significant differences between conventional generation units, whose output are directly controlled by regulating their fuel injection, and wind power plants, which suffer from the inherent unpredictable and variable nature of wind. For this reason, increasing penetration levels of this renewable energy resource is expected to create a unique set of challenges for grid planning, operation, and market processes. These challenges have not been greatly noticeable thus far because the participation of wind generation in the world is still relatively small, except for a few regions, mainly in Europe. This situation will undoubtedly vary as the share of this variable source of electricity continues to increase. The impacts of wind power penetration on power system operations could be divided in local and system-wide impacts. Local impacts happen near the wind farm, such as those that occur on voltage control, fault current, harmonic

distortion, and flicker. System-wide impacts, on the other hand, include load-generation imbalance, transmission congestion, reactive power generation, and reduced frequency control, which are strongly related to the wind power penetration level in the system as a whole [50].

This work concentrates on system-wide impacts affecting power system scheduling and dispatch operations, particularly load-generation imbalance and transmission congestion. Wind power production patterns and electricity demand profiles tend to be negatively correlated for most hours, with peak wind production typically occurring at night during periods of low demand and vice versa for peak demand periods. This causes, for example in the California system, during the load pick-up hours, when load is ramping up and wind generation is decreasing, the need for ramping generation in excess of 10 GW over a 3-hour period to cover the load increase. Similarly, during off-peak hours the system must be capable of ramping down in excess of 12 GW of resources over the same time period [136]. Furthermore, the variability and uncertainty of wind power production creates challenges when operational decisions must be made hours in advance of real-time operation. In particular, an inaccurate wind forecast in day-ahead generation scheduling can result in insufficient commitment of units, resulting in the unavailability of resources to meet load following and regulation requirements. It can also result in the over-commitment of resources, which impacts overall market efficiency and could produce significant wind curtailment [137]. Finally, wind power facilities are preferred to be sited where the most cost-effective resources are located, which are generally not close to major load centers. Therefore, wind energy must travel long distances before being consumed. This situation will contribute to increasing congestion on transmission

systems, which again will negatively impact overall market efficiency and could produce significant wind curtailment.

4.1.2 Managing High Wind Penetration in Day-ahead Scheduling Operations

System operators are already accustomed to dealing with daily load variability and load forecast errors. The increase of wind power penetration levels is, however, raising concerns on how they should properly manage the added variability and uncertainty of this non-dispatchable generation resource, especially in day-ahead scheduling operations. According to [137, 138], the integration of high penetration levels of wind power (greater than 30% in terms of energy) into large existing interconnected power systems will require a proactive step-by-step redesign of existing scheduling, real-time, and market power system operations.

The objective of power system operators should be to have the power system absorb the most amount of wind to achieve the best economic return on wind capacity investment and obtain the environmental benefits intended with current policies. The amount of wind energy that is ultimately absorbed by the power system is limited by the temporal constraints of conventional generation units and the spatial constraints imposed by the transmission network. The most straightforward approach for mitigating this problem is to perform power system infrastructure enhancements, including complementing wind power with more flexible conventional power plants, expansion of the transmission system, and/or the use of utility-scale energy storage technologies. The problem with this approach is that the cost of adding reserve back-up generation or energy storage can increase the total operating cost of wind power systems. According to [139, 140], the additional cost of back-up generation necessary to allow wind power to

reach high contribution levels would increase the cost of wind power by about 15-30%. In a study conducted by the DOE, the costs of new transmission lines required to support only a 20% wind power penetration would already represent about 7% of the total wind power costs [141]. Thus, with such a strategy, the cost reduction of wind electricity caused by up-scaling and technological learning will be counteracted by the cost required for additional generation and transmission capacity and/or any curtailed wind power because of supply-demand imbalance [50].

An alternative approach consists in extending traditional power system tools to account for the variability and uncertainty of wind power such that improved operational decisions are made and existing assets are better utilized. In this sense, two distinct lines of thinking have evolved on how to better manage high wind power penetration in day-ahead scheduling operations. These lines of thinking in essence differ on the way system reserves are computed. The first approach implicitly determines the required system reserves through the solution of a stochastic UC problem, where sufficient generation is committed to account for various possible wind scenarios weighted by their probability of occurrence [142, 143]. The main disadvantage of this method is that the UC problem, which is already in itself a highly dimensional and combinatorial problem, becomes computationally prohibitive when considering an adequate number of scenarios [144]. Because of this reason, such a strategy is not followed in this work. The second approach, on the other hand, is based on utilizing a cost-benefit analysis and wind forecast information to explicitly determine the required level of system reserves [145, 146]. The main disadvantage of this type of approach is that simplifications must be made to estimate the cost of providing system reserves, as this cost is not known a priori, leading

to suboptimal solutions. First steps being taken in the U.S. by ISOs to manage wind variability and uncertainty in their systems, such as the ones discussed below, are more in line with the latter strategy.

The approach explored in this research consists in extending the traditional day-ahead scheduling and real-time dispatch tools to incorporate two technologies that enhance the flexibility of power systems and could become available to system operators in the mid-term future. These two technologies are EVs and power routers (PRs). A more flexible power system will enable a less costly integration of wind power [50].

EVs are an ideal deferrable load, remaining idle 96% of the time [147] and hence can be flexibly charged with undetectable effects to the user. Because of this characteristic, EVs are widely regarded as a resource that could bring relief to the temporal constraints limiting wind power production, if their load is allowed to be flexibly scheduled. The benefits of balancing wind generation with flexible EV charging in this manner have been extensively reported in the literature and are confirmed later in this chapter. In general, additional system reserves are required to accommodate higher wind power penetration. This in turn requires the commitment of additional conventional generation, which defeats emission reduction goals, underpins RPS standards, and could be economically inefficient [137]. Therefore, in addition to flexibly scheduling EV load, added potential exist for EVs if introduced into the system reserves market. The potential benefits of allowing this are also explored in this chapter.

As with wind power, increasing EV penetration levels is expected to aggravate transmission congestion issues. Much of the research surrounding day-ahead scheduling operations in systems with high wind and EV penetration has been limited to variations

of the stochastic UC problem formulation. In an effort to achieve reasonable solution times, most of these studies do not consider the transmission system [148-150], completely neglecting the impact of transmission constraints on achieving the full benefits of matching wind generation with flexible EV charging. The few studies that do consider the transmission system still fail to acknowledge the negative impact of congestion and thus do not propose any solutions to this issue [151, 152]. Therefore, the requirement of relief for the spatial constraints imposed by transmission systems to accommodate higher levels of wind power in day-ahead scheduling operations has not yet been addressed in the literature. This is the subject of discussion of the following chapter, where the impact of PRs as a potential solution is analyzed.

4.2 UNIT COMMITMENT PROBLEM FORMULATION

The large variation of system load throughout a day and the operating constraints of generation units and the transmission network make the day-ahead scheduling of generation resource a crucial task for the economic operation of power systems, in both regulated and deregulated market environments. The problem of optimally scheduling generator start-ups/shutdowns and output levels in each time period to minimize total system operating cost over all units and a time horizon, while satisfying system operating constraints, is commonly referred to as the UC problem [153, 154].

First publications on the UC problem date back to the mid-1960s [155-157]. Since then, the UC problem formulation has been constantly evolving in complexity to address pressing power system issues. For example, one of the latest noticeable variations proposed in the literature is the stochastic UC [158], which would allow system operators to make better decisions when confronted with probabilistic variables. Also, different

solution techniques have become popular over the years for solving the UC problem, beginning with priority-list based methods, followed by more systemic approaches, such as dynamic programming and Lagrangian relaxation, and, more recently, mixed integer linear programming (MILP) and genetic algorithm optimization based methods [153, 154, 159].

The goal of this effort was to develop a comprehensive UC problem formulation so that an accurate assessment could be made on the impact that balancing wind power with flexible EV charging could have on wind power curtailment and total system operating cost. As such, the UC problem presented in this section was developed based on a number of previously proposed UC problem formulations [148, 151, 160-162]. The reviewed UC problems were modified to take into consideration the time the unit has been down prior to the first hour of operation in determining the start-up costs and extended to adequately model the different aspects considered in this work. The developed UC problem is based on a MILP formulation, since the availability of modern software has made this optimization technique an attractive option [163]. Furthermore, it requires a single type of binary variable, to achieve the advantages discussed in [162], and allows for an accurate modeling of the time-dependent constraints of conventional fossil-fuel generation units. A walk-through of the objective function and constraints of the developed UC problem formulation is done in the following sections. For convenience, Table 10 summarizes the nomenclature used in the problem formulation below.

Table 10. Nomenclature Used in the Developed UC Problem Formulation

Symbol	Meaning	Symbol	Meaning
a,b,c	Coefficients of quadratic fuel cost curve of conventional units	RD	Ramp down rate limit of conventional units
D^0	Time a conventional unit has been off before the first hour of operation	RU	Ramp up rate limit of conventional units
D^0_{SUC}	Parameter relating initial downtime with start-up costs of conventional units	r	Level of reserves provided by conventional units
DT	Minimum down time of conventional units	SD	Cost of shutting down a conventional unit
DT^0	Initial time a conventional unit must be off at the start of the operating horizon	SDC	Shutdown cost of conventional units
FC	Fuel cost of conventional units	SDR	Shutdown ramp rate limit of conventional units
I	Status indicator of conventional units	SU	Cost associated with segments of the start-up cost curve of conventional units
i	Index for conventional units	SUC	Start-up cost of conventional units
j	Index for non-EV loads	SUR	Start-up ramp rate limit of conventional units
L	Served non-EV load	s	Index for segments of the fuel cost curve of conventional units
L_D	Non-EV load demand	T	Number of time periods in the operating horizon
M	Slope of segments of the fuel cost curve of conventional units	TOC	Total system operating cost
m	Index for segments of the start-up cost curve of conventional units	t	Index for time periods
N	Number of segments in fuel/start-up cost curves of conventional units	U^0	Time a conventional unit has been on before the first hour of operation
P	Power output of conventional units	UT	Minimum up time of conventional units
$\overline{P}$	Maximum power output of conventional units because of operational constraints	UT^0	Initial time a conventional unit must be on at the start of the operating horizon
$P_{\max}$	Maximum generation capacity of conventional units	ΔP	Width of segments of the fuel cost curve of conventional units
$P_{\min}$	Minimum generation capacity of conventional units	δ	Power level of segments of the fuel cost curve of conventional units
R	Required level of system reserves	ρ	Penalty factor for unserved non-EV loads

4.2.1 Objective Function

The objective of the UC problem is to determine the generation schedule that satisfies the system load over an operating horizon while minimizing the total system operating cost. The total system operating cost, TOC, includes the fuel, start-up, and shutdown costs of the conventional fossil-fuel generation units as indicated in

$$TOC = \sum_{t}\sum_{i}\left[FC_{it} + SUC_{it} + SDC_{it}\right] + \sum_{t}\sum_{j}\rho_{j}\left(L_{D,jt} - L_{jt}\right). \quad (10)$$

Notice that in (10) an additional term was included to account for unserved load caused by insufficient generation or transmission resources. Values for the penalty factor ρ_j can be established based on the value of loss load (VOLL).

In a regulated environment, the fuel cost of a generation unit, FC, in (10) is determined by its input/output curve and its corresponding fuel cost. In deregulated markets, an insight into the fuel costs incurred by conventional generation units to produce electricity can be obtained through the bids power producers present to the market operator. Effective market designs result in competitive market outcomes, with prices reflecting, on average, the marginal cost to produce energy [164]; similar to what occurs in a regulated environment. Therefore, the developed UC problem formulation represents the fuel costs of conventional generation units with quadratic cost curves approximated with piecewise linear functions as shown in (11)-(14) and depicted in Figure 54.

$$FC_{it} = A_i I_{it} + \sum_{s=1}^{N_{si}} M_{si}\delta_{sit} \quad \forall i \ \ \forall t \quad (11)$$

$$A_i = a_i + b_i P_{\min,i} + c_i P_{\min,i}^2 \quad \forall i \quad (12)$$

$$P_{it} = \sum_{s=1}^{N_{si}} \delta_{sit} + P_{\min,i} I_{it} \quad \forall i \ \ \forall t \quad (13)$$

$$0 \le \delta_{sit} \le \Delta P_{si} \quad \forall i \ \ \forall t \ \ s = 1,\ldots,N_{si} \quad (14)$$

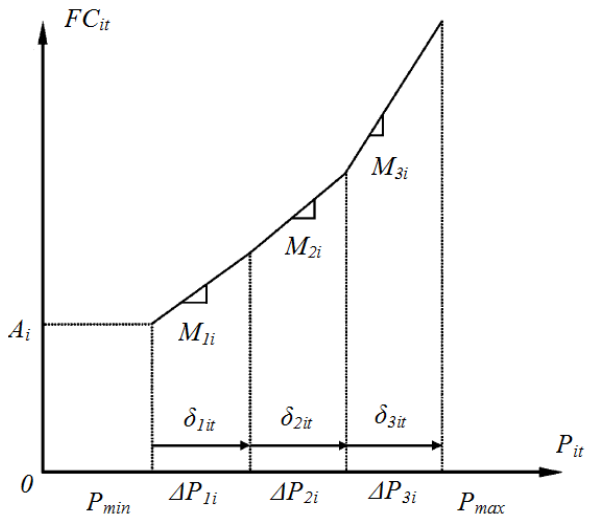

Figure 54. Piecewise linear approximation of a quadratic cost curve of a generation unit.

The start-up cost of a conventional generation unit, SUC, in (10) is generally dependent on the time since the unit was last turned off and is typically modeled with an exponential function [162]. This representation of the start-up cost of conventional units can readily be incorporated in a MILP formulation by approximating exponential start-up curves with stepwise functions, as depicted in Figure 55. By utilizing (15), conventional generation unit start-ups are monitored and the appropriate start-up cost is assigned based on the time the unit has remained off. This start-up cost is restricted to be a nonnegative quantity by (16), and (17)-(18) are included to take into account the time units have been off before the first hour of operation, if this is the case.

$$SUC_{it} \geq \begin{cases} SU_{mi}\left[I_{it} - \sum_{n=1}^{\min(m,t)} I_{i(t-n)}\right], & \text{if } (m < t) \text{ or} \\ & \text{if } \left(m \geq t \text{ and } D^0_{SUC,mit} > 0\right) \\ 0, & \text{if } m \geq t \text{ and } D^0_{SUC,mit} \leq 0 \end{cases} \quad \forall i \ \forall t \ m = 1,\ldots,N_{mi} \quad (15)$$

$$SUC_{it} \geq 0 \quad \forall i \ \forall t \quad (16)$$

$$D^0_{SUC,mit} = D^0_i, \quad m \le t \tag{17}$$

$$D^0_{SUC,mit} = D^0_{SUC,(m-1)it} - 1, \quad m = t+1, \ldots, N_{mi} \tag{18}$$

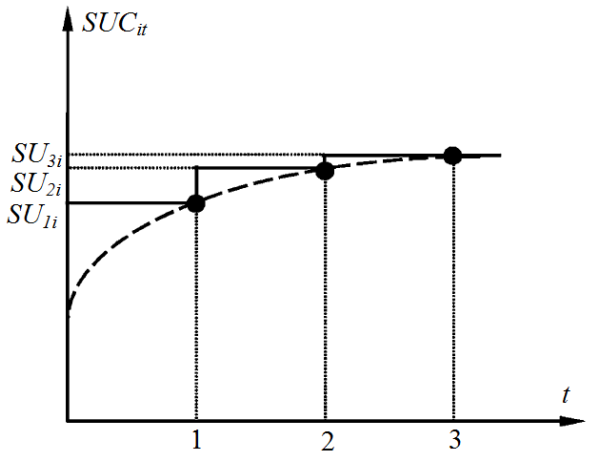

Figure 55. Approximation of an exponential start-up cost curve of a generation unit with a stepwise function.

Sometimes fuel and crew costs may be incurred when shutting down conventional generation units [159]. The hours in which a decision is made to turn a conventional unit off is monitored with (19), and, if applicable, a shutdown cost is assigned to the corresponding unit for those given hours. These shutdown costs are nonnegative quantities, as enforce by (20).

$$SDC_{it} \ge SD_i \left[I_{i(t-1)} - I_{it} \right] \quad \forall i \ \forall t \tag{19}$$

$$SDC_{it} \ge 0 \quad \forall i \ \forall t \tag{20}$$

4.2.2 System Reserves Constraints

The developed UC problem was formulated to include modeling of procurement of system reserves. System reserves products, technical requirements, and terminology vary from market to market [165]. Aspects related to system contingencies are outside of the

scope of this work. Therefore, here system reserves are restricted to the procurement of spinning reserves to account only for load and wind forecast errors. Furthermore, it is assumed that all conventional generation units are capable of outputting the requested amount of reserves in the allotted time, based on their operating limits. Constraint (21) ensures that the system reserves requirements are met at each time period. The amount of reserves a conventional generation unit can provide is dependent on its maximum possible output, $\overline{P}$, which is limited by its maximum generation capacity and ramp rate limits, as indicated in (22).

$$\sum_i r_{it} \geq R_t \quad \forall t \tag{21}$$

$$r_{it} = \overline{P}_{it} - P_{it} \quad \forall i \ \forall t \tag{22}$$

4.2.3 Operational Constraints of Conventional Fossil-fired Generation Units

The operational constraints of conventional fossil-fired generation units include capacity limits, ramp up/down rate limits, and minimum up/down time constraints. Minimum output capability of conventional generation units are generally limited by fuel combustion stability and inherent steam generator design constraints, while maximum output is limited by the maximum designed capability of the turbine [159]. Thus, if a decision is made for a conventional generation unit to be on during a given time period, its output must be limited between its absolute minimum and maximum output levels, as enforced by (23)-(24).

$$P_{\min,i} I_{it} \leq P_{it} \leq \overline{P}_{it} \quad \forall i \ \forall t \tag{23}$$

$$0 \leq \overline{P}_{it} \leq P_{\max,i} I_{it} \quad \forall i \ \forall t \tag{24}$$

Conventional fossil-fired generation units are constrained on the amount their output levels can vary between two consecutive time periods, because of mechanical and thermal stress that produce wear and tear and shorten the life of the units [159]. Constraints (25)-(27) guarantee that the change in the output levels of conventional generation units in two consecutive time periods do not exceed their corresponding ramp up/down rate limits. Notice that an additional pair of ramp rate limits, SUR and SDR, are enforced specifically in instances where units start-up and shutdown, respectively.

$$\overline{P}_{it} \le P_{i(t-1)} + RU_i I_{i(t-1)} + SUR_i \left[I_{it} - I_{i(t-1)} \right] + P_{\max,i} \left[1 - I_{it} \right] \quad \forall i \ \forall t \tag{25}$$

$$\overline{P}_{it} \le P_{\max,i} I_{i(t+1)} + SDR_i \left[I_{it} - I_{i(t+1)} \right] \quad \forall i \ t = 1, \ldots, T-1 \tag{26}$$

$$P_{i(t-1)} - P_{it} \le RD_i I_{it} + SDR_i \left[I_{i(t-1)} - I_{it} \right] + P_{\max,i} \left[1 - I_{i(t-1)} \right] \quad \forall i \ \forall t \tag{27}$$

Certain conventional fossil-fired generation units after they have been turned on/off are required to remain on/off for a minimum amount of time before they can be turned off/on again [159]. Constraints (28)-(31) enforce the minimum up time requirements of conventional generation units, while constraints (32)-(35) enforce their minimum down time. These set of constraints take into consideration the initial amount of time a given unit has remained on/off prior to the first hour of operation.

$$\sum_{n=1}^{UT_i^0} \left[1 - I_{in} \right] = 0 \quad \forall i \tag{28}$$

$$\sum_{n=t}^{t+UT_i-1} I_{in} \ge UT_i \left[I_{it} - I_{i(t-1)} \right] \quad \forall i \ t = UT_i^0 + 1, \ldots, T - UT_i + 1 \tag{29}$$

$$\sum_{n=t}^{T} \left\{ I_{in} - \left[I_{it} - I_{i(t-1)} \right] \right\} \ge 0 \quad \forall i \ t = T - UT_i + 2, \ldots, T \tag{30}$$

$$UT_i^0 = \min \left\{ T, \left[UT_i - U_i^0 \right] I_{i0} \right\} \tag{31}$$

$$\sum_{n=1}^{DT_i^0} I_{in} = 0 \quad \forall i \tag{32}$$

$$\sum_{n=t}^{t+DT_i-1} \left[1 - I_{in}\right] \geq DT_i \left[I_{i(t-1)} - I_{it} \right] \quad \forall i \; t = DT_i^0 + 1, \ldots, T - DT_i + 1 \tag{33}$$

$$\sum_{n=t}^{T} \left\{1 - I_{in} - \left[I_{i(t-1)} - I_{it} \right]\right\} \geq 0 \quad \forall i \; t = T - DT_i + 2, \ldots, T \tag{34}$$

$$DT_i^0 = \min\left\{T, \left[DT_i - D_i^0 \right]\left[1 - I_{i0}\right]\right\} \tag{35}$$

4.3 FLEXIBLE EV CHARGING MODELING

The advantages of flexible or controlled EV charging over an uncontrolled approach have already been thoroughly analyzed in the literature [166-168]. To avoid repeating the same efforts, the case in which EVs are charged in an uncontrolled manner is not considered here. Instead, this research directly delves into the future scenario where EV loads are allowed to be flexibly scheduled and starts by analyzing the implications of this strategy on wind curtailment and total system operating cost for varying levels of EV penetration on the network. For convenience, Table 11 summarizes the nomenclature used in the mathematical expressions presented in this section.

To incorporate flexible EV charging modeling into the developed UC framework, first, the objective function expressed in (10) was extended to include an additional term to account for unserved EV loads, in addition to unserved non-EV loads, because of insufficient generation or transmission resources, as shown below:

$$TOC = \sum_t \sum_i \left[FC_{it} + SUC_{it} + SDC_{it} \right] + \sum_t \sum_j \rho_j \left(L_{D,jt} - L_{jt} \right) + \sum_v \rho_v \left(dayE_{DR,v} - \sum_t L_{vt} \right). \tag{36}$$

Table 11. Nomenclature Used in the Mathematical Expressions for Modeling Flexible EV Charging

Symbol	Meaning	Symbol	Meaning
$CharR$	Maximum charging rate of EVs	L_D	Non-EV load demand
$dayE_{DR}$	Daily driving energy requirements of EVs	R	Required level of system reserves
E	Level of energy stored in EV batteries	r	Level of reserves provided by conventional units/EV loads
E_{DR}	Driving energy requirement of EVs	SDC	Shutdown cost of conventional units
$E_{\max}$	Maximum storable energy in EV batteries	SUC	Start-up cost of conventional units
$E_{\min}$	Minimum storable energy in EV batteries	TOC	Total system operating cost
FC	Fuel cost of conventional units	t	Index for time periods
I_{EVRes}	Indicator of amount of reserves provided by EVs	v	Index for EVs
i	Index for conventional units	η	Charging efficiency of EVs
j	Index for non-EV loads	ρ	Penalty factor for unserved non-EV/EV loads
L	Served non-EV/EV load		

As for penalty factor ρ_j, ρ_v can also be established based on the value of loss load (VOLL). Notice from (36) that while non-EV loads are dispatched according to the required level of demand at each time period, EV loads are dispatched based on the daily energy requirements for driving, hence allowing for flexible EV charging.

The system reserves constraints were also extended for the possibility to allow EVs to provide system reserves services in addition to conventional fossil-fired generation units. To accomplish this, an additional term was included in (21) to account for this possibility in meeting the system reserves requirement, yielding:

$$\sum_i r_{it} + \sum_v r_{vt} \geq R_t \quad \forall t. \tag{37}$$

Also, the following constraint, which captures the amount of reserves provided by EVs, was added to the developed UC problem formulation:

$$0 \leq r_{vt} \leq I_{EVRes} L_{vt} \quad \forall v \ \forall t. \tag{38}$$

If enabled, EVs provide system reserves by adjusting their charging rate from their scheduled charge level to balance out load and wind forecast errors. With all the debate surrounding vehicle-to-grid (V2G) technology, especially the impact that it would have on EV battery life, it was decided to not include this concept in the present analysis. However, the developed UC problem formulation can easily be augmented to model the impact of V2G in future work.

Finally, an additional set of constraints is specifically included in the developed UC problem to manage EV charging. These constraints are given as follows:

$$0 \le L_{vt} \le CharR_{vt} \quad \forall v \ \forall t \tag{39}$$

$$E_{\min,v} \le E_{vt} \le E_{\max,v} \quad \forall v \ \forall t \tag{40}$$

$$E_{vt} = E_{v(t-1)} + \eta_v L_{vt} - E_{DR,vt} \quad \forall v \ \forall t \tag{41}$$

$$E_{v(t-1)} \ge E_{DR,vt} + E_{\min,v} \quad \forall v \ \forall t. \tag{42}$$

As indicated in (39), the charging rate of EVs is limited by the maximum rating of their charging circuits and the amount of time they remain connected to the grid in a given time period. The minimum and maximum limits of the state of charge (SOC) of the EV batteries are enforced with (40). Constraint (41) establishes the relationship between the SOC of the EV batteries and the energy consumed by driving and obtained from charging the EVs. The charging efficiency is taken into account in this constraint. Since the primary purpose of EVs is to serve as a means of transportation to their owners, (42) ensures that all trips in the following time period can be completed with the energy stored in the EV battery in the previous time period. This is an important restriction that often is neglected, as some works in the literature assume that the primary role of EVs will be to support power system operations [148, 149, 169]. Notice that supply of the daily EV

driving energy requirements is accomplished with the unserved EV load penalty term included in (36).

Some implicit assumptions that are commonly made in the literature regarding EV charging are also applied in this work. First, to capture the full flexibility that EVs could provide to the power system, a future scenario in which a universal EV charging infrastructure is in place is assumed. In addition, each considered vehicle driving profile is assumed to represent an aggregation of EVs. Aggregators or load serving entities having control over the charging of a number of EVs, who coordinate the purchase of energy directly with the market operator, is considered a plausible future scenario [30, 47, 170]. Further, it is assumed that system operators have perfect knowledge of when EVs will be connected to the grid, the SOC of their batteries, and future driving patterns. This information could potentially be obtained in the future through prediction efforts or can be given directly by EV aggregators on behalf of the EV owners.

In this project, all EV driving profiles are constructed from light-duty vehicle transportation data made publicly available in the 2009 National Household Travel Survey (NHTS) [171]. The 2009 NHTS was conducted under the sponsorship of the U.S. Federal Highway Administration and serves as the national inventory of daily travel to assist transportation planners, policy makers, researchers, and others who need comprehensive data on travel and transportation patterns in the U.S. The NHTS dataset contains data for 150,147 completed households in the sample, including household, person, vehicle, and daily trip level data collected from March 2008 through May 2009. Data for 1,167,321 trips are included in the dataset. Among the daily trip level data reported in the NHTS are trip purpose, mode of transportation used, travel time, time of

day when the trip took place, day of the week, month, and vehicle attributes. Special care was exercised in using the NHTS dataset by filtering out faulty entries. Only sedans, minivans, and SUVs that traveled less than or equal to 100 mi in the recorded travel day were considered admissible candidates to be treated as EVs [172]. The 24-hour travel day in the NHTS was designated to start at 4:00 AM of the day assigned to a household being surveyed and continued until 3:59 AM of the following day. The reason for this is that, on a typical day, 4:00 AM represents the time when the fewest number of people are traveling, thus allowing the collection of more coherent data on trips [173].

Since the UC problem is generally formulated with a time resolution of an hour, additional assumptions are needed to properly model EV load scheduling. The maximum charging rate of a given EV profile at a particular hour, apart from being dependent on the maximum rating of the charging circuit and scaled by the number of vehicles assumed in the profile, is derated linearly based on the time the vehicle is parked during that given hour. In the same manner, the energy consumed by an EV profile during a particular hour depend on the electrical efficiency of the vehicle type, the number of vehicles considered in the profile, and the miles traveled during that particular hour. If a trip extends over multiple hours, the miles of that trip are distributed proportionally among those hours based on the time the trip took place in each of them. As noted above, the UC tool ensures that the daily EV energy requirement is met and that EVs have sufficient stored energy to complete all of their trips.

Although it is not expected that EVs will vary much their locations on the grid, because of their limited range, when analyzing bulk power systems from the perspective of an ISO, the UC tool was still designed to model EV mobility on the grid. Since the

purpose of this work is not to replicate an actual power system and the NHTS does not provide detailed geographical information on trips, the following simple approach was followed to establish the location of EVs on the grid. At the beginning of the day, the EVs are randomly located at load buses of the system. Because of the reason mentioned above, only limited EV mobility was considered in this work. Therefore, after each trip an EV is allowed to randomly move only among neighboring load buses of the initial location of the vehicle; with the only caveat that the location of the vehicle before and after its first and last trips, respectively, must be the same. To be consistent, driving profiles from the NHTS were filtered to meet this restriction. It is important to notice that, even though the above approach was used to define the mobility of EVs on the grid, the developed UC framework could be employed if actual geographical power system and light-duty transportation data were available.

4.4 MODELING THE EFFECTS OF WIND POWER VARIABILITY AND UNCERTAINTY

To evaluate the impact of EVs on increasing wind power production, the developed UC problem must have the capability of modeling generation from this renewable energy source. For this, the following constraint was incorporated into the above UC problem formulation:

$$0 \le W_{wt} \le W_{Fcst,wt} \quad \forall w \ \forall t, \tag{43}$$

where W is the scheduled wind power production, W_{Fcst} is the wind power forecast used in the day-ahead scheduling process, and w and t are the wind and time period indexes, respectively. Notice that the developed UC problem allows for wind energy to go unscheduled when technically and economically feasible to do so. Now that all

generation sources and loads have been defined, another constraint must be added to ensure that power balance is maintained for each time period, as indicated below:

$$\sum_{i} P_{it} + \sum_{w} W_{wt} = \sum_{j} L_{jt} + \sum_{v} L_{vt} \quad \forall t, \tag{44}$$

where P and L are the scheduled output of conventional generation units and the served non-EV/EV loads, and i, j, and v are the respective indexes used for these variables. It is important to mention that the objective function (36) is not updated with the modeling of wind power production, since to guarantee that the maximum forecasted wind power production could be scheduled, it is assumed that the cost of wind energy production is zero. This assumption is repeatedly made in previous works in the literature [148, 149, 151, 174-176] and is considered reasonable as the variable cost to produce electricity from wind is much lower than that of conventional generation units.

The Eastern Wind Integration and Transmission Study (EWITS) conducted by the National Renewable Energy Laboratory (NREL) [177] provides wind speed data points and plant output values for 1,326 simulated wind plants in the Eastern U.S., as well as next-day, six-hour, and four-hour forecasts for each plant, for 2004, 2005, and 2006. Wind speed data and power output time series for each wind plant were computed by combining a mesoscale model with composite turbine power curves, and other relevant data. Hourly forecasts were synthesized by running a statistical forecast synthesis tool based on Markov chains. Further details on the EWITS project, including modeling tools and input data can be found in [178]. For this research, the next-day forecast of the EWITS dataset was employed. These data contain hourly 24-hour-ahead forecasted maximum and observed maximum wind power production for a given plant. These

hourly wind power output values represent the average expected and observed wind power during each hour.

U.S. ISOs have been charged with the task of integrating renewable energy resources, especially wind, into their electric power systems. Particularly, they have to ensure that these resources provide energy to the system in a manner which is efficient, cost-effective, and, above all, that promotes system-wide reliability. Towards this goal, ISOs have been working diligently for last few years to incorporate wind power forecasts into power system operations. However, the experience with wind power forecasting in power system operations is relatively limited thus far, and strategies are not consistent across regions and are constantly being revised [179]. Still, in evaluating the impact of EVs on increasing wind power production, it was considered interesting to integrate some of these efforts with the developed UC framework. The Electric Reliability Council of Texas (ERCOT), which is the ISO with the highest level of wind power capacity in the U.S.(13.3% effective May 2014) [180], already takes into consideration wind power forecasts in a number of applications and processes. Specifically relating to day-ahead scheduling operations, ERCOT uses conservative forecasts for wind power generation as input to its day-ahead resource planning procedures and considers historical wind power forecasting errors in determining their system reserves requirement [179, 181]. Therefore, these two processes, which are the subject of discussion of the following sections, are implemented in this work.

4.4.1 Conservative Wind Forecasts

Wind power forecast values from the EWITS dataset provide the expected value of wind power production, also referred to as the 50% exceedance forecast. These forecasts

result in observed maximum production values greater than the forecasted amount 50% of the time. Based on current operating practices, under prediction, while economically disadvantageous, does not challenge security, as wind generators may be curtailed if required to avoid adverse effects to the grid. However, over prediction can compromise system security since conventional sources of generation may not be available in time to compensate for the shortage of wind production. Because of this, operators use an X% exceedance forecast, with X > 50, to ensure that sufficient wind energy will be available to maintain system reliability [182]. In an X% exceedance forecast, there is an X% chance the observed maximum wind power production will exceed the forecasted wind power production. Notice that wind energy produced in excess of the conservative forecasted value used in day-ahead scheduling operations can still be transacted in real-time dispatch operations. In some jurisdictions, X is set dynamically based on risk [182]. However, for this effort X is set at different fixed percentages to capture the effects of conservative forecasts on the present analysis.

The method presented in [183] was adapted to produce conservative wind power forecasts from the EWITS 24-hour-ahead forecasts. This procedure is based on representing wind power forecast errors with beta distribution functions and consists of the following steps. First, all maximum observed and forecasted wind power output pairs of a given wind plant are normalized and the (0, 1) pu interval is divided into bins of equal length. The normalized wind power forecast values are then used to determine in which bin to place its corresponding normalized observed wind power output pair. The parameters of the beta distribution, α and β, can now be computed for each bin using the following:

$$\mu_i = \frac{\sum_{n \in N} W_{Obs,n}}{count(N)} \quad \forall i \text{ and } N = \left\{ n : LL_i < W_{Fcst50\%,n} \leq UL_i \right\} \tag{45}$$

$$\sigma_i^2 = \frac{\sum_{n \in N} \left(W_{Obs,n} - \mu_i \right)^2}{count(N)} \quad \forall i \text{ and } N = \left\{ n : LL_i < W_{Fcst50\%,n} \leq UL_i \right\} \tag{46}$$

$$\alpha_i = \frac{\left(1 - \mu_i\right) \mu_i^2}{\sigma_i^2} - \mu_i \quad \forall i \tag{47}$$

$$\beta_i = \frac{\left(1 - \mu_i\right)}{\mu_i} \alpha_i \quad \forall i, \tag{48}$$

where LL_i, UL_i, μ_i, and σ_i^2 are the lower limit, upper limit, mean, and variance, respectively, of bin i. Notice that this creates a beta distribution of the probability of achieving a given observed maximum wind power production for each bin of wind power forecast values. So, the inverse cumulative beta distribution function, as seen in (49), is employed to finally obtain the X% exceedance forecast from the 50% exceedance forecast.

$$W_{FcstX\%,n} = BETAinv\left(1 - \mathrm{X}, \alpha_i, \beta_i\right) \quad \text{for } i, n : LL_i < W_{Fcst50\%,n} \leq UL_i \tag{49}$$

As an example, ERCOT utilizes an 80% exceedance forecast in its day-ahead resource planning procedures [179, 181]. In this case, to comply with ERCOT procedures, X in (49) should be assigned a value of 0.8. A comparison of the observed maximum potential production, the 50% exceedance forecast, and the 80% exceedance forecast for a wind plant in the EWITS dataset is shown in Figure 56.

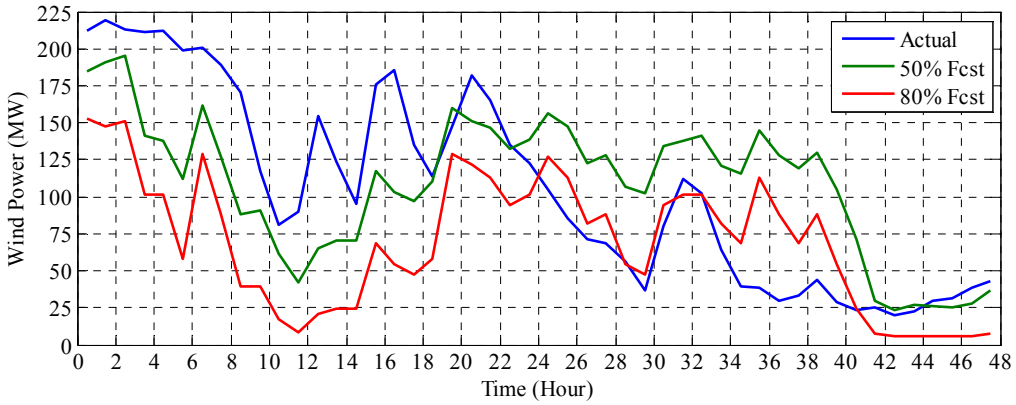

Figure 56. Observed maximum potential wind power output, 50% exceedance forecast, and 80% exceedance forecast of an EWITS wind plant over a 48-hour period.

4.4.2 Procurement of Reserves Based on Historical Wind Power Forecast Errors

The increasing level of wind power penetration has resulted in greater levels of operational risk. Specially, during periods of load pickup , when wind power generation tends to decrease, conventional generation resources are required to increase their output or come quickly on-line to compensate for this effective sudden increase in load. Indeed, the risk of load increases and wind power reductions that are not forecasted exists for all hours of the day. Therefore, methodologies are required for the determination of an adequate quantity of system reserves to mitigate these risks. System reserves and the procedures used to compute them are hence an important aspect when modeling day-ahead scheduling operations in systems with high wind penetration. In general, system reserves are deployed to replace loss of generating capacity, to compensate for load and wind forecast uncertainty, and when there is a limited amount of capacity available for real-time dispatch operations. In ERCOT, a range of different reserves products exists that could be provided by on-line and off-line generation, and demand-side resources [181, 184]. Starting in late 2008, ERCOT began considering wind power forecasts when

determining their system reserves requirement [181]. The method adopted by ERCOT [185], and that was employed in this work, is based on the net load forecast accuracy evaluation summarized in the paragraphs below.

In simple terms, ERCOT takes historical data and calculates a day-ahead net load forecast error. Net load is defined as the observed total system load minus the estimated aggregate potential maximum power output from wind generation resources:

$$netL_{Obs,t} = \sum_{j} L_{Obs,jt} - \sum_{w} W_{Obs,wt} \quad \forall t. \tag{50}$$

Net load cannot be directly forecasted, but load and wind power generation can be forecasted independently and then combined, as indicated in:

$$netL_{Fcst,t} = \sum_{j} L_{Fcst,jt} - \sum_{w} W_{Fcst,wt} \quad \forall t. \tag{51}$$

Net load uncertainty is then defined as the difference between the observed net load and the forecasted net load or, alternatively, as the difference between the load and wind uncertainties:

$$\begin{aligned} netL_{Unc,t} &= netL_{Obs,t} - netL_{Fcst,t} \quad \forall t \\ &= \sum_{j}\left(L_{Obs,jt} - L_{Fcst,jt}\right) - \sum_{w}\left(W_{Obs,wt} - W_{Fcst,wt}\right) \quad \forall t. \end{aligned} \tag{52}$$

The days that are used for this monthly analysis are the last 30 days prior to the study and the days from the same month in the previous year. For the purpose of determining the amount of system reserves that needs to be acquired to compensate for net load forecast errors for each hour of the day during the upcoming month, hours are placed into four hour blocks. The 95th percentile of the net load uncertainty for the analyzed days for all hours which are considered to be part of a four hour block will be calculated. The same calculation is done separately for each block. ERCOT then ensures that system

reserves that are procured for each block will result in a total capacity that is larger than or equal to 95% of the calculated uncertainties in the above net load forecast performance analysis. ERCOT realizes the procurement of this system reserves requirement through three of its system reserves products: the Regulation Service, the Responsive Reserve Service, and the Non-spinning Reserve Service. In this work, the system reserves requirement computed with the procedure discussed in this section is fulfilled with the single level of system reserves considered in the developed UC problem formulation, which was precisely included to compensate for load and wind forecast errors.

Additional analysis is performed to determine if the net load forecast tends to err in a particular direction. The average uncertainty in the net load forecast is calculated using the same days of study and four-hour blocks. If it is determined that the net load forecast on average over-forecasted the observed net load for a four hour block, then the average uncertainty is added back to the system reserves requirement value calculated with the percentile method described in the paragraph above. With this, provisions are made for hours in which the net load forecast is tending to over-forecast.

Furthermore, ERCOT applies a floor to the system reserves requirement to take into account additional factors. While the above net load analysis may cover reserves required for forecast uncertainty, it may not necessarily cover exposure to loss-of-generation contingencies. Because of this risk, it may be necessary for ERCOT to have additional reserves available during high risk hours. However, since in this research contingencies are not considered, a floor of zero is applied to the system reserves requirement calculation.

4.5 NUMERICAL RESULTS: INFINITE TRANSMISSION CAPACITY

A UC tool was developed by implementing the above UC problem formulation in a MATLAB®/CPLEX® simulation platform. MATLAB® was employed to read the input data and construct the objective function and constraints. The resulting MILP UC problem was then solved by invoking the CPLEX® for MATLAB® toolbox functions. For all simulations in this work, a relative MIP gap tolerance of 0.01% was used, and the operation horizon consisted of 24 hours. The conservative wind power forecast and system reserves requirement calculation were also implemented in MATLAB®. To capture the actual wind curtailment that occurs, as oppose to the wind power that goes unscheduled, and the effects of procuring system reserves, the developed UC tool was coupled with a real-time economic dispatch (ED) tool. This real-time ED tool was built based on the developed UC problem formulation, where temporal constraints were removed, and utilizes the optimal generation schedule determined by the UC and observed load and wind power values, instead of forecasted values, as inputs. Post analysis of the results was again realized in the MATLAB® environment.

The test case created for this research is based on the IEEE 39-bus system [186], which represents a reduced model of the power system in New England and has been widely used to study both static and dynamic problems in power systems. The topology of the modified 39-bus test system is displayed in Figure 57. Specific parameters used in this test system are included in Appendix C. In its original form, the IEEE 39-bus system consists of 46 branches, 10 conventional generation units, and 19 loads. For the results presented in this chapter, a single-bus system model is assumed, which is equivalent to assuming that the transmission lines have infinite capacity. Modeling the transmission

network and the negative impacts of congestion are topics covered in the following chapter.

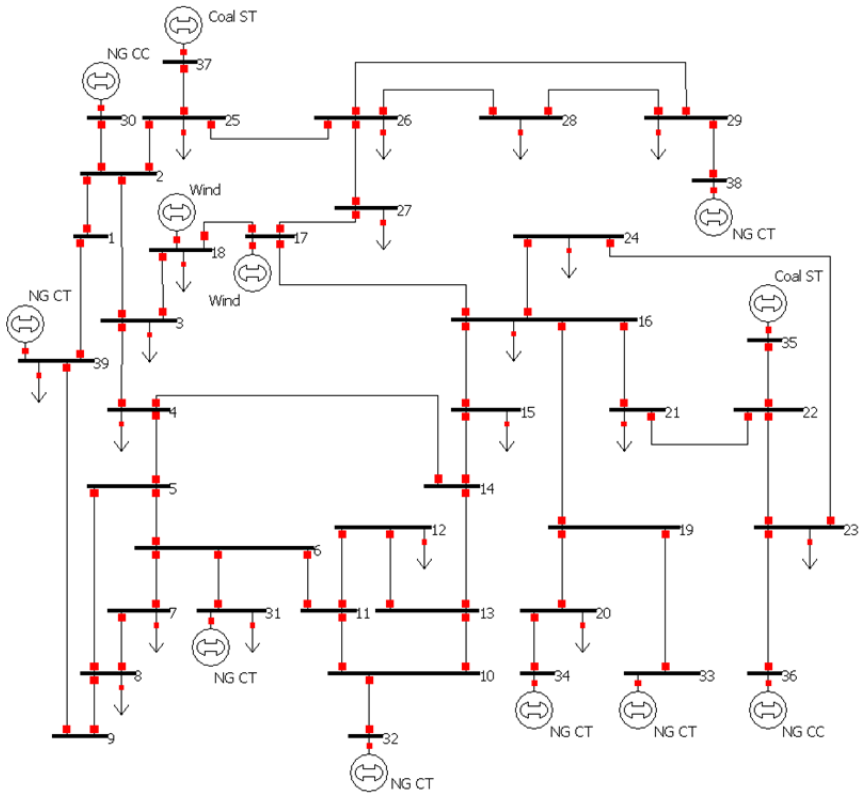

Figure 57. One-line diagram of the 39-bus test system.

The UC parameters of the conventional generation units had to be constructed, since the original IEEE 39-bus system does not provide such information. Three fossil-fired conventional generation technologies were considered in this work: coal steam turbine, natural gas combined cycle, and natural gas combustion turbine generation technologies. Coal steam turbine units were placed at buses 35 and 37, natural gas combined cycle units were place at buses 30 and 36, while natural gas combustion turbine units were placed at buses 31, 32, 33, 34, 38, and 39. UC parameters for these generation technologies, including minimum and maximum power output capabilities, ramp

down/up rates, minimum down/up times, quadratic cost parameters, and start-up costs, were averaged from data obtained from a variety of sources [159, 187-190]. Fuel costs of \$1.943/MBtu and \$6.208/MBtu were assumed for coal and natural gas, respectively, which were obtained from averaging the cost of these fuels for the electric power sector for years 2004 through 2012 published in [132]. The quadratic cost curves of the conventional generation units were approximated in the optimization process with five piecewise linear segments.

The original IEEE 39-bus system only presents a snapshot of the system conditions, meaning that it does not give information on the load variation throughout a day. To account for this, 19 normalized load profiles over a 24-hour period were randomly selected from [191] and then were randomly placed on the load buses of the 39-bus test system. These 19 normalized 24-hour load profiles were first scaled individually base on the load value given in the original IEEE 39-bus system for their respective buses and then scaled as a whole to achieve a typical system reserve margin of 20% [192]. To take into consideration load uncertainty in the day-ahead scheduling procedure and system reserves requirement calculation, it was necessary to construct load forecast profiles. This was done using the method presented in [193]. The forecast load is assumed to consist of the actual load plus an error, which is assumed to follow a Gaussian distribution with zero mean and a standard deviation proportional to the load:

$$L_{Fcst,jt} = L_{Obs,jt} + \varepsilon_{jt}, \tag{53}$$

where $L_{Fcst,jt}$, $L_{Obs,jt}$, and ε_{jt} are the forecasted value, the observed value, and the normally-distributed forecast error associated with load j at time t. Because of the

cyclical nature of the load and the maturity of load forecasting, it is assumed that the standard deviation of the load forecast error is equal to a percentage of the actual load:

$$\sigma_{jt} = \frac{k}{100} L_{Obs,jt}, \tag{54}$$

where k is dependent on the accuracy of the forecasting tool. Here, the value of k was set to 5.04%, which was the average forecast accuracy within NYISO for years 2011 through 2013 [194]. The resulting total system observed and forecasted load profiles are shown in Figure 58.

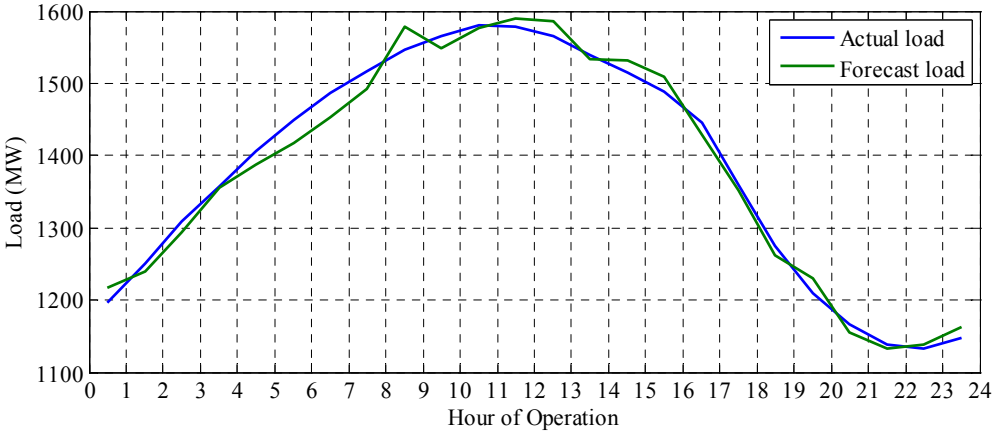

Figure 58. Total actual and forecasted system load.

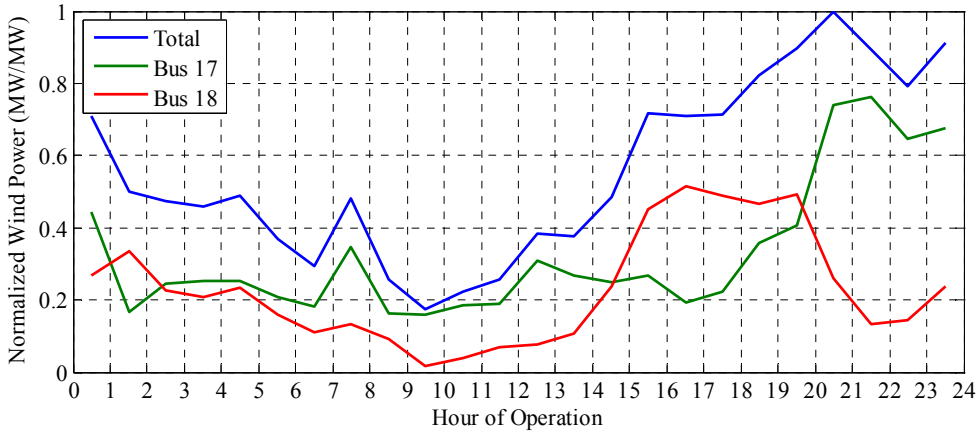

Figure 59. Normalized total actual wind power production and individual production levels of the two wind power plants.

Two wind power plants were located on buses 17 and 18, as indicated in Figure 57, representing a region with high wind penetration. Observed wind power and 24-hour-ahead 50% exceedance forecast profiles for these two wind power plants were taken from the EWITS dataset [177]. The observed total and individual normalized maximum potential wind power production profiles used in this work are shown in Figure 59. Since the intention of this project is to study the impact of flexible EV charging on systems with high wind penetration, different scenarios were considered in which the observed total maximum potential wind power production was scaled to reach 25%, 30%, 35%, and 40% of the daily total system load. As noted in Section 4.4, it was considered interesting to incorporate current strategies that ISOs are taking to manage high wind power penetration in their systems, such as employing conservative wind power forecasts and the computation of system reserves requirement based on historical forecast errors. To capture the effects of the former, six levels of conservative forecasts, 50%, 58%, 65%, 73%, and 80% exceedance forecasts, were utilized in the day-ahead scheduling process. The profiles of these wind power forecasts, together with the total observed maximum potential wind power production, are displayed in Figure 60. Since the system reserves requirement calculation is based on accounting for 95% of the historical load/wind forecast errors, this requirement increases with wind penetration, as depicted in Figure 61. Notice that these two strategies are followed to maintain reliability of supply in face of the variability and uncertainty of wind power production. No unserved non-EV/EV loads were observed in the simulations performed in this work, even for the scenarios in which a 50% exceedance forecast was used in the day-ahead scheduling procedure.

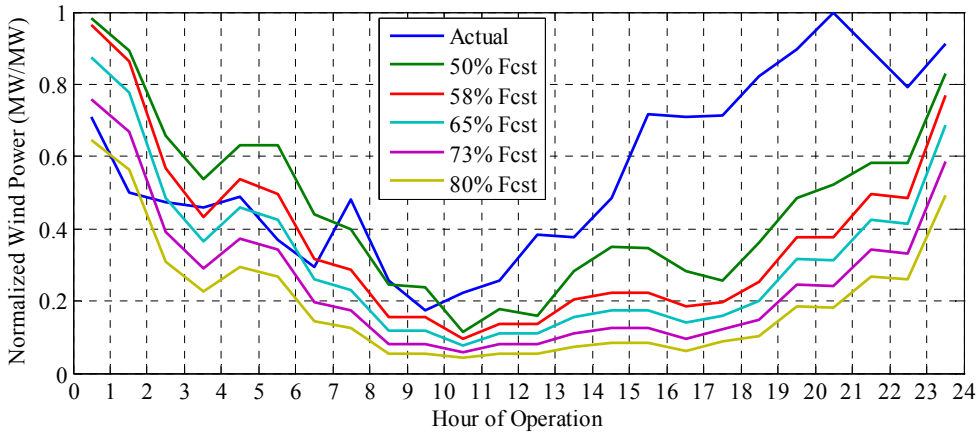

Figure 60. Normalized total actual wind power production and different conservative wind power forecasts.

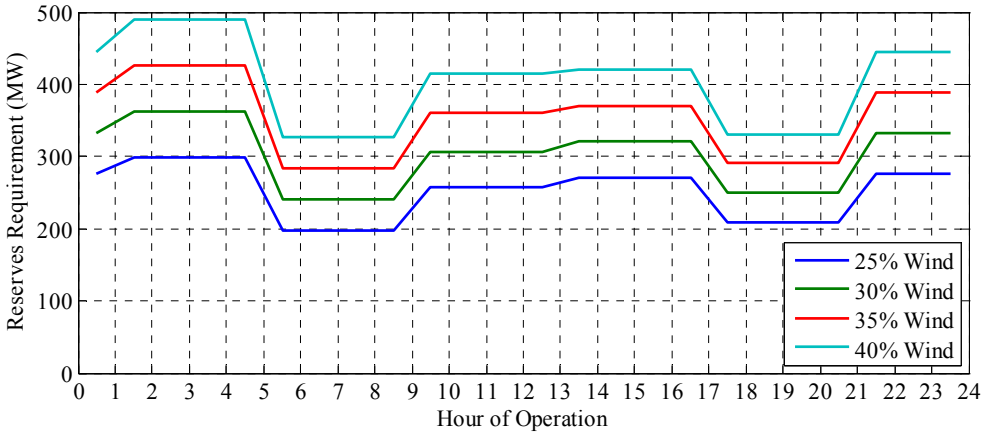

Figure 61. System reserves requirement at different wind penetration levels.

A hundred driving profiles were randomly selected from the 2009 NHTS [171] to account for the variability in driving behavior of vehicle owners. A driving electrical efficiency of 0.25 kWh/mi was assumed for sedans, 0.37 kWh/mi for minivans, and 0.435kW/mi for SUVs [195]. In this work, all EVs were considered to have an all-electric range of 100 mi. It was also presumed that when parked every EV had access to a 240 V, 30 A outlet for an effective maximum charging rate of 5.76 kW. All EV chargers were assumed to have an efficiency of 85%. Different EV penetration scenarios were considered in this analysis. The total number of EVs in the system was determined so that

the aggregated daily EV driving energy requirement represented 0%, 5%, 10%, 15%, and 20% of the daily total system load in each scenario. The total number of EVs was distributed equally among all driving profiles. Finally, to be consistent with the way trip data was collected in the 2009 NHTS, here it was assumed that the 24-hour operation horizon initiates at 5:00 AM. Since the developed UC tool takes into consideration the initial conditions of the conventional generation units and initial charging state of EVs, this assumption results inconsequential. Also, to avoid questions on properly establishing these initial conditions, the UC tool was executed five times, using as input the final conditions of the previous run, prior to the final execution in which results were recorded.

Two flexible EV charging cases are considered in this section. In both cases, EV charging is allowed to be flexibly scheduled; however, in one EVs do not provide system reserves services, while in the other they are allowed to do so. The results for these cases are discussed in the following sections.

4.5.1 Increasing Wind Power Production by Flexibly Charging EVs

The impact of flexibly scheduling EV load on systems with high wind penetration, but without allowing EVs to participate in the procurement of system reserves, is analyzed in this section. In this work, this impact is measured in terms of the amount of wind curtailed and the total system operating cost. But, before delving into the scenarios with EV penetration, results for the situation with no EVs in the system are first presented.

The total wind energy that is curtailed with no EVs as a function of the level of conservative wind forecast used in the day-ahead scheduling process at different wind penetration levels is shown in Figure 62. Notice that this figure indicates the actual

amount of wind power generation that gets curtailed, as oppose to the wind power generation that goes unscheduled in the day-ahead scheduling process. As observed, wind curtailment increases with conservative wind forecasts. This occurs because utilizing conservative forecasts in day-ahead scheduling operations leads to the commitment of additional conventional generation units, since a lower wind power production than expected is made available for this process (see Figure 60). This increases the aggregate minimum operating limits of the conventional generation units, constraining the amount of wind power that can be absorbed by the system. In addition, wind curtailment increases with the level of wind power penetration, as the variability and uncertainty of this generation resource becomes greater at higher penetration levels. The system hence grows incapable of absorbing additional wind power generation as more becomes available.

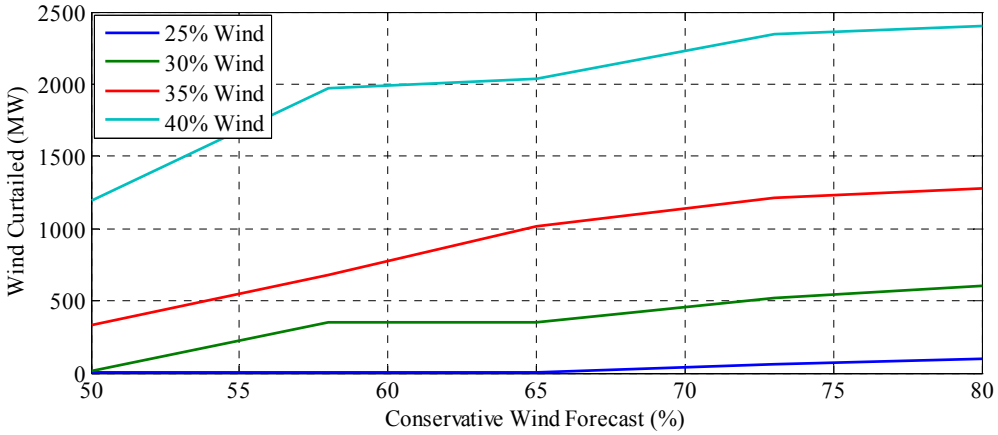

Figure 62. Wind curtailment with no EVs for different wind penetration and conservative wind forecast levels.

The total system operating cost for the case with no EVs in the system as a function of the level of conservative wind forecast employed at different wind penetration levels is

presented in Figure 63. As expected, the total system operating cost increases with conservative wind power forecasts. The reason for this is twofold. First, since wind curtailment increases with conservative wind power forecasts, load energy requirements not fulfilled with inexpensive wind power must be instead met with more expensive conventional generation. Second, conservative wind power forecasts progressively depart from the observed maximum potential wind power generation profile leading to the suboptimal commitment of conventional generation units, specifically the over-commitment of these units, with obvious economic consequences. The total system operating cost decreases with wind penetration, except for a wind power penetration of 40%. This happens because the cost reduction caused by the slightly greater wind power absorption at a 40% wind power penetration gets eclipsed by the commitment of more expensive conventional generation units to meet the higher system reserves requirement at this wind power penetration level (see Figure 61).

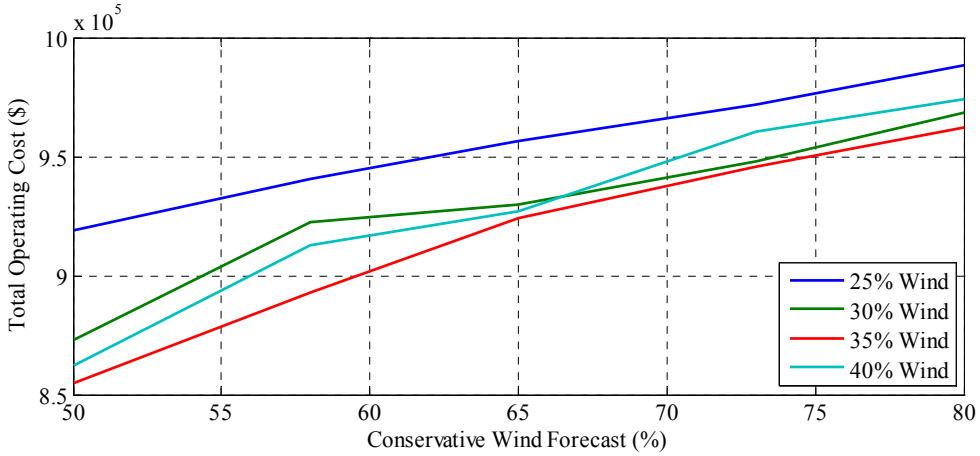

Figure 63. Total operating cost with no EVs for different wind penetration and conservative wind forecast levels.

The benefit of EVs in increasing wind power production when their load is allowed to be flexibly scheduled is clear from Figure 64. Considerable wind curtailment reduction is observed with increasing EV penetration in all considered wind penetration and conservative forecast scenarios. This is a direct result of optimally scheduling EV load to follow wind power availability and balance out the variability of this renewable generation resource. Additional benefits in terms of reducing the cycling of conventional generation units were also observed, as displayed in Figure 65. This could potentially mitigate wear and tear caused by the repeated turning on and off of conventional generation units to cope with the variability of wind power generation, helping extend the life of these units.

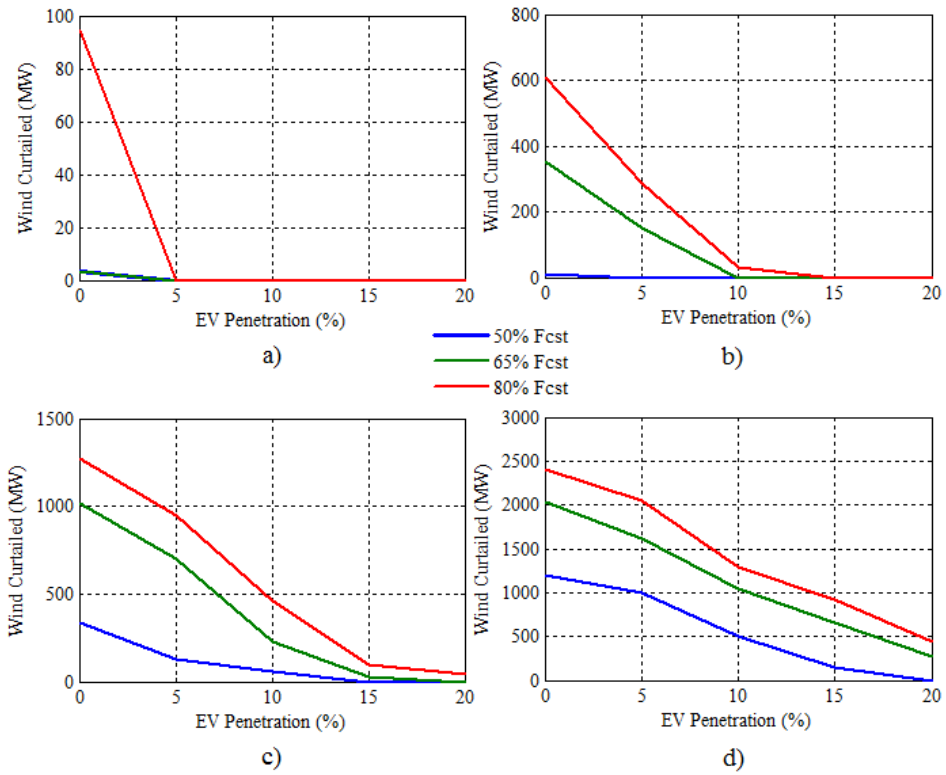

Figure 64. Wind curtailment for different conservative wind forecast and EV penetration levels at: a) 25%, b) 30%, c) 35%, and d) 40% wind penetration.

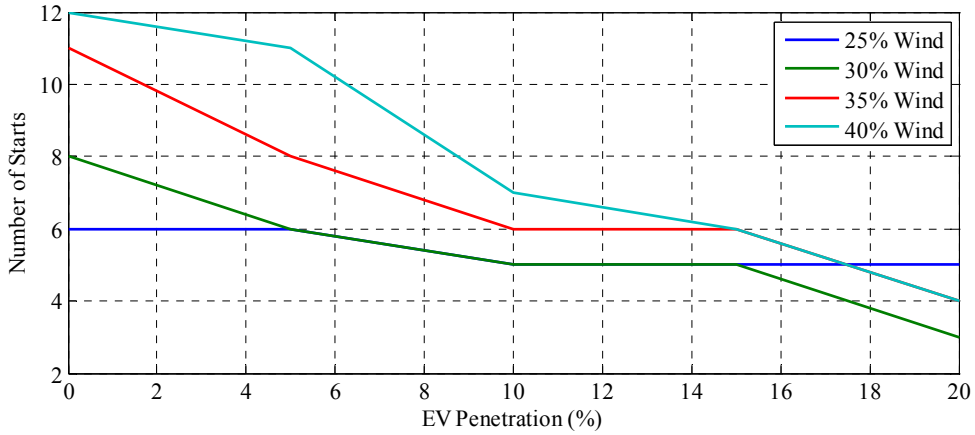

Figure 65. Number of starts of conventional generation units for different wind and EV penetration levels.

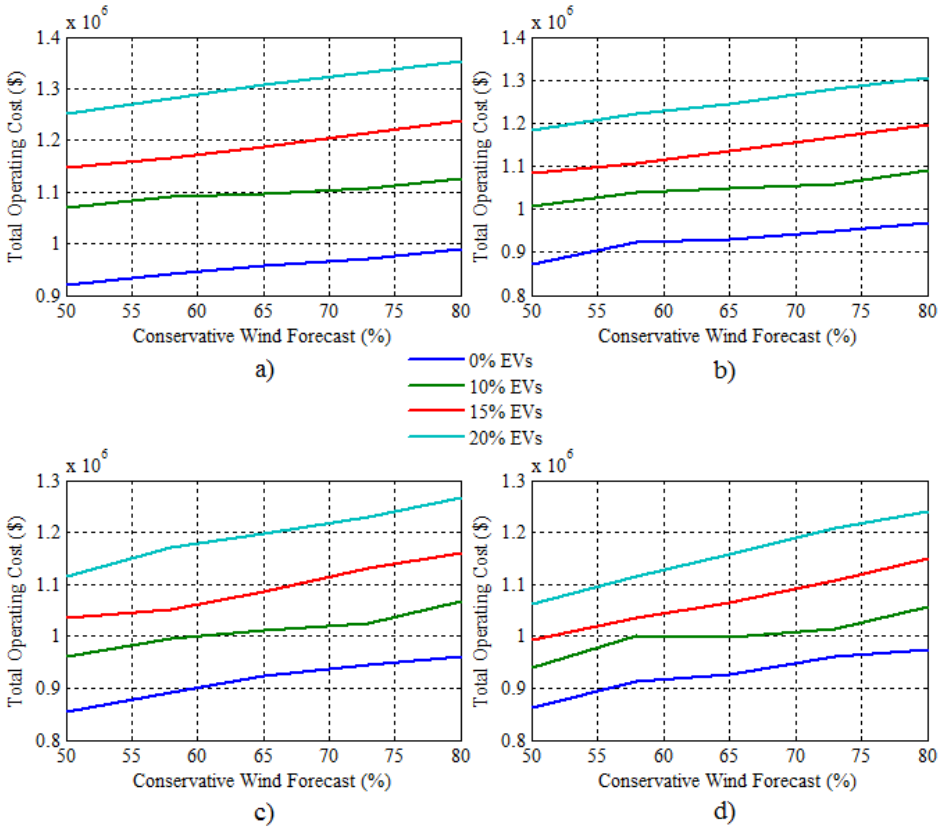

Figure 66. Total operating cost for different EV penetration and conservative wind forecast levels at: a) 25%, b) 30%, c) 35%, and d) 40% wind penetration.

However, a disadvantage of introducing a substantial number of EVs into the power system is evident from Figure 66. EVs are ultimately an electric load that when added to the system will increase the total system operating cost, negatively impacting electricity

prices for all users. This was one of the disadvantages of increasing EV penetration that was identified in Section 1.2 and that is currently a subject of active research. In this case, the increase in total system operating cost is exacerbated because the EV load does not adjust to the actual maximum potential wind power production, as observed in Figure 67, since EVs are not enabled to participate in the procurement of system reserves.

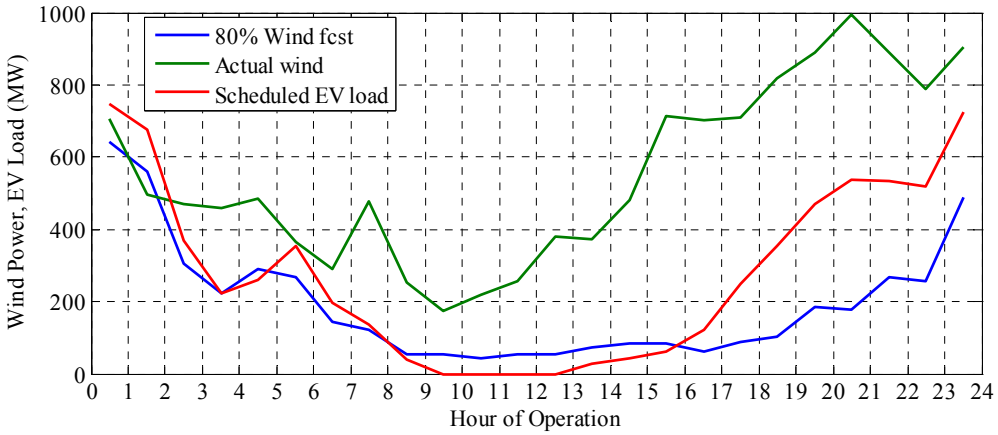

Figure 67. Total actual wind power, 80% exceedance forecast, and scheduled EV load profiles at a wind and EV penetration of 40% and 20%, respectively.

4.5.2 Additional Benefits from Enabling Reserves Provided by EVs

Results are presented in this section for the case in which EVs are not only allowed to be flexibly charged but also to provide system reserves services. As mentioned previously in Section 4.3, in this work it is considered that the deployment of reserves provided by EVs is done solely by adjusting their loads from their scheduled profiles, without supplying electricity back to the grid (i.e., no V2G). In this manner, the amount of the system reserves requirement that could potentially be fulfilled with EVs for a scenario in which wind and EV penetration are 40% and 20%, respectively, is depicted in Figure 68. Recall that in this work system reserves are only procured to compensate for

wind and load forecast errors, but in practice EVs could potentially be employed for other auxiliary services as well, such as reserves for contingencies, frequency regulation, and load following.

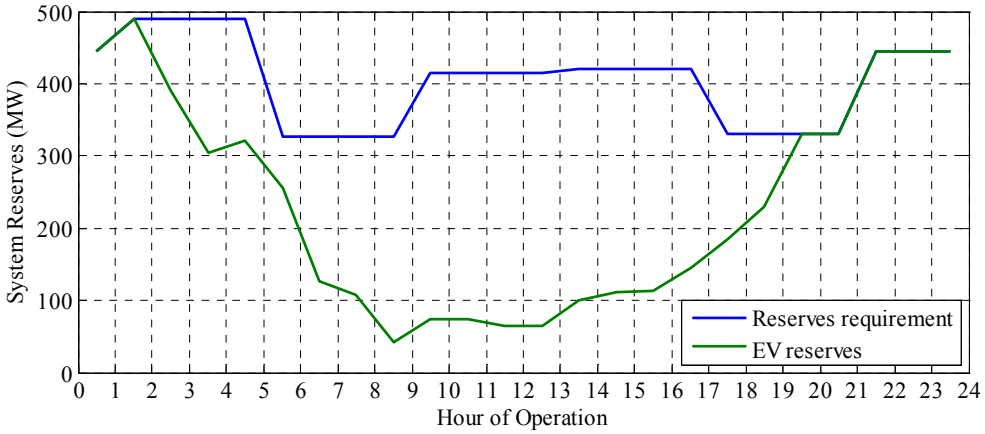

Figure 68. System reserves requirement fulfilled by EVs if enabled at a wind and EV penetration of 40% and 20%, respectively.

The capability of EVs in adjusting their charging profiles to actual wind power generation conditions is shown in Figure 69, which compares the 80% exceedance and observed wind power production profiles and the EV load resulting from the developed scheduling and dispatch tools. As observed, the scheduled and dispatched EV loads tend to follow the trend of the wind power generation profile used as input to their respective power system operation tool. In particular, the real-time dispatch tool in this scenario decides to defer a considerable portion of the total daily EV charging requirement to the latter hours of operation when the highest actual wind power production occurs.

The additional benefit in further increasing wind power production by enabling EVs to provide system reserves is clearly observed in Figure 70, which shows the amount of wind energy that is curtailed as a function of EV penetration and conservative wind

forecast at different wind power penetration levels. As indicated, in this case even with a low EV penetration of 5% wind curtailment was completely reduced in all scenarios, except for a wind power penetration of 40% where the same result is achieved with an EV penetration of 10%. Since a greater amount of inexpensive wind power generation is absorbed by the system compared to the case analyzed in the previous section, positive economic consequences are expected.

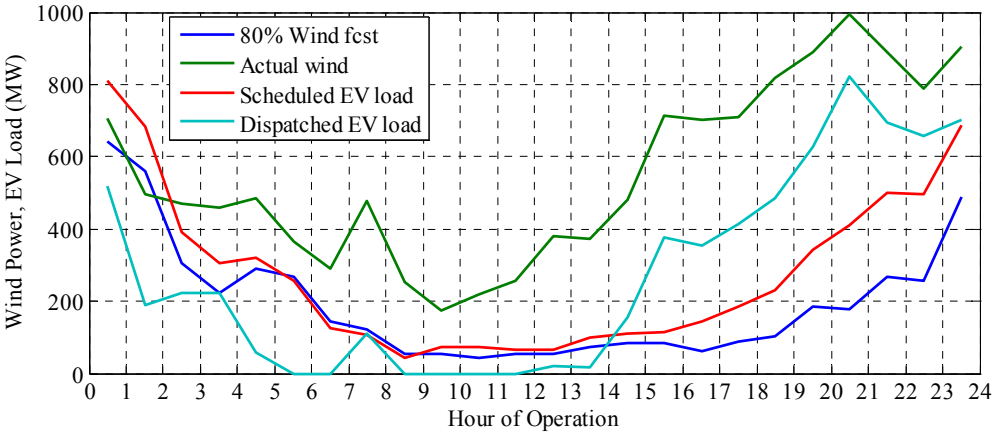

Figure 69. Total actual wind power, 80% exceedance forecast, scheduled and dispatched EV load profiles at a wind and EV penetration of 40% and 20%, respectively.

The total system operating cost as function of conservative wind forecast and EV penetration at different wind power penetration levels is presented in Figure 71. In this figure, the solid blue line represents the total system operating cost with no EVs in the system, the rest of the solid lines represent results for different EV penetrations when enabled to provide system reserves, while the dashed lines are the total system operating costs for the case in which EVs do not provide reserves. Notice that considerable cost reduction is achieved compared to the case of the previous section. In particular, for the scenario of high wind power penetration of 40% and low EV penetration of 10%,

virtually the same total system operating cost is obtained for this case as the case with no EVs in the system. These results demonstrate that flexibly integrating EVs into the day-ahead scheduling process and allowing them to participate in the system reserves market may result in a very cost-effective strategy for incorporating this technology into power system operations. The electricity market design that would develop the rules and pricing mechanisms that would encourage participation in such strategies is outside of the scope of this research. However, EV owners would somehow be compensated, perhaps with cheaper electricity prices for charging, by not having strict time of usage for their driving energy requirements, hence allowing their load to be deferred to support the power system. All this would serve as additional incentives to those discussed in Section 1.1 to further encourage the electrification of a significant portion of the light-duty vehicle fleet.

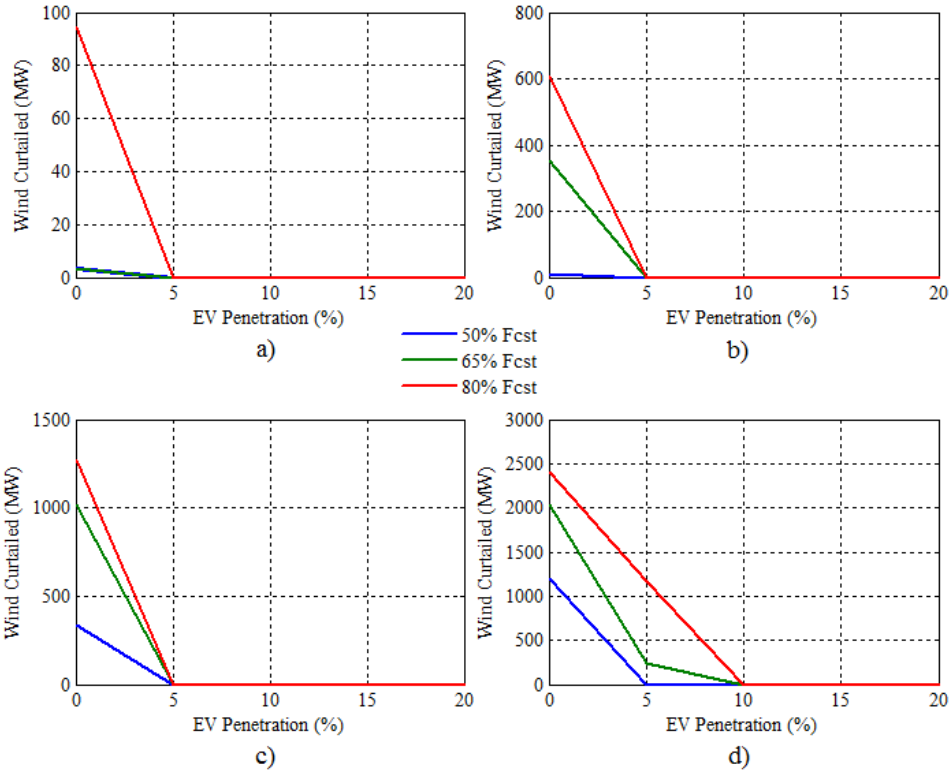

Figure 70. Wind curtailment when EVs are enabled to provide system reserves for different conservative wind forecast levels at: a) 25%, b) 30%, c) 35%, and d) 40% wind penetration.

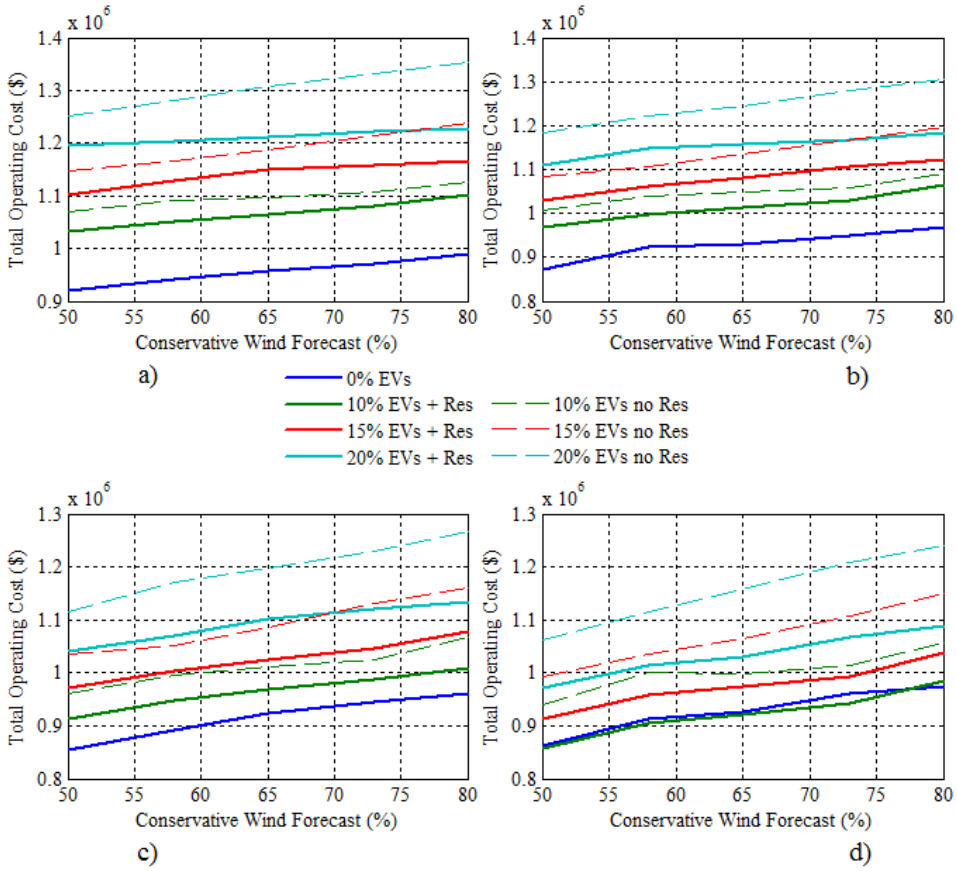

Figure 71. Total operating cost when EVs are and are not enabled to provide system reserves for different conservative wind forecast levels at: a) 25%, b) 30%, c) 35%, and d) 40% wind penetration.

4.6 SUMMARY

Because vehicles remain stationary most of the time, EVs are expected to be an ideal deferrable load that could be flexibly charged, providing a spectrum of opportunities for system operators. One such opportunity was explored in this chapter. Mainly driven by RPS requirements, wind power penetration has increased drastically in the U.S. in the last few years and is expected to continue growing in the decades that follow. The variability and uncertainty of this renewable energy resource makes the determination of the optimal generation schedule a very challenging process. Two purely operational strategies have

evolved in the literature to manage high wind power penetration in day-ahead scheduling operations. One is based on implicitly calculating the required system reserves to account for wind forecast errors through the solution of a stochastic UC problem; while the other is based on explicitly calculating the required system reserves using a cost-benefit analysis. Others, recognizing the potential benefits EVs have to offer, have proposed using this new load type as a resource for balancing out the variability and uncertainty of wind power generation. This is the approach that is studied in this work.

To determine the impact of flexible EV charging on day-ahead scheduling operations in systems with high wind power penetration, a detailed UC problem formulation was developed. The developed UC problem included modeling of the procurement of system reserves, the operational constraints of conventional generation units, flexible EV charging, and curtailment of wind power generation. Provisions were made to allow for EVs to participate in the procurement of system reserves if enabled to do so. Strategies currently being implemented by U.S. ISOs to manage wind power in their systems, such as employing conservative wind power forecasts and determining the system reserves requirement based on historical wind power forecast errors, were also integrated with the developed UC framework. The developed UC problem formulation was implemented in a MATLAB®/CPLEX® simulation platform, and simulations were performed on a modified version of the IEEE 39-bus system.

Simulation results were presented for the cases in which EVs were not and were enabled to provide system reserves in scenarios with varying wind and EV penetration levels. The impact of flexible EV charging was measured in terms of wind curtailment and total system operating cost. Considerable wind curtailment reduction was observed

for the case in which EVs were flexibly charged but were not enabled to participate in the procurement of reserves, demonstrating the benefits that this type of flexible load has on balancing the variability of wind power generation. However, since EVs ultimately represent additional electric load to the system, results for this case show a substantial increase in the total system operating cost with the introduction of EVs, which in turn would negatively impact electricity prices. On the other hand, when EVs are enabled to provide system reserves, greater wind curtailment reduction is achieved, considerably reducing the total system operating cost compared to the previous case. These results point to a potential cost-effective mechanism for incorporating flexible EV charging into power system operations.

It is important to mention that the effects of including the transmission network in the developed modeling framework, and hence the impact of transmission congestion, on perfectly balancing flexible EV charging with wind power generation was not considered in this chapter. Indeed, the increase in wind power and EV penetration levels is expected to aggravate transmission congestion issues, if the integration of these new highly dynamical energy sources and loads continue to outpace transmission system upgrades. The possible impact of transmission congestion on achieving the maximum benefits of balancing the variability and uncertainty of wind power production with the flexibility of EV charging is shown in the next chapter. A potential solution, based on augmenting the flexibility of the transmission network, is also proposed.

5 TRANSMISSION CONGESTION RELIEF TO FACILITATE EV-WIND BALANCING

In Chapter 4, the benefit of flexible electric vehicle (EV) charging in increasing wind power production was analyzed. Additional benefits in terms of further wind curtailment reduction and lower total system operating costs were determined if EVs were enabled to provide system reserves services. However, this analysis neglected a very important aspect in day-ahead scheduling and real-time dispatch operations: the effects of transmission constraints.

In this chapter, the effects of incorporating the transmission network in the developed unit commitment (UC) framework, specifically the impact of transmission congestion on achieving the maximum benefits of EV-wind balancing, are studied. This chapter begins by providing an overview of transmission congestion, including its origins and potential consequences. Modeling of the transmission network in the developed UC problem formulation is also discussed. The resulting scheduling and dispatch tools are applied to the 39-bus test system to quantify the benefit reduction caused by transmission congestion compared to the case covered in Section 4.5.2.

The most straightforward approach for alleviating transmission congestion is to build new transmission lines. However, much uncertainty surrounds the development of new transmission projects, owing to their elevated cost, long lead times, problems with the acquisition of the required real estate, and outdated and ineffective transmission investment policies. Because of this, an alternative approach consisting in adopting methods to improve the utilization of existing transmission assets are strongly being considered. This is the option explored in this chapter by employing power routers (PRs)

to alleviate transmission congestion. PRs are devices capable of rerouting power flows in the grid from heavily loaded lines to parallel lightly loaded transmission paths. Modeling of the functionality of these devices was included in the developed UC problem formulation. The final integrated day-ahead scheduling framework was applied to the 39-bus test system to show how PRs can facilitate EV-wind balancing in congested power systems.

5.1 TRANSMISSION CONGESTION

At the beginning of the electric power industry and for most part of the last century, the transmission network was conceived as a radial connection from energy generation to loads. However, as electricity became a basic infrastructure requirement, the reliable delivery of electricity became a major performance metric. To achieve higher reliability figures, utilities gradually moved from a radial structure to a more meshed network. A meshed system provides alternative paths of energy delivery from source to load in case of a fault, thus enhancing the system reliability. However, the increased reliability came at the cost of lower controllability. Furthermore, with deregulation, the U.S. transmission network has been effectively converted into an interstate highway system for wholesale electricity commerce. Increased competition in the wholesale electricity market has led to operating the power grid closer to its operational limits. Because of the inherent asymmetry of the path impedances of meshed networks, power flows through the parallel paths are unevenly distributed, causing asymmetrical stress on transmission assets, in turn giving rise to undesired effects, such as uneven line loading, loop flows, and transmission congestion.

Transmission congestion occurs on electric transmission facilities when actual or scheduled flows of electricity across a line or piece of equipment are restricted below desired levels [196]. In meshed transmission networks, this starts happening when the first line reaches its physical limits. The situation worsens when the N-1 or N-2 contingency scenarios are accounted for, whereby the power system is required to operate safely even with one or two of the worst possible contingencies. In such cases, lower operational limits are established to protect the security and reliability of the grid. All this leads to the underutilization of transmission assets. In 2010, the transmission asset utilization rate in the U.S. was reported at 43% [197]. Despite this low transmission asset utilization, the U.S. Department of Energy (DOE) has identified several congestion areas of concern in the Eastern and Western Interconnections [196]. In fact, in the Eastern Interconnection, Level 5 Transmission Loading Relief (TLR) procedures, the most critical process to mitigate operating security limit violations, have increased from 8 in 2000 to 43 in 2005 and 286 in 2012 [198], signaling an important increase in transmission congestion during the last decade.

Because power purchasers typically try to buy the least expensive energy available, when transmission congestion limits the amount of energy that can be delivered to load centers or exported from generation-rich areas, real economic consequences are imposed upon energy consumers. As an example, in 2008 PJM and NYISO experienced annual congestion costs of about $2.1 and $1.4 billion, respectively [199, 200]. In more severe congestion conditions, transmission constraints can impair grid reliability by reducing the availability of generation resources and rendering the area more vulnerable to system

outages. Because of these reasons, a general interest exists on alleviating transmission congestion.

5.2 MODELING THE TRANSMISSION NETWORK

In order to evaluate the impact of transmission congestion and the effectiveness of a potential solution to this issue in the day-ahead scheduling procedure, it is necessary to include a representation of the transmission network in the UC problem formulation that was developed in Chapter 4. The current industry practice is to model the transmission system in day-ahead scheduling operations using the DC power flow formulation, because of the high dimensionality and combinatorial nature of the UC problem [179]. The DC power flow formulation provides a linear description of the transmission system and only considers real power flows, while disregarding the effects on voltage magnitudes and reactive power flows [159]. Following this industry practice, the power flow constraints included in the developed UC problem formulation are as follows:

$$\sum_{i \in B_b} P_{it} + \sum_{w \in B_b} W_{wt} = \sum_{j \in B_b} L_{jt} + \sum_{v \in B_b} L_{vt} + \sum_{l \in B_{b=frBus} \cup B_{b=toBus}} LF_{lt} \quad \forall b \; \forall t \tag{55}$$

$$\theta_{(b=slack)t} = 0 \quad \forall t \tag{56}$$

$$LF_{lt} = \frac{\left(\theta_{(b=frBus)t} - \theta_{(b=toBus)t}\right)}{X_l} \quad \forall l \; \forall t \tag{57}$$

$$-LF_{\max,l} \le LF_{lt} \le LF_{\max,l} \quad \forall l \; \forall t \tag{58}$$

Table 12 summarizes the nomenclature used in the above mathematical expressions. Constraint (55) ensures that the power balance at each bus for all time periods of the operation horizon is maintained. The phase angle of the slack bus is set to 0º with (56).

The power flow in each transmission line is determined by (57). Constraint (58) enforces the power flow capacity limits of the transmission lines.

Table 12. Nomenclature Used in the Mathematical Expressions for Modeling the Transmission System

Symbol	Meaning	Symbol	Meaning
B	Set of elements connected to a bus	P	Power output of conventional units
b	Index for buses	t	Index for time periods
i	Index for conventional units	v	Index for EVs
j	Index for non-EV loads	W	Power output of wind power plants
L	Served non-EV/EV load	w	Index for wind power plants
LF	Power flow in a line	X	Reactance of a line
$LF_{\max}$	Maximum power flow capacity of a line	θ	Bus voltage phase angle
l	Index for transmission lines		

5.3 Numerical Results: Benefit Reduction Caused by Transmission Congestion

The impact of transmission congestion on achieving the maximum benefits of optimally balancing the variability and uncertainty of wind power generation with flexible EV charging is presented in this section. The same 39-bus test system described in Section 4.5 is utilized for this analysis, with the exception that in this case the transmission system is not assumed to have an infinite capacity. Since the main objective of this section is to determine the impact of transmission congestion on the maximum benefits of flexible EV charging, it is assumed that EV load is allowed to be flexibly scheduled and EVs are enabled to participate in the procurement of system reserves.

In its original form, the IEEE 39-bus system does not provide capacity limits for the transmission lines; therefore, a mechanism had to be developed for establishing these operational restrictions to be able to demonstrate the effects of transmission congestion. In this work, the capacity limits of the transmission lines were established based on an

optimal power flow (OPF) analysis performed on the base case of the 39-bus system for the peak loading condition. The capacity limits of transmission lines 3-4 and 15-16 were set at 80%, and that of line 17-27 was set at 100% of their respective power flows resulting from this analysis. These three lines are the bottleneck of the 39-bus system considered in this work. The capacity limits of the rest of the transmission lines were established such that the maximum power flowing through each respective line of all the considered scenarios was randomly between 50% and 80% of this limit. The resulting capacity limits of the transmission lines of the 39-bus system used in this work are included in Appendix C.

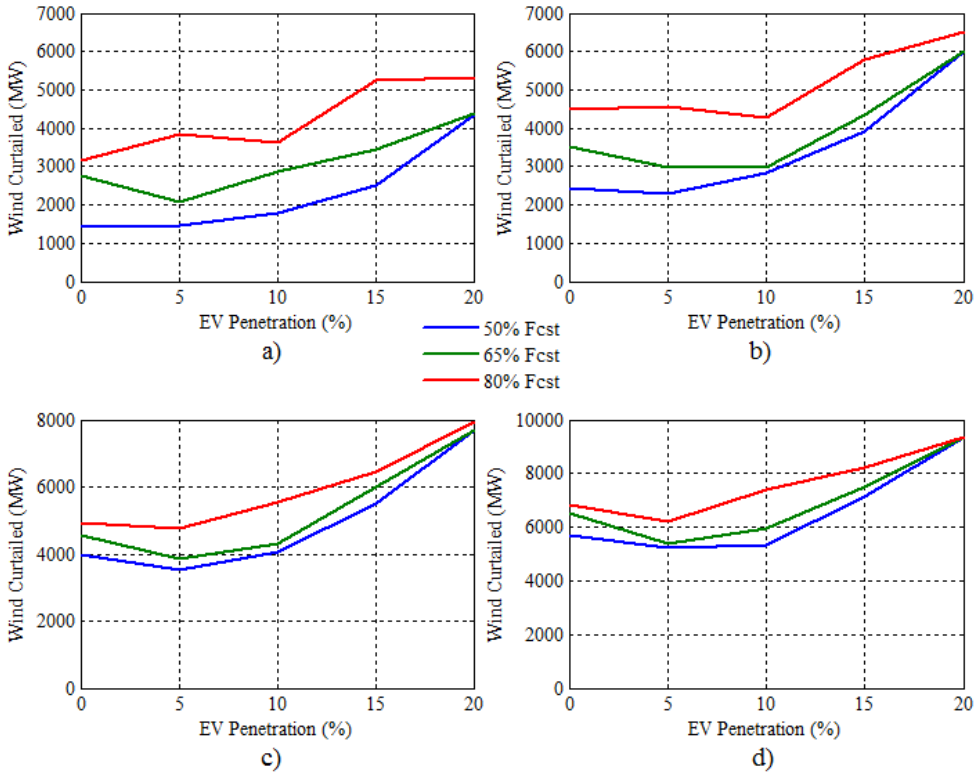

Figure 72. Wind curtailment for different conservative wind forecast and EV penetration levels when the transmission system has finite capacity at: a) 25%, b) 30%, c) 35%, and d) 40% wind penetration.

The amount of wind energy that is curtailed in this case for varying EV penetration, wind power forecast, and wind power penetration levels is presented in Figure 72. When compared to the wind curtailment shown in Figure 70 of Section 4.5.2, it is clear that the benefits of flexible EV charging in increasing wind power production when assuming that the transmission network has infinite capacity are not achieved in this case. This occurs because transmission congestion impedes effective delivery of available wind power to electricity consumers. Although in some scenarios a slight decrease in wind curtailment is observed with increasing EV penetration, because the benefits of flexible EV charging marginally exceed the negative impacts of transmission congestion, the general trend seen in Figure 72 is that wind curtailment increases with EV penetration, as greater EV loads aggravate transmission congestion issues. Wind curtailment increases with wind penetration as well, because the transmission system grows incapable of delivering energy from this renewable resource as more of it becomes available.

Since transmission congestion limits the amount of inexpensive wind energy that is absorbed by the system, it is expected that this will have negative economic consequences as well. The total system operating cost for varying EV penetration, wind power forecast, and wind power penetration levels is presented in Figure 73. The solid lines in this graph represent different EV penetrations for the case in which the transmission system had finite capacity, while the dash lines repeat the results for the case analyzed in Section 4.5.2 in which an infinite transmission capacity was assumed. When comparing these two cases, a substantial increase in total system operating cost is observed when the transmission network is taken into account. This gives an indication of the cost of transmission congestion for the 39-bus test system. The negative impacts of

transmission congestion are due in part to EV load departing from its optimal dispatched profile, where it no longer tends to follow the trend of wind power generation and hence does not absorb the variability and uncertainty of this generation resource, as depicted in Figure 74.

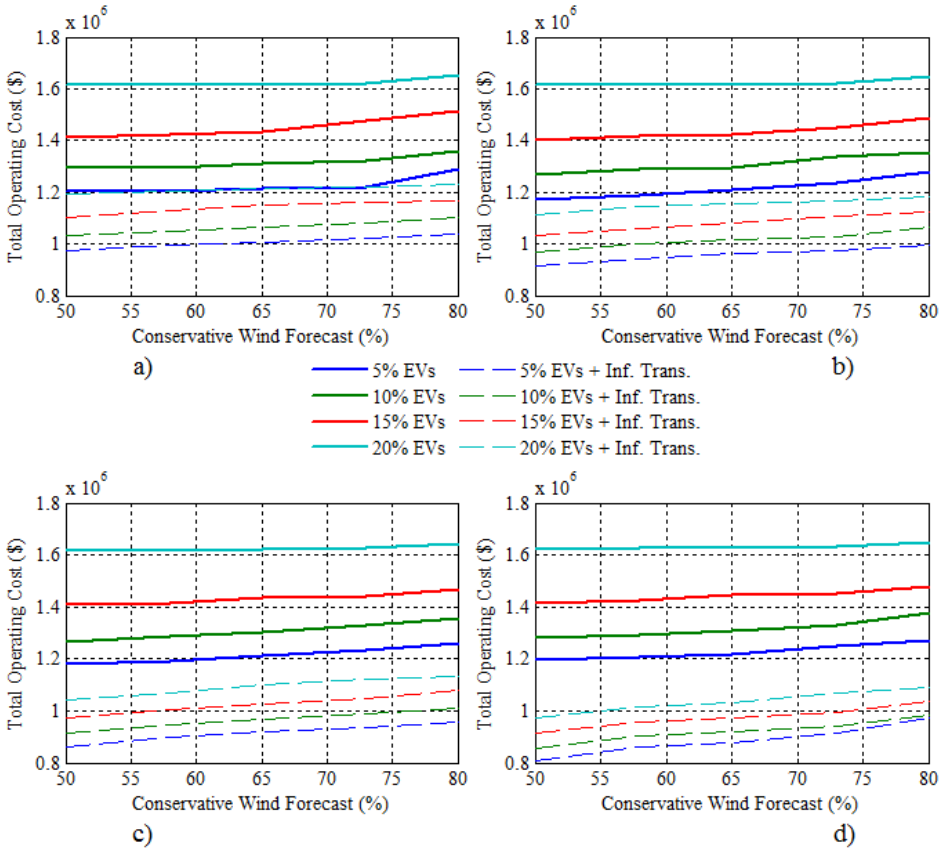

Figure 73. Total operating cost for different EV penetration and conservative wind forecast levels when the transmission system has finite and infinite capacity at: a) 25%, b) 30%, c) 35%, and d) 40% wind penetration.

The results presented in this section show that providing relief for the temporal constraints of conventional generation units to increase wind power penetration, such as with flexible loads, may not be sufficient in all circumstances. In already congested power systems, relief for the spatial constraints imposed by the transmission network may also be required. This demonstrates the importance of developing strategies for

alleviating transmission congestion, so that, for example, the expected benefits of joint policies of increasing wind power and EVs as complementary technologies can be fully achieved.

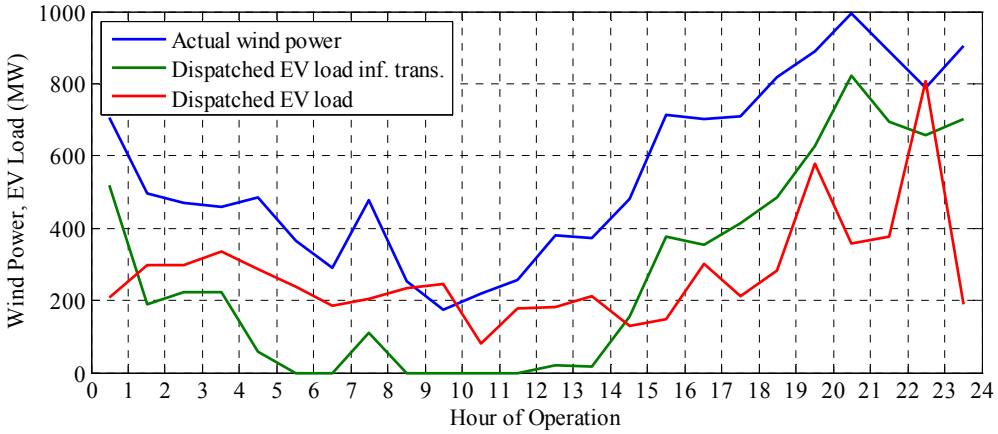

Figure 74. Total actual wind power and dispatched EV load profiles with infinite and finite transmission capacity at a wind and EV penetration of 40% and 20%, respectively.

5.4 Overview and Modeling of Power Routing Technology

The most straightforward approach, albeit the most expensive, to alleviate transmission congestion is to build new transmission lines. It is estimated that the cost of a new transmission line rated at 500 kV is about $3 million per mile [201]. Transmission projects do not only require huge capital expenditure but also involve long lead times, often up to10 years [202]. Another major obstacle towards constructing new transmission lines is the acquisition of the required real estate. The general public sentiment towards locating transmission lines near to their communities has become increasingly negative, and in many urban centers the cost of land required for transmission projects can be exorbitantly high. Furthermore, outdated and ineffective transmission investment policies fail to capture the full benefits of new transmission upgrades in the incentive structure

offered to investors [203]. As a result, investors have little or no incentive to invest in transmission projects that might be beneficial for consumers and society at large.

Considering the uncertainties in the development of new transmission infrastructure, an alternative approach for relieving congestion is to adopt methods to improve the overall utilization of existing transmission assets. In this sense, apart from distributed generation, energy efficiency, and demand response programs, the U.S. DOE is also promoting the development of high-impact advanced technologies to address transmission bottlenecks [204]. In particular, energy policy and planning agencies have started to evaluate the potential benefits of deploying devices that are able to reroute active power flows in their systems [205]. PRs are effectively devices that can increase the throughput of a transmission network by increasing the utilization of parallel lightly loaded paths, while preventing overloading of highly loaded lines. PRs are capable of this because they can alter the power flow in a line by modifying the bus voltage magnitudes, phase angles, and/or the impedance of the line. This research focuses on PRs that insert a phase angle injection in the line it is placed on, as depicted in Figure 75. In this case, the active power flow in the line varies according to:

$$LF = \frac{V_1 \cdot V_2 \cdot \sin(\theta_1 - \theta_2 + \alpha)}{X}. \tag{59}$$

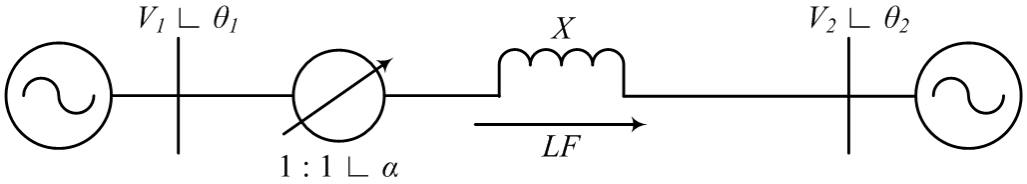

Figure 75. A PR varying the effective phase angle between two buses.

The phase-shifting transformer (PST) and the unified power flow controller (UPFC) are examples of two conventional PR devices that have been implemented in the field to vary the effective phase angle of a transmission path. A complete description of other traditional power routing technologies that have been either proposed or implemented is given in [206]. PSTs were developed to enhance the transmission system under steady-state conditions [207]. Their inability to provide continuous power flow control, their slow operation, and wear and tear resulting from frequent operation discourages their use as a dispatchable control resource by system operators. The UPFC, on the other hand, is a voltage source converter (VSC) based power flow controller capable of providing continuous, dynamic power flow control [208]. Unfortunately, the cost of the UPFC becomes prohibited because of its fully-rated back-to-back (BTB) converter and low-frequency transformers, preventing its widespread implementation. Recent advances in semiconductor technology, though, combined with new designs based on fractionally rated converters, such as the controllable network transformer [206, 209] and fractionally-rated BTB converter [210], has rekindled interest in the possible wide-scale deployment of power-electronics-based PRs. Thus, it seems appropriate to incorporate the functionality of these devices in current power system operations to evaluate their impact on the grid.

In order to model the functionality of PRs in day-ahead scheduling operations, first, the objective function of the developed UC problem formulation (36) was updated as follows:

$$TOC = \sum_t \sum_i \left[FC_{it} + SUC_{it} + SDC_{it} \right] + \sum_t \sum_j \rho_j \left(L_{D,jt} - L_{jt} \right) + \sum_v \rho_v \left(dayE_{DR,v} - \sum_t L_{vt} \right) + \sum_t \sum_{pr} \rho_{pr} \left| \alpha_{prt} \right|. \quad (60)$$

Table 13. Nomenclature Used in the Mathematical Expressions for Modeling PR Functionality

Symbol	Meaning	Symbol	Meaning
b	Index for buses	SUC	Start-up cost of conventional units
$dayE_{DR}$	Daily driving energy requirements of EVs	TOC	Total system operating cost
FC	Fuel cost of conventional units	t	Index for time periods
i	Index for conventional units	V	Bus voltage magnitude
j	Index for non-EV loads	v	Index for EVs
L	Served non-EV/EV load	X	Reactance of a line
L_D	Non-EV load demand	α	Phase angle injection of PRs
LF	Power flow in a line	$\alpha_{\max}$	Maximum phase angle injection of PRs
l	Index for transmission lines	$\alpha_{\min}$	Minimum phase angle injection of PRs
pr	Index for PRs	θ	Bus voltage phase angle
SDC	Shutdown cost of conventional units	ρ	Penalty factor for unserved non-EV/EV loads and PR operation

Table 13 summarizes the nomenclature used in the mathematical expressions of this section. The additional term is included only to avoid the superfluous operation of PRs in the absence of congestion. Therefore, penalty factor ρ_{pr} is set to a very low value to not influence the total system operating cost. In addition, the constraint that determines the power flow in each line (57) was update with the DC problem formulation of (59), as shown below:

$$LF_{lt} = \frac{\left(\theta_{(b=frBus)t} - \theta_{(b=toBus)t} + \alpha_{prt}\right)}{X_l} \quad \forall l \ \forall t. \tag{61}$$

Note that the PR phase angle injection variable, α_{prt}, is only included in this constraint if a PR has been installed on the corresponding line. Finally, a last constraint that enforces the PR phase angle injection limits was incorporated into the developed UC problem formulation:

$$\alpha_{\min,pr} \le \alpha_{prt} \le \alpha_{\max,pr} \quad \forall pr \ \forall t. \tag{62}$$

5.5 NUMERICAL RESULTS: INTEGRATED DAY-AHEAD SCHEDULING FRAMEWORK

Now that all the pieces of the day-ahead scheduling framework developed in this work have been introduced, in this section, they are all integrated to demonstrate that deployment of PRs can facilitate EV-wind balancing in congested power systems. Simulation results are again presented for the 39-bus system described in sections 4.5 and 5.3. In this case, PRs are located on the bottlenecks of the system, i.e., lines 3-4, 15-16, and 17-27. These locations were selected intuitively based on previous work that indicate that the sensitivities of power flows to a given PR control action are greatest for the line on which this device is installed [211]; and hence may not necessarily represent optimal PR placement in the system under study. The problem of determining optimal PR placement would most likely be done as part of power system planning operations, which is a subject outside of the scope of this work.

As in Section 5.3, in this case it is not only assumed that EV load is allowed to be flexibly scheduled but that EVs also participate in the procurement of system reserves. Because of space constraints, this case only considers a 20% EV penetration, which represents the scenario where the transmission system must deliver the most amount of electricity to consumers. Furthermore, the results for this case are limited to a 40% wind penetration and where an 80% exceedance forecast is used in the day-ahead scheduling process, which is the scenario that leads to the greatest amount of wind curtailment.

PowerWorld® was utilized to create contour graphs of the line loading conditions to give a visual illustration of the impact of PR operation on the 39-bus test system for a specific hour of operation. The contour graph in Figure 76 is for the case without PRs, while the one in Figure 77 shows the case with three PRs installed in the system. Note

that the locations of the PRs in the 39-bus test system are indicated in Figure 77. Two things are evident when comparing these figures. First, higher power flows are observed leaving the rich wind power generation region in the case with PRs, indicating a greater delivery of wind generated electricity. Second, a better utilization of transmission assets is also seen in the case with PRs, as dark blue contours are mainly limited to expensive generation regions, suggesting a more optimal dispatch of conventional generation resources in this case as well. As observed, PRs prevent the maximum operating limits of transmission lines from being exceeded, rerouting through parallel underutilized paths the additional power flows required through these heavily loaded lines to achieve the outcomes described above.

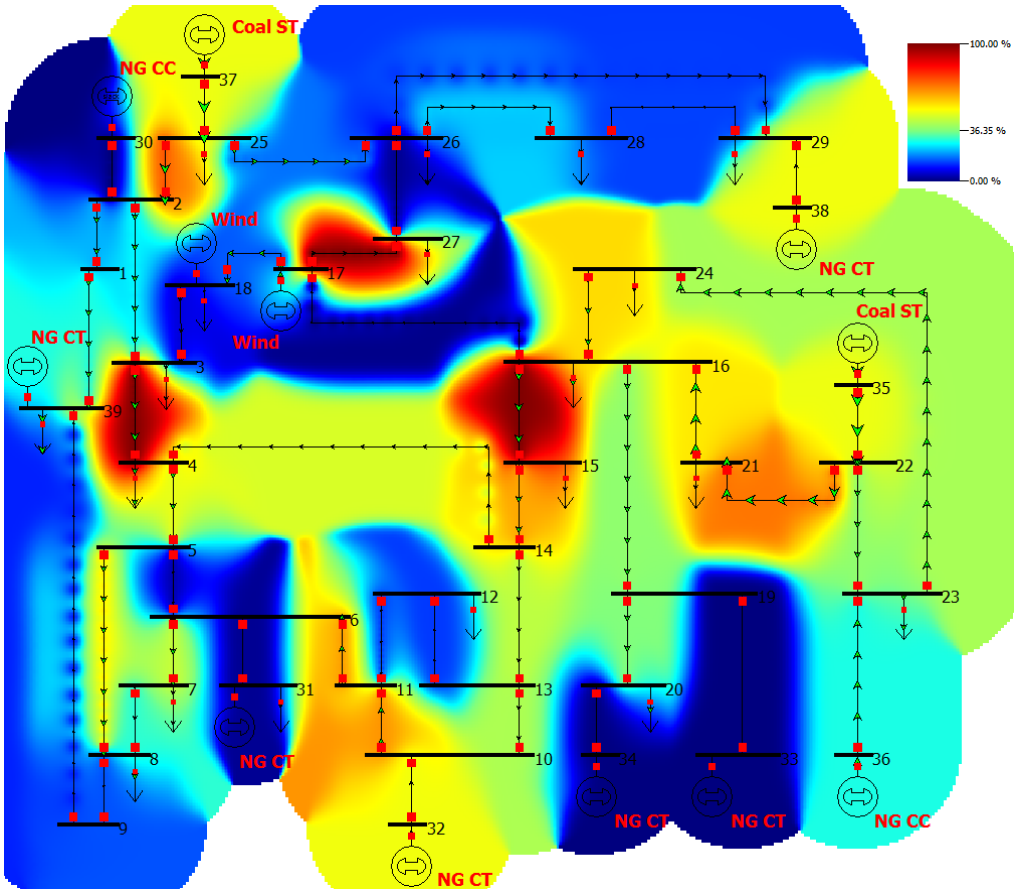

Figure 76. Contour graph of the line loading conditions without PRs installed on the system.

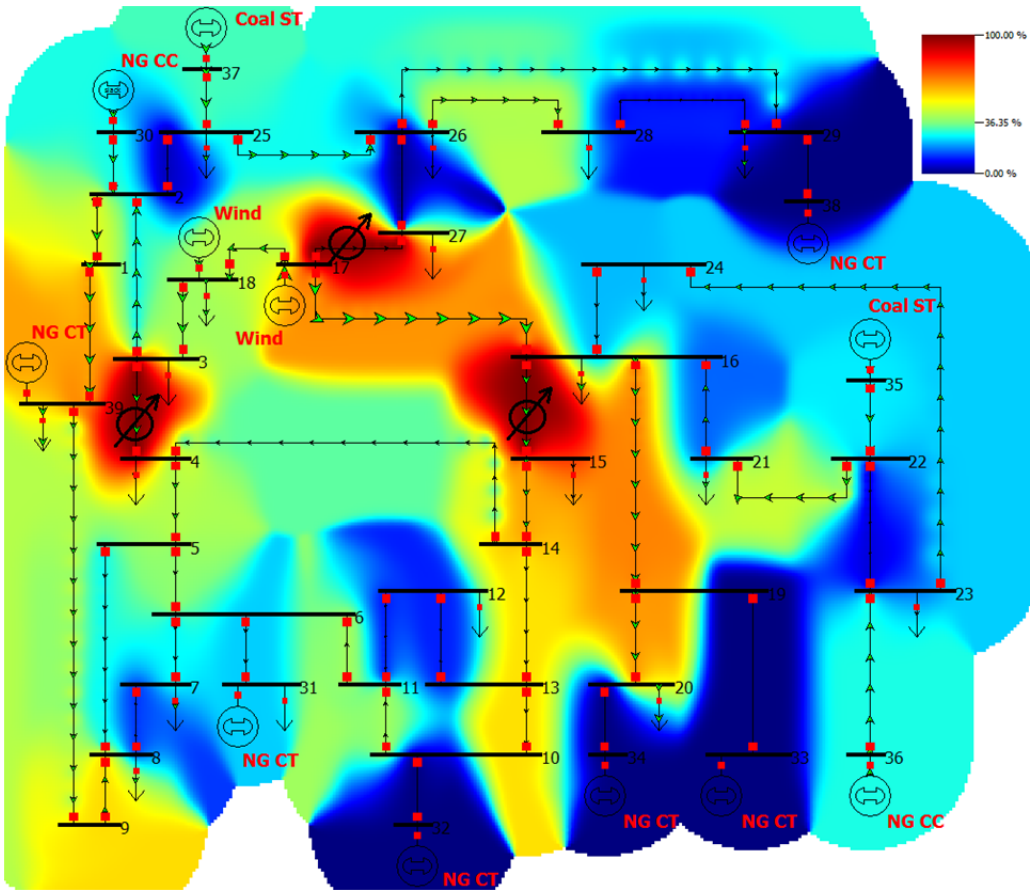

Figure 77. Contour graph of the line loading conditions with PRs installed on lines 3-4, 15-16, and 17-27.

The amount of wind energy that is curtailed in this case, as a function of the PR phase angle injection limit, is presented in Figure 78. The power rating of a PR, and hence the investment cost of this device, increases with its phase angle injection limit. For the results of this section, it is assumed that all PRs in the system have the same phase angle injection limit. As observed in Figure 78, for the scenario of a phase angle injection limit of 0º, the same amount of wind curtailment is obtained as for the case with transmission congestion analyzed in Section 5.3. The greatest wind curtailment reduction occurs within the first few degrees of PR phase angle injection limit. After this, wind curtailment continues to reduce steadily until converging to the same result of the case discussed in

Section 4.5.2, in which an infinite transmission capacity was assumed. When the PRs are rated to provide phase angle injections of 8º or greater, the system is capable of absorbing all wind power generation thanks to the added flexibility of the transmission network introduced with the deployment of these devices.

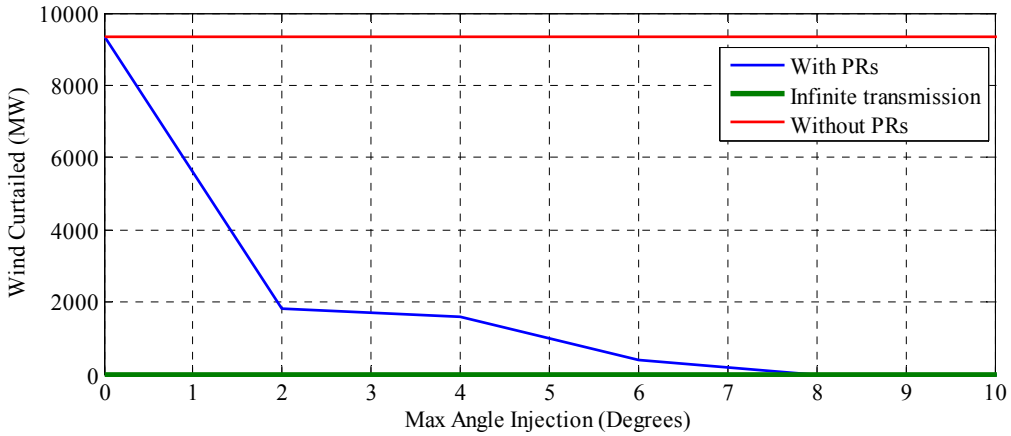

Figure 78. Wind curtailment reduction with increasing maximum PR phase angle injection.

The total system operating cost for this case as a function of the PR phase angle injection limit is displayed in Figure 79. A similar trend as for the wind curtailment is observed in this figure, except that the same result of the case in which the transmission network is assumed to have an infinite capacity is achieved at a higher PR phase angle injection of around 14º. This occurs because, even though wind curtailment is reduced to zero when PRs have a phase angle injection limit of 8º, these devices do not have additional capacity to reroute power away from the congested lines to ensure the optimal commitment and dispatch of conventional generation units. These results demonstrate that PRs are devices capable of seemingly increasing the transmission capacity of the grid by leveraging untapped parallel transmission resources.

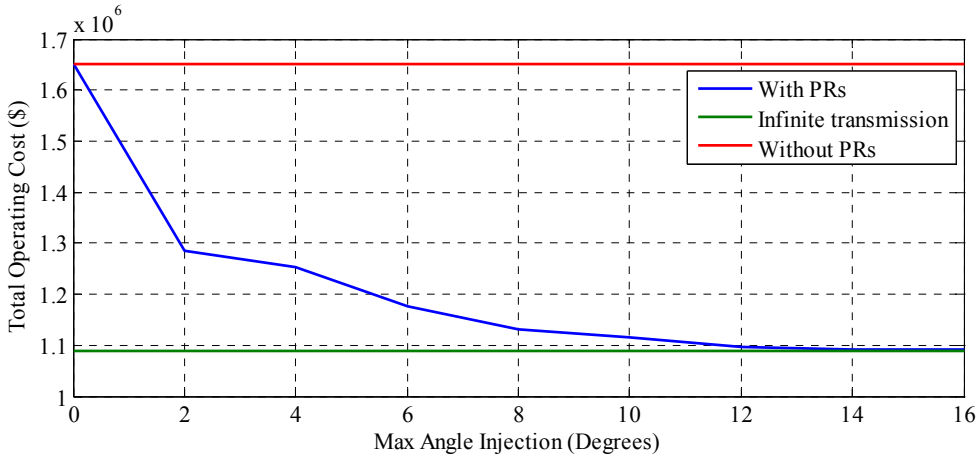

Figure 79. Total operating cost reduction with increasing maximum PR phase angle injection.

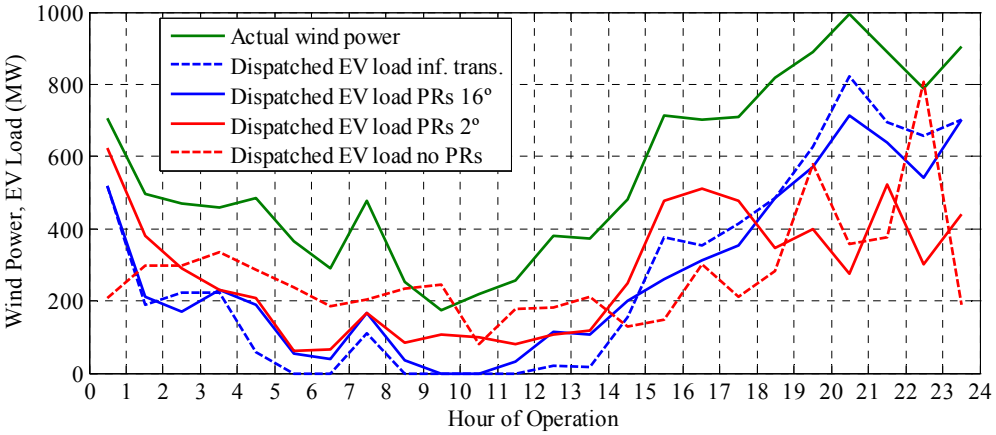

Figure 80. Total actual wind power and dispatched EV load profiles with infinite and finite transmission capacity, without and with PRs having a maximum phase angle injection of 2° and 16°.

Figure 80 compares the observed wind power generation profile with the total dispatched EV load for different scenarios. As observed, when the PRs have a phase angle injection limit of only 2°, the dispatched EV load significantly departs from that of the scenario with no PRs. On the other hand, when they are rated for a phase angle injection limit of 16°, the dispatched EV load resembles the optimal EV load profile for the case in which an infinite transmission capacity is assumed. This result shows the potential for achieving optimal EV-wind balancing if PRs are employed for relieving transmission congestion.

Finally, Table 14 summarizes the optimal phase angle injections of the PRs for each hour of the operation horizon, assuming they have a phase angle injection limit of 16º. The continuous and dynamic control requirements that the PR technology must possess for scheduling and dispatch operations are evident from this table. This result discourages the use of conventional PSTs for this particular application, pointing to the need for the development of power-electronics-based PR solutions. It is important to mention that the value of PRs was evaluated in this work only in the context of electricity market operations and facilitating EV-wind balancing. Other value propositions that are encouraging the development of low-cost power-electronics-based PRs exist as well, such as helping to mitigate loop flows and providing post-contingency remedial actions.

Table 14. Optimal Phase Angle Injections of the PRs for Each Hour of Operation

Hour of Operation	**PR Angle Injection (º)**			**Hour of Operation**	**PR Angle Injection (º)**		
	Line 3-4	***Line 15-16***	***Line 17-27***		***Line 3-4***	***Line 15-16***	***Line 17-27***
1	12.889	-16.000	12.210	13	13.056	-16.000	3.897
2	15.084	-16.000	5.268	14	13.417	-16.000	4.036
3	14.945	-16.000	4.180	15	14.208	-16.000	4.560
4	12.307	-16.000	4.619	16	15.054	-16.000	5.554
5	14.006	-16.000	4.783	17	16.000	-16.000	4.367
6	10.991	-12.521	3.665	18	14.298	-16.000	8.629
7	5.415	-5.764	2.643	19	11.016	-16.000	16.000
8	9.070	-9.829	3.730	20	12.088	-16.000	16.000
9	5.230	-5.585	1.739	21	14.845	-16.000	9.036
10	5.238	-5.975	1.469	22	13.331	-16.000	12.672
11	6.087	-7.300	2.546	23	14.972	-16.000	6.431
12	6.119	-7.033	2.407	24	12.630	-16.000	16.000

5.6 SUMMARY

The transmission system in the U.S. gradually evolved from a radial structure to a greatly meshed network as the reliable delivery of electricity became a major performance metric. The inherent asymmetry of the path impedances of meshed networks

causes uneven stress on transmission assets, giving rise to undesired effects. One of such effects is transmission congestion, which occurs on transmission facilities when actual or scheduled flows of electricity are restricted below desired levels. In meshed transmission networks, this starts happening when the first line reaches its operational limit, leading to the inefficient utilization of existing transmission assets. Transmission congestion imposes real economic consequences upon energy consumers and can impair grid reliability, rendering areas more vulnerable to system outages.

In order to capture the impact of transmission congestion on optimally balancing the variability and uncertainty of wind power generation with flexible EV charging, it was necessary to include a representation of the transmission network in the developed UC problem formulation. Following the current industry practice, the transmission system was modeled in this work using the DC power flow formulation. The resulting UC framework was applied to the 39-bus test system. The simulation results showed that, because of transmission congestion, the full benefit of flexible EV charging in increasing wind power production was not achieved; the total system operating cost became significantly greater; and, the dispatched EV load was unable to follow the trend of wind power generation. These results demonstrated that the relief of the temporal constraints of conventional generation units, by leveraging flexible EV charging, was not sufficient to increase wind power production in the 39-bus test system. In this case, relief for the spatial constraints imposed by the transmission system was also required to obtain the full benefits of optimally balancing wind power generation with flexible EV charging.

The most straightforward approach to alleviate transmission congestion is to build new transmission lines. However, because of their elevated costs, long lead times,

problems with the acquisition of real state, and outdated and ineffective transmission investment policies, much uncertainty surrounds the development of new transmission projects. A more cost-effective strategy that is currently receiving a great deal of attention is to improve the overall utilization of existing transmission assets by deploying PRs on the network. PRs are devices capable of rerouting power flows that could be used to increase the utilization of parallel lightly loaded paths, while preventing overloading of highly loaded lines.

The functionality of this device was incorporated into the developed UC problem formulation. All the different aspects modeled in this work were integrated into a single-day ahead scheduling framework that was applied to the 39-bus test system. Contour graphs of the line loading conditions for a given hour of operation showed higher power flows leaving the rich wind power generation region and a better utilization of transmission assets for the case with PRs installed in the system. In addition, simulation results demonstrated that PRs could increase the benefits of EV-wind balancing in congested power systems. If PRs with sufficient ratings are installed in the system, the same results as for the case in which an infinite transmission capacity was assumed could be achieved. Furthermore, the results showed that a power-electronics-based PR solution would be required for the particular application analyzed in this work, because of its continuous and dynamic control requirements.

It is important to mention that the wind curtailment and total system operating cost results presented in this chapter are system specific and dependent on, among other things, the level of congestion of the network, the available capacity in parallel transmission paths, and the ratings and placement of the PRs on the grid. However, there

is good indication that most power system operations are currently limited by only a few congested corridors, while the bulk of the transmission system remains underutilized, as assumed here.

The following chapter provides conclusions for the work on managing third harmonic currents from EV battery chargers and flexible EV charging to increase wind power production covered in this document. The contributions of this work and suggestions for future research are also discussed.

6 CONCLUSIONS

A tremendous potential exists in the U.S. for electrifying a significant portion of the light-duty vehicle (LDV) fleet. Since their short-lived popularity in the early 1900s, multiple failed attempts were made throughout the 20th century to revive the idea of mass adoption of electric vehicles (EVs). However, to address pressing concerns on energy security, the environment, and the sustainability of future transportation, EV development has gone into an accelerated pace in recent years, gaining the support of politicians, automakers, and consumers. So far, numerous studies have projected varying levels of market success for EVs, most predicting substantial market growth with time. Furthermore, the current shift in the automotive industry appears to be indicating a possible bright future for EVs. Therefore, the moment seems appropriate to develop mechanisms to prepare the power system for the introduction of this new device into the network. Because of its unique load characteristics, an extensive deployment of EVs will not only bring considerable challenges to power system operation, but will enable unique opportunities as well. The objective of this work was to address the increased third harmonic currents in distribution systems expected with the introduction of EVs and explore the potential of leveraging flexible EV charging to increase wind power production.

The proliferation of single-phase nonlinear residential loads in the last couple decades has shifted the concerns utilities have over power system harmonics from large industrial and commercial customers to their residential/small commercial distribution systems. Of particular interest are currents at the third harmonic frequency because of their negative impacts on the grid caused by their zero-sequence nature and negligible phase diversity.

The introduction of EVs is further raising concerns among utilities over the impact of this new load type on power system harmonics. Since EV chargers rely on power electronic systems to obtain a controllable DC source from the utility AC supply, it is expected that these devices will aggravate third harmonic current issues. In fact, utility harmonic field data indicate that, even without EVs, distribution feeders are already experimenting elevated levels of third harmonic currents, especially in the neutral conductor. To address present and future utility harmonic filtering needs, in this work, a practical third harmonic hybrid active filter for medium voltage (MV) applications was proposed. Its design was based on strict utility requirements of cost, reliability, and ease of system implementation. Simulation results were presented to demonstrate the good filtering and dynamic performance of the proposed filtering system; to draw comparisons with conventional third harmonic filtering approaches; and, to show cost versus performance curves of the proposed filter when existing capacitor banks are retrofitted for this particular application.

Two experimental setups were tested and a system impact study was conducted to demonstrate the operation and benefits of the proposed third harmonic hybrid active filtering solution. The first experimental setup, tested at 350 V, showed the directionality feature of the proposed filter and good filtering performance when compensating for an actual rectifier front-end load. The second experimental setup, tested at 7.2 kV, was used to demonstrate third harmonic hybrid active filtering at utility distribution MV levels. A detailed description of the design, simulation results, and experimental results for both setups were presented. The system impact study was realized utilizing actual data for a typical residential/small commercial distribution feeder provided by a National Electric

Energy Testing, Research and Applications Center (NEETRAC) utility member. Results of this system impact study show that considerable third harmonic neutral current and neutral-to-earth voltage (NEV) reduction can be achieved by deploying the proposed filter. The preliminary results of this work demonstrate the potential of the proposed filter as an effective tool for addressing the increase of third harmonic currents expected with the introduction of EVs.

Because vehicles remain stationary most of the time, EVs have the potential of being flexibly charged, providing a number of opportunities for system operators. Wind power penetration in the U.S. has increased drastically in the last few years and is projected to continue growing in the decades that follow. The variability and uncertainty of this renewable energy resource makes the determination of the optimal generation schedule a very challenging process. In this work, the potential benefits of leveraging flexible EV charging to balance out the variability and uncertainty of wind power generation was explored. A detailed unit commitment (UC) problem formulation was developed to determine the impact of flexible EV charging on the day-ahead scheduling process in systems with high wind power penetration. The developed UC framework included modeling of the operational constraints of conventional generation units, flexible EV charging, curtailment of wind power generation, conservative wind power forecasts, and procurement of system reserves based on historical wind power forecast errors. The resulting UC tool was employed to perform simulations on a modified version of the IEEE 39-bus system. The simulation results, assuming an infinite transmission capacity, showed a considerable increase in wind power production with EV penetration, with even

greater wind power production and lower total system operating cost if EVs were enabled to provide system reserves.

However, when the transmission network was included in the developed UC framework and transmission bottlenecks were introduced in the test system, simulation results showed that the full benefit of flexible EV charging in increasing wind power production was not achieved; the total system operating cost became significantly greater; and, the dispatched EV load was unable to follow the trend of wind power generation. These results indicate that the relief of the temporal constraints of conventional generation units, by leveraging flexible EV charging, to increase wind power production may not always be sufficient. Such a situation is very probable if the integration of wind power and EVs continue to outpace transmission system upgrades. In these cases, relief for the spatial constraints imposed by the transmission system is required to achieve the full benefits of EV-wind balancing. This work focuses on the strategy of improving the overall utilization of existing transmission assets by deploying power routers (PRs) on the network. The simulation results showed that PRs could help increase the benefits of EV-wind balancing in congested power systems; and if they are properly located and rated to provide the required phase angle injection, the same results as if the transmission network had infinite capacity could potentially be obtained.

6.1 CONTRIBUTIONS

The contributions of this work and the resulting publications are given below:

1. A practical third harmonic hybrid active filter for MV applications has been proposed. The design of the proposed filter was driven by strict utility requirements of low cost, high reliability, and ease of system implementation [117, 212].

2. Two experimental setups were designed, built, and tested. One was used to verify the directionality feature of the proposed filter and its filtering performance when compensating for an actual rectifier front-end load, while the other was employed to demonstrate third harmonic hybrid active filtering at utility distribution MV levels [117, 118, 212].
3. A system study was performed to evaluate the impact of deploying the proposed filter in terms of third harmonic neutral current and NEV reduction. For this study, actual data for a typical residential/small commercial distribution feeder was utilized [118].
4. An integrated day-ahead scheduling framework was developed, which included modeling of the operational constraints of conventional generation units, the transmission network, flexible EV charging, curtailment of wind power generation, conservative wind power forecasts, procurement of system reserves based on historical wind power forecast errors, and PR functionality. The resulting tool was employed to examine the benefits of balancing the variability and uncertainty of wind power generation with flexible EV charging [213].
5. It was determined that the full benefits of balancing wind power generation with flexible EV charging may not be achieved in congested power systems. A potential solution based on employing PRs to augment the flexibility of the transmission system has been proposed [213].

6.2 FUTURE WORK

6.2.1 Development of (Hybrid) Active Filter Designs Without a DC-Link Capacitor

Utility equipment that are deployed in the field are required to have a long expected life, typically measured in decades and sometimes exceeding 30 years, with very low maintenance. In this sense, the weak point of the proposed third harmonic hybrid active filter is its DC-link capacitor. Electrolytic capacitors are preferred in DC-link applications, and particularly in the proposed filter, because of their lower cost, but have the disadvantage of a very low lifetime, requiring frequent maintenance. As in this work, active filtering solutions proposed in the literature almost exclusively rely on a full-bridge power converter, which requires a DC-link capacitor. Therefore, it would be interesting to consider (hybrid) active filters with alternative topologies that do away with the DC-link capacitor, possibly a direct AC converter employing virtual quadrature sources (VQS) theory.

6.2.2 Third Harmonic Filtering in Networked Distribution Systems

Distribution systems are predominantly configured as radial feeders out of distribution substations. Therefore, in most situations a distributed third harmonic filtering approach based on the proposed filter can readily be implemented. However, not all distribution systems are radial, particularly in more urban areas, making the implementation of such an approach more complicated. In these cases, the development of a coordinated strategy to ensure adequate third harmonic filtering and proper sharing of the burden among multiple filters would be required. Comparison of the performance of the proposed shunt filtering approach with a series counterpart may also be warranted.

6.2.3 System Reserves Requirement in Systems with High Wind and EV Penetration

In this work, the amount of system reserves to be procured was calculated based on accounting for 95% of historical wind power forecast errors. A better approach has been proposed in the literature where this calculation not only considers wind power forecast errors but contingencies and the cost of providing these reserves as well, to avoid procuring excess system reserves. An attempt has yet to be made on employing such an approach in systems where EVs are enabled to provide system reserves services. This could lead to even lower costs of integrating EVs into power system operations.

6.2.4 Electricity Market Design of the Integrated Day-Ahead Scheduling Framework

The results presented in this work support the development of joint policies for increasing wind power and EV penetration. However, an implementation of the developed integrated day-ahead scheduling framework will require an appropriate electricity market design to establish the rules and pricing mechanisms, for example, to encourage EV owners to participate in programs such as flexible EV charging. Also, even though PRs have the potential of providing tremendous benefits to power system operations, beyond generation scheduling and dispatch processes, investment policies for this technology are still not yet clear.

APPENDIX A: PCB AND SCHEMATICS OF CONTROLLER BOARD

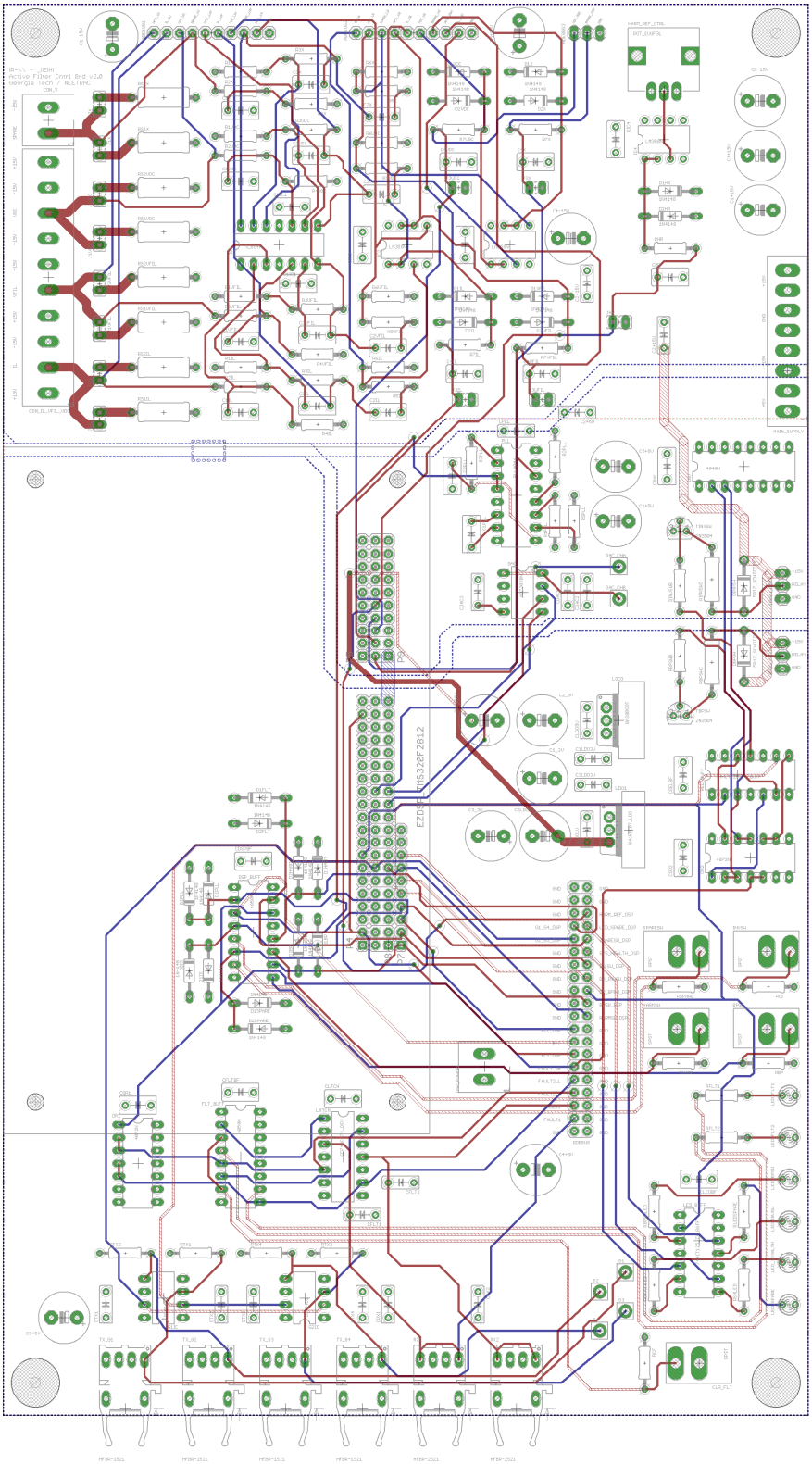

Figure 81. Printed circuit board (PCB) layout of the third harmonic hybrid active filter controller board.

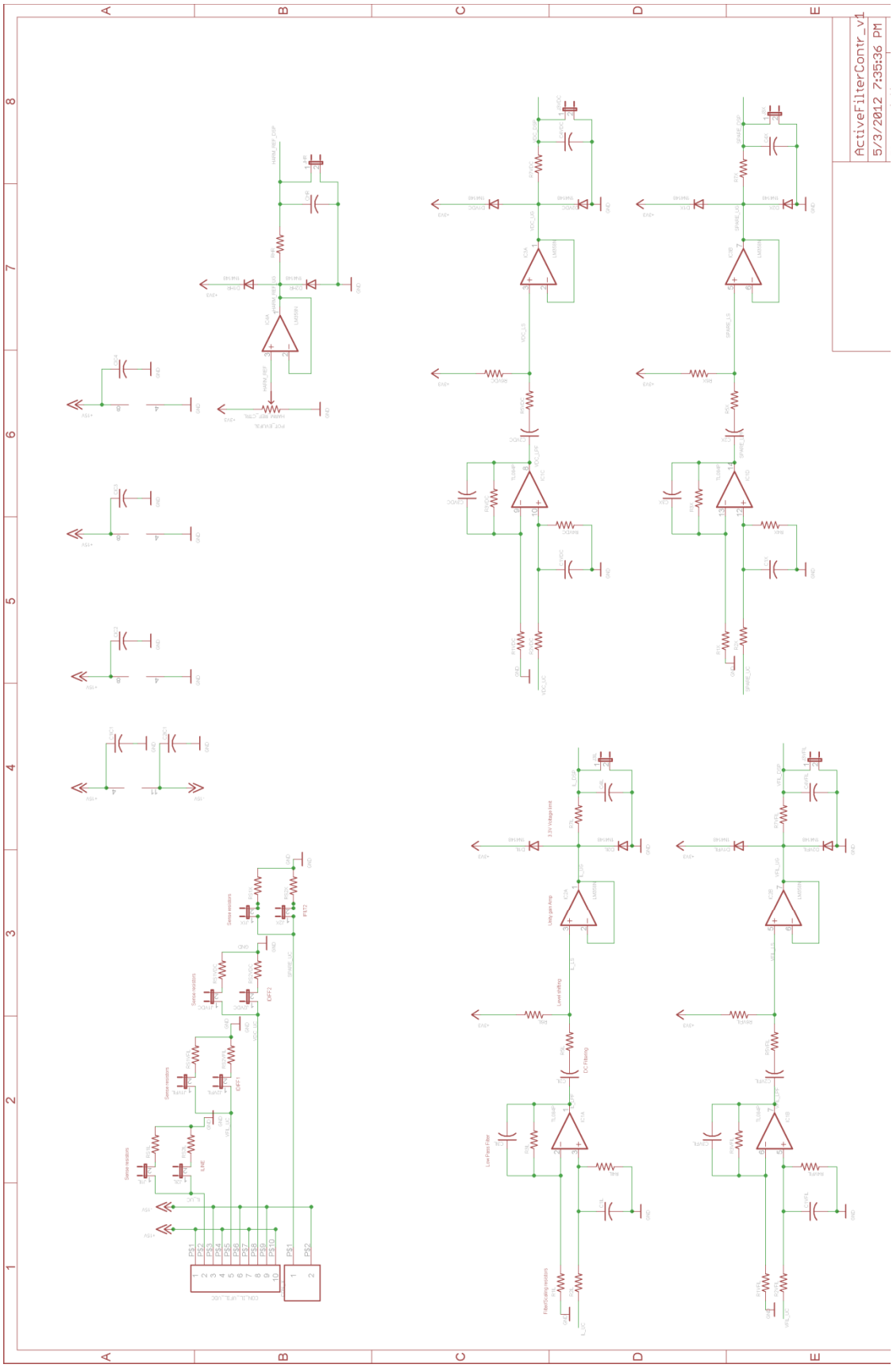

Figure 82. Schematic diagram of the third harmonic hybrid active filter controller board, sheet 1.

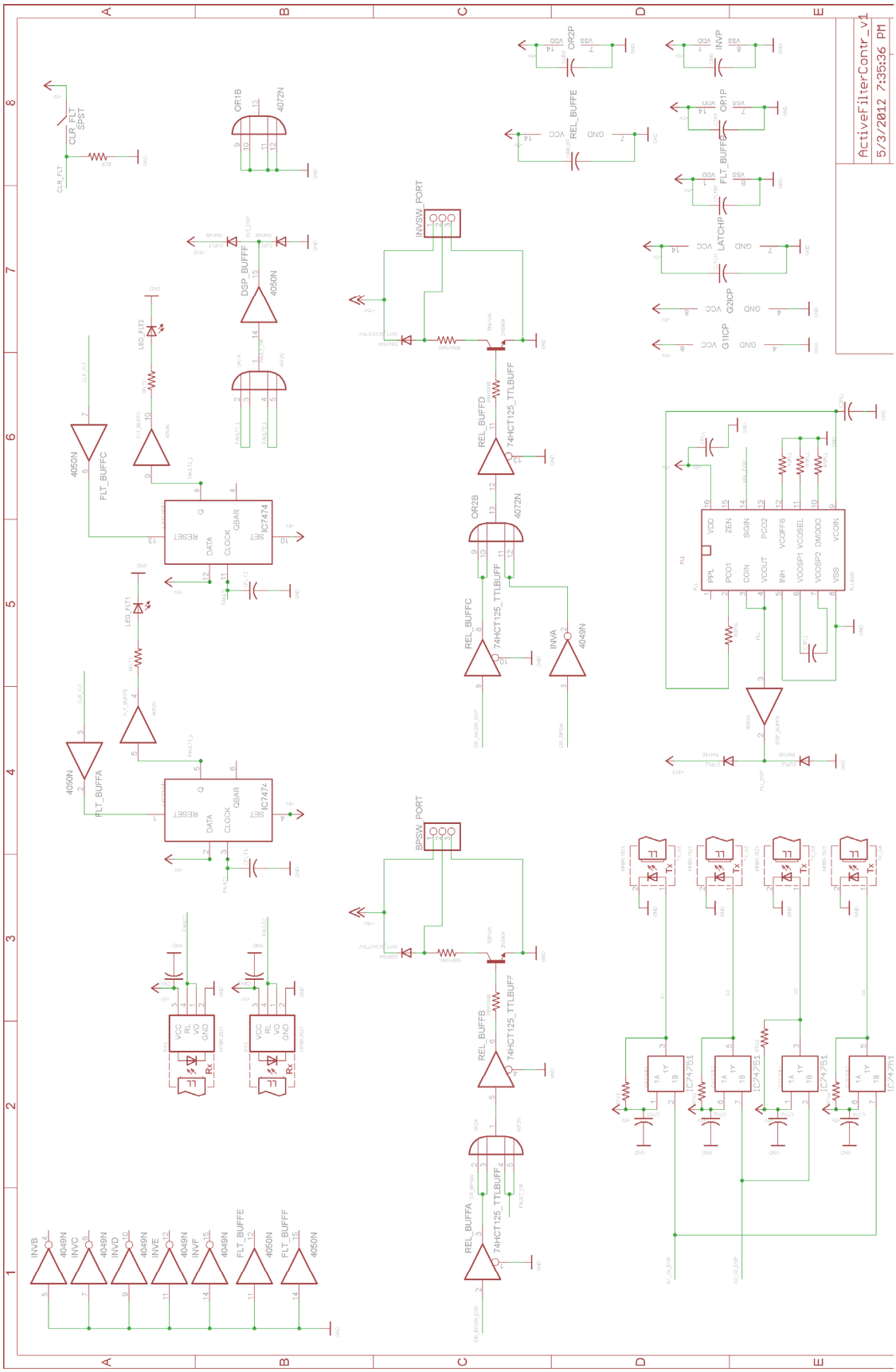

Figure 83. Schematic diagram of the third harmonic hybrid active filter controller board, sheet 2.

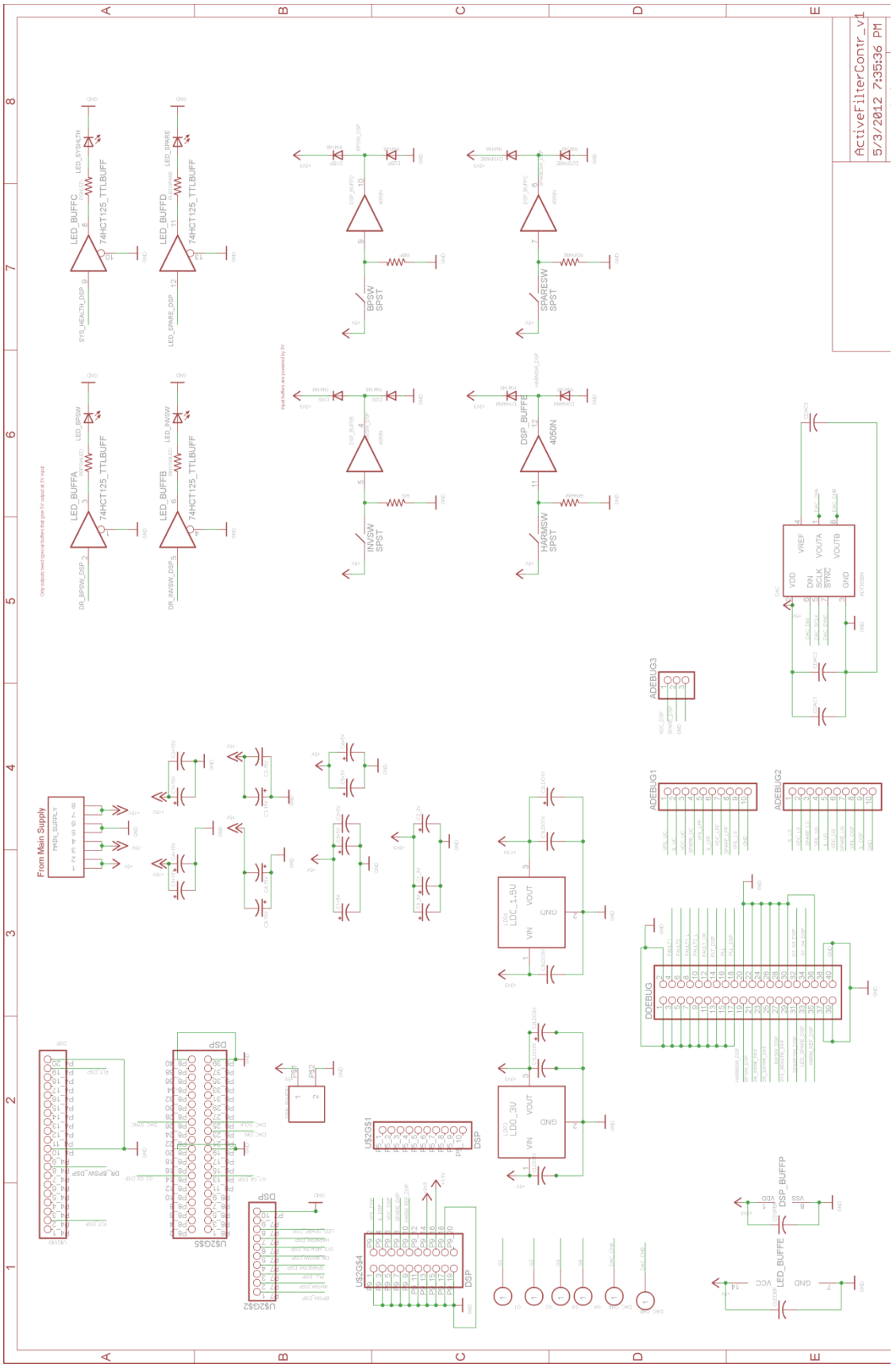

Figure 84. Schematic diagram of the third harmonic hybrid active filter controller board, sheet 3.

APPENDIX B: PARAMETERS USED TO CONTSTRUCT THE REDUCED FEEDER MODEL

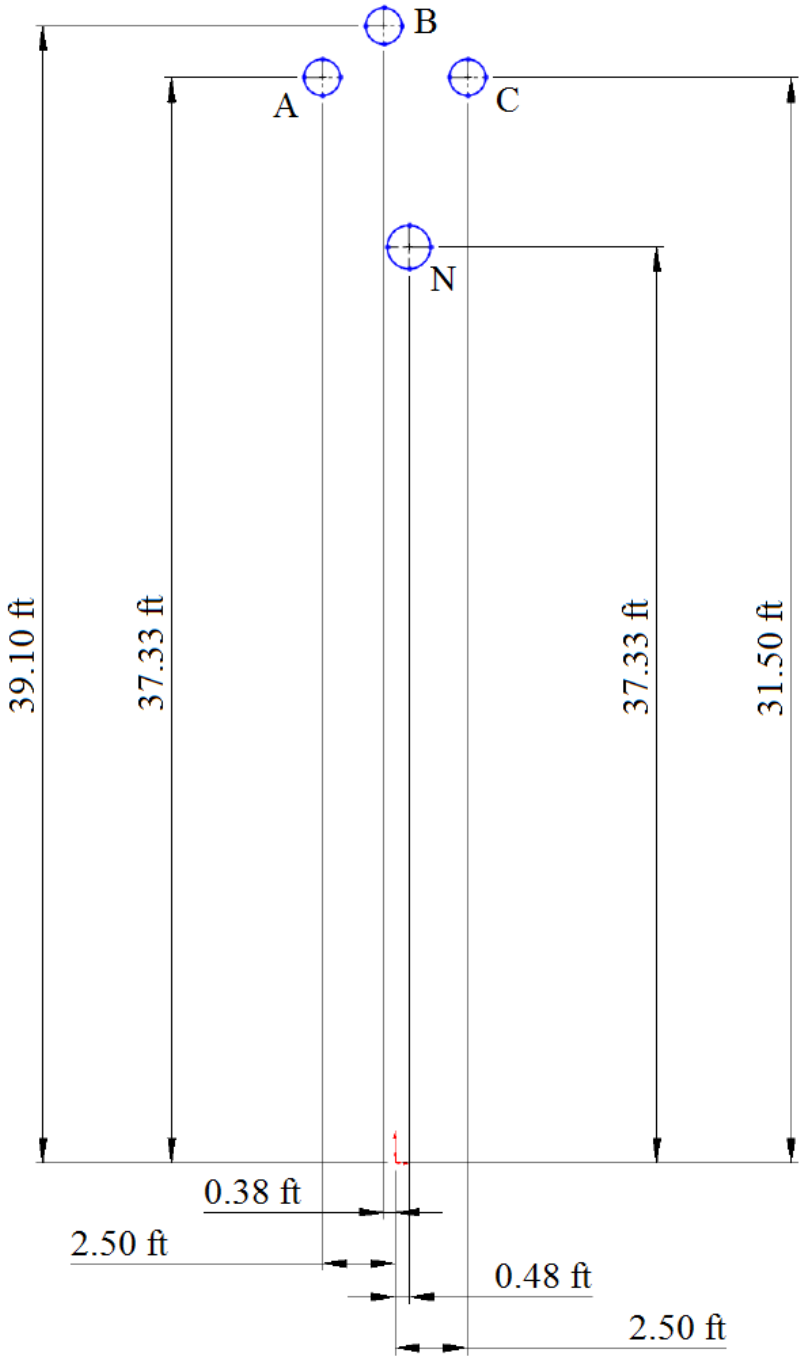

Figure 85. Arrangement of phase and neutral conductors of the residential/small commercial distribution feeder.

Table 15. Line and Load Parameters of Each Segment of the Residential/Small Commercial Distribution Feeder

Segment	Length (ft)	Phase Conductor	Neutral Conductor	Connected Load Phase A (kVA)	Connected Load Phase B (kVA)	Connected Load Phase C (kVA)
1	2831.2	397 ACSR	4/0 AL	275	15	75
2	2782.6	1/0 AL	2 AL	205	185	372
3	488.2	397 ACSR	4/0 AL	0	15	462.5
4	1498.5	397 ACSR	4/0 AL	334.5	165	145
5	6578.8	1/0 AL	2 AL	1013.5	196	306
6	3236.6	1/0 AL	2 AL	10	0	0
7	2067.9	1/0 AL	2 AL	669.5	982	1409.5
8	586.7	397 ACSR	4/0 AL	350	300	375
9	2521.1	397 ACSR	4/0 AL	1067.67	997.67	1421.17
10	3631.5	397 ACSR	4/0 AL	385	605.5	188
11	3379.8	1/0 AL	2 AL	607.5	115	205
12	1389.6	1/0 AL	2 AL	237.5	70	377.5
13	1113.9	1/0 AL	2 AL	742.5	915	867.5
14	4316.8	397 ACSR	4/0 AL	2276.67	1709.17	1681.67
15	3565.1	397 ACSR	4/0 AL	132.5	1017.5	640

APPENDIX C: PARAMETERS OF THE 39-BUS TEST SYSTEM

Table 16. Line Data for the 39-Bus Test System

From Bus	To Bus	X	MW Limit	From Bus	To Bus	X	MW Limit
1	2	0.0411	730	14	15	0.0217	195
1	39	0.025	545	15	16	0.0094	180
2	3	0.0151	595	16	17	0.0089	660
2	25	0.0086	440	16	19	0.0195	325
2	30	0.0181	560	16	21	0.0135	520
3	4	0.0213	165	16	24	0.0059	235
3	18	0.0133	955	17	18	0.0082	580
4	5	0.0128	260	17	27	0.00692	50
4	14	0.0129	125	19	20	0.0138	340
5	6	0.0026	120	19	33	0.0142	125
5	8	0.0112	230	20	34	0.018	125
6	7	0.0092	280	21	22	0.014	500
6	11	0.0082	195	22	23	0.0096	355
6	31	0.025	205	22	35	0.0143	965
7	8	0.0046	155	23	24	0.035	455
8	9	0.0363	175	23	36	0.0272	560
9	39	0.025	230	25	26	0.0323	715
10	11	0.0043	180	25	37	0.0232	965
10	13	0.0043	130	26	27	0.0147	80
10	32	0.02	125	26	28	0.0474	230
11	12	0.0435	60	26	29	0.0625	270
12	13	0.0435	70	28	29	0.0151	190
13	14	0.0101	145	29	38	0.0156	125

Table 17. Generation Unit Operational Data for the 39-Bus Test System

Bus	Min MW	Max MW	Shutdown/Start up Ramp Rate (MW/h)	Ramp Down/Up Rate (MW/h)	Min Down/Up Time (h)
30	163.05	280.73	163.05	79.81	5
31	30.09	63.3	63.3	63.3	1
32	30.09	63.3	63.3	63.3	1
33	30.09	63.3	63.3	63.3	1
34	30.09	63.3	63.3	63.3	1
35	193.43	483.57	193.43	142.33	15
36	163.05	280.73	163.05	79.81	5
37	193.43	483.57	193.43	142.33	15
38	30.09	63.3	63.3	63.3	1
39	30.09	63.3	63.3	63.3	1

Table 18. Generation Unit Cost Data for the 39-Bus Test System

Bus	Generation Technology	Fuel Cost ($/Btu)	Quadratic Cost Parameters			Start up Cost ($)
			a (Btu/h)	*b (Btu/MWh)*	*c (Btu/MW^{2}h)*	
30	NG CC	6.208	159.69	7.571	0.00427	22820
31	NG CT	6.208	121.00	11.491	0.00736	1410
32	NG CT	6.208	121.00	11.491	0.00736	1410
33	NG CT	6.208	121.00	11.491	0.00736	1410
34	NG CT	6.208	121.00	11.491	0.00736	1410
35	Coal ST	1.943	64.16	9.920	0.01059	52310
36	NG CC	6.208	159.69	7.571	0.00427	22820
37	Coal ST	1.943	64.16	9.920	0.01059	52310
38	NG CT	6.208	121.00	11.491	0.00736	1410
39	NG CT	6.208	121.00	11.491	0.00736	1410

Table 19. Normalized Wind Data for the 39-Bus Test System

Hour of Operation	Wind Power Bus 17 (MW/MW)		Wind Power Bus 18 (MW/MW)	
	Forecast	*Actual*	*Forecast*	*Actual*
1	0.5929	0.4420	0.3891	0.2690
2	0.4779	0.1648	0.4146	0.3347
3	0.3785	0.2460	0.2791	0.2261
4	0.4045	0.2520	0.1337	0.2086
5	0.4232	0.2540	0.2062	0.2350
6	0.4126	0.2081	0.2185	0.1609
7	0.3114	0.1822	0.1303	0.1117
8	0.2533	0.3451	0.1442	0.1344
9	0.1928	0.1638	0.0512	0.0920
10	0.1849	0.1574	0.0515	0.0172
11	0.0838	0.1838	0.0291	0.0375
12	0.1108	0.1903	0.0680	0.0677
13	0.0982	0.3074	0.0602	0.0756
14	0.1956	0.2685	0.0877	0.1078
15	0.2419	0.2480	0.1086	0.2369
16	0.2339	0.2663	0.1124	0.4524
17	0.1556	0.1924	0.1276	0.5157
18	0.0901	0.2242	0.1679	0.4900
19	0.2263	0.3582	0.1338	0.4647
20	0.2931	0.4050	0.1925	0.4927
21	0.3388	0.7409	0.1837	0.2591
22	0.4418	0.7613	0.1405	0.1330
23	0.4521	0.6474	0.1305	0.1452
24	0.6033	0.6749	0.2279	0.2375

Table 20. Load Data for the 39-Bus Test System

Bus	Load at Each Hour of Operation (MW)											
	1	*2*	*3*	*4*	*5*	*6*	*7*	*8*	*9*	*10*	*11*	*12*
3	61.4	63.2	66.4	69.2	72.5	75.4	77.7	80.3	82.3	83.6	84.0	82.9
4	96.9	105.9	113.2	117.2	124.0	125.7	129.5	129.5	129.7	128.8	130.4	129.0
7	48.2	52.3	55.5	57.3	58.9	59.5	60.0	60.2	60.1	60.0	60.8	61.0
8	106.7	112.0	118.6	123.1	127.1	128.5	129.6	131.3	132.6	133.0	134.0	135.2
12	1.5	1.6	1.6	1.7	1.8	1.8	1.8	1.8	1.9	1.9	2.0	1.9
15	58.3	59.5	62.2	65.3	68.3	71.8	75.6	79.2	81.4	82.8	83.5	82.9
16	62.7	63.4	67.4	71.0	73.6	75.2	79.0	81.7	84.4	85.8	85.6	84.6
18	30.0	30.7	31.6	33.1	34.8	36.5	37.8	39.2	39.8	40.7	41.2	41.2
20	129.7	135.5	140.3	145.2	149.1	153.4	156.7	159.8	162.1	163.8	162.9	160.5
21	48.0	49.2	51.7	54.2	56.6	58.6	60.9	62.8	65.1	67.6	69.9	71.4
23	45.3	49.2	54.3	56.9	58.7	60.4	60.9	62.5	63.4	64.2	64.4	64.6
24	56.7	60.9	65.8	69.5	72.0	75.0	76.7	77.4	79.5	80.5	79.2	80.2
25	39.7	41.1	40.8	41.7	41.9	43.6	44.4	45.6	49.2	52.8	57.3	58.1
26	28.2	30.1	31.4	32.4	33.5	34.3	34.6	35.3	35.8	35.9	36.3	36.1
27	54.6	58.3	60.5	63.5	66.8	68.1	69.8	71.7	72.3	73.0	73.3	71.8
28	37.8	42.3	47.2	49.8	50.9	51.8	52.8	52.8	53.0	53.0	53.7	53.3
29	51.6	52.6	55.1	58.3	63.0	67.6	69.9	71.3	73.1	73.7	73.9	73.5
31	1.6	1.6	1.7	1.8	1.8	1.9	1.9	2.1	2.2	2.3	2.4	2.4
39	238.4	240.8	242.8	246.3	251.9	259.5	266.7	273.0	278.5	282.7	286.1	287.8
Bus	**Load at Each Hour of Operation (MW)**											
	13	*14*	*15*	*16*	*17*	*18*	*19*	*20*	*21*	*22*	*23*	*24*
3	81.8	80.6	78.0	76.0	72.2	67.7	64.1	60.7	58.3	56.5	56.2	57.1
4	128.3	127.6	125.9	124.5	128.5	118.6	108.2	99.5	96.0	90.1	92.2	91.5
7	60.4	59.2	59.1	59.7	55.2	49.4	44.7	41.7	40.2	39.7	40.7	44.0
8	136.2	134.5	132.7	132.3	130.5	124.2	113.5	106.0	101.0	98.8	98.1	100.1
12	1.9	1.8	1.7	1.7	1.6	1.4	1.3	1.3	1.3	1.2	1.2	1.3
15	80.5	78.3	76.7	73.4	68.8	64.3	60.8	58.6	56.9	56.0	55.3	55.8
16	83.2	79.9	79.3	76.5	73.4	72.0	67.3	64.0	61.1	58.9	58.8	59.0
18	40.2	39.1	39.0	37.2	34.5	31.8	29.4	28.1	27.1	26.6	26.4	27.3
20	158.7	156.8	156.8	153.9	146.3	137.3	131.3	127.4	125.0	124.1	124.3	126.5
21	71.5	70.4	68.5	66.9	65.1	59.7	55.2	51.3	49.5	47.9	47.1	47.2
23	63.9	62.5	61.3	60.4	60.0	55.6	50.6	46.4	43.9	42.5	42.2	42.6
24	80.3	78.4	76.5	75.8	73.5	67.9	62.9	58.3	55.7	53.6	53.3	54.5
25	58.4	57.3	55.9	54.0	52.6	48.4	45.8	42.8	40.3	38.9	37.7	38.3
26	35.6	34.4	33.8	32.9	30.5	28.0	25.8	24.5	23.7	23.2	23.4	24.8
27	70.7	67.7	66.3	65.5	61.2	56.0	52.7	50.6	49.1	48.4	49.0	50.6
28	53.0	50.9	49.5	49.1	49.3	46.3	42.3	38.8	36.6	35.1	34.7	36.6
29	70.6	69.3	67.1	66.4	63.0	59.2	55.7	52.7	50.7	49.5	48.9	49.2
31	2.3	2.3	2.2	2.2	2.1	2.0	1.9	1.9	1.6	1.7	1.6	1.5
39	288.0	287.8	285.0	280.5	276.3	269.7	261.7	254.1	249.2	245.0	241.9	239.9

Table 21. System Reserves Requirement for the 39-Bus Test System

Hour of Operation	**System Reserves Requirement at Different Wind Penetration Levels (MW)**			
	25%	***30%***	***35%***	***40%***
1	276.4	332.6	388.3	444.5
2	298.5	362.3	426.1	490.0
3	298.5	362.3	426.1	490.0
4	298.5	362.3	426.1	490.0
5	298.5	362.3	426.1	490.0
6	197.2	240.2	283.3	326.0
7	197.2	240.2	283.3	326.0
8	197.2	240.2	283.3	326.0
9	197.2	240.2	283.3	326.0
10	256.8	307.0	360.3	415.0
11	256.8	307.0	360.3	415.0
12	256.8	307.0	360.3	415.0
13	256.8	307.0	360.3	415.0
14	271.3	320.9	370.5	420.1
15	271.3	320.9	370.5	420.1
16	271.3	320.9	370.5	420.1
17	271.3	320.9	370.5	420.1
18	209.6	250.1	290.6	331.1
19	209.6	250.1	290.6	331.1
20	209.6	250.1	290.6	331.1
21	209.6	250.1	290.6	331.1
22	276.4	332.6	388.3	444.5
23	276.4	332.6	388.3	444.5
24	276.4	332.6	388.3	444.5

APPENDIX D: PUBLICATIONS

1. **J. E. Hernandez**, R. P. Kandula, F. C. Lambert, and D. Divan, “A practical directional third harmonic hybrid active filter for medium-voltage utility applications,” IEEE Trans. Ind. Appl., vol. 49, no. 6, pp. 2674-2683, 2013.

2. **J. E. Hernandez**, J. J. Thomas, and S. Grijalva, "Providing flexibility for temporal and spatial constraints to increase wind power production," IEEE Trans. Sust. Energy, Submitted for review on Nov. 30, 2014.

3. R. P. Kandula, A. Iyer, R. Moghe, **J. E. Hernandez**, and D. Divan, “Power router for meshed systems based on a fractionally rated back-to-back converter,” IEEE Trans. Power Electron., vol. 29, no. 10, pp. 5172-5180, 2014.

4. A. R. Iyer, R. P. Kandula, R. Moghe, **J. E. Hernandez**, F. C. Lambert, and D. Divan, “Validation of the plug-and-play AC/AC power electronics building block (AC-PEBB) for medium-voltage grid control applications,” IEEE Trans. Ind. Appl., vol. 50, no. 5, pp. 3549-3557, 2014.

5. **J. E. Hernandez**, R. P. Kandula, F. Lambert, D. Divan, and S. Grijalva, "A 7.2 kV experimental setup of a third harmonic hybrid active filter for medium voltage utility applications," in IEEE Energy Conversion Congr. and Expo., 2013, pp. 5199-5206.

6. **J. E. Hernandez**, R. P. Kandula, F. Lambert, and D. Divan, "A practical directional third harmonic hybrid active filter for medium voltage utility applications," in IEEE Energy Conversion Congr. and Expo., 2012, pp. 219-226.

7. **J. E. Hernandez**, F. Kreikebaum, and D. Divan, "Flexible electric vehicle (EV) charging to meet renewable portfolio standard (RPS) mandates and minimize green house gas emissions," in IEEE Energy Conversion Congr. and Expo., 2010, pp. 4270-4277.

8. J. J. Thomas, **J. E. Hernandez**, and S. Grijalva, "An investigation of the impact of dispatchable power routers on electricity markets and market participants," in IEEE PES General Meeting, 2014, pp. 1-5.

9. A. Iyer, R. Moghe, R. Kandula, **J. E. Hernandez**, and D. Divan, "Validation of the plug-and-play AC/AC power electronics building block (AC-PEBB) for medium voltage grid control applications," in IEEE Energy Conversion Congr. and Expo., 2013, pp. 2544-2551.

10. J. J. Thomas, **J. E. Hernandez**, and S. Grijalva, "Power flow router sensititvities for post-contingency corrective control," in IEEE Energy Conversion Congr. and Expo., 2013, pp. 2590-2596.

11. R. P. Kandula, A. Iyer, R. Moghe, **J. E. Hernandez**, and D. Divan, "Power flow controller for meshed systems with a fractionally rated BTB converter," in IEEE Energy Conversion Congr. and Expo., 2012, pp. 4053-4060.

12. A. Iyer, R. Moghe, R. Kandula, **J. E. Hernandez**, and D. Divan, "Plug-and-play AC/AC power electronics building blocks (AC-PEBBs) for grid control," in IEEE Energy Conversion Congr. and Expo., 2012, pp. 1354-1361.

13. R. P. Kandula, **J. E. Hernandez**, and D. Divan, "Directional triplen hybrid active filter for radial systems," in IEEE Energy Conversion Congr. and Expo., 2011, pp. 4058-4065.

14. R. Moghe, F. Kreikebaum, **J. E. Hernandez**, R. P. Kandula, and D. Divan, "Mitigating distribution transformer lifetime degradation caused by grid-enabled vehicle (GEV) charging," in IEEE Energy Conversion Congr. and Expo., 2011, pp. 835-842.

15. F. Kreikebaum, D. Das, **J. E. Hernandez**, and D. Divan, "Ubiquitous power flow control in meshed grids," in IEEE Energy Conversion Congr. and Expo., 2009, pp. 3907-3914.

REFERENCES

[1] "Annual energy outlook 2013," U.S. EIA, Washington, DC, DOE/EIA-0383(2013), 2013.

[2] M. Guarnieri, “When cars went electric, part one,” IEEE Ind. Electron. Mag., vol. 5, no. 1, pp. 61-62, 2011.

[3] C. C. Chan, “The rise & fall of electric vehicles in 1828-1930: Lessons learned,” Proc. IEEE, vol. 101, no. 1, pp. 206-212, 2013.

[4] C. Sulzberger, “An early road warrior: electric vehicles in the early years of the automobile,” IEEE Power and Energy Mag., vol. 2, no. 3, pp. 66-71, 2004.

[5] M. Guarnieri, “When cars went electric, part 2,” IEEE Ind. Electron. Mag., vol. 5, no. 2, pp. 46-53, 2011.

[6] C. Sulzberger, “Early road warrior, part 2 - competing electric and gasoline vehicles,” IEEE Power and Energy Mag., vol. 2, no. 5, pp. 83-88, 2004.

[7] PBS: Timeline - History of the Electric Car [Online]. Available: http://www.pbs.org/now/shows/223/electric-car-timeline.html

[8] S. D'Agostino, “The electric car,” IEEE Potentials, vol. 12, no. 1, pp. 28-32, 1993.

[9] E. Hesla, “Electric propulsion,” IEEE Ind. Appl. Mag., vol. 15, no. 4, pp. 10-13, 2009.

[10] Electric Auto Association: EV History [Online]. Available: http://www.electricauto.org/?page=EVHistory

[11] U.S. EPA: Overview - The Clean Air Act Amendments of 1990 [Online]. Available: http://epa.gov/oar/caa/caaa_overview.html

[12] THOMAS (Library of Congress): Bill Text - 102nd Congress (1991-1992) H.R.776.ENR [Online]. Available: http://thomas.loc.gov/cgi-bin/query/F?c102:1:./temp/~c102808xcz:e411437:

[13] L. H. Reed Jr., “California low-emission vehicle program: Forcing technology and dealing effectively with the uncertainties,” BC Envtl. Aff. L. Rev., vol. 24, no. 4, pp. 695-793, 1997.

[14] "One million electric vehicles by 2015: February 2011 status report," U.S. DOE, Washington, DC, 2011.

[15] Federal Tax Credits for Electric Vehicles [Online]. Available: http://www.fueleconomy.gov/feg/taxevb.shtml

[16] Alternative Fuels Data Center: All Laws and Incentives Sorted by Type [Online]. Available: http://www.afdc.energy.gov/laws/matrix/incentive

[17] Alternative Fuels Data Center: Alternative Fuel Infrastructure Tax Credit [Online]. Available: http://www.afdc.energy.gov/laws/law/US/10513

[18] Alternative Fuels Data Center: U.S. Alternative Fueling Stations by Fuel Type [Online]. Available: http://www.afdc.energy.gov/data/search?q=sales

[19] Alternative Fuels Data Center: U.S. PEV Sales by Model [Online]. Available: http://www.afdc.energy.gov/data/search?q=sales

[20] A. Baum, "Electric vehicle market summary," Baum & Assoc., West Bloomfield, MI, 2014.

[21] Nissan LEAF: Price & Specs [Online]. Available: http://www.nissanusa.com/electric-cars/leaf/versions-specs/version.s.html

[22] Chevrolet Volt: Options and Standard Equipment [Online]. Available: http://www.chevrolet.com/volt-electric-car/specs/options.html

[23] N. Layne. Nissan Lifts U.S. Output of Electric Leaf as Sales Rise [Online]. Available: http://www.reuters.com/article/2014/01/14/autoshow-nissan-leaf-idUSL2N0KO1KC20140114

[24] A. Sharma. GM to Invest $450 Mln in Two Michigan Plants [Online]. Available: http://www.reuters.com/article/2014/04/08/gm-investment-idUSL3N0N00SY20140408

[25] Navigant Research: Plug-In Electric Vehicles on Roads in the United States Will Surpass 2.7 Million by 2023 [Online]. Available: http://www.navigantresearch.com/newsroom/plug-in-electric-vehicles-on-roads-in-the-united-states-will-surpass-2-7-million-by-2023

[26] Alternative Fuels Data Center: U.S. HEV Sales by Model [Online]. Available: http://www.afdc.energy.gov/data/search?q=sales

[27] Navigant Research: Electric Vehicle Geographic Forecasts [Online]. Available: http://www.navigantresearch.com/research/electric-vehicle-geographic-forecasts

[28] A. Cooper, L. Wood, I. Rohmund, D. Costenaro, and A. Duer, "Forecast of on-road electric transportation in the U.S. (2010-2035)," IEE Edison Found., Washington, DC, 2013.

[29] "The future of the electric grid: An interdisciplinary MIT study," MIT Energy Initiative, Cambridge, MA, 2011.

[30] W. Di, D. C. Aliprantis, and Y. Lei, “Load scheduling and dispatch for aggregators of plug-in electric vehicles,” IEEE Trans. Smart Grid, vol. 3, no. 1, pp. 368-376, 2012.

[31] F. K. Tuffner and M. C. Kintner-Meyer, "Using electric vehicles to meet balancing requirements associated with wind power," PNNL, Richland, WA, 2011.

[32] J. L. Sullivan, I. T. Salmeen, and C. P. Simon, "PHEV marketplace penetration: An agent based simulation," UMTRI, Ann Arbor, MI, UMTRI-2009-32, 2009.

[33] T. P. Cleary, K. G. Sikes, Z. Lin, J. L. Sullivan, J. Ward, and T. J. Gross, "PHEV market introduction study," ORNL, Oak Ridge, TN, ORNL/TM-2009/019, 2010.

[34] "Annual energy outlook 2011," U.S. EIA, Washington, DC, DOE/EIA-0383(2011), 2011.

[35] S. Y. Jeon, “Hybrid & electric vehicle technology and its market feasibility,” M.S. thesis, Syst. Design & Manag. Prog., Massachusetts Ints. of Tech., Cambridge, MA, 2010.

[36] M. C. Kuss, A. J. Markel, and W. E. Kramer, “Application of distribution transformer thermal life models to electrified vehicle charging loads using Monte-Carlo method,” in 25th World Battery, Hybrid and Fuel Cell Electric Vehicle Symp. & Exhib., 2010.

[37] Q. Li, T. Cui, R. Negi, F. Franchetti, and M. D. Ilic, “On-line decentralized charging of plug-in electric vehicles in power systems,” ArXiv e-prints, Nov. 2011.

[38] C. Gerkensmeyer, M. C. Kintner-Meyer, and J. G. DeSteese, "Technical challenges of plug-in hybrid electric vehicles and impacts to the US power system: Distribution system analysis," PNNL, Richland, WA, 2010.

[39] K. Clement-Nyns, E. Haesen, and J. Driesen, “The impact of charging plug-in hybrid electric vehicles on a residential distribution grid,” IEEE Trans. Power Syst., vol. 25, no. 1, pp. 371-380, 2010.

[40] J. A. P. Lopes, F. J. Soares, and P. M. R. Almeida, “Integration of electric vehicles in the electric power system,” Proc. IEEE, vol. 99, no. 1, pp. 168-183, 2011.

[41] C. Roe, E. Farantatos, J. Meisel, A. P. Meliopoulos, and T. Overbye, "Power system level impacts of PHEVs," in 42nd Int. Conf. on System Sciences, 2009, pp. 1-10.

[42] R. Moghe, F. Kreikebaum, J. E. Hernandez, R. P. Kandula, and D. Divan, "Mitigating distribution transformer lifetime degradation caused by grid-enabled vehicle (GEV) charging," in IEEE Energy Conversion Congr. and Expo., 2011, pp. 835-842.

[43] A. Ipakchi and F. Albuyeh, “Grid of the future,” IEEE Power and Energy Mag., vol. 7, no. 2, pp. 52-62, 2009.

[44] R. C. Green, L. Wang, and M. Alam, “The impact of plug-in hybrid electric vehicles on distribution networks: A review and outlook,” Renewable and Sust. Energy Rev., vol. 15, no. 1, pp. 544-553, 2011.

[45] M. Kintner-Meyer, K. Schneider, and R. Pratt, “Impacts assessment of plug-in hybrid vehicles on electric utilities and regional US power grids, part 1: Technical analysis,” in 2007 Electric Utilities Environmental Conf., 2007.

[46] S. W. Hadley and A. A. Tsvetkova, "Potential impacts of plug-in hybrid electric vehicles on regional power generation," ORNL, Oak Ridge, TN, 2008.

[47] M. D. Galus, M. Zima, and G. Andersson, “On integration of plug-in hybrid electric vehicles into existing power system structures,” Energy Policy, vol. 38, no. 11, pp. 6736-6745, 2010.

[48] M. Kintner-Meyer, T. B. Nguyen, C. Jin, P. Balducci, and T. Secrest, "Impact assessment of plug-in hybrid vehicles on the US power grid," in 25th World Battery, Hybrid and Fuel Cell Electric Vehicle Symp. & Exhib., 2010.

[49] S. D. Jenkins, J. R. Rossmaier, and M. Ferdowsi, "Utilization and effect of plug-in hybrid electric vehicles in the United States power grid," in IEEE Vehicle Power and Propulsion Conf., 2008, pp. 1-5.

[50] B. Soares M.C. Borba, A. Szklo, and R. Schaeffer, “Plug-in hybrid electric vehicles as a way to maximize the integration of variable renewable energy in power systems: The case of wind generation in northeastern Brazil,” Energy, vol. 37, no. 1, pp. 469-481, 2012.

[51] W. Kempton and J. Tomić, “Vehicle-to-grid power fundamentals: Calculating capacity and net revenue,” J. of Power Sources, vol. 144, no. 1, pp. 268-279, 2005.

[52] A. Brooks, E. Lu, D. Reicher, C. Spirakis, and B. Weihl, “Demand dispatch,” IEEE Power and Energy Mag., vol. 8, no. 3, pp. 20-29, 2010.

[53] SAE Electric Vehicle and Plug-in Hybrid Electric Vehicle Conductive Charge Coupler, SAE Standard J1772-201210, 2012.

[54] J. Arrillaga and N. R. Watson, Power system harmonics, 2nd ed. Chichester, England: Wiley, 2003.

[55] T. A. Short, Distribution Reliability and Power Quality, Boca Raton, FL: CRC Press, 2006.

[56] R. Dugan, S. Santoso, and M. F. McGranaghan, Electrical Power Systems Quality, 2nd ed. New York, NY: McGraw-Hill, 2002.

[57] E. L. Owen, “A history of harmonics in power systems,” IEEE Ind. Appl. Mag., vol. 4, no. 1, pp. 6-12, 1998.

[58] G. I. Rhodes, “Parallel operation of three-phase generators, with their neutrals interconnected,” Trans. AIEE, vol. XXIX, no. 1, pp. 765-790, 1910.

[59] A. H. Griswold and R. W. Mastick, “Inductive interference as a practical problem,” Trans. AIEE, vol. XXXV, no. 2, pp. 1051-1094, 1916.

[60] F. C. Orchard, Mercury Arc Rectifier Practice, London, England: Chapman & Hall, 1935.

[61] P. W. Blye and H. E. Kent, “Effects of rectifiers on system wave shape,” Trans. AIEE, vol. 53, no. 1, pp. 54-63, 1934.

[62] R. P. Stratford, “Analysis and control of harmonic current in systems with static power converters,” IEEE Trans. Ind. Appl., vol. IA-17, no. 1, pp. 71-81, 1981.

[63] C. K. Duffey and R. P. Stratford, “Update of harmonic standard IEEE-519: IEEE recommended practices and requirements for harmonic control in electric power systems,” IEEE Trans. Ind. Appl., vol. 25, no. 6, pp. 1025-1034, 1989.

[64] IEEE Guide for Harmonic Control and Reactive Compensation of Static Power Convertors, ANSI/IEEE Std 519-1981, 1981.

[65] IEEE Recommended Practices and Requirements for Harmonic Control in Electrical Power Systems, IEEE Std 519-1992, 1993.

[66] C. Sankaran, Power Quality, Boca Raton, FL: CRC Press, 2002.

[67] F. C. De La Rosa, Harmonics and Power Systems, Boca Raton, FL: CRC Press, 2006.

[68] U.S. EIA: Residential Energy Consumption Survey (RECS) [Online]. Available: http://www.eia.gov/consumption/residential/

[69] A. Mansoor, W. M. Grady, R. S. Thallam, M. T. Doyle, S. D. Krein, and M. J. Samotyj, “Effect of supply voltage harmonics on the input current of single-phase diode bridge rectifier loads,” IEEE Trans. Power Del., vol. 10, no. 3, pp. 1416-1422, 1995.

[70] A. Mansoor, W. M. Grady, P. T. Staats, R. S. Thallam, M. T. Doyle, and M. J. Samotyj, “Predicting the net harmonic currents produced by large numbers of distributed single-phase computer loads,” IEEE Trans. Power Del., vol. 10, no. 4, pp. 2001-2006, 1995.

[71] IEEE Draft Guide for Applying Harmonic Limits on Power Systems, IEEE P519.1/D12, 2012.

[72] Electromagnetic Compability (EMC) - Part 3-2: Limits - Limits for Harmonic Current Emissions (Equipment input current ≤ 16 A per phase), IEC 61000-3-2, 2009.

[73] Electromagnetic Compatibility (EMC) - Part 3-12: Limits - Limits for Harmonic Currents Produced by Equipment Connected to Public Low-voltage Systems with Input Current >16 A and ≤ 75 A per Phase, IEC 61000-3-12, 2011.

[74] W. Jewell and D. J. Ward, "Single phase harmonic limits," in PSERC EMI, Power Quality, and Safety Workshop, 2002.

[75] T. A. Short, Electric Power Distribution Handbook, Boca Raton, FL: CRC Press, 2004.

[76] A. A. Sallam and O. P. Malik, Electric Distribution Systems, Hoboken, NJ: Wiley-IEEE Press, 2011.

[77] J. Schonek, "The singularities of the third harmonic," Cahier Technique Schneider Electric, no. 202, pp. 8-9, 2001.

[78] J. C. Balda, A. R. Oliva, D. W. McNabb, and R. D. Richardson, "Measurements of neutral currents and voltages on a distribution feeder," IEEE Trans. Power Del., vol. 12, no. 4, pp. 1799-1804, 1997.

[79] V. E. Wagner, J. C. Balda, D. C. Griffith, A. McEachern, T. M. Barnes, D. P. Hartmann, D. J. Phileggi, A. E. Emannuel, W. F. Horton, W. E. Reid, R. J. Ferraro, and W. T. Jewell, "Effects of harmonics on equipment," IEEE Trans. Power Del., vol. 8, no. 2, pp. 672-680, 1993.

[80] S. E. Zocholl and G. Benmouyal, "How microprocessor relays respond to harmonics, saturation, and other wave distortions," in Proc. 24th Annu. Western Protective Relay Conf., 1997, pp. 1-15.

[81] A. Medina and M. Martinez-Cardenas, "Analysis of the harmonic distortion impact on the operation of digital protection systems," in IEEE PES General Meeting, 2005, pp. 741-745.

[82] I. Zamora, A. J. Mazon, V. Valverde, J. I. S. Martin, G. Buigues, and A. Dysko, "Influence of power quality on the performance of digital protection relays," in IEEE Power Tech, 2005, pp. 1-7.

[83] T. Q. Tran, L. E. Conrad, and B. K. Stallman, "Electric shock and elevated EMF levels due to triplen harmonics," IEEE Trans. Power Del., vol. 11, no. 2, pp. 1041-1049, 1996.

[84] A. Maitra, W. Sunderman, and D. Dorr, "Studying the impact of elevated neutral to earth voltage on distribution systems due to triplen harmonics," in IEEE PES General Meeting, 2006.

[85] A. Lefcourt, “Effects of electrical voltage/current on farm animals: how to detect and remedy problems USDA Handbook 696,” USDA, Washington, DC, 1991.

[86] D. Dorr, W. Howe, P. Lim, and C. Bray, "Understanding nuisance shocking from an electric power utility perspective," in IEEE Int. Power Engineering Conf., 2007, pp. 505-509.

[87] E. R. Collins and J. Jian, “Analysis of elevated neutral-to-earth voltage in distribution systems with harmonic distortion,” IEEE Trans. Power Del., vol. 24, no. 3, pp. 1696-1702, 2009.

[88] W. G. Sunderman, R. C. Dugan, and D. S. Dorr, "The neutral-to-earth voltage (NEV) test case and distribution system analysis," in IEEE PES General Meeting, 2008, pp. 1-6.

[89] O. C. Onar and A. Khaligh, "Grid interactions and stability analysis of distribution power network with high penetration of plug-in hybrid electric vehicles," in IEEE Applied Power Electronics Conf. and Expo., 2010, pp. 1755-1762.

[90] R. Liu, L. Dow, and E. Liu, "A survey of PEV impacts on electric utilities," in IEEE PES Innovative Smart Grid Tecnologies, 2011, pp. 1-8.

[91] V. Monteiro, H. Gonçalves, J. C. Ferreira, and J. L. Afonso, “Batteries charging systems for electric and plug-in hybrid electric vehicles,” in New Advances in Vehicular Technology and Automotive Engineering, Rijeka, Croatia: InTech, 2012, ch. 5, pp. 149-168.

[92] Y. Lu and J. Jiang, "Harmonic-study of electric vehicle chargers," in Proc. 8th Int. Conf. Electrical Machines and Systems, 2005, pp. 2404-2407.

[93] J. C. Gomez and M. M. Morcos, “Impact of EV battery chargers on the power quality of distribution systems,” IEEE Trans. Power Del., vol. 18, no. 3, pp. 975-981, 2003.

[94] P. T. Staats, W. M. Grady, A. Arapostathis, and R. S. Thallam, “A statistical method for predicting the net harmonic currents generated by a concentration of electric vehicle battery chargers,” IEEE Trans. Power Del., vol. 12, no. 3, pp. 1258-1266, 1997.

[95] M. M. Morcos, N. G. Dillman, and C. R. Mersman, “Battery chargers for electric vehicles,” IEEE Power Eng. Rev., vol. 20, no. 11, pp. 8-11, 2000.

[96] S. H. Berisha, G. G. Karady, R. Ahmad, R. Hobbs, and D. Karner, "Current harmonics generated by electric vehicle battery chargers," in Proc. Int. Conf. Power Electronics, Drives, and Energy Systems for Industrial Growth, 1996, pp. 584-589.

[97] F. Lambert, "Secondary distribution impacts of residential electric vehicle charging," California Energy Commision, Sacramento, CA, P600-00-039, 2000.

[98] C. Mersman, M. Morcos, and N. Dillman, "On the design of a novel microprocessor-based battery charger for electric vehicles," in Proc. 8th Europe Power Electronics Conf., 1999.

[99] J. A. Orr, A. E. Emanuel, and K. W. Oberg, "Current harmonics generated by a cluster of electric vehicle battery chargers," IEEE Trans. Power App. Syst., vol. PAS-101, no. 3, pp. 691-700, 1982.

[100] J. A. Orr, A. E. Emanuel, and D. J. Pileggi, "Current harmonics, voltage distortion, and powers associated with electric vehicle battery chargers distributed on the residential power system," IEEE Trans. Ind. Appl., vol. IA-20, no. 4, pp. 727-734, 1984.

[101] P. T. Staats, W. M. Grady, A. Arapostathis, and R. S. Thallam, "A statistical analysis of the effect of electric vehicle battery charging on distribution system harmonic voltages," IEEE Trans. Power Del., vol. 13, no. 2, pp. 640-646, 1998.

[102] R. Bass, R. G. Harley, F. Lambert, V. Rajasekaran, and J. Pierce, "Residential harmonic loads and EV charging," in IEEE PES Winter Meeting, 2001, pp. 803-808.

[103] D. K. Jackson, A. M. Schultz, S. B. Leeb, A. H. Mitwalli, G. C. Verghese, and S. R. Shaw, "A multirate digital controller for a 1.5-kW electric vehicle battery charger," IEEE Trans. Power Electron., vol. 12, no. 6, pp. 1000-1006, 1997.

[104] R. P. Kandula, J. E. Hernandez, and D. Divan, "Directional triplen hybrid active filter for radial systems," in IEEE Energy Conversion Congr. and Expo., 2011, pp. 4058-4065.

[105] IEEE Guide for the Application of Shunt Power Capacitors, IEEE Std 1036-2010, 2011.

[106] S. Peele, D. Guinn, and J. Grappe, "Progress energy tackles the third harmonic," Transm. & Distr. World, vol. 63, no. 12, pp. 48-52, 2011.

[107] M. E. L. Tostes, U. H. Bezerra, R. Silva, J. A. L. Valente, C. C. M. de Moura, and T. M. M. Branco, "Impacts over the distribution grid from the adoption of distributed harmonic filters on low-voltage customers," IEEE Trans. Power Del., vol. 20, no. 1, pp. 384-389, 2005.

[108] S. Bhattacharya and D. Divan, "Active filter solutions for utility interface of industrial loads," in Proc. Int. Conf. Power Electronics, Drives and Energy Systems for Industrial Growth, 1996, pp. 1078-1084.

[109] K. Schipman and F. Delincé, “The importance of good power quality,” ABB Power Qual. Prod., Charleroi, Belgium, ABB Review, 2010.

[110] L. Gyugyi and E. C. Strycula, "Active ac power filters," in IEEE Industry Applications Society Annu. Meeting, 1976, pp. 529-535.

[111] B. Singh, K. Al-Haddad, and A. Chandra, “A review of active filters for power quality improvement,” IEEE Trans. Ind. Electron., vol. 46, no. 5, pp. 960-971, 1999.

[112] V. Khadkikar, A. Chandra, and B. Singh, “Digital signal processor implementation and performance evaluation of split capacitor, four-leg and three H-bridge-based three-phase four-wire shunt active filters,” IET Power Electron., vol. 4, no. 4, pp. 463-470, 2011.

[113] B. Singh, V. Verma, A. Chandra, and K. Al-Haddad, “Hybrid filters for power quality improvement,” IEE Proc. Gen., Transm. and Distr., vol. 152, no. 3, pp. 365-378, 2005.

[114] J. Hurng-Liahng, W. Kuen-Der, W. Jinn-Chang, and C. Wen-Jung, “A three-phase four-wire power filter comprising a three-phase three-wire active power filter and a zig-zag transformer,” IEEE Trans. Power Electron., vol. 23, no. 1, pp. 252-259, 2008.

[115] P. N. Enjeti, W. Shireen, P. Packebush, and I. J. Pitel, “Analysis and design of a new active power filter to cancel neutral current harmonics in three-phase four-wire electric distribution systems,” IEEE Trans. Ind. Appl., vol. 30, no. 6, pp. 1565, 1994.

[116] G. Kamath and N. Mohan, "A novel, reduced rating active filter for 3-phase, 4-wire loads," in IEEE Industry Applications Society Annu. Meeting, 1994, pp. 936-940.

[117] J. E. Hernandez, R. P. Kandula, F. C. Lambert, and D. Divan, “A practical directional third harmonic hybrid active filter for medium-voltage utility applications,” IEEE Trans. Ind. Appl., vol. 49, no. 6, pp. 2674-2683, 2013.

[118] J. E. Hernandez, R. P. Kandula, F. Lambert, D. Divan, and S. Grijalva, "A 7.2 kV experimental setup of a third harmonic hybrid active filter for medium voltage utility applications," in IEEE Energy Conversion Congr. and Expo., 2013, pp. 5199-5206.

[119] IEEE Standard for Shunt Power Capacitors, IEEE Std 18-2012, 2013.

[120] S. Bhattacharya, C. Po-Tai, and D. M. Divan, “Hybrid solutions for improving passive filter performance in high power applications,” IEEE Trans. Ind. Appl., vol. 33, no. 3, pp. 732-747, 1997.

[121] D. ZhanFeng, J. Xinjian, and Z. Dongqi, "A novel hybrid filter to cancel the neutral harmonic current," in IEEE IAS Annu. Meeting, 2002, pp. 59-63.

[122] R. P. Kandula, A. Iyer, and D. Divan, "Stable operation of multiple power routers," in IEEE Energy Conversion Congr. and Expo., 2013, pp. 1435-1442.

[123] J. Kueck, B. Kirby, T. Rizy, F. Li, and N. Fall, "Reactive power from distributed energy," The Electricity J., vol. 19, no. 10, pp. 27-38, 2006.

[124] "Economics and application of shunt capacitors on utility systems," McGraw-Edison Co., Pittsburgh, PA, Bulletin No. 71011, 1981.

[125] A. M. Bryantsev, M. D. Galperin, and G. A. Evdokunin, "Magnetically controlled reactors enhance transmission capability & save energy—Especially in compact Increased surge-impedance-loading power lines," in NSF/EPRI Urgent Opportunities for Transmission System Enhancement Workshop, 2001.

[126] S. Inoue, T. Shimizu, and K. Wada, "Control methods and compensation characteristics of a series active filter for a neutral conductor," IEEE Trans. Ind. Electron., vol. 54, no. 1, pp. 433-440, 2007.

[127] N. Mohan, T. M. Undeland, and W. P. Robbins, Power Electronics: Converters, Applications, and Design, 3rd ed. Hoboken, NJ: Wiley, 2003.

[128] "Assessment of elevated neutral to earth voltages in distribution systems: Modeling and simulation guidelines," EPRI, Palo Alto, CA, Tech. Rep. 1012439, 2006.

[129] "PSCAD user's guide," Manitoba HVDC Research Centre, Winnipeg, Canada, 2010.

[130] A. Morched, B. Gustavsen, and M. Tartibi, "A universal model for accurate calculation of electromagnetic transients on overhead lines and underground cables," IEEE Trans. Power Del., vol. 14, no. 3, pp. 1032-1038, 1999.

[131] B. Gustavsen, G. Irwin, R. Mangelrød, D. Brandt, and K. Kent, "Transmission line models for the simulation of interaction phenomena between parallel AC and DC overhead lines," in Proc. Int. Conf. Power System Transients, 1999, pp. 61-67.

[132] "Electric power monthly with data for July 2014," U.S. EIA, Washington, DC, 2014.

[133] "Monthy energy review," U.S. EIA, Washington, DC, DOE/EIA-0035(2014/09), 2014.

[134] U.S. EPA: Renewable Portfolio Standards [Online]. Available: http://www.epa.gov/agstar/tools/funding/renewable.html

[135] R. Wiser, C. Namovicz, M. Gielecki, and R. Smith, “The experience with renewable portfolio standards in the United States,” The Electricity J., vol. 20, no. 4, pp. 8-20, 2007.

[136] C. Loutan and D. Hawkins, "Integration of renewable resources: Transmission and operating issues and recommendations for integrating renewable resources on the California ISO-controlled Grid," CAISO, Folsom, CA, 2007.

[137] C. Loutan, Y. Taiyou, S. Chowdhury, A. A. Chowdhury, and G. Rosenblum, "Impacts of integrating wind resources into the California ISO market construct," in IEEE PES General Meeting, 2009, pp. 1-7.

[138] T. Ackermann, Wind Power in Power Systems, Hoboken, NJ: Wiley, 2005.

[139] S. V. Valentine, “Understanding the variability of wind power costs,” Ren. and Sust. Energy Rev., vol. 15, no. 8, pp. 3632-3639, 2011.

[140] L. E. Benitez, P. C. Benitez, and G. C. van Kooten, “The economics of wind power with energy storage,” Energy Econ., vol. 30, no. 4, pp. 1973-1989, 2008.

[141] "20% Wind energy by 2030: Increasing wind energy's contribution to U.S. electricity supply," U.S. DOE, Washington, DC, DOE/GO-102008-2567, 2008.

[142] F. Bouffard and F. D. Galiana, “Stochastic security for operations planning with significant wind power generation,” IEEE Trans. Power Syst., vol. 23, no. 2, pp. 306-316, 2008.

[143] A. Tuohy, P. Meibom, E. Denny, and M. O'Malley, “Unit commitment for systems with significant wind penetration,” IEEE Trans. Power Syst., vol. 24, no. 2, pp. 592-601, 2009.

[144] Z. Chaoyue and G. Yongpei, “Unified stochastic and robust unit commitment,” IEEE Trans. Power Syst., vol. 28, no. 3, pp. 3353-3361, 2013.

[145] M. A. Ortega-Vazquez and D. S. Kirschen, “Estimating the spinning reserve requirements in systems with significant wind power generation penetration,” IEEE Trans. Power Syst., vol. 24, no. 1, pp. 114-124, 2009.

[146] M. A. Matos and R. J. Bessa, “Setting the operating reserve using probabilistic wind power forecasts,” IEEE Trans. Power Syst., vol. 26, no. 2, pp. 594-603, 2011.

[147] W. Kempton and J. Tomić, “Vehicle-to-grid power implementation: From stabilizing the grid to supporting large-scale renewable energy,” J. of Power Sources, vol. 144, no. 1, pp. 280-294, 2005.

[148] L. Cong, W. Jianhui, A. Botterud, Z. Yan, and A. Vyas, “Assessment of impacts of PHEV charging patterns on wind-thermal scheduling by stochastic unit commitment,” IEEE Trans. Smart Grid, vol. 3, no. 2, pp. 675-683, 2012.

[149] A. Y. Saber and G. K. Venayagamoorthy, "Resource scheduling under uncertainty in a smart grid with renewables and plug-in vehicles," IEEE Syst. J., vol. 6, no. 1, pp. 103-109, 2012.

[150] J. Kiviluoma and P. Meibom, "Methodology for modelling plug-in electric vehicles in the power system and cost estimates for a system with either smart or dumb electric vehicles," Energy, vol. 36, no. 3, pp. 1758-1767, 2011.

[151] M. E. Khodayar, W. Lei, and M. Shahidehpour, "Hourly coordination of electric vehicle operation and volatile wind power generation in SCUC," IEEE Trans. Smart Grid, vol. 3, no. 3, pp. 1271-1279, 2012.

[152] Z. JunHua, W. Fushuan, D. Zhao Yang, X. Yusheng, and W. Kit-Po, "Optimal dispatch of electric vehicles and wind power using enhanced particle swarm optimization," IEEE Trans. Ind. Informat., vol. 8, no. 4, pp. 889-899, 2012.

[153] R. Baldick, "The generalized unit commitment problem," IEEE Trans. Power Syst., vol. 10, no. 1, pp. 465-475, 1995.

[154] N. P. Padhy, "Unit commitment-a bibliographical survey," IEEE Trans. Power Syst., vol. 19, no. 2, pp. 1196-1205, 2004.

[155] R. H. Kerr, J. L. Scheidt, A. J. Fontanna, and J. K. Wiley, "Unit commitment," IEEE Trans. Power App. Syst., vol. PAS-85, no. 5, pp. 417-421, 1966.

[156] P. G. Lowery, "Generating unit commitment by dynamic programming," IEEE Trans. Power App. Syst., vol. PAS-85, no. 5, pp. 422-426, 1966.

[157] K. Hara, M. Kimura, and N. Honda, "A method for planning economic unit commitment and maintenance of thermal power systems," IEEE Trans. Power App. Syst., vol. PAS-85, no. 5, pp. 427-436, 1966.

[158] S. Takriti, J. R. Birge, and E. Long, "A stochastic model for the unit commitment problem," IEEE Trans. Power Syst., vol. 11, no. 3, pp. 1497-1508, 1996.

[159] A. J. Wood and B. F. Wollenberg, Power Generation, Operation, and Control, 2nd ed. Hoboken, NJ: Wiley, 1996.

[160] W. Lei, M. Shahidehpour, and L. Tao, "Stochastic security-constrained unit commitment," IEEE Trans. Power Syst., vol. 22, no. 2, pp. 800-811, 2007.

[161] H. Ma and S. M. Shahidehpour, "Unit commitment with transmission security and voltage constraints," IEEE Trans. Power Syst., vol. 14, no. 2, pp. 757-764, 1999.

[162] M. Carrion and J. M. Arroyo, "A computationally efficient mixed-integer linear formulation for the thermal unit commitment problem," IEEE Trans. Power Syst., vol. 21, no. 3, pp. 1371-1378, 2006.

[163] J. Ostrowski, M. F. Anjos, and A. Vannelli, “Tight mixed integer linear programming formulations for the unit commitment problem,” IEEE Trans. Power Syst., vol. 27, no. 1, pp. 39-46, 2012.

[164] "State of the market report for PJM 2012," Monitoring Analytics, Eagleville, PA, 2013.

[165] Y. G. Rebours, D. S. Kirschen, M. Trotignon, and S. Rossignol, “A survey of frequency and voltage control ancillary services—Part I: Technical features,” IEEE Trans. Power Syst., vol. 22, no. 1, pp. 350-357, 2007.

[166] Z. Peng, Q. Kejun, Z. Chengke, B. G. Stewart, and D. M. Hepburn, “A methodology for optimization of power systems demand due to electric vehicle charging load,” IEEE Trans. Power Syst., vol. 27, no. 3, pp. 1628-1636, 2012.

[167] A. Foley, B. Tyther, P. Calnan, and B. Ó Gallachóir, “Impacts of electric vehicle charging under electricity market operations,” Applied Energy, vol. 101, no. 0, pp. 93-102, 2013.

[168] L. Rong-Ceng, S. Chun-Lien, and L. Chan-Nan, “Stochastic analyses of electric vehicle charging impacts on distribution network,” IEEE Trans. Power Syst., vol. 29, no. 3, pp. 1055-1063, 2014.

[169] I. Momber, G. Morales-Espana, A. Ramos, and T. Gomez, “PEV storage in multi-bus scheduling problems,” IEEE Trans. Smart Grid, vol. 5, no. 2, pp. 1079-1087, 2014.

[170] J. Chenrui, T. Jian, and P. Ghosh, “Optimizing electric vehicle charging: A customer's perspective,” IEEE Trans. Veh. Technol., vol. 62, no. 7, pp. 2919-2927, 2013.

[171] U.S. FHWA: National Household Travel Survey [Online]. Available: http://nhts.ornl.gov

[172] T. A. Becker, I. Sidhu, and B. Tenderich, "Electric vehicles in the United States: A new model with forecasts to 2030," CET Univ. of California, Berkeley, CA, Rep. 2009.1.v.2.0, 2009.

[173] "2009 National household travel survey: User's guide," U.S. FHWA, Washington, DC, Version 2, 2011.

[174] A. Botterud, Z. Zhi, W. Jianhui, J. Sumaili, H. Keko, J. Mendes, R. J. Bessa, and V. Miranda, “Demand dispatch and probabilistic wind power forecasting in unit commitment and economic dispatch: A case study of Illinois,” IEEE Trans. Sust. Energy, vol. 4, no. 1, pp. 250-261, 2013.

[175] Z. Chaoyue, W. Jianhui, J. P. Watson, and G. Yongpei, “Multi-stage robust unit commitment considering wind and demand response uncertainties,” IEEE Trans. Power Syst., vol. 28, no. 3, pp. 2708-2717, 2013.

[176] W. Hongyu and M. Shahidehpour, “Stochastic SCUC solution with variable wind energy using constrained ordinal optimization,” IEEE Trans. Sust. Energy, vol. 5, no. 2, pp. 379-388, 2014.

[177] NREL: Transmission Grid Integration - Eastern Wind Dataset [Online]. Available: http://www.nrel.gov/electricity/transmission/eastern_wind_methodology.html

[178] M. Brower, "Development of eastern regional wind resource and wind plant output datasets," AWS Truewind, Albany, NY, Subcontract Rep. NREL/SR-550-46764, 2009.

[179] A. Botterud, J. Wang, V. Miranda, and R. J. Bessa, “Wind power forecasting in U.S. electricity markets,” The Electricity J., vol. 23, no. 3, pp. 71-82, 2010.

[180] ERCOT: Quick Facts [Online]. Available: http://www.ercot.com/content/news/presentations/2014/ERCOT_Quick_Facts_091114.pdf

[181] D. Maggio, C. D'Annunzio, H. Shun-Hsien, and C. Thompson, "Utilization of forecasts for wind-powered generation resources in ERCOT operations," in IEEE PES General Meeting, 2010, pp. 1-5.

[182] D. G. Choi, F. Kreikebaum, V. M. Thomas, and D. Divan, “Coordinated EV adoption: Double-digit reductions in emissions and fuel use for $40/vehicle-year,” Environ. Science & Technol., vol. 47, no. 18, pp. 10703-10707, 2013.

[183] H. Bludszuweit, J. A. Dominguez-Navarro, and A. Llombart, “Statistical analysis of wind power forecast error,” IEEE Trans. Power Syst., vol. 23, no. 3, pp. 983-991, 2008.

[184] R. Baldick, M. Webber, and C. King, "Techno-economic modeling of the integration of 20% wind and large-scale energy storage in ERCOT by 2030," Univ. of Texas, Austin, TX, DE-EE0001385, 2012.

[185] "ERCOT methodologies for determining ancillary service requirements," ERCOT, Austin, TX, 2013.

[186] IEEE 10-Generator 39-Bus System [Online]. Available: http://sys.elec.kitami-it.ac.jp/ueda/demo/WebPF/39-New-England

[187] FERC: RTO Unit Commitment Test System [Online]. Available: http://www.ferc.gov/industries/electric/indus-act/market-planning/rto-commit-test.asp

[188] F. N. Lee, “A fuel-constrained unit commitment method,” IEEE Trans. Power Syst., vol. 4, no. 3, pp. 1208-1218, 1989.

[189] J. Price. Reduced Network Modeling of WECC as a Market Design Prototype [Online]. Available: http://www.pserc.wisc.edu/research/public_reports/markets.aspx

[190] WECC, “Generator parameters and outage data,” in DWG Meeting, 2013.

[191] FERC: Form No. 714 - Annual Electric Balancing Authority Area and Planning Area Report [Online]. Available: http://www.ferc.gov/docs-filing/forms/form-714/data.asp

[192] FERC: Electric Power Markets - National Overview [Online]. Available: http://www.ferc.gov/market-oversight/mkt-electric/overview.asp

[193] M. A. Ortega-Vazquez and D. S. Kirschen, "Economic impact assessment of load forecast errors considering the cost of interruptions," in IEEE PES General Meeting, 2006.

[194] NYISO: Markets & Operations - Market Data - Load Data [Online]. Available: http://www.nyiso.com/public/markets_operations/market_data/load_data/index.jsp

[195] M. Duvall, “Comparing the benefits and impacts of hybrid electric vehicle options for compact sedan and sport utility vehicles,” EPRI Palo Alto, CA, Rep. 1006892, 2002.

[196] "National electric transmission congestion study," U.S. DOE, Washington, DC, 2009.

[197] S. Pullins, I. Volkova, and I. Danilin, "Joint Russian/American study on legal/regulatory, market, consumer and technical impediments to smart grid technology deployment," USAID and USEA, Washington, DC, 2012.

[198] NERC: TLR Logs [Online]. Available: http://www.nerc.com/pa/rrm/TLR/Pages/TLR-Logs.aspx

[199] "State of the market report for PJM," Monitoring Analytics, Eagleville, PA, 2011.

[200] "2009 State of the market report New York ISO electricity markets," Potomac Economics, Fairfax, VA, 2010.

[201] "Transmission facts," AEP, Columbus, OH, 2008.

[202] "Transmission investment: Adequate returns and regulatory certainty are key," Edison Electric Institute, Washington, DC, 2013.

[203] "Green power superhighways: Building a path to America's clean energy future," AWEA & SEIA, Washington, DC, 2009.

[204] "National transmission grid study," U.S. DOE, Washington, DC, 2002.

[205] "Flexible AC transmission systems benefits study," California Energy Commission, Sacramento, CA, P600-00-037, 1999.

[206] D. Das, "Dynamic control of grid power flow using controllable network transformers," Ph.D. dissertation, School of Elect. and Comp. Eng., Georgia Tech, Atlanta, GA, 2012.

[207] W. Breuer, D. Povh, D. Retzmann, E. Teltsch, and X. Lei, "Role of HVDC and FACTS in future power systems," in Ciger Symp., 2004.

[208] L. Gyugyi, C. D. Schauder, S. L. Williams, T. R. Rietman, D. R. Torgerson, and A. Edris, "The unified power flow controller: A new approach to power transmission control," IEEE Trans. Power Del., vol. 10, no. 2, pp. 1085-1097, 1995.

[209] D. Das, D. M. Divan, and R. G. Harley, "Power flow control in networks using controllable network transformers," IEEE Trans. Power Electron., vol. 25, no. 7, pp. 1753-1760, 2010.

[210] R. P. Kandula, A. Iyer, R. Moghe, J. E. Hernandez, and D. Divan, "Power router for meshed systems based on a fractionally rated back-to-back converter," IEEE Trans. Power Electron., vol. 29, no. 10, pp. 5172-5180, 2014.

[211] J. J. Thomas, J. E. Hernandez, and S. Grijalva, "Power flow router sensititvities for post-contingency corrective control," in IEEE Energy Conversion Congr. and Expo., 2013, pp. 2590-2596.

[212] J. E. Hernandez, R. P. Kandula, F. Lambert, and D. Divan, "A practical directional third harmonic hybrid active filter for medium voltage utility applications," in IEEE Energy Conversion Congr. and Expo., 2012, pp. 219-226.

[213] J. E. Hernandez, J. J. Thomas, and S. Grijalva, "Providing flexibility for temporal and spatial constraints to increase wind power production," IEEE Trans. Sust. Energy, submitted for publication.